NUMERICAL MODELLING OF ROTORCRAFT AEROELASTIC STABILITY

by

HEJUN DU, B.Sc., M.Sc.

June, 1991

A thesis submitted for the degree of

Doctor of Philosophy of the University of London

and for the

Diploma of Membership of the Imperial College

Department of Aeronautics

Imperial College of Science, Technology and Medicine

London, SW7 2BY

ACKNOWLEDGEMENTS

The author wishes to express his sincere gratitude to his supervisor Mr D. Hitchings for his invaluable instruction, deep understanding, great help and very special caring throughout the course. The author benefited a lot from the wealth of knowledge and experience of his supervisor. The author gratefully thanks Professor G. A. O. Davies for the launch of this project and for his consistent encouragement, invaluable advise and great help throughout the course.

The author gratefully acknowledge the Westland Helicopters Ltd for sponsoring this work, special thanks go to Mr S. Holton and Mr. P. Juggins for their valuable discussions and suggestions.

The author would like to thank the Nanjing Aeronautical Institute in China, where he was educated for six and half years; and to especially thank all his colleagues in the Helicopter Technology Research Institute at NAI.

The author is very grateful to his parents, sisters and brothers in China for their enthusiastic encouragement and concern, and especially indebted to his wife for her understanding, patience and invaluable help.

ABSTRACT

Firstly, the whirl flutter of a tilt-rotor aircraft of interest is studied. The tilt-rotor aircraft in aeroplane forward flight mode is modelled as a coupled tilt-rotor/nacelle system. The system's degrees of freedom consist of the rigid blade torsion about a pitch bearing, the universal joint or gimbal degrees of freedom at the hub, and the nacelle's rigid body motions. Aerodynamic loads are computed based on a two-dimensional quasisteady thin airfoil theory including both circulatory and noncirculatory aerodynamic forces. The nonlinear differential equations of motion are derived by Newton's method based on a ordering scheme and are linearised using the perturbation method. The system stability is analysed by solving the eigenvalue problem associated with the linearised differential equations. This model was validated against existing experimental and theoretical results for a propeller and a tilt-rotor, and then applied to study a universal joint tilt-rotor and an ideal gimbal tilt-rotor aircraft. The whirl flutter characteristics of these systems were evaluated and compared. The effects of significant parameters were identified.

More efforts were subsequently made to develop a general lumped mass finite element model for analysing the structural dynamic and aeroelastic problems of a general three dimensional elastic beam with arbitrary and large base movements. This was done by combining finite elements with the multibody dynamics method. The general models developed have great modelling flexibility and can model the complex geometry of beams and the arbitrary coupling of a beam with other substructures as well as any large and arbitrary base motions of a beam.

Firstly, a general finite element structural dynamic model was developed for a beam attached to an arbitrary moving base described by three angular velocities (accelerations) and three translational velocities (accelerations). The equations of motion were derived using the virtual work principal. Large deflections and small strains of the beam are assumed. The axial and torsional deformation of the beam element are represented by linear polynomials, while the bending deflections are represented by cubic polynomials. Numerical examples were performed for both an eigenvalue problem of a spinning beam and the dynamic response of a space-based robotic manipulator arm with complex base motions. The former was found to give almost identical results to a precise analytical solution. The second example was found to be basically identical to the numerical simulation results from a recently developed multibody dynamics model. Some inconsistencies in the previous model are addressed. The great modelling flexibility of the hybrid finite element and multibody dynamics model was demonstrated.

The above lumped mass finite element structural dynamic model was further developed as a finite element aeroelastic beam model for rotorcraft blades in an axial flow by including the aerodynamic loads. A two dimensional quasi-steady thin airfoil theory was used to compute the aerodynamic loads. The arbitrary blade base motions were included in the aerodynamic formulation. The aerodynamics model is valid for both high inflow and low inflow cases. Again, the resulting nonlinear differential equations of motion were linearised using the perturbation method in order to analyse the system aeroelastic stability. This general model can be used as a basic element to analyse the isolated blade aeroelastic stability and the coupled rotor/body system aeroelastic stability by making use of the arbitrary base motion variables of the blades. A number of numerical examples are analysed with a wide range of parametric variations. The adequacy and great modelling flexibility of the present model were verified.

To my parents

CONTENTS

LIST OF FIGURES

LIST OF TABLES

LIST OF SYMBOLS

A	Blade section area
a	Blade section lift curve slope
$\vec{a}$	Accelleration of a point on blade
$\vec{a}_{( )}$	Accelleration vector of ( )
$\vec{a}_0$	Accelleration of the gimball centre
$\vec{a}_r$	Accelleration of a point on blade relative to moving frame
$\{ a^e \}, \{ a_b \}$	Node degrees of freedom of a beam element, and quasi-coordinates due to the moving base, respectively
b	Blade semi-chord
c_1	Blade section lift coefficient
c_{10}	Trim value of blade section lift coefficient
c_d	Blade section drag coefficient
c_{d0}	Trim value of c_d
c_{mac}	Blade section moment coefficient
c_{mac0}	Trim value of c_{mac}
D	Blade section drag
Δc_1	Perturbation value of blade section lift coefficient
Δc_d	Perturbation value of c_d
Δc_{mac}	Perturbation value of c_{mac}
ΔU_p	Perturbation value of U_R
ΔU_T	Perturbation value of U_T
E	Young's modulus
e_p	Blade pitch bearing offset
e_x, e_y, e_z	Position coordinates of nacelle gravity centre relative to the hub centre
$\vec{E}_{( )}$	Unit vector column of ( ) system
F_I^*, F_s^*	Generalised inertial force and generalised structual force, respectively
F_I	Inertial loads due to the lumped mass
$F_{AR}^x, F_{AR}^y, F_{AR}^z$	Components of $\vec{F}_{AR}$ in $x_{2g}y_{2g}z_{2g}$ system
$F_{IR}^x, F_{IR}^y, F_{IR}^z$	Components of $\vec{F}_{IR}$ in $x_{2g}y_{2g}z_{2g}$ system
F_y, F_z	Blade section aerodynamic force components
$\vec{F}_A$	Blade section aerodynamic force vector
$\vec{F}_{IR}, \vec{F}_{AR}$	Resultant forces transmitted to nacelle from a blade, respectively due to

	intertial loads and aerodynamic loads
$\vec{F}_R$	Resultant force transmitted to nacelle from a blade
G	Shear modulus
gc	mass centre
H_1 - H_4 , L_1 - L_2	Hermitte interpolation functions
$\vec{H}_0$	Position vector of gimball centre relative to nacelle G.C.
I	Central inertial dyadic of the lumped mass
I_2, I_3	Sectional principal inertial moments of Unit-length blade about cross-section axes
I_{xx}, I_{xy}, I_{xz}, I_{yy}, I_{yz}, I_{zz}	The rigid body nacelle or the lumped beam mass moments of inertia
$\vec{i}_g$, $\vec{j}_g$, $\vec{k}_g$	Unit vector of $x_g y_g z_g$ system
k_A	Beam cross-section polar radius of gyration
K_{β_s}, K_{β_c}	Rotor gimball hinge restrain spring stiffness in pitch and yawing
K_ϕ	Blade pitch control link stiffness
K_{pg}	Kinematic pitch/gimball couping
K_x, K_y, K_z $K_{\theta x}$, $K_{\theta y}$, $K_{\theta z}$	Translational and rotational spring stiffness representing restrain between nacelle and aircraft wing, respectively
l_e	Length of an element
l_x, l_y, l_z	Position of restrain spring representing nacelle-wing restrain, relative to the gravity centre of nacelle
$\vec{L}$	Blade section lift vector
$\vec{L}_c$, $\vec{L}_{nc}$	Circulatory and noncirculatory parts of blade section lift
M	Blade section aerodynamic moment
m	Unit-length blade mass or lumped beam mass
M_I	Inertial moment of the lumped mass about the mass centre
M_{na}	Nacelle mass
M_E^{pitch}	spring restraint loads respectively
M_I^{pitch}, M_A^{pitch},	Moments about feathering bearing due to ineatial, aerrodynamic and
$\vec{M}$	Blade section aerodynamic moment vection
$\vec{M}_c$, $\vec{M}_{nc}$	Steady and unsteady parts of $\vec{M}$
$\vec{M}_D$, $\vec{M}_E$	loads
$\vec{M}_I$, $\vec{M}_A$,	Moment vectors due to ineatial, aerodynamic, damping, spring restraint
$\vec{M}_{IR}$, $\vec{M}_{AR}$	Resultant moments transmitted to nacelle from proprotor respectively due to ineatial loads aerodynamic loads

$\vec{M}_R$	Resultant moments transmitted to nacelle from proprotor
[M] [C] [K]	Inertia, gyroscopic (or damping) and stiffness matrices of the whole system, respectively
$[M_j]$ $[C_j]$ $[K_j]$	Element inertia, gyroscopic and stiffness matrices, respectively
N_e	Number of elements
P_x, P_y, P_z	Inertial force components of unit - length blade
P_R^x, P_R^y, P_R^z	Components of $\vec{P}_R$ in $x_{1g}y_{1g}z_{1g}$ system
$\vec{P}_E$	Force applied on nacelle due to nacelle's restraint spring
$\vec{P}_G$	Resultant force at nacelle G.C. due to loads from proprotor
$\vec{P}_I$	Inertial force on unit - length blade
$\vec{P}_R$	Resultant force transmitted to nacelle from whole proprotor
q_x,q_y,q_z	Inertial moment components of unit - length blade)
Q_E^x, Q_E^y, Q_E^z	Components of $\vec{Q}_E$ in $x_{1g}y_{1g}z_{1g}$ system
Q_R^x, Q_R^y, Q_R^z	Components of $\vec{Q}_R$ in $x_{1g}y_{1g}z_{1g}$ system
$\vec{Q}_E$	Moment applied about nacelle G.C. due to nacelle restraint springs
$\vec{Q}_G$	Result moment applied at nacelle gravity centre due to the loads transmitted from ehole proprotor
$\vec{q}_I$	Inertial moment on unit - length blade
$\vec{Q}_R$	Resultant moment transmitted to nacelle from whole proprotor
R	Rotor radius
R_x, R_y, R_z	Perturbation displacement vector of nacelle gravity centre or beam base
r_x, r_y, r_z	x, y, z components of $\vec{R}_{gc}$
$\vec{r}$	Position vector of pint on blade
$\vec{R}_{(\ )}$	Position vector of ( )
$\vec{R}_E^0$	Position of nacelle restraint springs relative to nacelle gravity centre
$\vec{r}_e$	Postion vector of point on blade elastic axis
$\vec{R}_g$	Perturbation displacement vector of gimball centre
T	The centrifugal force caused by the beam outboard a cross-section
$[T_{ij}]$	Transformation matrix between $x_iy_iz_i$ and $x_jy_jz_j$
U	Blade section resultant velocity magnitude
u	Axial displacement of the elaticity centre of the beam cross-section

U_n	Blade section velocity component vertical to blade chord
U_p	Blade section out-of-plane velocity
U_R	Blade section velocity component Parallel to blade chord
U_T	Blade section inplane velocity
v	Lead-lag displacement of the elaticity centre of the beam cross-section
v_F	Aircraft forward speed or rotor forward speed normalised with respect to ΩR
v_i	Induced velocity of rotor normalised with respect to ΩR
v_x, v_y, v_z	x,y,z components of $\vec{v}_{gc}$
$\vec{v}$	Blade section resultant velocity
$\vec{V}_{(\,)}$	Traanslational veloccity of ( )
$\vec{v}_0$	Velocity of gimball centre
$\vec{v}_{\text{blade motion}}$	Moving velocity of blade section
$\vec{v}_{\text{free airflow}}$	Free airflow velocity of blade section
$\vec{v}_r$	Velocity of point on blade relaative to moving nacelle frame
w	Flap displacement of the elaticity centre of the beam cross-section
x	Blade radial station
x_A	Blade section aerodynamic centre offset
x_e	Local axial coordinate of a beam element
x_g, y_g, z_g	Displacement components of gimball centre
x_{Gc}	Blade section gravity centre position
x_{gc}, y_{gc}	Blade sectional mass centre offsets in y and z direction, respectively
x_T	Tension centre offset from elasticity centre
y, z	Blade ccross-sectional coordinate
z_h	Gimbal undersling
α	Blade section attack angle
α_G	Pitch angle due to gimball motion
β	Rotational angle in flap
β_G	Flap angle due to gimball motion
β_{Gs}, β_{Gc}	Gimball yawing and pitch degree of freedom
β_p	Blade precone angle
β_{sw}	Blade feathering hinge sweep angle
$\Delta_i = \delta U_j - \delta W_{Ij}$	Contribution of j'th element to $\delta U - \delta W_I$
δU	Variation of strain enegy
δW	Virtual work
$\dot{\varepsilon}$	Pitch velosity of blade section

$\varepsilon_{xx}, \varepsilon_{x\eta}, \varepsilon_{x\xi}$	Engineering strain components
$\vec{\varepsilon}_{(\,)}$	Angular accelleration vector of ( )
$\hat{\phi}$	Geometric twist angle
ϕ	Blade torsion deformation
ϕ	Elastic twist angle
ϕ_0	Trim torsion pitch aangle of blade
ϕ_{1s}, ϕ_{1c}	Generalized sine and cosine cyclic torsion coordinates
ϕ_c	Generalized collecteive torsion coordinate
θ_0	coordinateBlade colletive angle
θ_{1s}, θ_{1c}	Blade cyclic
θ_G	Blade geometry pitch angle
θ_{tw}	Blade pre-twist angle
$\theta_x, \theta_y, \theta_z$	Nacelle regid-body rotation degree of freedom or beam base rotations
ρ	Density of air
$\sigma_{xx}, \sigma_{x\eta}, \sigma_{x\xi}$	Enginerring stress components
Ω	Rotor rotation speed
$\omega_x, \omega_y, \omega_z$	x,y,z components of $\vec{\omega}_h$
$\vec{\omega}_{(\,)}$	Angular velocity of ( )
$\vec{\omega}, \dot{\vec{\omega}}$	Angular velocity and accelleration includeing nacelle rotation and rotor rotation speed
$\vec{\omega}_{na}$	Angular velocity due to nacelle rotatioon
$\vec{\omega}_{p1}$	Angular velocity of beam sction in base-fixed frame x,y,z
ξ	Rotational angle in lead-lag
ξ, η	Blade cross-section principal axis
ψ, ψ_k	Azimuth of kth blade

$(\,)' = \frac{\partial(\,)}{\partial x}$ or $\frac{\partial(\,)}{\partial r}$

$\dot{(\,)} = \frac{d(\,)}{dt}$ (or $\frac{d(\,)}{d\Omega t}$ in chapter 3 and 4. see p.52)

$\ddot{(\,)} = \frac{d^2(\,)}{dt^2}$ (or $\frac{d^2(\,)}{d(\Omega t)^2}$ in chapter 3 and 4)

$[\,]^T$ Transpose of matrix [ ]

CHAPTER 1 INTRODUCTION

1.1 PURPOSES

Rotorcraft make use of rotors to produce lift or thrust. Examples of such aircraft are helicopters and tilt-rotor aircraft. Inevitably, the aeroelastic stability problem is of particular significance since the blades are a flexible structure and they carry all of the aerodynamic loads. The aeroelastic stability associated with rotorcraft is a broad and complex subject. The complexity is caused by two basic sources: One is the unusual flexibility of rotor blades, and the other is the complexity introduced by the fact that they are rotating.

Although the analysis of rotorcraft aeroelasticity can be traced back to the nineteen fifties, early work in this field made use of simple physical models such as spring restrained, centrally hinged, rigid blades [Loewy 1969, Ormiston & Hodges 1972]. Later work treated configurations that were somewhat more complex, including some with elastic blades [Houbolt & Brooks 1958, Hodges & Dowell 1974, Friedmann 1975], fuselage body degrees of freedom and inflow dynamics [Johnson 1977, Ormiston 1985, Gaonkar & Peters 1986b]. These models provide us with a physical insight into the complicated dynamic phenomena of rotorcraft blades and coupled rotor/fuselage structures, and are very valuable for this reason. However, since they are based on only one physical model they are limited as a general analytical model when the aim is to accurately analyse various realistic rotorcraft configurations. With the advent of the promising bearingless rotor systems, a great deal of modelling flexibility is required as various configurations may be very different. It is desirable to develop a general dynamic model with a great modelling flexibility capable of dealing with realistic and relatively complicated geometries and structural coupling effects in rotorcraft dynamics. The Finite Element Method provides us with an ideal technique well suited to modelling the complicated structural configurations such as the nonuniform blades and blades with complex root

geometries. Moreover, the Finite Element Method leads to a significant reduction in the algebraic manipulative labour in the rotorcraft aeroelasticity analysis. A considerable part of rotorcraft structural mechanics research efforts has begun to focus in this direction.

Recent implementations applying the finite element method to rotorcraft dynamic problems contain several significant efforts to explore the application of the Finite Element Method to rotorcraft aeroelasticity [Friedmann & Straub 1980, Sivaneri & Chopra 1982]. These models discretize a simply spinning beam, but they are still limited to one configuration. Furthermore, they lack the capability to model the general coupling of the beam with a fuselage or to model blade/root kinematics of an arbitrary configuration.

Meanwhile, investigations of rotating beam dynamics are also being actively conducted in a number of other relevant disciplines [Likins 1974, Luh et al 1980, Kamman & Huston 1984, Turcic & Midha 1984, Kane & Ryan 1987]. Especially important is the so-called "multi-body system" dynamics, where a number of rigid and flexible bodies are inter-connected and may be largely rotating and/or translating relative to each other. The central theme of multibody dynamics is to develop a general set of dynamic equations of motion for such a large system. This is realised by considering the motion of a typical body in an arbitrary moving reference frame. This moving reference frame consists of six rigid body degrees of freedom and hence can model the arbitrary connections of a body to other bodies. This consequently leads to a general dynamics model with a high degree of modelling flexibility. A rotorcraft has many similarities with such a system. Unfortunately although a number of multibody dynamics codes exist, most of them treat the structure as rigid body components. None possess the capability to model the aeroelastic phenomena and the nonlinear elastic equations of motion since they were developed primarily for spacecraft applications. A very recent work in multibody dynamics treats the structural dynamics of a beam attached to an arbitrary moving base

using the global modal method [Kane & Ryan 1987]. That is quite close to the problem of a general rotating beam dynamics model, but the structural dynamics model is a linear one and can not model some important structural effects of a rotor blade such as the blade pretwist. It also excludes the aerodynamic terms.

It can naturally be expected from the above discussions that the combination of the finite element method with the "multibody" dynamics method will result in a quite general dynamic model for complex systems. One of the aims of this thesis is to develop a lumped mass finite element model for a general rotor blade, which can model the aeroelastic stability of both high-inflow rotorcraft such as tilt-rotor aircraft and low-inflow rotorcraft. The finite element and "multibody" dynamics modelling concepts are used to advantage to develop a general dynamics model capable of modelling the complex geometries of rotor blades, blade/root kinematics and the coupling between rotor blades and the fuselage degrees of freedom. Meanwhile, the other aim of this thesis is to provide a general hybrid finite element-multibody structural dynamics model relevant to other disciplines where rotating beams occur, such as robotics, spacecraft dynamics etc. This structural dynamics model can treat both the natural characteristics problems and the dynamic response of a beam with an arbitrary moving base.

On the other hand, the tilt-rotor aircraft is a special type of rotorcraft and is being developed as a new and promising type of air vehicle. The tilt-rotor aircraft can both fly like a normal helicopter (helicopter mode) and like a propeller aeroplane (aeroplane mode). Consequently, it may meet a special type of instability at high speed forward flight in the aeroplane mode. This is the so-called whirl flutter. It was initially found to occur with propeller aircraft. With the development of the tilt-rotor aircraft, increasing efforts are being made to improve the understanding and analysis capability of the tilt-rotor aeroelastic stability. As a part of the efforts of this thesis, the whirl flutter problems of the tilt-rotor aircraft configurations of interests are studied. This whirl flutter model is

aimed at obtaining an understanding of the fundamental whirl characteristics of two different tilt-rotor configurations. One is a universal joint tilt-rotor. The other is an ideal gimbal tilt-rotor. An understanding of the whirl flutter characteristics of the gimbal tilt-rotor is lacking in the literature.

Therefore, this thesis consists of three dynamics models developed step-by-step. They are briefly reviewed in the following sections.

1.2 A WHIRL FLUTTER MODEL OF A TILT-ROTOR AIRCRAFT (CHAPTER 3, 4)

As the first step for the investigations of the rotorcraft aeroelasticity, a tilt-rotor aircraft whirl flutter problem is considered in Chapter 3. Since the emphasis is placed on obtaining physical insight into the dynamic behaviour of the system, a simple model is taken. The aircraft fuselage and wings are assumed as rigid and in a stable forward flight. The tilt-rotor is assumed to work in an axial flow mode. The rotor blades are assumed to be rigidly fixed to the hub in flap and lead-lag, but can twist about the pitch bearings with torque spring restraints which represent the control link stiffness. The rotor hub is joined to the nacelle through either a universal joint or a gimbal, and hence has two different construction configurations. Both have two degrees of freedom one each in pitch and yaw with viscous damping and spring restraints. The nacelle is modelled as a rigid body with six space degrees of freedom and has spring and viscous damping restraints with the wing. The total number of degrees of freedom is 12.

The equations of motion are derived by the Newton method. In the formulation, the nonlinear terms are retained using a normal ordering scheme. While the previous whirl flutter models usually used a linear model. The aerodynamic loads are computed based on a two-dimensional quasi-steady aerodynamics theory and include both circulatory forces and noncirculatory forces. The latter is usually neglected in the previous whirl

flutter models. The rotor equations of motion are obtained by the equilibrium of the aerodynamic loads, inertial loads applied on the whole rotor, and the universal joint (or gimbal) restraint moments. The blade torsion equation of motion is determined by the equilibrium of the aerodynamic moment and the inertial moment about the blade pitch axis and the elastic restraint moment due to the stiffness of the control system. The nacelle equations of motion are established according to general rigid body dynamics with the aerodynamic loads and the inertial loads transmitted from the rotor and with the restraint loads. Finally we obtain 12 linearised perturbation differential equations and an equilibrium algebraic equation for the blade torsion deformation.

The system stability is evaluated by solving the eigenvalue problem of the linearised differential equations. For this system, an instability may be occur at high forward speed. This is the whirl flutter problem. Numerical results include two principal groups for this whirl flutter model. The first one investigates a classical propeller whirl flutter model with only two degrees of freedom of the nacelle's pitch and yaw, and a four degrees of freedom flap-hinged tilt-rotor whirl including two cyclic flap modes, nacelle pitch and yaw modes. Both of these have been studied both theoretically and experimentally and results reported in the Literature. This part of the thesis is mainly aimed at confirming the validity of the present analytical model. The second group concentrates on a universal joint tilt-rotor and an ideal gimbal tilt-rotor and finding whirl characteristics for these.

1.3 A FINITE ELEMENT STRUCTURE DYNAMICS MODEL FOR A BEAM WITH AN ARBITRARY MOVING BASE (CHAPTER 5)

Subsequently, in Chapter 5, a general finite element structural dynamics model is developed for a general space elastic beam with an arbitrary moving base. This model can incorporate the coupling of a blade with fuselage or any large and arbitrary base motions. The physical model is idealised as:

1) A general elastic beam is set on a rigid base.
2) The rigid base may have an arbitrary space motion which is described by the three translational velocities of the connecting point and three rigid body angular velocities of the base.
3) The beam can be pretwisted.
4) Sectional mass centre is offset from the elasticity centre.
5) The beam undergoes a three-dimensional deformation which is described by the three translational displacements of the elasticity centre and three successive rotations of the section.
6) The deflections may be large.
7) The Euler-Bernoulli assumptions are used.
8)The effect of the section warping on the torsion is taken into account.

The equations of motion are obtained by using the virtual work principle. The equations are discretized by the finite element method. The beam is divided into a number of elements. The beam inertia is lumped at the end nodes of each element. This lumped mass model simplifies the formulation of the generalised inertia forces. As usual, the lumped rotary inertia in flexure (flap and lag) are taken to be small values. The effect of cross section warping on the inertial forces are negligible and are not considered.

The generalised forces contributed from the internal forces are obtained by the derivation of the strain energy . Although the deflections may be large, the strain is assumed to be small. The nonlinear strain-displacement relations are presented. The centrifugal stiffness and gyroscopic terms caused by the base motion are specifically treated so that this dynamics model can be conveniently applied to both nonlinear and liner problems. The final mathematical models can be readily applied to solve not only the eigenvalue problem but also the dynamic response problem of a beam with arbitrary base motions as in a multibody dynamics algorithm.

Two groups of numerical examples are solved to validate the model and show its application to a general dynamic simulation of a beam under complex base motions. The first case is for a simply spinning beam which has an analytical solution to compare with. The second case is simulating the behaviour of a space-based robotic manipulator which has a complex base motion. Results of this problem from a modal method specifically developed for a general multibody code are available to compare with.

1.4 A FINITE ELEMENT AEROELASTICITY BEAM MODEL (CHAPTER 6)

Based on the physical model given in the last section, Chapter 6 considers the beam as a rotorcraft blade which is subject to aerodynamic actions. The aeroelasticity problem of this blade can be modelled by adding the aerodynamic loads to the generalised active forces. The aerodynamics of the blade are developed for an axial flow state of a rotor. A two-dimensional quasisteady aerodynamic theory is used. Noncirculatory aerodynamic loads are also included. The induced velocity is assumed to be uniform over the rotor. The aerodynamic loads are calculated so as to be valid both for high inflow cases such as a tilt-rotor aircraft in a aeroplane-mode forward flight and for low inflow problems such as a normal helicopter in hover or vertical flight. The nonlinear differential equations of motion are obtained for the rotorcraft aeroelasticity problem by combining the aerodynamic loads with the previous structural dynamics model. This set of nonlinear differential equations of motion are linearised about a set of equilibrium positions using the perturbation method. This finally leads to a set of nonlinear algebraic equations for the equilibrium solution and a set of linearised differential perturbation equations that depend on the equilibrium values. This procedure is incorporated into the computer program.

A number of numerical examples are presented to analyse the aeroelastic stability of hingeless rotor blades. The results from the present model are compared with an existing and reliable result from the Literature which includes both the equilibrium solutions and the stability characteristics. The modelling flexibility of the present model is demonstrated.

1.5 STRUCTURE OF THIS THESIS

This chapter, chapter 1 highlights the purposes of this work and the models developed in this thesis.

The next chapter presents a literature review in the rotorcraft dynamics and aeroelasticity together with several significant works regarding rotating beam dynamics conducted in other disciplines.

Chapter 3 is contributed to formulate the equations of motion for the tilt-rotor aircraft whirl flutter model briefly described in section 1.2.

Chapter 4 introduces the solution procedures for the tilt-rotor whirl flutter problem and presents the numerical results.

Chapter 5, 6 expand in detail the contents briefly discussed in section 1.3, 1.4. They are for the finite element structural dynamics model and finite element aeroelasticity model of a beam with an arbitrary moving base respectively.

Finally, chapter 7 draws the conclusions of this thesis and gives some comments on possible further developments.

CHAPTER 2 ROTORCRAFT DYNAMICS AND AEROELASTICITY STABILITY ANALYSIS

2.1 INTRODUCTION

Rotary beam-like structures are widely used in various fields, such as industrial robots, rotating machinery, satellites, and rotorcraft. Therefore, the dynamics of rotary beams have been a subject of interest in a number of diverse disciplines and have received an extensive investigation and development over the last four decades.

In the field of industrial robots, various approaches were developed to compute the forces and torques needed to drive all the joints accurately in order to control a manipulator which carries a variable or unknown load and moves along a planned path [Luh et al. 1980]. In the design of high speed machines and mechanisms, analyses have recently been conducted to study the vibration effects on the performance of the mechanism [Turcic and Midha, 1984]. In the field of satellites, the demand of precise orientation of a satellite relative to an inertial or an orbiting frame of reference has resulted in a number of research endeavours [Modi, 1974, Kulla,1972, Likins,1974, Kamman and Huston,1984, Kane et al.,1987].

For rotorcraft, the rotating blade dynamics is closely linked to the rotorcraft aeroelasticity problems due to the special working environment. Virtually, every rotary-wing aircraft potentially has aeroelastic stability problems. These represent some of the most complex problems in the area of aeroelasticity. The complexity is caused by two basic sources: one is the unusual flexibility of rotor blades, and the other is the complexity introduced by the rotation. Blade flexibility not only adds more degrees of freedom, but also introduces complicated geometrically nonlinear problems by allowing large blade deflections. The rotation results in much more complicated inertia loads such as centrifugal and coriolis forces which bring additional stiffness and couplings. This is

inherent for all rotating beams. It also gives rise to a complex unsteady aerodynamic environment. The investigations of the rotorcraft aeroelasticity has been extensively conducted during the last 40 years, especially since the 1970's. and substantial progress has been achieved.

This chapter is intended to present a brief review of the research of rotorcraft dynamics and aeroelasticity stability. The modelling of an aeroelasticity problem involves three basic aspects, namely :

1) structural modelling,

2) inertial modelling,

3) aerodynamic modelling.

The first two items form the basis for the structural dynamic modelling, which is also essential for rotary beam dynamics in other fields. In the next section, therefore, we shall firstly discuss the development of the rotorcraft structural dynamics. Subsequently, the aerodynamic modelling in rotorcraft aeroelasticity stability analysis is introduced. The last section is concerned with the application of the Finite Element technique to rotorcraft aeroelasticity problems.

2.2 STRUCTURAL DYNAMICS MODELLING

The development of rotorcraft structural dynamics modelling will be discussed in two parts. That is:

1) rotating blade structure dynamics, and

2) coupled rotor/body system dynamics.

2.2.1 Structural Dynamics of Rotating Blades

2.2.1.1 Rigid Blade Model

Early rotor blade and rotorcraft analyses usually treated both hinged and cantilever elastic blades as hinged, rigid blades for aeroelastic stability analysis. Early analysis of rotor

aeroelastic problems was generally undertaken in terms of the classical fixed-wing flutter model. The flap-pitch flutter of blades, similar to the counterpart found in fixed-wing aircraft, is naturally derived [Loewy,1969]. The pitch-lag and flap-lag instabilities were found by Pei [Loewy,1969]. More complicated flap-lag-pitch flutter models were subsequently developed [Loewy,1969]. These rigid blade models are appropriate for some rotorcraft configurations. The equations of motion are easier to derive and need much less computation time to solve them than for flexible blades. They are very valuable when a physical insight into the dynamic behaviour of a system is needed.

2.2.1.2 Elastic Blade Model

Although the rigid blade models can be used to approximate the dynamics of a rotorcraft blade, rotor blades are fundamentally rotating elastic beams. Houbolt and Brooks's work [1958] was used as the classic and standard equations of motion for elastic blades from the middle 1950's to 1970's. They developed a set of linear differential equations for nonuniform rotor blades. However these linear equations contain the geometrical stiffening owing to centrifugal force, normally considered a nonlinear effect. For articulated rotor blades, it is quite adequate.

However, it has been clear from the early work on rotorcraft dynamics that the governing equations are not of the linear type [Loewy,1969]. Attempts at further understanding of this nonlinearity was not made until the 1970's. During the late 1960's, interest in the hingeless rotor was intensified. Hingeless rotor blades are cantilevered to the hub. The lack of hinges leads to a simpler mechanism but large bending and torsional deformations of the blades arise. These large deformations give rise to geometrically nonlinear structural and inertial terms in the dynamic equations, even when the strains are small. Since the 1970's, extensive efforts have been devoted to the development of suitable structural dynamic models for cantilever rotating blades.

In linear structural analysis, the deflection of the structure is assumed to be infinitesimally small, so that the difference between the deformed and undeformed configurations of the structure can be neglected. The equilibrium formulation of the structure can be referred to either the deformed or the undeformed configurations. However, in large displacement nonlinear analysis of structures, the deformed and the undeformed configurations can no longer be considered identical. The geometry of the beam must be defined both in its undeformed state and in its deformed state. This requires the development of the transformation relation between the undeformed blade coordinate unit vectors and the deformed blade coordinate unit vectors. Transformation matrices for various rotation sequence are hence derived [Peters and Ormiston, 1973, Hodges et al. 1980]. A survey of methods of treating finite rotation in relation to nonlinear beam kinematics was published by Hodges [1987a]. Based on this type of transformation relationships and combined with the Euler-Bernoulli assumption, a number of elastic blade dynamics equations have been developed.

Ormiston and Hodges [1972] considered elastic flap-lag blade models. The well-known kinematical foreshortening of the beam axis caused by bending is addressed. This leads to centrifugal and coriolis forces. These effects are essential to model the nonlinear features of hingeless rotor dynamics. (An illustration of foreshortening is given in fig.2.1).

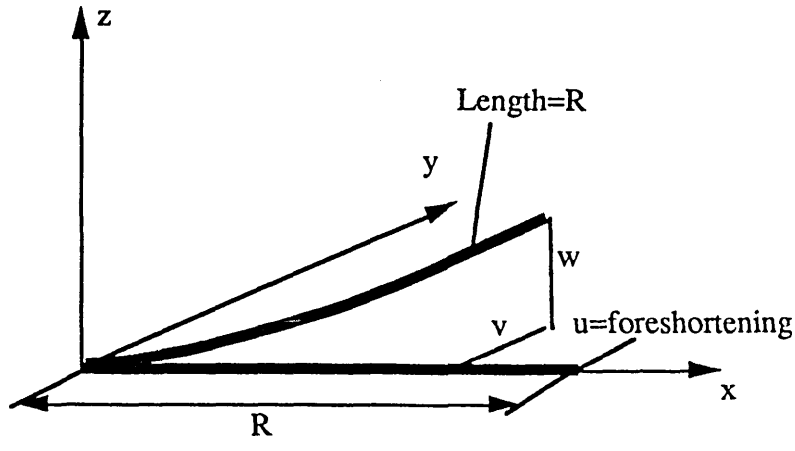

Fig 2.1 Illustration of the beam foreshortening caused by bendings

Nonlinear equations for coupled bending and torsion of elastic rotor blades were subsequently developed by a number of researchers [Friedmann, 1975, Hodges and Dowell,1974]. In these investigations, an ordering scheme was utilised to systematically neglect the higher order nonlinear terms that arise from the geometrical nonlinearity. In such an ordering scheme, all of the important parameters of the problem are assigned orders of magnitude in terms of a typical nondimensional displacement quantity ε which represents typical blade slopes. This ordering scheme is used with the assumption that terms of $O(\varepsilon^2)$ are usually negligible when compared to terms of order one. That is $1+ O(\varepsilon^2) =1$. This approach is based on the so called moderate rotation assumption of rotor blades.

Meanwhile, the significant nonlinear coupling between torsion and combined flapwise and chordwise bending were properly modelled [Hodges and Dowell,1974, Friedmann, 1975,1977a]. This coupling is found to be significant in hingeless rotor blade aeroelasticity stability analysis. Fig.2.2 illustrates the origin of the nonlinear torsion caused by simultaneous flapwise and chordwise bending. To evaluate the accuracy of the theory, the Princeton beam experiments were conducted [Dowell et al,1977]. The Hodges-Dowell equations were further extended to include variable flap-lag structural coupling and to investigate their effects on rotor blade aeroelasticity stability in hover [Hodges and Ormiston,1976].

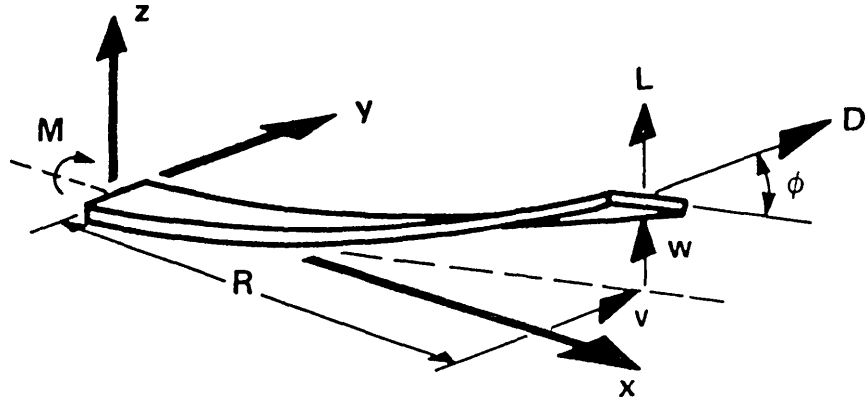

Fig 2.2 Nonlinear torsion of an elastic cantilever beam resulting from simultaneous flapwise and chordwise bending

The equations introduced above are developed based upon the assumption that the structural deformations of the rotor blades are limited to be only moderately large, where the formulation of the dynamic equations usually utilise an ordering scheme to neglect higher order nonlinear terms. This approach leads to equations which contain up to second order nonlinear terms. In an analysis by Crespo Da Silva and Hodges [1986b], the influence of retaining the next level of higher order terms in the equations of motion was considered. This yields equations including a third order nonlinearity. The influence of these third order terms on blade response and stability was investigated. The results indicated that the influence is limited for practical rotorcraft configurations [Friedmann, 1990].

The moderate rotation assumptions can be adequately applied to many rotor blade dynamic and aeroelastic analyses, but this gives some limitation to the equations of motion derived based on the assumptions used. In more recent studies, Hodges [1985, 1987*b*] have developed a nonlinear structural dynamics model for rotor blades in which the assumption of moderate rotations were abandoned. The common ordering scheme is not used to model the beam kinematics. A less restrictive assumption is that the extensional strain is ignored compared to unity. Such a large displacement model for composite beams was also addressed in a recent publication [Bauchau and Hong,1987b].

2.2.1.3 Bearingless and Composites Materials Rotor Blade Model

The application of bearingless rotor systems poses a new class of problems to rotorcraft dynamists. The bearingless rotor systems eliminate blade root hinges and bearings by using a beam that is sufficiently flexible in torsion to accommodate all of the blade-pitch-control motion usually provided by the pitch change bearing of articulated and hingeless rotors. The flexible structure makes the dynamic modelling of the systems much more complicated and difficult to analyse. The first effort was made to derive the differential equations for a composite bearingless rotors using the global modal method by Bielawa

[1976]. For complex structures, such as bearingless rotors, the Finite Element Method is an ideal solution technique. Further investigations on bearingless rotor blades usually applied the Finite Element Method and will be discussed in section 2.4 which deals with the application of the Finite Element Method to rotary wing dynamics.

Composites materials are more and more widely used within rotorcraft structures, especially for the rotor blades. However, most of the dynamic models developed to date have been restricted to isotropic material properties. The development of composite rotor blades has lead to substantial research efforts in recent years to develop dynamic models which are suitable for the structural dynamic and aeroelastic analysis of composite rotor blades. The work in this area can be divided into two categories: 1) Modelling approaches which lead to the determination of the stiffness properties of arbitrary composite blade cross sections. Anisotropic materials and the composite nature of the blades are taken into account in this category. 2) Structural models which use one-dimensional beam kinematics suitable for composite rotor blade analysis [Friedmann,1990].

The determination of the shear centre location and warping functions of composite blade sections is the centre of the research in the first category. Cross section properties can then be evaluated and further be applied to the research in the second category. A large number of studies have been conducted in the first area during recent years [Borri and Merlini,1986, Bauchau,1985, Lee and Kim,1987, Stemple and Lee,1988, Friedmann,1990]. More recently, some work was aimed at the structural dynamic modelling of composite blades [Kosmatka and Friedmann, 1987, 1989, Bauchau and Hong,1987a,1987b, Minguet and Dugundji, 1989a,1989b, Rand,1990]. However, work in the aeroelastic analysis of composites blades is limited, so far only by Chopra and his associates [Hong and Chopra, 1985, 1986, Panda and Chopra, 1987]. The

results show that there is a great potential for aeroelastic tailoring of composites rotor blades.

2.2.2 Coupled Rotor/body Models

The previous sections mainly discussed the structural dynamic models of isolated rotor blades including rigid body blades, elastic blades and the modelling of bearingless rotors and composites blades. However, the coupling between a rotor and other components, such as fuselages, rotor shaft, tilt-rotor aircraft nacelle and wings, is an important factor in the system dynamic modelling.

The first significant analytical study is attributed to Coleman and Feingold [1957]. They considered a rotorcraft system of a rigid rotor/fuselage and described the well-known "ground resonance" phenomena. Possible rotorcraft airborne aeroelastic instability was mentioned by Loewy [1969] and later was widely known as "air resonance". The transformation relations between the rotating coordinates system fixed to blades and the non-rotating coordinates system fixed to the body was developed by Hohenemser and Yin [1972]. This is an important technique used to couple the rotor equations of motion written in the rotating system with the body equations of motion in the non-rotating system. The relationship between the rotating and non-rotating coordinates is called the multiblade coordinates transformation.

A further development based on the Coleman model was made by Hammond [1974]. These equations include periodic coefficients and were solved using the Floquet theory. A more complete analysis for rotorcraft rotor/body aeroelasticity stability was subsequently developed by Johnson [1977]. This model was further extended to a more comprehensive analysis which is capable of modelling coupled rotor/fuselage problems such as ground resonance in hover and forward flight, in addition to a number of other

aerodynamic and dynamic problems. It has been quite successful for hingeless rotor ground resonance prediction [Johnson,1981a, 1981b].

An analytical model was also developed by Hodges [1979a] to analyse the aeroelastic stability of coupled bearingless rotor/fuselage. The analysis treated the blades as rigid bodies and was limited to hovering.

Warmbrodt and Friedmann [1979] derived the governing equations of motion of a helicopter rotor coupled to a rigid body fuselage. A consistent formulation was used to derive nonlinear periodic coefficient equations of motion which can be used for steady coupled rotor/fuselage dynamics in forward flight. A more recent work in coupled rotor/body analysis was developed to model multi-rotor hybrid heavy lift vehicles [Venkatesan and Friedmann, 1984, 1987], where the rotor blades are considered as hinged rigid blades. Two dimensional quasi-steady aerodynamics were included.

All of the models described above were developed based upon certain specific rotorcraft configurations. They lack the generality to model arbitrary rotorcraft configurations and the rotor/body coupling effect. To remedy this situation, a Finite Element model was developed by Hodges et al. [1986], which will be discussed in more detail in section 2.4.

The formulation of the nonlinear equations of motion for a rotorcraft aeroelasticity problem is complex and toilsome work. When the rotor/body coupling or higher order terms are required the situation becomes even worse. Several efforts have, therefore, been made to use symbolic algebraic manipulation on a computer [Reddy and Warmbrodt, 1985, Crespo Da Silva and Hodges, 1986a]. These approaches are based on an ordering scheme but algebraic tasks are relegated to a computer. Another approach to generate rotary wing equations of motion is based on the implicit approach [Gibbons

and Done, 1984, Patel and Done, 1985, Done et al, 1988, Hodges et al., 1986]. In this approach the equations of motion are never explicitly written out since they are generated numerically by the computer during the solution process [Friedmann, 1990].

Another class of rotorcraft dynamics problem is the aeroelastic stability of the tilt-rotor aircraft. Tilt-rotor aircraft aeroelastic stability analysis is fundamentally similar to coupled rotor/body helicopter dynamics. However, there are some difference between them, such as the larger rotating speed and the high inflow aerodynamics in the tilt-rotors. A more detailed review in this area is given in the introduction of the next chapter which deals with the tilt-rotor whirl flutter problem.

2.3 AERODYNAMIC MODELLING IN ROTORCRAFT AEROELASTICITY

It was pointed out in the previous section that there are two major aspects in the rotorcraft aeroelastic modelling, namely, the structural dynamic modelling and the aerodynamic modelling. Aerodynamic modelling for rotor blades was developed against the background of fixed wing aerodynamics. However, the aerodynamic theory for rotary wing aeroelasticity is much more complex than that of fixed wings and hence much less well developed. The simplest type of unsteady aerodynamics used for rotor blade aeroelasticity analysis is Theodorsen's theory [Theodorsen, 1934]. It is well known that Theodorsen's theory is not directly valid for rotary wings because the unsteady wake beneath a rotor is quite different from the wake postulated by Theodorsen's theory. Nevertheless, various quasi-steady and unsteady models for aerodynamic loads based on this theory have been developed in rotorcraft aeroelasticity [Friedmann, 1983].

Greenberg [1947] has derived expressions for unsteady lift and moment on a two dimensional airfoil executing harmonic motion in a pulsating stream of incompressible fluid. This theory was subsequently widely used in rotorcraft aeroelasticity analysis. Greenberg's theory is essentially a fixed wing type unsteady aerodynamic theory because

the effect of the unsteady wake beneath rotor is not included. When the effect of the unsteady wake beneath rotor is required, Loewy's extension of Theodorsen's theory provides a useful approximation to the unsteady wake beneath a hovering rotor [Loewy, 1957]. Greenberg's and Loewy's theories are discussed in detail by Johnson [1980b]. Some significant applications of the various theories mentioned above to rotorcraft aeroelasticity stability analysis were presented by a number of authors [Johnson, 1980a, Friedmann and Yuan, 1977, Kaza and Kvaternik, 1981].

A simple and most convenient representation of rotor unsteady aerodynamics useful in rotorcraft aeroelasticity analysis is the dynamic inflow model, which captures low frequency aerodynamic effects associated with the wake [Friedmann, 1983]. The inflow is defined as a combination of the steady inflow and a perturbation inflow,

$$\lambda = \bar{\lambda} + \delta\lambda, \qquad \text{and} \quad \delta\lambda = \lambda_0 + \lambda_c \cos\Psi + \lambda_s \sin\Psi$$

where $\bar{\lambda}$ is the steady inflow component while $\delta\lambda$ is the perturbation inflow component. The dynamic perturbation inflow components can be related to unsteady aerodynamic forces and moments on the rotor using a differential form:

$$[m]\begin{Bmatrix}\dot{\lambda}_0\\ \dot{\lambda}_s\\ \dot{\lambda}_c\end{Bmatrix} + [L]^{-1}\begin{Bmatrix}\lambda_0\\ \lambda_s\\ \lambda_c\end{Bmatrix} = \begin{Bmatrix}C_T\\ -C_{mx}\\ -C_{my}\end{Bmatrix}$$

where C_T, C_{mx}, C_{my} are the rotor aerodynamic lift coefficient, the rotor aerodynamic moment coefficients in x and y directions respectively.

This model is based on the assumption that the dynamic inflow is related to the aerodynamic loads in a linear, first order fashion.

A simple static inflow model was first established by Ormiston and Peters [1972]. Subsequently, a dynamic inflow model including the first order time lag between the load perturbation and inflow perturbations was developed by Peters [1974]. The correlation with experiment was conducted by Hohenemser and Crews [1973]. An analytical

method to obtain the L matrix for the dynamic inflow theory was formulated by Pitt and Peters [1981], and was extensively compared with experiment by Gaonkar and Peters [1986a]. The dynamic inflow theory was applied to rotor blade aeroelasticity stability analysis to evaluate the unsteady aerodynamics by a number of authors [Ormiston, 1976, Gaonkar et al., 1982, Johnson, 1982, Gaonkar and Peters, 1986a, 1986b].

Forward flight of a rotorcraft in helicopter mode introduces some additional, substantial difficulties in the aerodynamic modelling process. The reversed flow region on the retreating blade can produce time-varying nonlinear stall effects. Due to the importance of the dynamic stall phenomenon, it has been the subject of a number of studies which have resulted in a relatively good physical understanding of this complex, unsteady aerodynamic effect [McCroskey et al., 1981, Carr et al., 1977]. The complexity of such models however, preclude their incorporation in conventional rotary wing aeroelastic analysis. Therefore numerous semi-empirical models have been developed for rotorcraft aeroelastic analysis [Friedmann, 1983].

A quasi steady stall analysis was used by Ormiston and Bousman [1975] in a flap-lag blade stability analysis. Beddoes's dynamic stall model [1976] consists of two distinct flow regimes: the attached flow regime and the separated flow regime. This model is a convenient one to use. A similar model was developed by Ganwani [1981]. The treatment of the attached flow regime is very similar to Beddoes's. However, the treatment of the separated flow regime is substantially different. Tran and Petot's model [1981] developed a theory valid for an airfoil performing a completely arbitrary motion rather than just simple harmonic motion. Further work aimed at an improved physical understanding of this model was carried out by Peters [1985]. Tran and Petot's stall model is gaining acceptance in rotary wing aeroelasticity as other researchers introduce refinements into the model.

Another significant portion of recent research in unsteady aerodynamics of rotor blades has been aimed at developing two dimensional unsteady airfoil theory in the time domain. Two dimensional aerodynamic theories, which provides analytical expressions for unsteady loads on a moving airfoil, are usually based on the assumption of simple harmonic motion. This assumption implies that they are strictly valid only at the stability boundary and thus they provide no information on system damping before or after the onset of flutter. Another important limitation of these theories is evident when one tries to apply them to the rotorcraft aeroelasticity problems in forward flight, which is governed by equations with periodic coefficients. In this case the complex lift deficiency factor associated with the frequency domain unsteady aerodynamic theory is not consistent with the numerical method employed in the treatment of periodic systems [Friedmann, 1983, 1987]. Thus many of the rotary wing analyses in forward flight are based on quasisteady aerodynamics. Therefore, several recent studies were developed to transform the rotor unsteady aerodynamic theory from the frequency domain to the time domain [Dinyervari and Friedmann, 1985, Friedmann, 1986].

The aerodynamic theories mentioned above are all two dimensional unsteady aerodynamic theories. Their applications show that two dimensional quasi-steady aerodynamics is a valuable and powerful tool for predicting rotor blade aeroelasticity stability in axial flow states. But there are serious theoretical limitations for forward flight application. In this case, unsteady aerodynamics including a dynamic stall model and a dynamic inflow model must be considered. Obviously, a complete three dimensional unsteady aerodynamic theory is also very useful for application to rotor aeroelastic stability analysis in forward flight. However, only a few linear three dimensional unsteady aerodynamic applications have been developed by a few researchers for the rotor blade aeroelasticity analysis [Dat, 1984, Runyan and Tai, 1986]. There is, therefore, much to be done in this area.

2.4 APPLICATION OF THE FINITE ELEMENT METHOD TO ROTORCRAFT AEROELASTICITY ANALYSIS

The previous two sections discussed the structural dynamic modelling and aerodynamic modelling of the rotorcraft aeroelasticity problem. These two aspects form the basis for the rotorcraft equations of motion. All of the studies mentioned above use traditional global modal methods to discretize the partial differential equations. There are a number of limitations in applying them to realistic complex configurations. It is difficult to apply modal methods to nonuniform blades and blades with complex root geometries. Also, the formulation has to be modified considerably when a different rotor configuration is considered. This gives a limitation on the generality of the models. Moreover, when complex structures, such as bearingless composite rotors and coupled rotor/body system, are considered, the global modal method leads to extremely cumbersome algebraic manipulations and the lack of the generality of the models is a significant barrier. The Finite Element method provides us with an ideal technique well suited to modelling the complicated structural geometries. This is especially true when the Finite Element method is combined with the multibody dynamics approach, the general dynamics model can be created relatively easily.

The Finite Element Method was originally developed in the field of structural mechanics in the 1950's, and has been extensively developed in this field since then. However, it was not until the 1980's that the Finite Element Method was applied to rotorcraft aeroelasticity analysis.

The first effort to utilise the Finite Element Method in rotorcraft dynamics was made by Hohenemser and Yin [1977]. They actually used the transfer matrix technique. A strict finite element discretisation was developed for the helicopter aeroelasticity stability analysis in 1980's [Friedmann and Straub, 1980, Sivaneri and Chopra, 1982]. Friedmann and Straub used a weighted residual Galerkin type finite element method to

discretize a set of coupled blade flap-lag-torsion partial differential equations. Sivaneri and Chopra applied a conventional local Rayleigh-Ritz finite element method to study the flap-lag-torsion aeroelasticity stability of hingeless rotor blades in hover. Sivaneri and Chopra subsequently extended their work to analyse a bearingless rotor blade stability in hover [1984]. Celi and Friedmann [1987] also applied Friedmann and Straub's finite element model to the aeroelasticity analysis of a swept tip rotor blade. It is also worthwhile mentioning that Finite Element analyses have been frequently used to solve the free vibration problem of rotating beams by a number of researchers [Nagaraj and Shanthakumar, 1975, Hoa, 1979, Hodges, 1979b, Hodges and Rutkowski 1981]. These studies indicate conclusively the Finite Element Method is a practical tool for solving rotorcraft aeroelasticity problems and leads not only to the modelling flexibility but also to a significant reduction in the algebraic manipulation in the formulation. Later on, the Finite Element Method was widely applied to the aeroelasticity stability analysis of composites rotor blades due to its modelling advantages [Hong and Chopra, 1985, 1986, Panda and Chopra, 1987].

All of the Finite Element models mentioned above only dealt with the aeroelasticity stability problems of simply spinning rotor blades and are limited to one configuration. Although these models gives us a capability to model the complex blade geometries, this is not sufficient to let us obtain a general dynamic element, especially when the rotor/body coupling is included where there may be large and arbitrary relative translational and rotational motion between the rotor and the body. Hodges et al. recently developed a program that goes toward providing such a general finite element model [1986]. The essential part of that work is the development of a general aeroelasticity beam element in a moving reference frame. This moving reference frame has an arbitrary space motion and thus can model the coupling with other substructures. Hodges et al [1986] used an implicit approach to generate the system equations of motion and developed a consistent mass aeroelastic beam element. This model was especially

developed for the rotorcraft aeromechanical stability analysis. Results show that the model is a very practical and general tool for rotorcraft aeromechanical stability analysis. This is the first and so far , the sole effort to develop such a general rotorcraft aeroelasticity stability analysis model.

CHAPTER 3 A TILT-ROTOR/NACELLE WHIRL FLUTTER MODEL---FORMULATION OF THE EQUATIONS OF MOTION

3.1. INTRODUCTION

The tilt-rotor aircraft is being developed as a new type of air vehicle. One of its principal dynamic problems is the aeroelastic stability. Investigation of the aeroelasticity stability of the tilt-rotor aircraft is one of the aims of this thesis. The tilt-rotor aircraft contains not only helicopter rotor type instabilities, but also propeller type instabilities, because a tilt-rotor can works both in the helicopter mode and in the normal aeroplane mode. When a tilt-rotor aircraft flies forward like a normal aircraft, the well-known propeller type instability--whirl flutter is likely to appear. This is one of the problems to be studied in this thesis.

A great many investigations were made in relation to the propeller whirl flutter in the early 1960's, where only the nacelle pitch and yaw degrees of freedom were considered. In these models, it was found that a propeller whirl flutter always developed from the backward whirl mode [Reed and Bland, 1961, Bland and Bennett, 1963, Reed, 1965].

With the development of the tilt-rotor aircraft, similar tilt-rotor whirl flutter problems were subsequently investigated and found to be much more complicated than the propeller whirl flutter characteristics. The forward whirl instability is found for the flap-hinged or gimbaled (universal joint) tilt-rotor models [Reed, 1965].

Further development and testing of the tilt-rotor aircraft in the 1970's lead to increasing efforts being made to improve the analysis capability and the understanding of the tilt-rotor aircraft aeroelastic stability. The wing, nacelle, aircraft and rotor blade degrees of freedom were subsequently modelled in the analysis. The effects of various couplings and parameters on the aeroelasticity stability were experimentally and analytically

studied. Aero-mechanical instabilities similar to helicopter ones were involved [Kvaternik and Kohn, 1977, Kvaternik, 1973a, 1973b, Johnson, 1977, Johnson, 1974].

This and the next chapter are concerned with the whirl flutter problem of the tilt-rotor aircraft. A simple coupled rigid rotor/nacelle model is developed since the emphasis was placed on the understanding of the fundamental characteristics of this kind of instability. This newly developed model applies the ordering scheme widely used in helicopter aeroelasticity formulation to retain the nonlinear terms in the equations of motion for whirl flutter problems. The previous whirl flutter models do not consider the nonlinearity. The quasi-steady aerodynamics includes not only the circulatory part, but also the non-circulatory part which was neglected in the previous whirl flutter models. Two different types of connections between rotor and rotor shaft are considered. One is the ordinary universal joint connection. Another is a suggested possible gimbal configuration. Their whirl flutter features are compared. The whirl flutter characteristics of the tilt-rotor of an ideal gimbal configuration is not found in the literature.

3.2 PHYSICAL MODEL AND BASIC ASSUMPTIONS

3.2.1 Physical Model Description

Assume that the tilt-rotor aeroplane with a rigid fuselage and rigid wings is in stable forward flight. Hence no aeroplane fuselage perturbation motions are considered and also the couplings of the tilt-rotor/nacelle system with the wing and fuselage are not included.

The nacelle, considered as a rigid body, is attached to the wing with spring and damping restraints at a certain positions on the nacelle. The nacelle is linked to the tilt-rotor through a hinge (universal joint or gimbal) with pitch and yaw spring restraints at the hub end of the nacelle.

The whole tilt-rotor (including blades) is idealised as rigid, and installed on the gimbal hinge at the gimbal centre. However the blades can be feathered about the pitch bearings. The flexibility of the control system is modelled.

Therefore the degrees of freedom of the whole system are:

a). Six degrees of freedom of the nacelle rigid body motions

b). Two universal joint (or gimbal) degrees of freedom, pitch and yaw motion of the tilt-rotor

c). Individual blade pitch degree of freedom for each blade

Fig 3.1--3.4 are the graphical descriptions of the physical model.

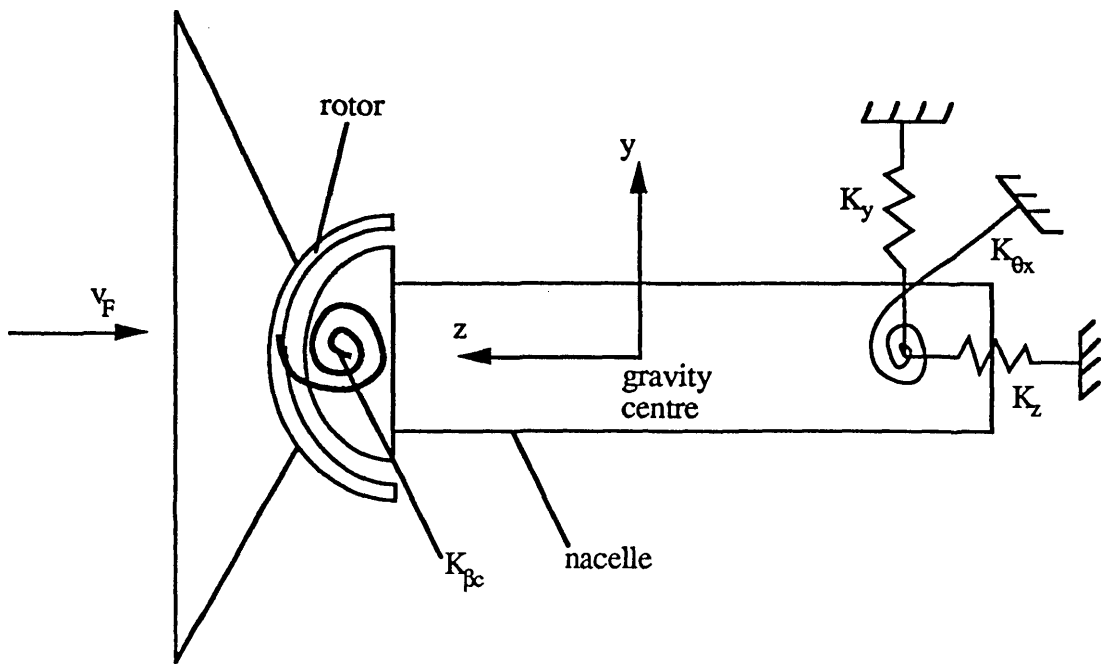

Fig 3.1 The motion in yawing direction (top view)

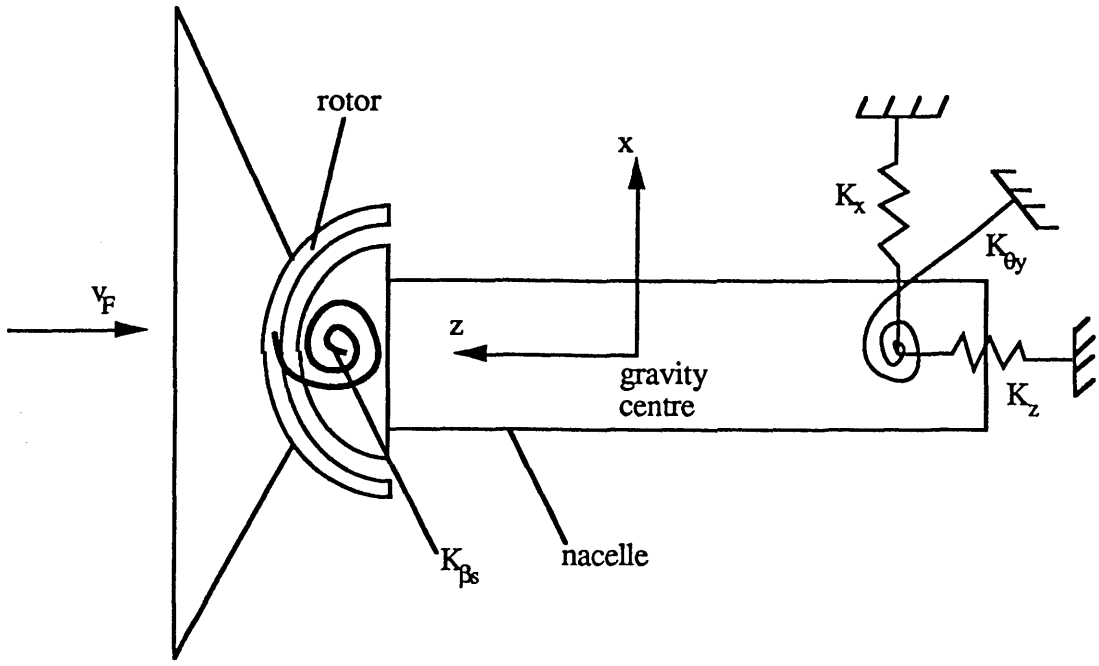

Fig 3.2 The motion in pitch direction (side view)

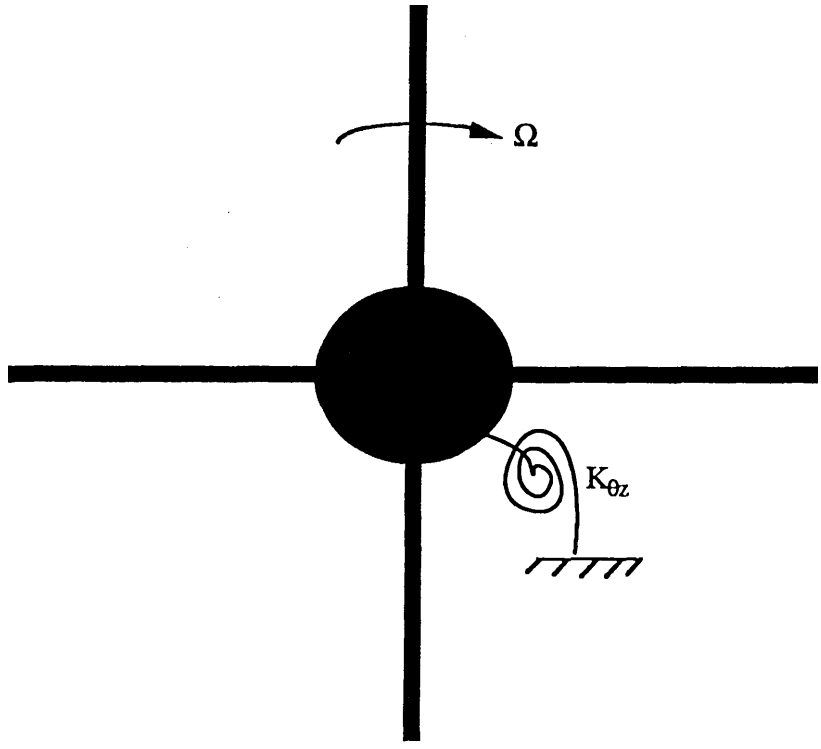

Fig 3.3 The roll motion of nacelle (forward view)

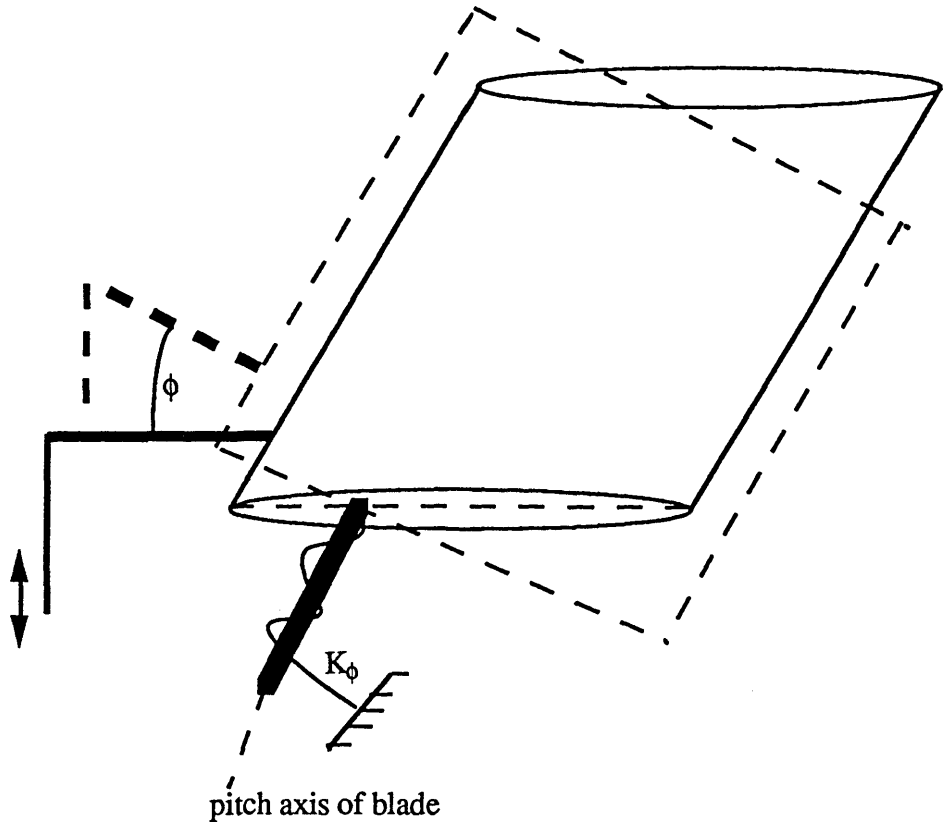

Fig 3.4 The feathering motion of blades about pitch bearings

3.2.2 Basic Assumptions and Ordering Scheme

3.2.2.1 Basic Assumptions

Certain assumptions are introduced before formulating the dynamic equations for this model. These are:

1. The fuselage of the aeroplane is assumed to be a rigid body and the wings also rigid. The rigid body perturbations of the fuselage are not included.
2. The aeroplane is in stable forward flight and the tilt-rotor works in an axial flow state.
3. The rotor speed is constant.
4. The blade feathering axis coincides with the blade elasticity axis.
5. The blade feathering axis is preconed by the angle β_p and swept by the angle βsw.
6. The blades are attached to the hub with an offset e_p from the rotation axis.
7. The rotor is underslung by a distance z_h from the gimbal centre.

8. The blade cross--section is symmetric, with distinct elastic centre, mass centre and aerodynamic centre.
9. The aerodynamic loads are calculated using a two dimensional quasisteady aerodynamic theory. No stall, no reverse flow and no compressibility effect are considered.
10. A constant induced velocity is assumed.

3.2.2.2 Ordering Scheme

In the derivation of the rotor aeroelastic equations of motion, a large number of higher order terms will appear. Previous researchers have shown that many of these can be neglected systematically by using an ordering scheme in the helicopter aeroelasticity formulations [Friedmann, 1983, 1990].

The basis of an ordering scheme is a small dimensionless parameter ε, which usually represents typical blade slopes due to blade deflection. ε is about 0.1 to 0.2 for normal helicopter rotor blades.

The ordering scheme is based on the assumption that

$$1 + 0(\varepsilon^2) = 1 \qquad (2.2.1)$$

A similar principle is used in this research for simplification of the derivation of the equations of motion.

The orders of the various variables magnitude for this problem are given as below:

$$a = 0(1/\varepsilon)$$

$$\theta_0, \theta_G = 0(\varepsilon^{1/2})$$

$$x/R,\ \sin\psi,\ \cos\psi,\ R\partial(\ )/\partial x,\ \partial(\ )/\partial\psi,\ C_l,\ \rho abR/m = 0(1)$$

$$\beta_G,\ \alpha_G,\ \beta_{Gs},\ \beta_{Gc},\ \beta_p,\ \beta_{sw},\ e_p/R,\ z_h/R,\ b/R,\ \dot{\theta}_G,\ \ddot{\theta}_G,\ C_{mac} = 0(\varepsilon)$$

$$C_d, R_x/R, R_y/R, R_z/R, \theta_x, \theta_y, \theta_z = 0(\varepsilon^{3/2})$$

$$x_A/R, x_{GO}/R = 0(\varepsilon^2)$$

$$I_3/mR^2 = 0(\varepsilon^3)$$

$$I_2/mR^2 = 0(\varepsilon^7)$$

.....(2.2.2)

Where $\psi=\Omega t$ is the azimuth angle of the blade.

3.2.3 Coordinate Systems and Transformations

In the formulation of the equations of motion, various reference coordinate systems are used. These are introduced in this following section.

A. The fixed inertial coordinate system $X_0\ Y_0\ Z_0$ " o " system.

This has an origin at the gravity centre of the nacelle. Z_0 is parallel to the static equilibrium longitudinal axis of the nacelle. Y_0 is parallel to the horizontal plane. It is fixed in space.

B. The nacelle--fixed non-inertia coordinate system $X_{10}\ Y_{10}\ Z_{10}$ "10 " system.

This has it origin at the centre of gravity of the nacelle. It is fixed with the nacelle body and is initially parallel to $X_0Y_0Z_0$ system without perturbations.

C. The fixed inertia gimbal centre coordinate system $X_gY_gZ_g$ " g " system.

It has its origin at the gimbal centre. It is parallel to $X_0Y_0Z_0$ system.

D. The nacelle--fixed gimbal centre coordinate system $X_{1g}Y_{1g}Z_{1g}$ "1g " system.

It is fixed with the nacelle, and parallel to $X_{10}Y_{10}Z_{10}$ system.

E. The rotating nacelle--fixed system $X_{2g}Y_{2g}Z_{2g}$ "2g" system.

It is obtained by rotating the "1g" system $\psi=\Omega t$ about Z_{1g} axis.

F. The hub--fixed coordinate system $X_hY_hZ_h$ "h" system.

This has its origin at the gimbal centre. It is fixed with on tilt-rotor hub, and coincides with the "2g" system without gimbal perturbations.

G. The Blade coordinate system $X_bY_bZ_b$ "b" system.

It has its origin at the pitch bearing of blades. It is obtained by including the blade precone angle and sweep angle in $X_hY_hZ_h$ system.

H. The blade cross--section--fixed system $X_{cs}Y_{cs}Z_{cs}$ "cs" system.

It has its origin at the pitch axis centre of the blade cross--section. It is obtained by perturbing with blades and is initially parallel to $X_bY_bZ_b$ without the pitch motion of blades.

I. The blade cross--section major principal axis system $X_{pa}Y_{pa}Z_{pa}$ "pa" system.

It has its origin at the pitch centre of blade cross--section. It is obtained by rotating the $X_{cs}Y_{cs}Z_{cs}$ system about X_{cs} axis to include the geometry attack angle θ_G.

The transformation relations between these coordinate systems are listed in Appendix 3A.

3.3 FORMULATION OF THE EQUATIONS OF MOTION

The rotor equations of motion are obtained by the equilibrium of the gimbal spring restraint moments and the inertia loads, the aerodynamic loads, and the damping loads applied on the rotor. The pitch equation of motion of blades is derived by the equilibrium of the aerodynamic moment, the inertia moment about blade pitch axis and the elastic restoring moment due to the flexibility of the control system. The inertial loads and the aerodynamic loads on a unit-length of the blade are derived first. Secondly, the loads at the blade root caused by one whole blade are calculated. These loads lead to the blade torsion equation of motion for each blade. Subsequently, the aerodynamic and inertial loads transmitted from the whole rotor to the gimbal are obtained. These loads can be finally used to obtain the rotor equations of motion and the nacelle equations of motion. In total these consist of 12 coupled differential equations.

3.3.1 Inertia Loads Applied on Blades and the Rotor

Taking an infinitely small mass at point "p" on the blade, then its mass is dm. The motion of this point "p" in a blade comprises the relative motion of the point relative to the moving frame "2g" and, simultaneously, the motion of the "2g" system relative to the fixed inertia frame "g" system.

Therefore the absolute acceleration of a point "p" is

$$\vec{a} = \vec{a}_0 + \vec{\omega} \times (\vec{\omega} \times \vec{r}) + \dot{\vec{\omega}} \times \vec{r} + \vec{a}_r + 2\vec{\omega} \times \vec{v}_r \qquad (3.1.1)$$

Where a_0 is the translational acceleration of the gimbal centre point, and is equal to

$$\vec{a}_0 = \ddot{x}_g \vec{i}_g + \ddot{y}_g \vec{j}_g + \ddot{z}_g \vec{k}_g \qquad (3.1.2)$$

$\vec{\omega}$ is the angular velocity of the moving frame "2g" system, and is equal to $\Omega\vec{k}_{1g} + \vec{\omega}_{na}$ where $\vec{\omega}_{na}$ is the angular velocity due to the nacelle motions.

$\vec{r}$ is the position vector of the general point "p" in the blade relative to gimbal centre.

$\vec{a}_r$ is the relative acceleration of the point "p" relative to the moving frame "2g" system.

$\vec{v}_r$ is the relative velocity of the point "p" relative to the moving frame "2g"

And hence $\vec{v}_r = \dot{\vec{r}}$ $\qquad$ $\vec{a}_r = \ddot{\vec{r}}$ $\qquad (3.1.3)$

Where $\dot{(\,)}$ indicates derivative with respect to the time t.*

The position vector $\vec{r}$ is (See Fig 3.5, Fig 3.6)

$$\vec{r} = -z_h \vec{k}_h + e_p \vec{i}_h + e_p \tan\beta_p \vec{k}_h + x\vec{i}_b + y\vec{j}_{cs} + z\vec{k}_{cs} \qquad (3.1.4)$$

* $\dot{(\,)}$ *is usually defined as derivative with respect to the time t* (*i.e.* $\frac{d(\,)}{dt}$). *For the convenience of nondimensionalisation, however,* $\dot{(\,)}$ *at the right hand of the subsequent expanded equations for the terms* $\frac{d(\,)}{dt}$ *indicates derivative with respect to the nondimensional parameter* $\psi = \Omega t$ (*i.e.* $\frac{d(\,)}{d\psi}$) *in chapter 3. And hence,* $\dot{(\,)}$ *in chapter 4 also represents* $\frac{d(\,)}{d\psi}$.

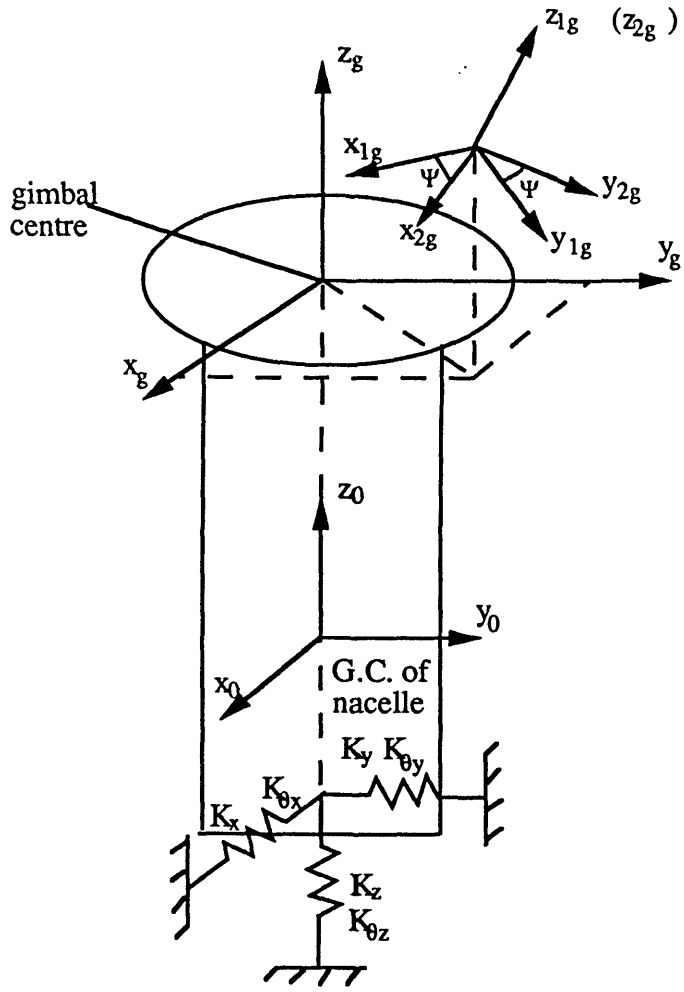

Fig 3.5 Motions of nacelle and gimbal centre

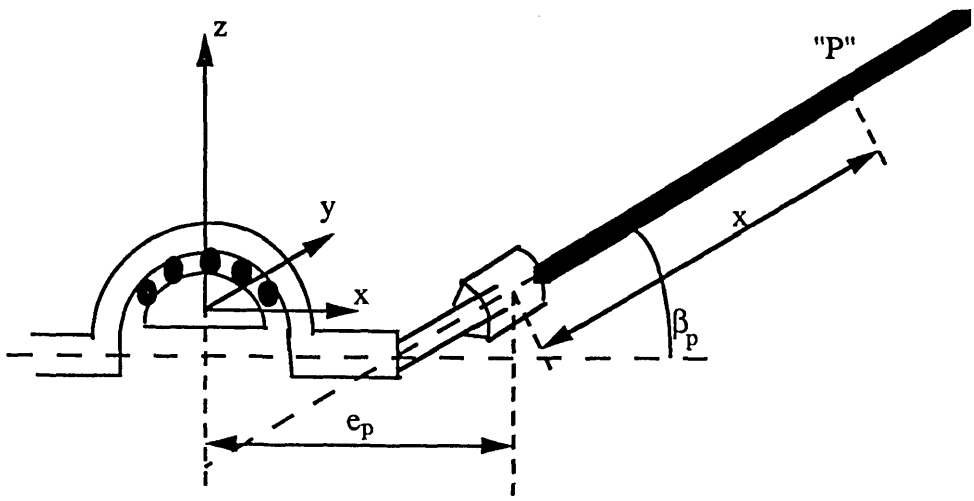

Fig 3.6 Motion of a general point "P" on blade

Writing $\vec{r}$ in the "2g" system

$$\vec{r} = [e_p + e_p\beta_p\beta_G - z_h\beta_G + x(1 + \beta_G\beta_p) + y(\beta_{sw} - \beta_p\phi + \beta_G\phi)$$
$$+ z(-\phi\beta_{sw} - \beta_p + \beta_G),\ -e_p\beta_p\alpha_G + z_h\alpha_G - x\beta_{sw} + y - z\phi,\ -e_p\beta_G + e_p\beta_p - z_h$$
$$+x(\beta_p - \beta_G) + y((\beta_p - \beta_G)\beta_{sw} + \beta_G\beta_p\phi + \phi)$$
$$+ z((\beta_G - \beta_p)\beta_{sw}\phi + \beta_G\beta_p + 1)]\ \vec{E}_{2g} \qquad (3.1.5)$$

Neglecting the higher order terms by applying the ordering scheme:

$$\vec{r} \approx [e_p + x + y(\beta_{sw} - \beta_p\phi + \beta_G\phi) + z(-\phi\beta_{sw} - \beta_p + \beta_G),$$
$$z_h\alpha_G - x\beta_{sw} + y - z\phi,\ -e_p\beta_G + e_p\beta_p - z_h$$
$$+x(\beta_p - \beta_G) + y((\beta_p - \beta_G)\beta_{sw} + \phi) + z]\ \vec{E}_{2g} \qquad (3.1.6)$$

It must be noted that a general point "p" in a blade is located in $X_{cs}Y_{cs}Z_{cs}$ system as

$$y\,\vec{j}_{cs} + z\,\vec{k}_{cs}$$

And also located in $X_{pa}Y_{pa}Z_{pa}$ system as

$$\eta\,\vec{j}_{pa} + \xi\,\vec{k}_{pa}$$

Where $X_{pa}Y_{pa}Z_{pa}$ is rotated from $X_{cs}Y_{cs}Z_{cs}$ by the geometry angle θ_G

$$\theta_G = \theta_0 + \theta_{tw} + \theta_{1c}\cos\psi + \theta_{1s}\sin\psi - K_{PG}\beta_G \qquad (3.1.7)$$

Where:

θ_0 — Collective pitch angle of blades

θ_{tw} — Pre–twist angle of the blades

θ_{1s}, θ_{1c} — Cyclic pitch control angle of blades

$K_{PG}\beta_G$ — Pitch angle change due to kinematic pitch/gimbal coupling

And hence:
$$\begin{Bmatrix} y \\ z \end{Bmatrix} = \begin{bmatrix} \cos\theta_G & -\sin\theta_G \\ \sin\theta_G & \cos\theta_G \end{bmatrix} \begin{Bmatrix} \eta \\ \xi \end{Bmatrix}$$

$$\begin{Bmatrix} \dot{y} \\ \dot{z} \end{Bmatrix} = \begin{Bmatrix} -z \\ y \end{Bmatrix} \dot{\theta}_G \qquad (3.1.8)$$

$$\begin{Bmatrix} \ddot{y} \\ \ddot{z} \end{Bmatrix} = \begin{Bmatrix} -z \\ y \end{Bmatrix} \ddot{\theta}_G - \dot{\theta}_G^2 \begin{Bmatrix} y \\ z \end{Bmatrix}$$

These relations are important in the derivation of the relative velocity and accelleration of the general point "p" given below.

Taking the derivative of $\vec{r}$ and applying the ordering scheme gives:

$$\vec{v}_r = \dot{\vec{r}}_{2g} \approx \Omega\{e_p\beta_p\dot{\beta}_G - z_h\dot{\beta}_G + x\,\dot{\beta}_G\beta_p + y[(\beta_G-\beta_p)\dot{\phi} + \phi\dot{\beta}_G + \dot{\theta}_G(-\phi\beta_{sw}-\beta_p+\beta_G)]$$

$$+z(-\dot{\phi}\beta_{sw}+\dot{\beta}_G-\beta_{sw}\dot{\theta}_G),\ -e_p\beta_p\dot{\alpha}_G + z_h\dot{\alpha}_G - z(\dot{\phi}+\dot{\theta}_G) - y\phi\dot{\theta}_G,$$

$$-e_p\dot{\beta}_G - x\dot{\beta}_G + y(-\dot{\beta}_G\beta_{sw} + \dot{\theta}_G+\dot{\phi}) + z[\dot{\beta}_G\beta_{sw}\phi + \dot{\beta}_G\beta_p + \beta_G\beta_{sw}\dot{\phi} - \beta_p\beta_{sw}\dot{\phi}$$

$$-\dot{\theta}_G((\beta_p-\beta_G)\beta_{sw}+\phi)]\}\,\vec{E}_{2g} \qquad (3.1.9)$$

$$\vec{a}_r = \ddot{\vec{r}}_{2g} \approx \Omega^2\{e_p\beta_p\ddot{\beta}_G - z_h\ddot{\beta}_G + x\,\ddot{\beta}_G\beta_p + z[-\ddot{\phi}\beta_{sw}+\ddot{\beta}_G-\ddot{\theta}_G\beta_{sw}] + y[-\beta_p\ddot{\phi} + \beta_G\ddot{\phi}$$

$$+2\dot{\beta}_G\dot{\phi}+\phi\ddot{\beta}_G+\ddot{\theta}_G(-\beta_p+\beta_G-\phi\beta_{sw})+2\dot{\theta}_G\dot{\beta}_G-2\beta_{sw}\dot{\theta}_G\dot{\phi}-\beta_{sw}\dot{\theta}_G^2],$$

$$-e_p\beta_p\ddot{\alpha}_G + z_h\ddot{\alpha}_G - z(\ddot{\phi}+\ddot{\theta}_G) - y(2\dot{\phi}\dot{\theta}_G+\phi\ddot{\theta}_G+\dot{\theta}_G^2),$$

$$-e_p\ddot{\beta}_G - x\ddot{\beta}_G + y[-\ddot{\beta}_G\beta_{sw} + \ddot{\phi} + \ddot{\theta}_G]$$

$$+z[2\dot{\beta}_G\beta_{sw}\dot{\phi}+\ddot{\beta}_G\beta_{sw}\phi + \ddot{\beta}_G\beta_p + \beta_G\beta_{sw}\ddot{\phi} - \beta_p\beta_{sw}\ddot{\phi} - \ddot{\theta}_G(\phi+\beta_p\beta_{sw}-\beta_G\beta_{sw})$$

$$-2\dot{\theta}_G(-\dot{\beta}_G\beta_{sw}+\dot{\phi}) - \dot{\theta}_G^2]\}\vec{E}_{2g} \qquad (3.1.10)$$

The angular velocity due to the nacelle rigid body motion is:

$$\vec{\omega}_{na} = \Omega[(\dot{\theta}_x - \dot{\theta}_y\theta_z)\,\vec{i}_g + (\dot{\theta}_y + \dot{\theta}_x\theta_z)\,\vec{j}_g + (\dot{\theta}_z - \dot{\theta}_x\theta_y)\vec{k}_g] \qquad (3.1.11)$$

The angular velocity of the moving frame "2g" :

$$\vec{\omega} = \Omega\vec{k}_{2g} + \vec{\omega}_{na}$$

$$= \Omega[(\dot{\theta}_x - \theta_y\dot{\theta}_z)\cos\psi + (\dot{\theta}_y + \theta_x\dot{\theta}_z)\sin\psi]\,\vec{i}_{2g} + \Omega[(-\dot{\theta}_x + \theta_y\dot{\theta}_z)\sin\psi$$

$$+ (\dot{\theta}_y + \theta_x\dot{\theta}_z)\cos\psi]\,\vec{j}_{2g} + \Omega[1 + \dot{\theta}_z - \theta_x\dot{\theta}_y]\,\vec{k}_{2g}$$

$$= \Omega[\omega_x\,\vec{i}_{2g} + \omega_y\,\vec{j}_{2g} + (1+\omega_z)\,\vec{k}_{2g}] \qquad (3.1.12)$$

The angular accelleration :

$$\vec{\omega} = \Omega^2[(\ddot{\theta}_x - \dot{\theta}_y\dot{\theta}_z - \theta_y\ddot{\theta}_z + \dot{\theta}_y + \theta_x\dot{\theta}_z)\cos\psi + (\ddot{\theta}_y + \dot{\theta}_x\dot{\theta}_z + \theta_x\ddot{\theta}_z - \dot{\theta}_x + \theta_y\dot{\theta}_z)\sin\psi]\,\vec{i}_{2g}$$

$$+ \Omega^2[(\ddot{\theta}_y + \dot{\theta}_x\dot{\theta}_z - \dot{\theta}_x + \theta_y\dot{\theta}_z + \theta_x\ddot{\theta}_z)\cos\psi + (-\ddot{\theta}_x - \theta_x\dot{\theta}_z + \theta_y\ddot{\theta}_z - \dot{\theta}_y + \dot{\theta}_y\dot{\theta}_z)\sin\psi]\,\vec{j}_{2g}$$

$$+ \Omega^2[\ddot{\theta}_z - \dot{\theta}_x\dot{\theta}_y - \theta_x\ddot{\theta}_y]\,\vec{k}_{2g}$$

$$= \Omega^2[\dot{\omega}_x\,\vec{i}_{2g} + \dot{\omega}_y\,\vec{j}_{2g} + \dot{\omega}_z\vec{k}_{2g}] \qquad (3.1.13)$$

In case of no perturbations, the position of the gimball centre in "o" system is assumed as

$$\vec{H}_0 = l_x\,\vec{i}_0 + l_y\,\vec{j}_0 + l_z\vec{k}_0 \qquad (3.1.14)$$

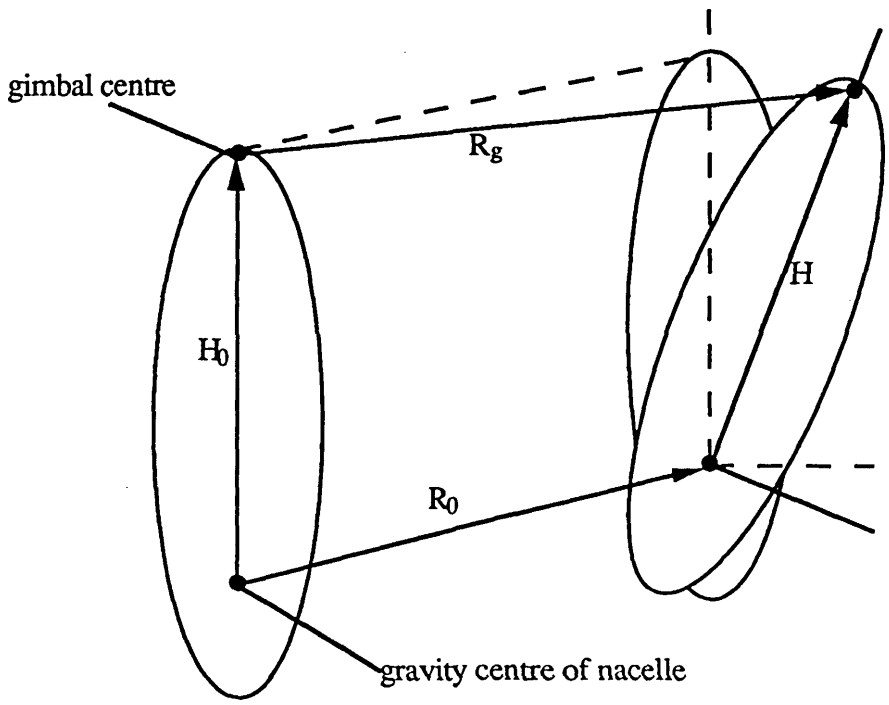

Fig 3.7 Displacement of gimbal centre

Assuming that the gravity centre of the nacelle undergoes a displacement $\vec{R}_0$ in the perturbations, and the nacelle, considered as a rigid body, has Euler angle series rigid rotations θ_x, θ_y, θ_z around the gravity centre. (Fig 3.7)

Therefore,

$$\vec{R}_g=-\vec{H}_0+\vec{R}_0+\vec{H}$$

$$=-(l_x\vec{i}_g+l_y\vec{j}_g+l_z\vec{k}_g)+R_x\vec{i}_g+R_y\vec{j}_g+R_z\vec{k}_g+l_x\vec{i}_{1g}+l_y\vec{j}_{1g}+l_z\vec{k}_{1g}$$

$$=[R_x+l_y(\theta_x\theta_y-\theta_z)+l_z(\theta_y+\theta_x\theta_z),\ R_y+l_x\theta_z+l_z(\theta_y\theta_z-\theta_x),$$

$$R_z-l_x\theta_y+l_y\theta_x]\vec{E}_g \qquad (3.1.15)$$

$$\vec{a}_0=\ddot{\vec{R}}_g=\Omega^2[\ddot{R}_x+l_y(\ddot{\theta}_x\theta_y+2\dot{\theta}_x\dot{\theta}_y+\theta_x\ddot{\theta}_y-\ddot{\theta}_z)$$

$$+l_z(\ddot{\theta}_y+\ddot{\theta}_x\theta_z+2\dot{\theta}_x\dot{\theta}_z+\theta_x\ddot{\theta}_z),$$

$$\ddot{R}_y+l_x\ddot{\theta}_z+l_z(\ddot{\theta}_y\theta_z+2\dot{\theta}_y\dot{\theta}_z+\theta_y\ddot{\theta}_z-\ddot{\theta}_x),\ \ddot{R}_z-l_x\ddot{\theta}_y+l_y\ddot{\theta}_x]\vec{E}_g$$

$$=\Omega^2(\ddot{x}_g\vec{i}_g+\ddot{y}_g\vec{j}_g+\ddot{z}_g\vec{k}_g)$$

$$=\Omega^2\{\ddot{x}_g[\cos\psi-\theta_z\sin\psi]+\ddot{y}_g[\sin\psi+\theta_z\cos\psi]+\ddot{z}_g[\theta_x\sin\psi-\theta_y\cos\psi]\}\vec{i}_{2g}$$

$$+\Omega^2\{\ddot{x}_g[-\sin\psi-\theta_z\cos\psi]+\ddot{y}_g[\cos\psi-\theta_z\sin\psi]+\ddot{z}_g[\theta_x\cos\psi+\theta_y\sin\psi]\}\vec{j}_{2g}$$

$$+\Omega^2\{\ddot{x}_g(\theta_y+\theta_x\theta_z)+\ddot{y}_g(\theta_y\theta_z-\theta_x)+\ddot{z}_g\}\vec{k}_{2g} \qquad (3.1.16)$$

Applying (3.1.12) and (3.1.6) and the ordering scheme:

$$\vec{\omega}\times(\vec{\omega}\times\vec{r})\approx\Omega^2\{-(e_p+x)-2x\omega_z+y[-(\beta_{sw}-\beta_p\phi+\beta_G\phi)-2\omega_z\beta_{sw}+\omega_x\phi]$$

$$+z[-(-\beta_{sw}\phi-\beta_p+\beta_G)-2\omega_z(-\beta_p+\beta_G)+\omega_x]\}\vec{i}_{2g}+\Omega^2\{-(z_h\alpha_G-x\beta_{sw})$$

$$+2\omega_z\beta_{sw}x+\omega_y[-z_h+x(\beta_p-\beta_G)]+y[-1-2\omega_z]+z[\phi(1+2\omega_z)+\omega_y]\}\vec{j}_{2g}$$

$$+\Omega^2\{\omega_x(e_p+x)+\omega_x\omega_z x+\omega_y(-x\beta_{sw})+y[\omega_x\beta_{sw}+\omega_y+\omega_y\omega_z]$$

$$+z[\omega_x(-\beta_{sw}\phi-\beta_p+\beta_G)+\omega_x\omega_z(-\beta_p+\beta_G)-\omega_y(1+\omega_z)\phi-(\omega_x^2+\omega_y\omega_y)]\}\vec{k}_{2g} \qquad (3.1.17)$$

Applying (3.1.13) and (3.1.6) and the ordering scheme,

$$\dot{\vec{\omega}}\times\vec{r}\approx\Omega^2\{\dot\omega_y[-e_p\beta_G+e_p\beta_p-z_h+x(\beta_p-\beta_G)]-\dot\omega_z(z_h\alpha_G-x\beta_{sw})+y[-\dot\omega_z+\dot\omega_y\phi]$$

$$+z[\dot\omega_y+\dot\omega_z\phi]\}\vec{i}_{2g}+\Omega^2\{\dot\omega_z(e_p+x)-\dot\omega_x[-z_h+x(\beta_p-\beta_G)]+y[\dot\omega_z(\beta_{sw}-\beta_p\phi+\beta_G\phi)$$

$$-\dot\omega_x((\beta_p-\beta_G)\beta_{sw}+\phi)]+z[-\dot\omega_x+\dot\omega_z(-\beta_p+\beta_G)]\}\vec{j}_{2g}+\Omega^2\{-\dot\omega_x x\beta_{sw}-\dot\omega_y(e_p+x)$$

$$+y[\dot\omega_x-\dot\omega_y\beta_{sw}]+z[-\dot\omega_x\phi-\dot\omega_y(-\phi\beta_{sw}-\beta_p+\beta_G)]\}\vec{k}_{2g} \qquad (3.1.18)$$

Applying (3.1.12) and (3.1.9) and the ordering scheme :

$$2\times\vec{\omega}\times\vec{v}_r\approx2\Omega^2\{-[-e_p\beta_p\dot\alpha_G+z_h\dot\alpha_G]-z_h\dot\alpha_G\omega_z+\omega_y[-e_p\dot\beta_G-x\dot\beta_G]$$

$$+y[\omega_y(-\dot\beta_G\beta_{sw}+\dot\theta_G+\dot\phi)+\phi\dot\theta_G+\omega_z\phi\dot\theta_G]+z[(1+\omega_z)(\dot\theta_G+\dot\phi)],$$

$$e_p\beta_p\dot\beta_G-z_h\dot\beta_G+x\dot\beta_G\beta_p+\omega_z(-z_h\dot\beta_G+x\dot\beta_G\beta_p)+\omega_x(e_p\dot\beta_G+x\dot\beta_G)$$

$$+y[-\omega_x(-\dot\beta_G\beta_{sw}+\dot\theta_G+\dot\phi)-\beta_p\dot\phi+\beta_G\dot\phi+\phi\dot\beta_G+\dot\theta_G(-\phi\beta_{sw}-\beta_p+\beta_G)$$

$$+\omega_z(-\beta_p\dot\phi+\beta_G\dot\phi+\phi\dot\beta_G)+\omega_z\dot\theta_G(-\beta_p+\beta_G)]+z[-\dot\phi\beta_{sw}+\dot\beta_G-\beta_{sw}\dot\theta_G$$

$$+\omega_z\dot\beta_G],\ \omega_x[-e_p\beta_p\dot\alpha_G+z_h\dot\alpha_G]-\omega_y(e_p\beta_p\dot\beta_G-z_h\dot\beta_G+x\dot\beta_G\beta_p)$$

$$+y[-\omega_x\phi\dot\theta_G-\omega_y(-\beta_p\dot\phi+\beta_G\dot\phi+\phi\dot\beta_G+\dot\theta_G(-\phi\beta_{sw}-\beta_p+\beta_G))]$$

$$+z[-\omega_x(\dot\theta_G+\dot\phi)-\omega_y(-\phi\beta_{sw}+\dot\beta_G-\beta_{sw}\dot\theta_G)]\}\vec{E}_{2g} \qquad (3.1.19)$$

Therfore,

$$\vec{a}=\vec{a}_0+\dot{\vec{\omega}}\times(\vec{\omega}\times\vec{r})+\vec{\omega}\times\dot{\vec{r}}+\vec{a}_r+2\vec{\omega}\times\vec{v}_r$$

$$\approx\Omega^2\{\ddot{x}_g\cos\psi+\ddot{y}_g\sin\psi-(e_p+x)-2x\omega_z+y[-\beta_{sw}+2\omega_y(\dot\phi+\dot\theta_G)$$

$$+2\phi\dot\theta_G-\dot\omega_z+\phi\dot\omega_y-\beta_p\ddot\phi+\beta_G\ddot\phi+2\dot\phi\dot\beta_G+\phi\ddot\beta_G+\ddot\theta_G(\beta_G-\beta_p)+2\dot\theta_G\dot\beta_G-\phi(\beta_G-\beta_p)$$

$$-2\omega_z\beta_{sw}+\omega_x\phi]+z[-\beta_{sw}\ddot\phi+\ddot\beta_G-\beta_{sw}\ddot\theta_G+\dot\omega_y+\dot\omega_z\phi$$

$$+2(1+\omega_z)(\dot\theta_G+\dot\phi)-(-\beta_p+\beta_G)+\omega_x+\phi\beta_{sw}-2\omega_z(-\beta_p+\beta_G)]\}\vec{i}_{2g}$$

$$+\Omega^2\{-\ddot{x}_g \sin\psi + \ddot{y}_g \cos\psi + x\beta_{sw} + \dot{\omega}_z (e_p + x) - \dot{\omega}_x[-z_h + x(\beta_p - \beta_G)]$$

$$+z_h\ddot{\alpha}_G - 2z_h\dot{\beta}_G + 2x\dot{\beta}_G\beta_p + 2\omega_z x\beta_{sw} + 2\omega_x x\dot{\beta}_G - \omega_y z_h + \omega_y x(\beta_p - \beta_G) + \omega_z\dot{\beta}_G]$$

$$+y[-1-2\omega_z] + z[\phi + \omega_y - \dot{\omega}_x + \dot{\omega}_z(-\beta_p + \beta_G) - \ddot{\theta}_G - \ddot{\phi} - 2\dot{\phi}\beta_{sw} + 2\dot{\beta}_G - 2\beta_{sw}\dot{\theta}_G$$

$$+2\omega_z\dot{\beta}_G + 2\phi\omega_z]\}\vec{j}_{2g} + \Omega^2\{\ddot{z}_g + \omega_x(x + e_p) - \dot{\omega}_x x\beta_{sw} - \dot{\omega}_y(e_p + x) - e_p\ddot{\beta}_G - x\ddot{\beta}_G$$

$$-x\beta_{sw}\omega_y + y[\omega_y + \dot{\omega}_x - \dot{\omega}_y\beta_{sw} - \ddot{\beta}_G\beta_{sw} + \ddot{\phi} + \ddot{\theta}_G + \omega_x\beta_{sw}] + z[[\omega_x(-\beta_{sw}\phi - \beta_p + \beta_G)$$

$$-\omega_y\phi - (\omega_x^2 + \omega_y\omega_y) - \dot{\omega}_x\phi - \dot{\omega}_y(-\phi\beta_{sw} - \beta_p + \beta_G) + 2\beta_{sw}\dot{\phi}\dot{\beta}_G + \beta_{sw}\phi\ddot{\beta}_G + \beta_{sw}\ddot{\phi}\beta_G$$

$$-\beta_p\beta_{sw}\ddot{\phi} + \beta_p\ddot{\beta}_G - \ddot{\theta}_G(\phi - \beta_{sw}\beta_G + \beta_{sw}\beta_p) + 2\beta_{sw}\dot{\beta}_G\dot{\theta}_G - 2\dot{\phi}\dot{\theta}_G - \dot{\theta}_G^2 - 2\omega_x(\dot{\phi} + \dot{\theta}_G)$$

$$-2\omega_y(-\beta_{sw}\dot{\phi} + \dot{\beta}_G - \beta_{sw}\dot{\theta}_G)]\}\vec{k}_{2g}$$

$$= \Omega^2\vec{i}_{2g}(a_x^0 + ya_x^y + za_x^z) + \Omega^2\vec{j}_{2g}(a_y^0 + ya_y^y + za_y^z) + \Omega^2\vec{k}_{2g}(a_z^0 + ya_z^y + za_z^z) \qquad (3.1.20)$$

The inertial forces per unit length of the blade is obtained from the D'Alembert's principle,

$$\vec{p}_I = -\int\int \rho d_A . \vec{a} = p_I^x\vec{i}_{2g} + p_I^y\vec{j}_{2g} + p_I^z\vec{k}_{2g} \qquad (3.1.21)$$

Applying the results from (3.1.20) and the relations in (3.1.8),

$$p_I^x = -\int\int \rho(a_x^0 + ya_x^y + za_x^z)\Omega^2 d_A$$

$$= \Omega^2\left\{-ma_x^0 - \int\int \rho[\eta,\zeta]\begin{bmatrix}\cos\theta_G & \sin\theta_G \\ -\sin\theta_G & \cos\theta_G\end{bmatrix}\begin{Bmatrix}a_x^y \\ a_x^z\end{Bmatrix} d_A\right\}$$

$$= \Omega^2\{-ma_x^0 - a_x^y\cos\theta_G mx_{Gc} - a_x^z mx_{Gc}\sin\theta_G\} \qquad (3.1.22)$$

$$p_I^y = \Omega^2\{-ma_y^0 - a_y^y\cos\theta_G mx_{Gc} - a_y^z mx_{Gc}\sin\theta_G\} \qquad (3.1.23)$$

$$p_I^z = \Omega^2\{-ma_z^0 - a_z^y\cos\theta_G mx_{Gc} - a_z^z mx_{Gc}\sin\theta_G\} \qquad (3.1.24)$$

The inertial moments per unit length of blades can similarly be obtained as :

$$\vec{q_I}=\int\int -\rho d_A(y\vec{j}_{cs}+z\vec{k}_{cs})\times\vec{a}=q_I^x\vec{i}_{2g}+q_I^y\vec{j}_{2g}+q_I^z\vec{k}_{2g} \qquad (3.1.25)$$

$$\begin{aligned}q_I^x=&-\Omega^2\int\int\rho\{[y-\phi z](a_z^0+ya_z^y+za_z^z)-[y(\phi-\beta_{sw}\beta_G+\beta_{sw}\beta_p)+z](a_y^0+ya_y^y+za_y^z)\}d_A\\&=-\Omega^2[a_z^0-a_y^0\phi]mx_{Gc}\cos\theta_G-\Omega^2[-a_z^0\phi-a_y^0]mx_{Gc}\sin\theta_G\\&+\Omega^2(I_3\sin^2\theta_G+I_2\cos^2\theta_G)(a_y^z+a_z^z\phi)+\Omega^2(I_3-I_2)\sin\theta_G\cos\theta_G(a_z^y\phi+a_y^y\\&-a_z^z+a_y^z\phi)-\Omega^2(I_3\cos^2\theta_G+I_2\sin^2\theta_G)(a_z^y-a_y^y\phi)\end{aligned} \qquad (3.1.26)$$

$$\begin{aligned}q_I^y=&-\Omega^2\int\int\rho\{[y(\phi-\beta_{sw}\beta_G+\beta_{sw}\beta_p)+z](a_x^0+ya_x^y+za_x^z)-[y(\beta_{sw}-\phi\beta_p+\phi\beta_G)\\&+z(-\phi\beta_{sw}-\beta_p+\beta_G)](a_z^0+ya_z^y+za_z^z)\}d_A\\&=-\Omega^2mx_{Gc}\cos\theta_G\phi a_x^0-\Omega^2mx_{Gc}\sin\theta_G a_x^0+\Omega^2mx_{Gc}\sin\theta_G(-\phi\beta_{sw}-\beta_p+\beta_G)a_z^0\\&+\Omega^2mx_{Gc}\cos\theta_G(\beta_{sw}-\phi\beta_p+\phi\beta_G)a_z^0+\Omega^2(I_3\cos^2\theta_G+I_2\sin^2\theta_G)[-a_x^y\\&(\phi-\beta_{sw}\beta_G+\beta_{sw}\beta_p)+a_z^y(\beta_{sw}-\phi\beta_p+\phi\beta_G)]+\Omega^2(I_3-I_2)\sin\theta_G\cos\theta_G[-a_x^y\\&-a_x^z(\phi-\beta_{sw}\beta_G+\beta_{sw}\beta_p)+a_z^y(-\phi\beta_{sw}-\beta_p+\beta_G)+a_z^z(\beta_{sw}-\phi\beta_p+\phi\beta_G)]\\&+\Omega^2(I_3\sin^2\theta_G+I_2\cos^2\theta_G)[-a_x^z+a_z^z(-\phi\beta_{sw}-\beta_p+\beta_G)]\end{aligned} \qquad (3.1.27)$$

$$\begin{aligned}q_I^z=&-\Omega^2\int\int\rho\{[y(\beta_{sw}-\phi\beta_p+\phi\beta_G)+z(-\phi\beta_{sw}-\beta_p+\beta_G)](a_y^0+ya_y^y+za_y^z)\\&-[y-z\phi](a_x^0+ya_x^y+za_x^z)\}d_A\\&=-\Omega^2mx_{Gc}\cos\theta_G a_y^0(\beta_{sw}-\phi\beta_p+\phi\beta_G)-\Omega^2mx_{Gc}\sin\theta_G a_y^0(-\phi\beta_{sw}-\beta_p+\beta_G)\\&-\Omega^2mx_{Gc}\cos\theta_G a_x^0+\Omega^2mx_{Gc}\sin\theta_G\phi a_x^0+\Omega^2(I_3\cos^2\theta_G+I_2\sin^2\theta_G)\\&[-a_y^y(\beta_{sw}-\phi\beta_p+\phi\beta_G)+a_x^y]+\Omega^2(I_3\sin^2\theta_G+I_2\cos^2\theta_G)[-a_y^z(-\phi\beta_{sw}-\beta_p+\beta_G)-\phi a_x^z]\\&+\Omega^2(I_3-I_2)\sin\theta_G\cos\theta_G\{-a_y^y(-\phi\beta_{sw}-\beta_p+\beta_G)-a_y^z(\beta_{sw}-\phi\beta_p+\phi\beta_G)-\phi a_x^y+a_x^z\}\end{aligned} \qquad (3.1.28)$$

Where, $I_2=\iint \rho\zeta^2 d_A$ $I_3=\iint \rho\eta^2 d_A$

$m=\iint \rho d_A$ $mx_{Gc}=\iint \rho\eta d_A$ (3.1.29)

And assume, $\iint \rho\zeta d_A=0$ $\iint \rho\zeta\eta d_A=0.$

Noting the following relations

$a_x^0=O(1)$ $a_x^y=O(\varepsilon)$ $a_x^z=O(\varepsilon)$

$a_y^0=O(\varepsilon)$ $a_y^y=O(1)$ $a_y^z=O(\varepsilon)$

$a_z^0=O(\varepsilon)$ $a_z^y=O(\varepsilon)$ $a_z^z=O(\varepsilon^2)$ (3.1.30)

And after applying the ordering scheme, we have :

$$p_I^x=-m\Omega^2\{\ddot{x}_g\cos\psi+\ddot{y}_g\sin\psi-(e_p+x)-2x\dot{\theta}_z\} \quad (3.1.31)$$

$$p_I^y=-m\Omega^2\{x\beta_{sw}+\ddot{\theta}_z(e_p+x)+z_h\ddot{\alpha}_G-2z_h\dot{\beta}_G+2x\beta_p\dot{\beta}_G+2x\dot{\theta}_z\beta_{sw}-x_{Gc}\cos\theta_G$$
$$+\sin\psi[-\ddot{x}_g-\ddot{\theta}_y(-z_h+x(\beta_p-\beta_G))+2x\dot{\theta}_y\dot{\beta}_G]+\cos\psi[\ddot{y}_g-\ddot{\theta}_x(-z_h+x(\beta_p-\beta_G))$$
$$+2x\dot{\theta}_x\dot{\beta}_G]\} \quad (3.1.32)$$

$$p_I^z=-m\Omega^2\{\ddot{z}_g-e_p\ddot{\beta}_G-x\ddot{\beta}_G+\sin\psi[-x\beta_{sw}(\ddot{\theta}_y-2\dot{\theta}_x)-(e_p+x)(-\ddot{\theta}_x-2\dot{\theta}_y)]$$
$$+\cos\psi[-x\beta_{sw}(\ddot{\theta}_x+2\dot{\theta}_y)-(e_p+x)(\ddot{\theta}_y-2\dot{\theta}_x)]\} \quad (3.1.33)$$

$$q_I^x=-m\Omega^2\{x_{Gc}\cos\theta_G[\ddot{z}_g-e_p\ddot{\beta}_G-x\ddot{\beta}_G-\phi x\beta_{sw}-\phi x\ddot{\theta}_z+\sin\psi[-x\beta_{sw}(\ddot{\theta}_y-2\dot{\theta}_x)$$
$$-(e_p+x)(-\ddot{\theta}_x-2\dot{\theta}_y)+\phi\ddot{x}_g]+\cos\psi[-x\beta_{sw}(\ddot{\theta}_x+2\dot{\theta}_y)-(e_p+x)(\ddot{\theta}_y-2\dot{\theta}_x)-\phi\ddot{y}_g]$$
$$+x_{Gc}\sin\theta_G[-x\beta_{sw}-\ddot{\theta}_z(e_p+x)-z_h\ddot{\alpha}_G+2z_h\dot{\beta}_G-2x\dot{\theta}_z\beta_{sw}-2x\beta_p\dot{\beta}_G-\phi\ddot{z}_g$$
$$+x\phi\ddot{\beta}_G+\sin\psi[\ddot{x}_g+\ddot{\theta}_y(-z_h+x(\beta_p-\beta_G))-2x\dot{\theta}_y\dot{\beta}_G]+\phi x(-\ddot{\theta}_x-2\dot{\theta}_y)]$$
$$+\cos\psi[-\ddot{y}_g+\ddot{\theta}_x(-z_h+x(\beta_p-\beta_G))-2x\dot{\theta}_x\dot{\beta}_G+\phi x(\ddot{\theta}_y-2\dot{\theta}_x)]\}$$
$$+\Omega^2(I_3\sin^2\theta_G+I_2\cos^2\theta_G)\{\phi+(-\beta_p+\beta_G)\ddot{\theta}_z-\ddot{\theta}_G-\ddot{\phi}+2\dot{\beta}_G-2\beta_{sw}\dot{\theta}_G-2\beta_{sw}\dot{\phi}$$
$$+2\dot{\theta}_z\dot{\beta}_G+2\phi\dot{\theta}_z-\ddot{\theta}_y\sin\psi-\ddot{\theta}_x\cos\psi\}+\Omega^2(I_3-I_2)\sin\theta_G\cos\theta_G(-1-2\dot{\theta}_z)$$

$$-\Omega^2(I_3\cos^2\theta_G+I_2\sin^2\theta_G)\{-\beta_{sw}\ddot{\beta}_G+\ddot{\phi}+\ddot{\theta}_G+\phi(1+2\dot{\theta}_z)+\sin\psi[\ddot{\theta}_y-2\dot{\theta}_x$$

$$-\beta_{sw}(-\ddot{\theta}_x-2\dot{\theta}_y)]+\cos\psi[\ddot{\theta}_x+2\dot{\theta}_y-\beta_{sw}(\ddot{\theta}_y-2\dot{\theta}_x)]\} \qquad (3.1.34)$$

$$q_I^y=-m\Omega^2\{x_{Gc}\cos\theta_G[-(e_p+x)\phi-2x\dot{\theta}_z\phi-\beta_{sw}\ddot{z}_g+x\beta_{sw}\ddot{\beta}_G+\sin\psi<\phi\ddot{y}_g$$

$$+(e_p+x)\beta_{sw}(-\ddot{\theta}_x-2\dot{\theta}_y)>+\cos\psi<\phi\ddot{x}_g+(e_p+x)\beta_{sw}(\ddot{\theta}_y-2\dot{\theta}_x)>]$$

$$+x_{Gc}\sin\theta_G[-(e_p+x)-2x\dot{\theta}_z+\ddot{x}_g\cos\psi+\ddot{y}_g\sin\psi]\}+\Omega^2(I_3\cos^2\theta_G+I_2\sin^2\theta_G)$$

$$\{\phi\beta_{sw}-2\phi^2\dot{\theta}_G+\phi\ddot{\theta}_z-2\phi\dot{\theta}_G\dot{\beta}_G-\phi^2\ddot{\beta}_G-2\phi\dot{\phi}\dot{\beta}_G-\phi^2(\beta_G-\beta_p)+2\phi\beta_{sw}\dot{\theta}_z$$

$$+\beta_{sw}(\beta_G-\beta_p)(-\beta_{sw}-\ddot{\theta}_z)-\beta_{sw}^2\ddot{\beta}_G+\beta_{sw}\ddot{\phi}+\beta_{sw}\ddot{\theta}_G+\sin\psi[-2\phi(\dot{\phi}+\dot{\theta}_G)(-\dot{\theta}_x)$$

$$+\phi^2\ddot{\theta}_x+\beta_{sw}(\ddot{\theta}_y-2\dot{\theta}_x)-\beta_{sw}^2(-\ddot{\theta}_x-2\dot{\theta}_y)+\phi(\beta_G-\beta_p)(\ddot{\theta}_x+2\dot{\theta}_y)]\}$$

$$+\cos\psi[-2\phi(\dot{\phi}+\dot{\theta}_G)\dot{\theta}_y-\phi^2\ddot{\theta}_y+\beta_{sw}(\ddot{\theta}_x+2\dot{\theta}_y)-\beta_{sw}^2(\ddot{\theta}_y-2\dot{\theta}_x)$$

$$+\phi(\beta_G-\beta_p)(\ddot{\theta}_x+2\dot{\theta}_y)]\}$$

$$+\Omega^2(I_3-I_2)\sin\theta_G\cos\theta_G\{\beta_{sw}-2\phi\dot{\theta}_G+\ddot{\theta}_z-2\dot{\theta}_G\dot{\beta}_G-\phi\ddot{\beta}_G-2\dot{\phi}\dot{\beta}_G+2\phi(\beta_G-\beta_p)$$

$$+2\beta_{sw}\dot{\theta}_z-\phi\ddot{\beta}_G-2\phi(\dot{\phi}+\dot{\theta}_G)+\sin\psi[-2(\dot{\phi}+\dot{\theta}_G)(-\dot{\theta}_x)-2\phi\ddot{\theta}_x+(\beta_G-\beta_p)(\ddot{\theta}_y-2\dot{\theta}_x)$$

$$+\cos\psi[-2(\dot{\phi}+\dot{\theta}_G)\dot{\theta}_y-2\phi\ddot{\theta}_y+(\beta_G-\beta_p)(\ddot{\theta}_x+2\dot{\theta}_y)]\}+\Omega^2(I_3\sin^2\theta_G+I_2\cos^2\theta_G)$$

$$\{\beta_{sw}\ddot{\phi}-\ddot{\beta}_G+\beta_{sw}\ddot{\theta}_G-\phi\ddot{\theta}_z-2(1+\dot{\theta}_z)(\dot{\phi}+\dot{\theta}_G)+(\beta_G-\beta_p)-\phi\beta_{sw}+2(\beta_G-\beta_p)\dot{\theta}_z$$

$$+\sin\psi\,\ddot{\theta}_x+\cos\psi\,(-\ddot{\theta}_y)\} \qquad (3.1.35)$$

$$q_I^z=-m\Omega^2\{x_{Gc}\cos\theta_G[\ddot{x}_g\cos\psi+\ddot{y}_g\sin\psi-(e_p+x)-2x\dot{\theta}_z]+x_{Gc}\sin\theta_G[(\beta_G-\beta_p)$$

$$(x\beta_{sw}+(e_p+x)\ddot{\theta}_z)+\phi(e_p+x)+2\phi x\dot{\theta}_z+\sin\psi(-\ddot{x}_g(\beta_G-\beta_p)-\phi\ddot{y}_g)+\cos\psi$$

$$(\ddot{y}_g(\beta_G-\beta_p)-\phi\ddot{x}_g)]\}+\Omega^2(I_3\cos^2\theta_G+I_2\sin^2\theta_G)\{2\phi\dot{\theta}_G-\ddot{\theta}_z+\ddot{\phi}(\beta_G-\beta_p)$$

$$+2\dot{\theta}_G\dot{\beta}_G+\phi\ddot{\beta}_G+2\dot{\phi}\dot{\beta}_G+(\beta_G-\beta_p)\ddot{\theta}_G+\sin\psi[2(\dot{\phi}+\dot{\theta}_G)(-\dot{\theta}_x)-\phi\ddot{\theta}_x]$$

$$+\cos\psi[2(\dot{\phi}+\dot{\theta}_G)\dot{\theta}_y+\phi\ddot{\theta}_y]\}+\Omega^2(I_3\sin^2\theta_G+I_2\cos^2\theta_G)\{\phi(\beta_{sw}\ddot{\phi}-\ddot{\beta}_G+\beta_{sw}\ddot{\theta}_G$$

$$-\phi\ddot{\theta}_z-2(1+\dot{\theta}_z)(\dot{\phi}+\dot{\theta}_G)-\phi\beta_{sw}+2(\beta_G-\beta_p)\dot{\theta}_z)+\phi^2\beta_{sw}-(\beta_G-\beta_p)^2\ddot{\theta}_z$$

$$+(\beta_G-\beta_p)\ddot{\theta}_G+(\beta_G-\beta_p)\ddot{\phi}-2(\beta_G-\beta_p)\dot{\beta}_G+2\beta_{sw}(\beta_G-\beta_p)(\dot{\theta}_G+\dot{\phi})$$

$$-2(\beta_G-\beta_p)\dot{\beta}_G\dot{\theta}_z-2\phi(\beta_G-\beta_p)\dot{\theta}_z+\phi\beta_{sw}(-\ddot{\theta}_G-\ddot{\phi}+2\dot{\beta}_G)$$

$$+\sin\psi[\phi\ddot{\theta}_x+(\beta_G-\beta_p)\ddot{\theta}_y-\phi\beta_{sw}\ddot{\theta}_y]+\cos\psi[-\phi\ddot{\theta}_y$$

$$+(\beta_G-\beta_p)\ddot{\theta}_x-\phi\beta_{sw}\ddot{\theta}_x]\}+\Omega^2(I_3-I_2)\sin\theta_G\cos\theta_G\{\ddot{\beta}_G+2\phi\ddot{\theta}_z$$

$$+2(1+\dot{\theta}_z)(\dot{\phi}+\dot{\theta}_G)-2\beta_{sw}\dot{\beta}_G+\sin\psi[-\ddot{\theta}_x+\beta_{sw}\ddot{\theta}_y]+\cos\psi[\ddot{\theta}_y+\beta_{sw}\ddot{\theta}_x]\} \quad (3.1.36)$$

3.3.2. Aerodynamic Loads Applied on a Unit Length of Blade

The two dimensional quasisteady thin airfoil aerodynamic model is used for the calculation of the aerodynamic loads [Johnson, 1977]. Fig.3.8 gives a description of the sectional aerodynamic environment.

Section lift $\vec{L}=\vec{L}_c+\vec{L}_{nc}$ (3.2.1)

Section drag $D=\rho b c_d U^2$ (3.2.2)

Section moment $\vec{M}=\vec{M}_c+\vec{M}_{nc}$ (3.2.3)

$\vec{M}$ positive nose up

Where, $L_c=\rho b c_l U^2$ (3.2.4)

That is the circulatory part of the lift and *normal* to the resultant velocity

$$L_{nc}=\rho ab\left\{\frac{b}{2}\dot{U}_n-\frac{b}{2}\left(x_A-\frac{b}{2}\right)\ddot{\varepsilon}\right\} \quad (3.2.5)$$

That is the noncirculatory part of the lift and *normal* to the chord line

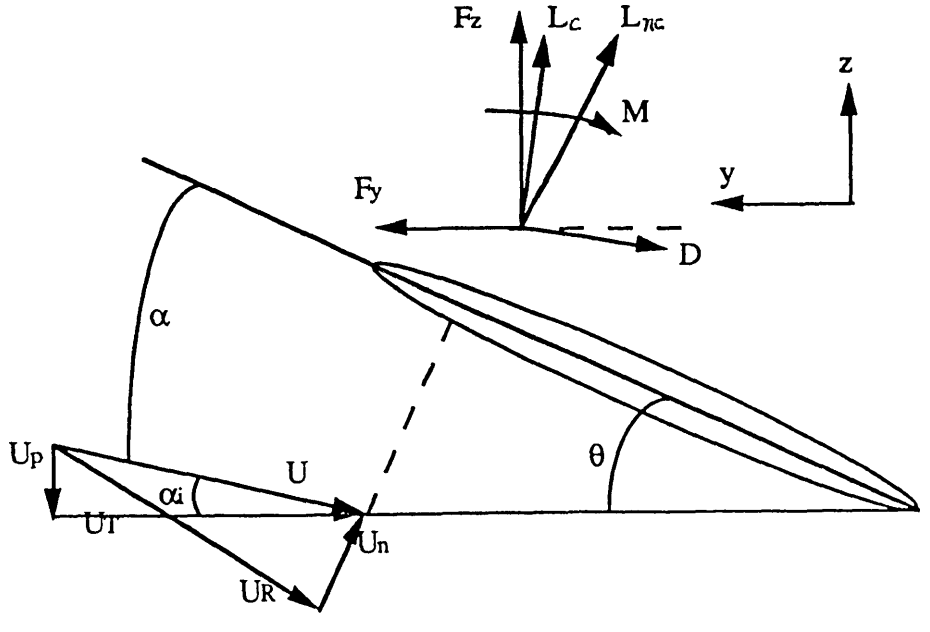

Fig 3.8 Blade section aerodynamics

$$M_c=x_A L_s+2\rho b^2 c_{mac} U^2 \qquad (3.2.6)$$

$$M_{nc}=\rho ab\left\{\frac{b}{2}\left(x_A-\frac{b}{2}\right)\dot{U}_n-\frac{b^2}{4}U_R\dot{\varepsilon}+\frac{b}{2}\left(x_A^2-x_A b+\frac{3b^2}{8}\right)\ddot{\varepsilon}\right\} \qquad (3.2.7)$$

And from Fig.3.8, $U^2=U_T^2+U_P^2$ (3.2.8)

$$U_n=U_T\sin\theta-U_p\cos\theta \qquad (3.2.9)$$

$$U_R=U_T\cos\theta+U_p\sin\theta \qquad (3.2.10)$$

$$\dot{\varepsilon}=\Omega(\dot{\theta}-\beta_G+\beta_p) \qquad (3.2.11)$$

The resultant on–coming airflow velocity is

$$\vec{v}=\vec{v}_{\text{free airflow}}-\vec{v}_{\text{blade motion}} \qquad (3.2.12)$$

$$\vec{v}_{\text{free airflow}}=-(v_F+v_i)\Omega R\vec{k}_g \qquad (3.2.13)$$

$$\vec{v}_{\text{blade motion}}=\vec{v}_0+\vec{\omega}\times\vec{r}_e+\dot{\vec{r}}_e \qquad (3.2.14)$$

Where,

$\vec{r}_e$ is the position vector of a general point on blade elasticity axis

$$\vec{v}_0=(\dot{x}_g\vec{i}_g+\dot{y}_g\vec{j}_g+\dot{z}_g\vec{k}_g)\Omega \qquad (3.2.15)$$

$$\dot{x}_g=\dot{R}_x+l_y(\dot{\theta}_x\theta_y+\theta_x\dot{\theta}_y-\dot{\theta}_z)+l_z(\dot{\theta}_y+\dot{\theta}_x\theta_z+\dot{\theta}_z\theta_x) \qquad (3.2.16)$$

$$\dot{y}_g=\dot{R}_y+l_x\dot{\theta}_z+l_z(\dot{\theta}_y\theta_z+\dot{\theta}_z\theta_y-\dot{\theta}_x) \qquad (3.2.17)$$

$$\dot{z}_g=\dot{R}_z-l_x\dot{\theta}_y+l_y\dot{\theta}_x \qquad (3.2.18)$$

$$\vec{r}_e=-z_h\vec{k}_h+e_p\vec{i}_h+e_p\beta_p\vec{k}_h+x\vec{i}_b$$

$$=\{e_p+x,\ z_h\alpha_G-x\beta_{sw},\ -e_p(\beta_G-\beta_p)-z_h+x(\beta_p-\beta_G)\}\vec{E}_{2g} \qquad (3.2.19)$$

(see Fig.3.5, 3.6)

$$\dot{\vec{r}}_e=\Omega\{e_p\beta_p\dot{\beta}_G-z_h\dot{\beta}_G+x\beta_p\dot{\beta}_G,\ -e_p\beta_p\dot{\alpha}_G+z_h\dot{\alpha}_G,\ -e_p\dot{\beta}_G-x\dot{\beta}_G\}\vec{E}_{2g} \qquad (3.2.20)$$

$$\vec{\omega}\times\vec{r}_e=\Omega[\omega_x\vec{i}_{2g}+\omega_y\vec{j}_{2g}+(1+\omega_z)\vec{k}_{2g}]\times\vec{r}_e$$

$$=\Omega\{-(z_h\alpha_G-x\beta_{sw})+\omega_z x\beta_{sw}+\omega_y[-z_h+x(\beta_p-\beta_G)]\}\vec{i}_{2g}+\Omega\{\{e_p+x+\omega_z x\}\vec{j}_{2g}$$

$$+\Omega\{-x\beta_{sw}\omega_x-(e_p+x)\omega_y\}\vec{k}_{2g} \qquad (3.2.21)$$

$$\vec{v}_{\text{blade motion}}=\Omega(\dot{x}_g\vec{i}_g+\dot{y}_g\vec{j}_g+\dot{z}_g\vec{k}_g)+\Omega\vec{i}_{2g}\{-(z_h\alpha_G-x\beta_{sw})+\omega_z x\beta_{sw}$$

$$+\omega_y[-z_h+x(\beta_p-\beta_G)]-z_h\dot{\beta}_G+x\beta_p\dot{\beta}_G\}+\Omega\{\{e_p+x+\omega_z x\}\vec{j}_{2g}+\Omega\{-x\beta_{sw}\omega_x$$

$$-(e_p+x)\omega_y-e_p\dot{\beta}_G-x\dot{\beta}_G\}\vec{k}_{2g} \qquad (3.2.22)$$

$$\vec{v}=\vec{v}_{\text{free airflow}}-\vec{v}_{\text{blade motion}}=-(v_F+v_i)\Omega R\vec{k}_g-\vec{v}_{\text{blade motion}} \qquad (3.2.23)$$

Rewriting (3.2.23) in components in $x_by_bz_b$system and using the ordering scheme

$$\vec{v}\approx\Omega\{[-(v_F+v_i)R-\dot{z}_g](\beta_p-\beta_G)+z_h\alpha_G+z_h\dot{\beta}_G+e_p\beta_{sw}-x\beta_G\dot{\beta}_G+\sin\psi[-(v_F+v_i)R$$

$$(\theta_x-\beta_{sw}\theta_y)-\dot{x}_g\beta_{sw}-\dot{y}_g-z_h\dot{\theta}_x]+\cos\psi[-(v_F+v_i)R(-\theta_y-\beta_{sw}\theta_x)-\dot{x}_g+\dot{y}_g\beta_{sw}$$

$$\dot{z}_g\theta_y+z_h\dot{\theta}_y],(v_F+v_i)R\beta_{sw}(\beta_G-\beta_p)-(e_p+x)-x\dot{\theta}_z+\sin\psi[-(v_F+v_i)R(\theta_y+\beta_{sw}\theta_x)$$

$$+\dot{x}_g-\beta_{sw}\dot{y}_g+\theta_z\dot{y}_g-\theta_y\dot{z}_g]+\cos\psi[-(v_F+v_i)R(\theta_x-\beta_{sw}\theta_y)-\dot{x}_g\beta_{sw}-\dot{y}_g+\dot{x}_g\theta_z-\dot{z}_g\theta_x],$$

$$-(v_F+v_i)R-\dot{z}_g+x\dot{\beta}_G+\sin\psi[-(\beta_G-\beta_p)\dot{y}_g+x\beta_{sw}\dot{\theta}_y-(e_p+x)\dot{\theta}_x]+\cos\psi[-(\beta_G-\beta_p)\dot{x}_g$$

$$+x\beta_{sw}\dot{\theta}_x+(e_p+x)\dot{\theta}_y]\}\vec{E}_b \qquad (3.2.24)$$

After applying the ordering scheme,

$$U_T=-v_{yb}=\Omega\{(e_p+x)+x\dot{\theta}_z-\sin\psi[-(v_F+v_i)R(\theta_y+\beta_{sw}\theta_x)+\dot{x}_g-\beta_{sw}\dot{y}_g]$$

$$-\cos\psi[-(v_F+v_i)R(\theta_x-\beta_{sw}\theta_y)-\dot{x}_g\beta_{sw}-\dot{y}_g]\} \qquad (3.2.25)$$

$$U_p=-v_{zb}=\Omega\{(v_F+v_i)R+\dot{z}_g-x\dot{\beta}_G-\sin\psi[-(\beta_G-\beta_p)\dot{y}_g+x\beta_{sw}\dot{\theta}_y-(e_p+x)\dot{\theta}_x]$$

$$-\cos\psi[-(\beta_G-\beta_p)\dot{x}_g+x\beta_{sw}\dot{\theta}_x+(e_p+x)\dot{\theta}_y]\} \qquad (3.2.26)$$

After applying the ordering scheme,

$$U_T^2\approx\Omega^2\{x^2+2e_px+2x^2\dot{\theta}_z+\sin\psi<-2(e_p+x)[-(v_F+v_i)R\theta_y+\dot{x}_g]>$$

$$+\cos\psi<-2(e_p+x)[-(v_F+v_i)R\theta_x-\dot{y}_g]>\} \quad (3.2.27)$$

$$U_p^2\approx\Omega^2\{(v_F+v_i)^2R^2+2(v_F+v_i)R\dot{z}_g-2(v_F+v_i)Rx\dot{\beta}_G+\sin\psi<2(v_F+v_i)Rx\dot{\theta}_x>$$

$$+\cos\psi<-2(v_F+v_i)Rx\dot{\theta}_y>\} \quad (3.2.28)$$

From (3.2.9),

$$\dot{U}_n=\Omega(U_T\cos\theta+U_p\sin\theta)\dot{\theta}+\dot{U}_T\sin\theta-\dot{U}_p\cos\theta \quad (3.2.29)$$

Where,

$$\dot{U}_T=\Omega^2\{-(v_F+v_i)R\beta_{sw}\dot{\beta}_G-x\ddot{\theta}_z-\sin\psi[-(v_F+v_i)R(\dot{\theta}_y+\beta_{sw}\dot{\theta}_x)$$

$$+\ddot{x}_g-\beta_{sw}\ddot{y}_g+\dot{\theta}_z\dot{y}_g+\theta_z\ddot{y}_g-\dot{\theta}_y\dot{z}_g-\theta_y\ddot{z}_g]+\cos\psi[-(v_F+v_i)R(\dot{\theta}_x-\beta_{sw}\dot{\theta}_y)-$$

$$\ddot{x}_g\beta_{sw}-\ddot{y}_g+\ddot{x}_g\theta_z+\dot{x}_g\dot{\theta}_z-\dot{z}_g\dot{\theta}_x-\ddot{z}_g\theta_x]-\cos\psi[-(v_F+v_i)R(\theta_y+\beta_{sw}\theta_x)$$

$$+\dot{x}_g-\beta_{sw}\dot{y}_g+\theta_z\dot{y}_g-\theta_y\dot{z}_g]-\sin\psi[-(v_F+v_i)R(\theta_x-\beta_{sw}\theta_y)-\dot{x}_g\beta_{sw}-\dot{y}_g+\dot{x}_g\theta_z-\dot{z}_g\theta_x] \quad (3.2.30)$$

$$\dot{U}_p=\Omega^2\{\ddot{z}_g-x\ddot{\beta}_G-\sin\psi[-(\beta_G-\beta_p)\ddot{y}_g-\dot{\beta}_G\dot{y}_g+x\beta_{sw}\ddot{\theta}_y-(e_p+x)\ddot{\theta}_x+[-z_h-x(\beta_G-\beta_p)]\ddot{\theta}_x$$

$$-x\dot{\beta}_G\dot{\theta}_x]-\cos\psi[-(\beta_G-\beta_p)\ddot{x}_g-\dot{\beta}_G\dot{x}_g+x\beta_{sw}\ddot{\theta}_x+(e_p+x)\ddot{\theta}_y-[-z_h-x(\beta_G-\beta_p)]\ddot{\theta}_y$$

$$+x\dot{\beta}_G\dot{\theta}_y]-\cos\psi[-(\beta_G-\beta_p)\dot{y}_g+x\beta_{sw}\dot{\theta}_y-(e_p+x)\dot{\theta}_x]+\sin\psi[-(\beta_G-\beta_p)\dot{x}_g$$

$$+x\beta_{sw}\dot{\theta}_x+(e_p+x)\dot{\theta}_y]\} \quad (3.2.31)$$

$$U_TU_p\approx\Omega^2\{(e_p+x)(v_F+v_i)R+x(v_F+v_i)R\dot{\theta}_z+(e_p+x)\dot{z}_g-x(e_p+x)\dot{\beta}_G$$

$$+\sin\psi[-(v_F+v_i)R\theta_y+\dot{x}_g][-(v_F+v_i)R]+\cos\psi[-(v_F+v_i)R\theta_x-\dot{y}_g][-(v_F+v_i)R]$$

$$+\sin\psi[x(e_p+x)\dot{\theta}_x]+\cos\psi[-x(e_p+x)\dot{\theta}_y]\} \quad (3.2.32)$$

$$U_R=U\cos\alpha\approx U \quad (3.2.33)$$

From Fig.3.8, the aerodynamic components in the y,z diretions are,

$$F_y=-D\cos\alpha_i-L_c\sin\alpha_i-L_{nc}\sin\theta \quad (3.2.34)$$

$$F_z=L_c\cos\alpha_i-D\sin\alpha_i+L_{nc}\cos\theta \quad (3.2.35)$$

$$\sin\alpha_i = \frac{U_p}{U} \qquad \cos\alpha_i = \frac{U_T}{U} \tag{3.2.36}$$

$$F_y = -\rho b c_d U^2 \frac{U_T}{U} - \rho b c_l U^2 \frac{U_p}{U} - L_{nc}\sin\theta$$

$$= -\rho b c_d U U_T - \rho b c_l U U_p - L_{nc}\sin\theta \tag{3.2.37}$$

$$F_z = \rho b c_l U U_T - \rho b c_d U U_p + L_{nc}\cos\theta \tag{3.2.38}$$

Applying equations (3.2.27) through (3.2.33), then, after using the ordering scheme:

$$F_y = -\rho b c_d [U_T^2\cos\theta + U_T U_p \sin\theta] - \rho b c_l [U_T U_p \cos\theta + U_p^2 \sin\theta] - L_{nc}\sin\theta$$

$$= -\rho b c_d \Omega^2 \{x^2 + 2e_p x + 2x^2\dot{\theta}_z + \sin\psi <-2(e_p+x)[-(v_F+v_i)R\theta_y + \dot{x}_g]>$$

$$+\cos\psi <-2(e_p+x)[-(v_F+v_i)R\theta_x - \dot{y}_g]>\}\cos\theta - (\rho b c_d \sin\theta + \rho b c_l \cos\theta)$$

$$\times\Omega^2\{(e_p+x)(v_F+v_i)R + x(v_F+v_i)R\dot{\theta}_z + (e_p+x)\dot{z}_g - x(e_p+x)\dot{\beta}_G$$

$$+\sin\psi[-(v_F+v_i)R\theta_y + \dot{x}_g][-(v_F+v_i)R] + \cos\psi[-(v_F+v_i)R\theta_x - \dot{y}_g][-(v_F+v_i)R]$$

$$+\sin\psi[x(e_p+x)\dot{\theta}_x] + \cos\psi[-x(e_p+x)\dot{\theta}_y]\} - \rho b c_l \sin\theta\Omega^2\{(v_F+v_i)^2R^2 + 2(v_F+v_i)R\dot{z}_g$$

$$-2(v_F+v_i)Rx\dot{\beta}_G + \sin\psi <2(v_F+v_i)Rx\dot{\theta}_x> + \cos\psi <-2(v_F+v_i)Rx\dot{\theta}_y>\} - L_{nc}\sin\theta \tag{3.2.39}$$

$$F_z = \rho b c_l [[U_T^2\cos\theta + U_T U_p \sin\theta] - \rho b c_d [U_T U_p \cos\theta + U_p^2 \sin\theta] + L_{nc}\cos\theta$$

$$= \rho b c_l \cos\theta\Omega^2\{x^2 + 2e_p x + 2x^2\dot{\theta}_z + \sin\psi <-2(e_p+x)[-(v_F+v_i)R\theta_y + \dot{x}_g]>$$

$$+\cos\psi <-2(e_p+x)[-(v_F+v_i)R\theta_x - \dot{y}_g]>\} - \rho b c_d \sin\theta\Omega^2\{(v_F+v_i)^2R^2 + 2(v_F+v_i)R\dot{z}_g$$

$$-2(v_F+v_i)Rx\dot{\beta}_G + \sin\psi <2(v_F+v_i)Rx\dot{\theta}_x> + \cos\psi <-2(v_F+v_i)Rx\dot{\theta}_y>\}$$

$$+(\rho b c_l \sin\theta - \rho b c_d \cos\theta)\Omega^2\{(e_p+x)(v_F+v_i)R + x(v_F+v_i)R\dot{\theta}_z + (e_p+x)\dot{z}_g - x(e_p+x)\dot{\beta}_G$$

$$+\sin\psi[-(v_F+v_i)R\theta_y + \dot{x}_g][-(v_F+v_i)R] + \cos\psi[-(v_F+v_i)R\theta_x - \dot{y}_g][-(v_F+v_i)R]$$

$$+\sin\psi[x(e_p+x)\dot{\theta}_x] + \cos\psi[-x(e_p+x)\dot{\theta}_y]\} + L_{nc}\cos\theta \tag{3.2.40}$$

Applying equations (3.2.4), (3.2.8) and (3.2.27) , (3.2.28), and neglecting higher order terms, we obtain :

$$M=x_A L_c+2\rho b^2 c_{mac}U^2+M_{nc}$$

$$=(2\rho b^2 c_{mac}+x_A\rho b c_l)\Omega^2\{x^2+2e_p x+2x^2\dot{\theta}_z+(v_F+v_i)^2R^2+2(v_F+v_i)R\dot{z}_g-2(v_F+v_i)Rx\dot{\beta}_G$$

$$+\sin\psi[<-2(e_p+x)[-(v_F+v_i)R\theta_y+\dot{x}_g]>+<2(v_F+v_i)Rx\dot{\theta}_x>]$$

$$+\cos\psi[<-2(e_p+x)[-(v_F+v_i)R\theta_x-\dot{y}_g]>+<-2(v_F+v_i)Rx\dot{\theta}_y>]\}+M_{nc} \qquad (3.2.41)$$

L_{nc} and M_{nc} in the above equations can be obtained by using (3.2.29) through (3.2.31) :

$$L_{nc}=\rho ab\left\{\frac{b}{2}\dot{U}_n-\frac{b}{2}\left(x_A-\frac{b}{2}\right)\ddot{\varepsilon}\right\}$$

$$=\rho ab\left\{\frac{b}{2}[\Omega^2\dot{\theta}\cos\theta_G x+\Omega^2\dot{\theta}\sin\theta_G(v_F+v_i)R+\Omega^2\sin\theta_G x\ddot{\theta}_z-\Omega^2\cos\theta_G(\ddot{z}_g-x\ddot{\beta}_G)]\right.$$

$$-\frac{b}{2}\left(x_A-\frac{b}{2}\right)(\ddot{\theta}-\dot{\beta}_G)\Omega^2+\sin\psi<\frac{b}{2}\{-\Omega^2\sin\theta_G[-(v_F+v_i)R(\dot{\theta}_y-\theta_x)+\ddot{x}_g+\dot{y}_g]$$

$$+\Omega^2\cos\theta_G x(-\ddot{\theta}_x-\dot{\theta}_y)\}>+\cos\psi<\frac{b}{2}\{-\Omega^2\sin\theta_G[-(v_F+v_i)R(\theta_y+\dot{\theta}_x)+\dot{x}_g-\ddot{y}_g]$$

$$\left.+\Omega^2\cos\theta_G x(\ddot{\theta}_y-\dot{\theta}_x)\}>\right\} \qquad (3.2.42)$$

$$M_{nc}=\rho ab\left\{\frac{b}{2}\left(x_A-\frac{b}{2}\right)\dot{U}_n-\frac{b^2}{4}U_R\dot{\varepsilon}+\frac{b}{2}\left(x_A^2-x_A b+\frac{3b^2}{8}\right)\ddot{\varepsilon}\right\}$$

$$=\rho ab\left\{\frac{b}{2}\left(x_A-\frac{b}{2}\right)\dot{U}_n^0-\frac{b^2}{4}U_R^0\Omega(\dot{\theta}-\beta_G+\beta_p)+\frac{b}{2}\left(x_A^2-x_A b+\frac{3b^2}{8}\right)(\ddot{\theta}-\dot{\beta}_G)\Omega^2\right.$$

$$+\sin\psi\left[\frac{b}{2}\left(x_A-\frac{b}{2}\right)\dot{U}_n^s-\frac{b^2}{4}U_R^s\Omega(\dot{\theta}-\beta_G+\beta_p)\right]+\cos\psi\left[\frac{b}{2}\left(x_A-\frac{b}{2}\right)\dot{U}_n^c\right]\Big\}$$

$$\left.+\cos\psi\left[\frac{b}{2}\left(x_A-\frac{b}{2}\right)\dot{U}_n^c-\frac{b^2}{4}U_R^c\Omega(\dot{\theta}-\beta_G+\beta_p)\right]\right\} \qquad (3.2.43)$$

Where,

$$U_T=U_T^0+U_T^s\sin\psi+U_T^c\cos\psi$$

$$U_p=U_p^0+U_p^s\sin\psi+U_p^c\cos\psi$$

$$\dot{U}_T=\dot{U}_T^0+\dot{U}_T^s\sin\psi+\dot{U}_T^c\cos\psi$$

$$\dot{U}_p=\dot{U}_p^0+\dot{U}_p^s\sin\psi+\dot{U}_p^c\cos\psi \qquad (3.2.44)$$

And therefore,

$$\dot{U}_n=\Omega\dot{\theta}(U_T\cos\theta+U_p\sin\theta)+\dot{U}_T\sin\theta-\dot{U}_p\cos\theta$$

$$=\dot{U}_n^0+\dot{U}_n^s\sin\psi+\dot{U}_n^c\cos\psi \qquad (3.2.45)$$

The detailed expressions for U_T , U_P , U_n and their derivatives are listed in appendix 3.D.

Combining (3.2.39) through (3.2.41) with (3.2.42) through (3.2.43), F_y , F_z , and M can be obtained, therefore, the aerodynamic force applied per unit length of blade is obtained:

$$\vec{F}_A=F_y\vec{j}_b+F_z\vec{k}_b \qquad (3.2.46)$$

$$\vec{M}_A=M\vec{i}_b \qquad (3.2.47)$$

Writing these components in $x_{2g}y_{2g}z_{2g}$ system, we have :

$$\vec{F}_A=[\beta_{sw}F_y+(\beta_G-\beta_p)F_z]\vec{i}_{2g}+F_y\vec{j}_{2g}+F_z\vec{k}_{2g} \qquad (3.2.48)$$

$$\vec{M}_A=M\vec{i}_{2g}-\beta_{sw}M\vec{j}_{2g}-(\beta_G-\beta_p)M\vec{k}_{2g} \qquad (3.2.49)$$

3.3.3. The Resultant Loads Caused by One Blade

1. The Resultant Inertial Forces Applied at Blade Root

$$\vec{F}_{IR}=\int_0^{R-e_p}\vec{p}_I dx=F_{IR}^x\vec{i}_{2g}+F_{IR}^y\vec{j}_{2g}+F_{IR}^z\vec{k}_{2g} \qquad (3.3.1)$$

$$F_{IR}^x=\int_0^{R-e_p}p_I^x dx \qquad (3.3.2)$$

$$F_{IR}^y=\int_0^{R-e_p}p_I^y dx \qquad (3.3.3)$$

$$F_{IR}^z=\int_0^{R-e_p}p_I^z dx \qquad (3.3.4)$$

2. The Resultant Inertial Moments about the Gimbal Centre

$$\vec{M}_{IR}=\int_0^{R-e_p}\vec{q}_I d_x+\int_0^{R-e_p}\vec{r}_e\times\vec{p}_I d_x=\vec{M}_{IR}=M_{IR}^x\vec{i}_{2g}+M_{IR}^y\vec{j}_{2g}+M_{IR}^z\vec{k}_{2g} \qquad (3.3.5)$$

Where, $\vec{r}_e$ is given as in (3.2.19)

$$\vec{r}_e\times\vec{p}_I=\{r_y p_I^z-r_z p_I^y,\ r_z p_I^x-r_x p_I^z,\ r_x p_I^y-r_y p_I^x\}\begin{Bmatrix} i_{2g} \\ j_{2g} \\ k_{2g}\end{Bmatrix} \qquad (3.3.6)$$

$$M_{IR}^x=\int_0^{R-e_p}(q_I^x+r_y p_I^z-r_z p_I^y)d_x \qquad (3.3.7)$$

$$M_{IR}^y=\int_0^{R-e_p}(q_I^y+r_z p_I^x-r_x p_I^z)d_x \qquad (3.3.8)$$

$$M_{IR}^z=\int_0^{R-e_p}(q_I^z+r_x p_I^y-r_y p_I^x)d_x \qquad (3.3.9)$$

3. The Resultant Aerodynamic Forces Applied at Blade Root

$$\vec{F}_{AR}=\int_0^{R-e_p}\vec{F}_A d_x$$

$$=\int_0^{R-e_p}(F_y\vec{j}_b+F_z\vec{k}_b)d_x$$

$$=F_{AR}^x\vec{i}_{2g}+F_{AR}^y\vec{j}_{2g}+F_{AR}^z\vec{k}_{2g} \qquad (3.3.10)$$

Where,

$$F_{AR}^x=\int_0^{R-e_p}[\beta_{sw}F_y+(\beta_G-\beta_p)F_z]d_x \qquad (3.3.11)$$

$$F_{AR}^y=\int_0^{R-e_p}F_y d_x \qquad (3.3.12)$$

$$F_{AR}^z=\int_0^{R-e_p}F_z d_x \qquad (3.3.13)$$

4. The Resultant Aerodynamic Moments about Gimbal Centre

$$\vec{M}_{AR}=\int_0^{R-e_p}\vec{q}_A d_x+\int_0^{R-e_p}\vec{r}_e\times\vec{P}_A d_x=M_{AR}^x\vec{i}_{2g}+M_{AR}^y\vec{j}_{2g}+M_{AR}^z\vec{k}_{2g} \qquad (3.3.14)$$

$$\vec{q}_A=M\vec{i}_b \qquad (3.3.15)$$

$$\vec{P}_A=F_y\vec{j}_b+F_z\vec{k}_b$$

$$=\{[\beta_{sw}F_y+(\beta_G-\beta_p)F_z],F_y,F_z\}\begin{Bmatrix} i_{2g} \\ j_{2g} \\ k_{2g}\end{Bmatrix} \qquad (3.3.17)$$

$$M_{AR}^x=\int_0^{R-e_p}(q_A^x+r_y p_A^z-r_z p_A^y)d_x \qquad (3.3.18)$$

$$M_{AR}^y=\int_0^{R-e_p}(q_A^y+r_z p_A^x-r_x p_A^z)d_x \qquad (3.3.19)$$

$$M_{AR}^z=\int_0^{R-e_p}(q_A^z+r_x p_A^y-r_y p_A^x)d_x \qquad (3.3.20)$$

The expressions of $F_{AR}^x,F_{AR}^y,F_{AR}^z,M_{AR}^x,M_{AR}^y,M_{AR}^z,F_{IR}^x,F_{IR}^y,F_{IR}^z,M_{IR}^x,M_{IR}^y,M_{IR}^z$ after applying the ordering scheme are listed in appendix 3B.

It should be noted in the ordering scheme application that the orders of these magnitudes for the above terms are:

$$F_{AR}^x = O(\varepsilon^2) \quad F_{AR}^y = O(\varepsilon) \quad F_{AR}^z = O(\varepsilon)$$
$$M_{AR}^x = O(\varepsilon^2) \quad M_{AR}^y = O(\varepsilon) \quad M_{AR}^z = O(\varepsilon)$$
$$F_{IR}^x = O(1) \quad F_{IR}^y = O(\varepsilon) \quad F_{IR}^z = O(\varepsilon)$$
$$M_{IR}^x = O(\varepsilon^2) \quad M_{IR}^y = O(\varepsilon) \quad M_{IR}^z = O(\varepsilon) \qquad (3.3.21)$$

3.3.4 The Blade Torsion Equation of Motion

The torsion equation of motion for each blade is obtained by the moment equilibrium about the pitch axis, that is

$$M_A^{pitch}+M_I^{pitch}+M_E^{pitch}=0 \qquad (3.4.1)$$

The inertial pitch moment about the feathering axis is

$$M_I^{pitch}=\int_0^{R-e_p}[q_I^x+(\beta_p-\beta_G)q_I^z-\beta_{sw}q_I^y]d_x \qquad (3.4.2)$$

$$M_A^{pitch}=\int_0^{R-e_p} Md_x \qquad (3.4.3)$$

$$M_E^{pitch}=-K_\phi\phi \qquad (3.4.4)$$

K_ϕ is the stiffness of the blade pitch control link system

M_I^{pitch},M_A^{pitch} after using the ordering sheme are listed in Appendix 3E.

3.3.5 The Equations of Motion of the Nacelle and Rotor

We have obtained the resultant forces and resultant moments transmitted to the nacelle due to both aerodynamic loads and inertial loads of a blade in section (3.3.3).

Therfore, the total loads transmitted to nacelle from a blade are:

Force : $\vec{F}_R=\vec{F}_{IR}+\vec{F}_{AR}$

$$=(F_{IR}^x+F_{AR}^x)\vec{i}_{2g}+(F_{IR}^y+F_{AR}^y)\vec{j}_{2g}+(F_{IR}^z+F_{AR}^z)\vec{k}_{2g}$$

$$=F_R^x\vec{i}_{2g}+F_R^y\vec{j}_{2g}+F_R^z\vec{k}_{2g} \qquad (3.5.1)$$

Moment : $\vec{M}_R=\vec{M}_{IR}+\vec{M}_{AR}$

$$=(M_{IR}^x+M_{AR}^x)\vec{i}_{2g}+(M_{IR}^y+M_{AR}^y)\vec{j}_{2g}+(M_{IR}^z+M_{AR}^z)\vec{k}_{2g}$$

$$=M_R^x\vec{i}_{2g}+M_R^y\vec{j}_{2g}+M_R^z\vec{k}_{2g} \qquad (3.5.2)$$

Rewriting these loads in $x_{1g}y_{1g}z_{1g}$ system using the relations in Appendix 3A .

$$\vec{F}_R=(F_R^x\cos\psi-F_R^y\sin\psi)\vec{i}_{1g}+(F_R^x\sin\psi+F_R^y\cos\psi)\vec{j}_{1g}+F_R^z\vec{k}_{1g}$$

$$\vec{M}_R=(M_R^x\cos\psi-M_R^y\sin\psi)\vec{i}_{1g}+(M_R^x\sin\psi+M_R^y\cos\psi)\vec{j}_{1g}+M_R^z\vec{k}_{1g}$$

The total loads transmitted from the whole rotor (N blades) to the nacelle are

$$\vec{P}_R=\sum_{k=1}^{N}\vec{F}_R=P_R^x\vec{i}_{1g}+P_R^y\vec{j}_{1g}+P_R^z\vec{k}_{1g} \qquad (3.5.5)$$

$$\vec{Q}_R=\sum_{k=1}^{N}\vec{M}_R=Q_R^x\vec{i}_{1g}+Q_R^y\vec{j}_{1g}+Q_R^z\vec{k}_{1g} \qquad (3.5.6)$$

These results are in detail listed in Appendix 3C.

Therefore the rotor equations of motion are :

$$Q_R^x-K_{\beta_c}\beta_{Gc}-C_{\beta c}\dot{\beta}_{Gc}=0 \qquad (3.5.7)$$

$$Q_R^y-K_{\beta_s}\beta_{Gs}-C_{\beta s}\dot{\beta}_{Gs}=0 \qquad (3.5.8)$$

K_{β_s},K_{β_c} ,$C_{\beta s}$,$C_{\beta c}$ are respectively the rotor gimbal hinge restraint stiffness and the damping coefficients in pitch and yawing directions.

Transmitting these loads to the centre of gravity of the nacelle again, we obtain the resultant forces applied on gravity centre and the resultant moments about the gravity centre :

$$\vec{P}_G=\vec{P}_R=P_R^x\vec{i}_{1g}+P_R^y\vec{j}_{1g}+P_R^z\vec{k}_{1g} \qquad (3.5.9)$$

$$\vec{Q}_G=\vec{Q}_R+(l_x\vec{i}_{1g}+l_y\vec{j}_{1g}+l_z\vec{k}_{1g})\times\vec{P}_R$$

$$=\vec{Q}_R+(l_yP_R^z-l_zP_R^y)\vec{i}_{1g}+(l_zP_R^x-l_xP_R^z)\vec{j}_{1g}+(l_xP_R^y-l_yP_R^x)\vec{k}_{1g} \qquad (3.5.10)$$

Where l_x , l_y , l_z are the position coordinates of the gimbal centre relative to the centre of gravity.

And rewriting $\vec{P}_G$ in $x_gy_gz_g$ system

$$\vec{P}_G=[P_R^x+(\theta_x\theta_y-\theta_z)P_R^y+(\theta_y+\theta_x\theta_z)P_R^z]\vec{i}_g+[P_R^x\theta_z+P_R^y+(\theta_y\theta_z-\theta_x)P_R^z]\vec{j}_g$$

$$+[-\theta_yP_R^x+\theta_xP_R^y+P_R^z]\vec{k}_g \qquad (3.5.11)$$

Finally, we can obtain the nacelle equations of motion according to the force and moment, they are:

The translational equations of motion

$$M_{Na}(\ddot{R}_x\vec{i}_g+\ddot{R}_y\vec{j}_g+\ddot{R}_z\vec{k}_g)=\vec{P}_G+\vec{P}_E \qquad (3.5.12)$$

The rotational motion equations are:

$$Q_E^x+Q_R^x+(l_yP_R^z-l_zP_R^y)=\dot{\Delta}_xI_{xx}+\Delta_y\Delta_z(I_{zz}-I_{yy})+I_{xy}(\Delta_z\Delta_x-\dot{\Delta}_y)-I_{xz}(\dot{\Delta}_z+\Delta_y\Delta_x)$$
$$-I_{yz}(\Delta_y^2-\Delta_z^2) \qquad (3.5.13)$$

$$Q_E^y+Q_R^y+(l_zP_R^x-l_xP_R^z)=\dot{\Delta}_yI_{yy}+\Delta_z\Delta_x(I_{xx}-I_{zz})+I_{yz}(\Delta_y\Delta_x-\dot{\Delta}_z)-I_{xy}(\dot{\Delta}_x+\Delta_z\Delta_y)$$
$$-I_{xz}(\Delta_z^2-\Delta_x^2) \qquad (3.5.14)$$

$$Q_E^z+Q_R^z+(l_xP_R^y-l_yP_R^x)=\dot{\Delta}_zI_{zz}+\Delta_y\Delta_x(I_{yy}-I_{xx})+I_{xz}(\Delta_z\Delta_y-\dot{\Delta}_x)-I_{yz}(\dot{\Delta}_y+\Delta_z\Delta_x)$$
$$-I_{xy}(\Delta_x^2-\Delta_y^2) \qquad (3.5.15)$$

Where, $\begin{bmatrix} I_{xx} & I_{xy} & I_{xz} \\ & I_{yy} & I_{yz} \\ & & I_{zz} \end{bmatrix}$ is inertia tensor of the nacelle

$$\vec{\omega}_{na}=\Delta_x\vec{i}_{1g}+\Delta_y\vec{j}_{1g}+\Delta_z\vec{k}_{1g} \qquad (3.5.16)$$

$$\Delta_x=\Omega(\dot{\theta}_x-\theta_y\dot{\theta}_z) \qquad \Delta_y=\Omega(\dot{\theta}_y+\theta_x\dot{\theta}_z) \qquad \Delta_z=\Omega(\dot{\theta}_z-\theta_x\dot{\theta}_y)$$

$$\dot{\Delta}_x=\Omega^2(\ddot{\theta}_x-\dot{\theta}_y\dot{\theta}_z-\theta_y\ddot{\theta}_z) \quad \dot{\Delta}_y=\Omega^2(\ddot{\theta}_y+\dot{\theta}_x\dot{\theta}_z+\theta_x\ddot{\theta}_z) \quad \dot{\Delta}_z=\Omega^2(\ddot{\theta}_z-\dot{\theta}_x\dot{\theta}_y-\theta_x\ddot{\theta}_y) \qquad (3.5.17)$$

Replacing (3.5.17) into (3.5.13) through (3.5.15), then :

$$Q_E^x+Q_R^x+(l_yP_R^z-l_zP_R^y)=\Omega^2[I_{xx}(\ddot{\theta}_x-\dot{\theta}_y\dot{\theta}_z-\theta_y\ddot{\theta}_z)+(I_{zz}-I_{yy})(\dot{\theta}_y\dot{\theta}_z-\theta_x\dot{\theta}_y^2+\theta_x\dot{\theta}_z^2)$$
$$-I_{xy}(\ddot{\theta}_y+\theta_x\ddot{\theta}_z)\ -I_{xz}(\ddot{\theta}_z-\theta_x\ddot{\theta}_y)-I_{yz}(\dot{\theta}_y^2-\dot{\theta}_z^2)] \qquad (3.5.18)$$

$$Q_E^y+Q_R^y+(l_zP_R^x-l_xP_R^z)=\Omega^2[I_{yy}(\ddot{\theta}_y-\dot{\theta}_x\dot{\theta}_z-\theta_x\ddot{\theta}_z)+(I_{xx}-I_{zz})(\dot{\theta}_x\dot{\theta}_z-\theta_x\dot{\theta}_x\dot{\theta}_y-\theta_y\dot{\theta}_z^2)$$
$$+I_{yz}(2\dot{\theta}_x\dot{\theta}_y-\ddot{\theta}_z+\theta_x\ddot{\theta}_y)\ -I_{yx}(\ddot{\theta}_x-\theta_y\ddot{\theta}_z)$$
$$-I_{zx}(\dot{\theta}_z^2-\dot{\theta}_x^2-2\theta_x\dot{\theta}_y\dot{\theta}_z+2\dot{\theta}_x\theta_y\dot{\theta}_z)] \qquad (3.5.19)$$

$$Q_E^z+Q_R^z+(l_xP_R^y-l_yP_R^x)=\Omega^2[I_{zz}(\ddot{\theta}_z-\dot{\theta}_x\dot{\theta}_y-\theta_x\ddot{\theta}_y)+(I_{yy}-I_{xx})(\dot{\theta}_x\dot{\theta}_y+\theta_x\dot{\theta}_x\dot{\theta}_z-\theta_y\dot{\theta}_y\dot{\theta}_z)$$
$$+I_{xz}(2\dot{\theta}_z\dot{\theta}_y-\ddot{\theta}_x+\theta_y\ddot{\theta}_z)-I_{yz}(\ddot{\theta}_y+\dot{\theta}_x\dot{\theta}_z+\theta_x\ddot{\theta}_z)$$
$$-I_{xy}(\dot{\theta}_x^2-\dot{\theta}_y^2-2\dot{\theta}_x\theta_y\dot{\theta}_z-2\theta_x\dot{\theta}_y\dot{\theta}_z)] \qquad (3.5.20)$$

Where, $\vec{P}_E$, Q_E^x, Q_E^y, Q_E^z are respectively the forces applied on the nacelle and moments acting about the nacelle centre of gravity due to nacelle's spring restraints with the wing.

Assume the position vector of spring restraint point relative to the nacelle gravity centre is (Before perturbation) (Fig 3.9)

$$\vec{R}_E^0 = e_x \vec{i}_g + e_y \vec{j}_g + e_z \vec{k}_g \qquad (3.5.21)$$

The displacement vector of the gravity centre is (Fig 3.9)

$$\vec{R}_0 = R_x \vec{i}_g + R_Y \vec{j}_g + R_z \vec{k}_g \qquad (3.5.22)$$

Then the displacement vector of the restraint point is

$$\vec{R}_E = -\vec{R}_E^0 + \vec{R}_0 + \vec{H}$$

$$= [R_x + e_y(\theta_x\theta_y - \theta_z) + e_z(\theta_y + \theta_x\theta_z), R_y + e_x\theta_z + e_z(\theta_y\theta_z - \theta_x),$$

$$R_z - e_x\theta_y + e_y\theta_x] \begin{Bmatrix} i_g \\ j_g \\ k_g \end{Bmatrix}$$

$$= x_e \vec{i}_g + y_e \vec{j}_g + z_e \vec{k}_g \qquad (3.5.23)$$

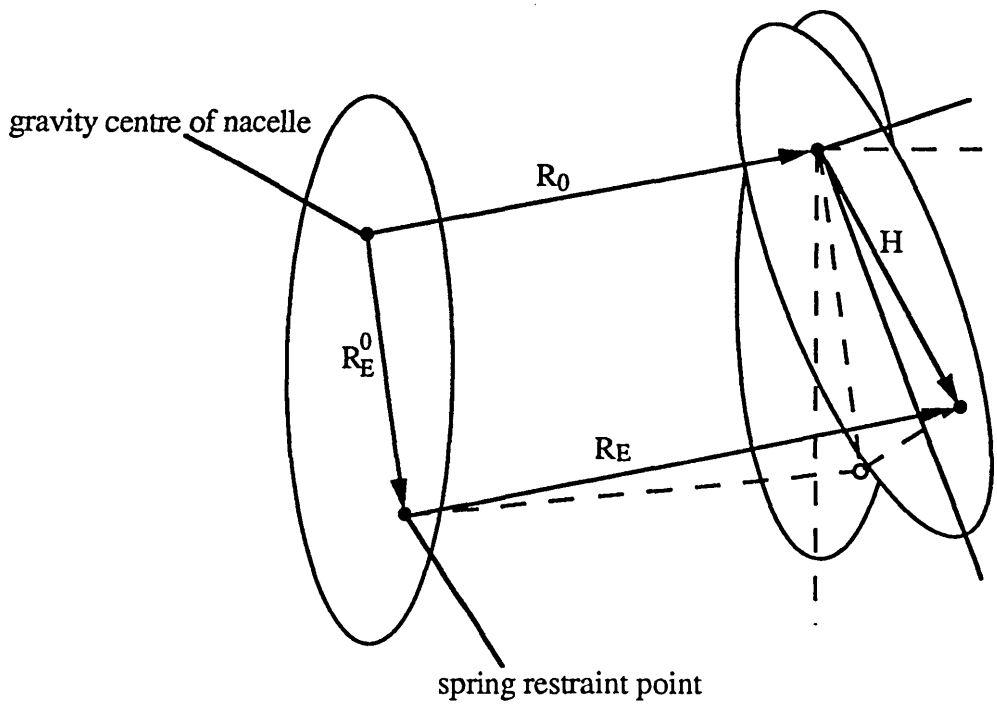

Fig 3.9 Displacement of spring restraint point between nacelle and wing

Therefore, $\vec{P}_E=-K_x x_e \vec{i}_g-K_y y_e \vec{j}_g-K_z z_e \vec{k}_g$ (3.5.24)

$$\vec{Q}_E=\vec{Q}_E^{e}+(e_x \vec{i}_{1g}+e_y \vec{j}_{1g}+e_z \vec{k}_{1g})\times\vec{P}_E \qquad (3.5.25)$$

$$\begin{aligned}\vec{Q}_E^{e}=&-K_{\theta x}(-\theta_y\theta_z+\theta_x)\vec{i}_g-K_{\theta y}(\theta_y+\theta_x\theta_z)\vec{j}_g-K_{\theta z}(-\theta_x\theta_y+\theta_z)\vec{k}_g\\ =&[-K_{\theta x}(-\theta_y\theta_z+\theta_x)-K_{\theta y}(\theta_y+\theta_x\theta_z)\theta_z+K_{\theta z}(-\theta_x\theta_y+\theta_z)\theta_y\\ &-K_{\theta y}(\theta_y+\theta_x\theta_z)-K_{\theta z}(-\theta_x\theta_y+\theta_z)\theta_x-K_{\theta x}(-\theta_y\theta_z+\theta_x)(\theta_x\theta_y-\theta_z)\\ &-K_{\theta z}(-\theta_x\theta_y+\theta_z)-K_{\theta x}(-\theta_y\theta_z+\theta_x)(\theta_y+\theta_x\theta_z)\\ &-K_{\theta y}(\theta_y+\theta_x\theta_z)(\theta_y\theta_z-\theta_x)]\begin{Bmatrix} i_{1g}\\ j_{1g}\\ k_{1g}\end{Bmatrix}\end{aligned} \qquad (3.5.26)$$

Writing $\vec{P}_E$ in equation (3.2.24) in the x_{1g} y_{1g} z_{1g} system :

$$\begin{aligned}\vec{P}_E=&[-K_x x_e-K_y y_e\theta_z+K_z z_e\theta_y,-K_y y_e-K_x x_e(\theta_x\theta_y-\theta_z)-K_z z_e\theta_x,\\ &-K_z z_e-K_x x_e(\theta_y+\theta_x\theta_z)-K_y y_e(\theta_y\theta_z-\theta_x)]\begin{Bmatrix} i_{1g}\\ j_{1g}\\ k_{1g}\end{Bmatrix}\end{aligned} \qquad (3.5.27)$$

Finally combining the relations (3.5.26) and (3.5.27) to obtain $\vec{Q}_E$.

Applying the ordering scheme to neglect the higher order terms, then we determine the moments about the nacelle gravity centre due to the restraint springs,

$$\vec{Q}_E=Q_E^x\vec{i}_{1g}+Q_E^y\vec{j}_{1g}+Q_E^z\vec{k}_{1g} \qquad (3.5.28)$$

Where,

$$\begin{aligned}Q_E^x=&-K_{\theta x}\theta_x-e_yK_z(R_z-e_x\theta_y+e_y\theta_x)+e_zK_y(R_y+e_x\theta_z-e_z\theta_x)\\ Q_E^y=&-K_{\theta y}\theta_y-e_zK_x(R_x-e_y\theta_z+e_z\theta_y)+e_xK_z(R_z-e_x\theta_y+e_y\theta_x)\\ Q_E^z=&-K_{\theta z}\theta_z-e_xK_y(R_y+e_x\theta_z-e_z\theta_x)+e_yK_x(R_x-e_y\theta_z+e_z\theta_y)\end{aligned} \qquad (3.5.29)$$

The nacelle equations of motion are obtained by applying (3.5.5–6), (3.5.27), and (3.5.29) to (3.5.12) and (3.5.18–20).

Note that the relations between displacements of nacelle's gravity centre and displacements of gimbal centre are:

$$\begin{Bmatrix} x_g \\ y_g \\ z_g \end{Bmatrix} = \begin{bmatrix} 1 & 0 & 0 & 0 & l_z & -l_y \\ 0 & 1 & 0 & -l_z & 0 & l_x \\ 0 & 0 & 1 & l_y & -l_x & 0 \end{bmatrix} \begin{Bmatrix} R_x \\ R_y \\ R_z \\ \theta_x \\ \theta_y \\ \theta_z \end{Bmatrix} \qquad (3.5.30)$$

Therefore, the variables x_g, y_g, z_g in the previous expressions for forces and moments can be expressed in terms of the variables R_x, R_y, R_z, θ_x, θ_y, θ_z. These are adopted as the six degrees of freedom associated with the nacelle's rigid body motion in the final equations of motion of the system.

These equations of motion are for a universal joint rotor configuration. The formulation of the equations for an ideal gimbal configuration are introduced in section 4.4.4.

CHAPTER 4 A TILT-ROTOR/NACELLE WHIRL FLUTTER MODEL---SOLUTION AND NUMERICAL RESULTS

4.1 INTRODUCTION

In the previous chapter the equations of motion for the coupled tilt-rotor/nacelle system have been derived. They consist of six rigid body equations of motion of the nacelle, two equilibrium equations for the two degrees of freedom of the universal joint, and N blade torsion equations of motion for the N blades. These coupled equations of motion can be used to obtain the stability solution of the system. That is, the whirl flutter characteristics of the system. We shall firstly introduce the solution procedure of the problem in section 2. Then, two groups of numerical results are presented in section 4. In the last section, some conclusions are drawn from the whirl flutter model.

4.2 SOLUTION PROCEDURE

We have obtained 12 dynamic equations for the coupled tilt-rotor/nacelle system in chapter 3. These equations are nonlinear ordinary differential equations. To obtain the system stability, the solution procedure consists of the following steps:

1) linearising the nonlinear equations,
2) transforming the linearised equations with periodic coefficients to linearised equations with constant coefficients by applying multiblade coordinate transformation relation,
3) evaluating the eigenvalues of the linearised equations with constant coefficients to analyse the system stability. These steps are discussed below.

The linearisation of the nonlinear differential equations is undertaken by assuming that the motion of the system degrees of freedom consists of two parts, the first part is the steady state equilibrium value and the second is the small perturbational motion of the system about the equilibrium position. It should be pointed out that the degrees of freedom associated with the nacelle and gimbal motions are essentially perturbational

quantities. Therefore, only the blade torsion degrees of freedom have both the steady state value and the perturbational value. These can be expressed as :

$$\phi = \phi_0 + \Delta\phi \tag{2.1}$$

Substituting equation (2.1) into the blade torsion equation of motion and the equations of motion for the nacelle and universal joint degrees of freedom which were obtained in the previous chapter gives us an algebraic equation for the equilibrium value of the blade torsion:

$$f(\phi_0) = 0 \tag{2.2}$$

and a set of linearised perturbation differential equation which can be written in matrix form:

$$[M(\phi_0)]\{\ddot{q}\} + [C(\phi_0)]\{\dot{q}\} + [K(\phi_0)]\{q\} = 0 \tag{2.3}$$

where {q} represents all the degrees of freedom of the coupled tilt-rotor/nacelle system. We note that [M], [C], [K] matrices are functions of ϕ_0 which is the equilibrium value solved from (2.2). They also contain some periodic coefficients $\sin\psi$, $\cos\psi$, where $\psi=\Omega t$ is the blade azimuth angle. One usually applies a transformation relation, known as a multiblade coordinate transformation, to eliminate the time dependent coefficients for the coupled rotor/body aeroelasticity stability analysis in an axial flow state.

The multiblade coordinate transformation is implemented by applying the following operators to the blade torsion equations (3.4.1) in the previous chapter :

$\frac{1}{N}\sum_{k=1}^{N}(.....)$ collective operator

$\frac{1}{N}\sum_{k=1}^{N}(-1)^k(.....)$ alternative operator

$$\frac{1}{N}\sum_{k=1}^{N}\cos n\psi_k(.....) \qquad \text{n-cosine operator}$$

$$\frac{1}{N}\sum_{k=1}^{N}\sin n\psi_k(.....) \qquad \text{n-sine operator} \qquad (2.4)$$

where N is the number of blades and n=1, ...m, m=(N-1)/2 (for odd N), or m=(N-2)/2 (for even N). These are similar to cyclic symmetry coordinates applied to cyclically symmetric structures.

Then utilising the multiblade coordinate transformation relation listed in appendix 4A to the blade torsion equation, and to the forces and moments transmitted from the rotor to the universal joint and nacelle, we can obtain the blade torsion equations and the equations for the nacelle and universal joint degrees of freedom expressed in the multiblade coordinates. The application of the operator in (2.4) to the blade torsion equation is straightforward and results in N equations of motion expressed in the multiblade coordinates. Appendix 3C lists the forces and moments transmitted from the rotor to the nacelle written in the multiblade coordinates. Finally, we have 12 coupled equations of motion for the tilt-rotor/nacelle system written in the multiblade coordinates:

$$[M]\{\ddot{x}\} + [C]\{\dot{x}\} + [K]\{x\} = 0 \qquad (2.5)$$

where $\{x\} = [R_x, R_y, R_z, \theta_x, \theta_y, \theta_z, \beta_{Gs}, \beta_{Gc}, \phi_c, \phi_{1s}, \phi_{1c}, \phi_{al}]$

Therefore, to obtain the stability solution of the system, the algebraic equation (2.2) is firstly solved for the equilibrium value ϕ_0, and then ϕ_0 is substituteed into the matrices [M], [C], [K] in equation (2.5), subsequently, the eigenvalue problem associated with equation (2.5) is solved. This gives either real eigenvalues or complex conjugate pairs of eigenvalues as :

$$\lambda_i = \sigma_i + i\omega_i \qquad (2.6)$$

σ_i reflects the system mode damping and hence the stability, ω_i represents the mode frequencies. The system is stable when σ_i is negative, otherwise an instability occurs

4.3 PROGRAMMING STRUCTURE

The above algorithm is coded into a FORTRAN program to numerically assess the whirl flutter problems of tilt-rotor aircraft. Two different rotor hub configurations are considered. One of them has a conventional universal joint connection between the rotor and nacelle. The other has an ideal gimbal connection. The whirl flutter characteristics of the ideal gimbal rotor configuration has not been found in any previous publications. The configuration data of both of the tilt-rotors include the gimbal undersling, blade pitch bearing offset, blade precone angle, blade pitch bearing sweep angle, blade sectional mass centre offset and aerodynamic centre offset. The induced velocity is assumed uniform over the rotor and calculated based on the formulae :

$$v_i = \frac{\sigma a}{16}\left(-1+\sqrt{1+\frac{24\theta_0}{\sigma a}}\right)$$

where σ is the solidity of the rotor, a is the lift curve slope, θ_0 is the blade collective pitch angle at 3/4 radius of the blade.

The integrals of blade properties along with the blade length is numerically evaluated based on a four-point finite difference formulae [NAG Library]. The algebraic equation for the torsion equilibrium value is explicitly written out and computed. The equilibrium value is subsequently replaced into the nonlinear differential equations of motion to obtain the mass, damping and stiffness matrices. The second order differential equations are transformed to equivalent first order state equations. The eigenvalue problem $[A]\{x\}=\lambda[B]\{x\}$ associated with this set of state equations are solved using the QZ algorithm [NAG Library]. The flutter characteristics can be analysed from the system eigenvalues. The flow chart of this program is presented below.

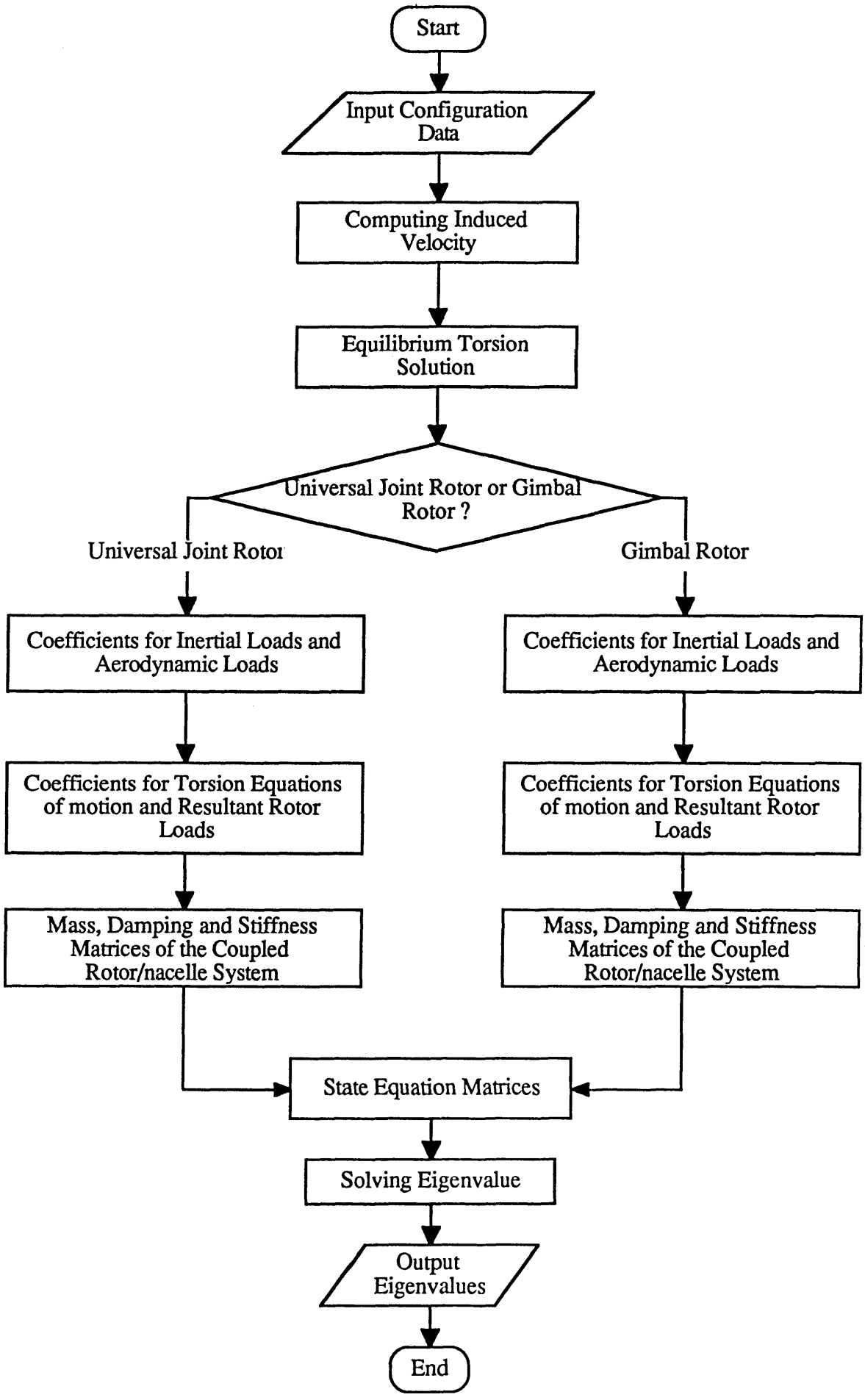
Start
Input Configuration Data
Computing Induced Velocity
Equilibrium Torsion Solution
Universal Joint Rotor or Gimbal Rotor ?
Universal Joint Rotor
Gimbal Rotor
Coefficients for Inertial Loads and Aerodynamic Loads
Coefficients for Inertial Loads and Aerodynamic Loads
Coefficients for Torsion Equations of motion and Resultant Rotor Loads
Coefficients for Torsion Equations of motion and Resultant Rotor Loads
Mass, Damping and Stiffness Matrices of the Coupled Rotor/nacelle System
Mass, Damping and Stiffness Matrices of the Coupled Rotor/nacelle System
State Equation Matrices
Solving Eigenvalue
Output Eigenvalues
End

4.4 NUMERICAL RESULTS

Numerical results include two principal groups. The first one investigates a classical propeller whirl flutter model with two degrees of freedom of nacelle pitch and yaw, and a four degrees of freedom flap-hinged tilt-rotor whirl including two cyclic flap modes, nacelle pitch and yaw modes. Both of these have been studied both theoretically and experimentally in the literature [Reed and Bland, 1961, Bland and Bennett, 1963, Kvaternik and Kohn, 1977]. This part of the thesis is mainly aimed at confirming the validity of the present analytical model. The second group concentrates on a universal joint tilt-rotor and an ideal gimbal tilt-rotor whirl flutter characteristics.

4.4.1 A Two Degrees of Freedom Classical Whirl Flutter

(Basic Configuration Data Is Listed in Table 4.1)

Table 4.1

A Classical Propeller Whirl Flutter Model

Propeller inertia moment about rotation axis I_x=0.0116 kgm^2
Nacelle inertia moment about pitch or yaw axis I_y=0.086 kgm^2
Propeller radius R=0.257 m, Blade semi-chord b=0.0278 m
Air density ρ_a=1.132 kg/m^3, Blade pretwist θ_{tw}=-40° root to tip
Nacelle pitch and yaw frequency $\omega_{\theta x}=\omega_{\theta y}$=57.525 rad/sec
Blade mass per unit length m=0.513 kg/m

Fig 4.1,4.2 show typical graphs of the whirl mode frequencies and damping against propeller forward speed at a constant advance ratio $J=V_F/2nR=\pi V_F/\Omega R=1.8$. Two families of curves are given in Fig 4.1,4.2 for two aerodynamic models. The quasisteady aerodynamic model was used as described in the previous chapter. The so-called unsteady aerodynamic model approximates unsteady aerodynamic effect according to the

idea of Reed and Bland [1961] (p27). The phase lag angle of the aerodynamic force is approximately given a 10^0 value in the present calculation.

Also given in Fig 4.2 are the experimental result and analytical result based on the measured static derivatives published by Bland & Bennett [1963]. A good agreement is observed between the present model and those results from Bland & Bennett. The approximate unsteady aerodynamic model gives a better agreement than the quasisteady aerodynamic model.

Fig 4.3, 4.4 indicate the effect of the propeller pitch axis location on the whirl flutter. Fig 4.5 is taken from [Bland & Bennett, 1963] to show the effect of the propeller pitch axis location (l_z/R). The result was obtained based on the measured static derivatives. Fig 4.3 and 4.4 show an identical trend of the l_z/R effect to Fig 4.5. The approximate unsteady aerodynamics model (Fig 4.4) gives a better result than the quasi-steady aerodynamics model (Fig 4.3).

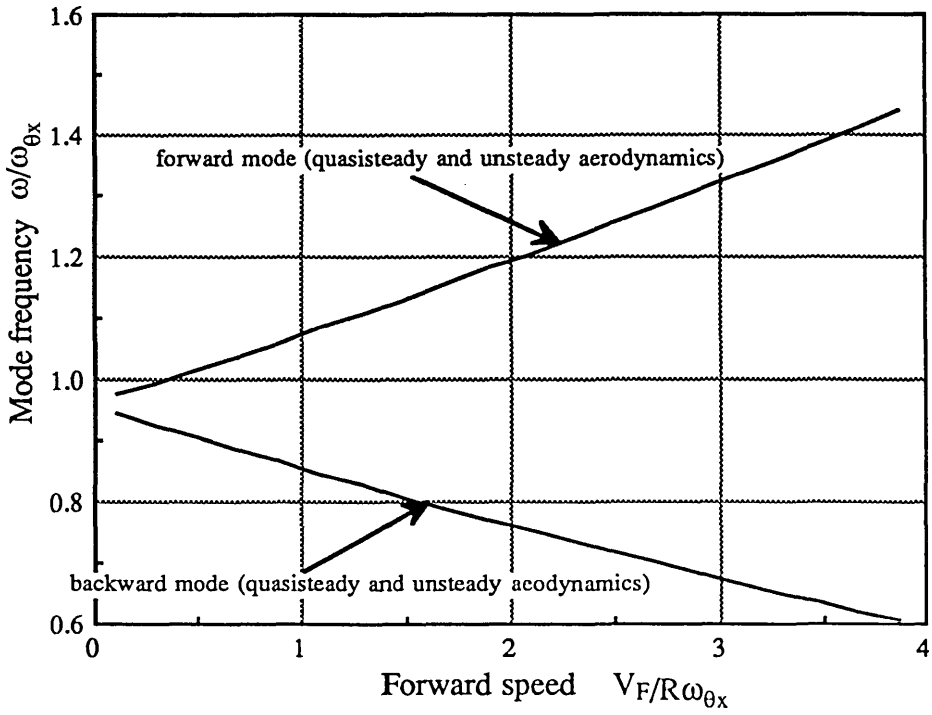

Fig 4.1 Typical variation of frequency with forward speed

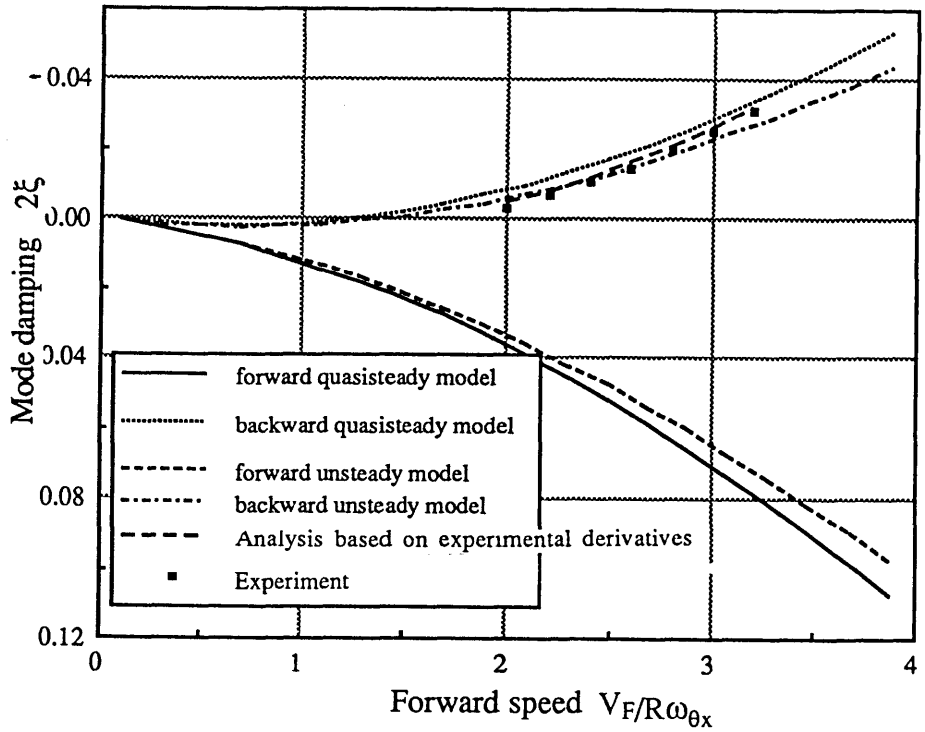

Fig 4.2 Typical variation of damping with forward speed

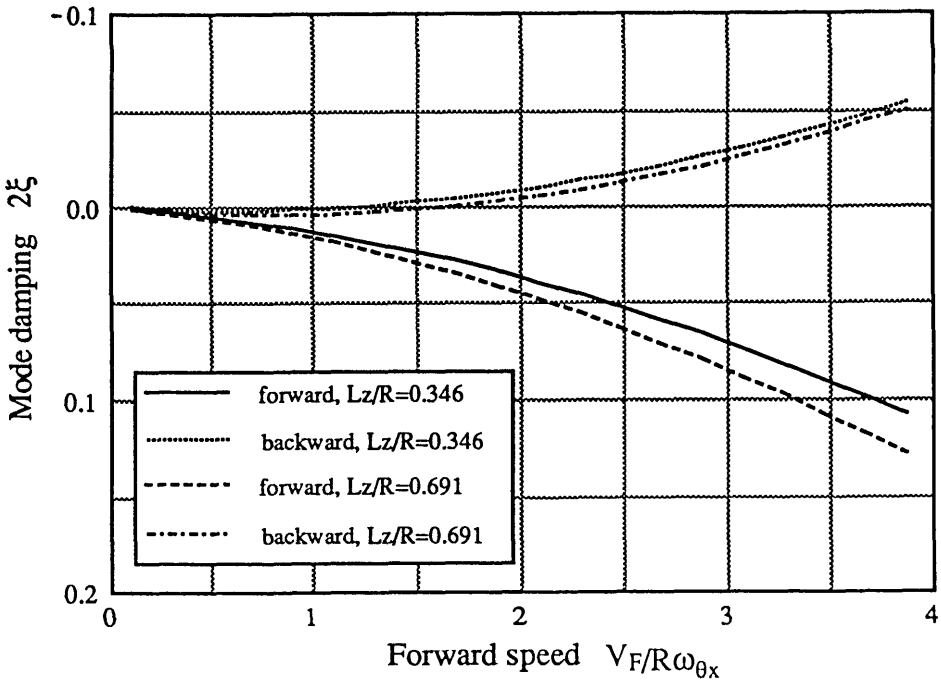

Fig 4.3 Effect of Lz/R on whirl flutter (quasisteady aerodynamics model)

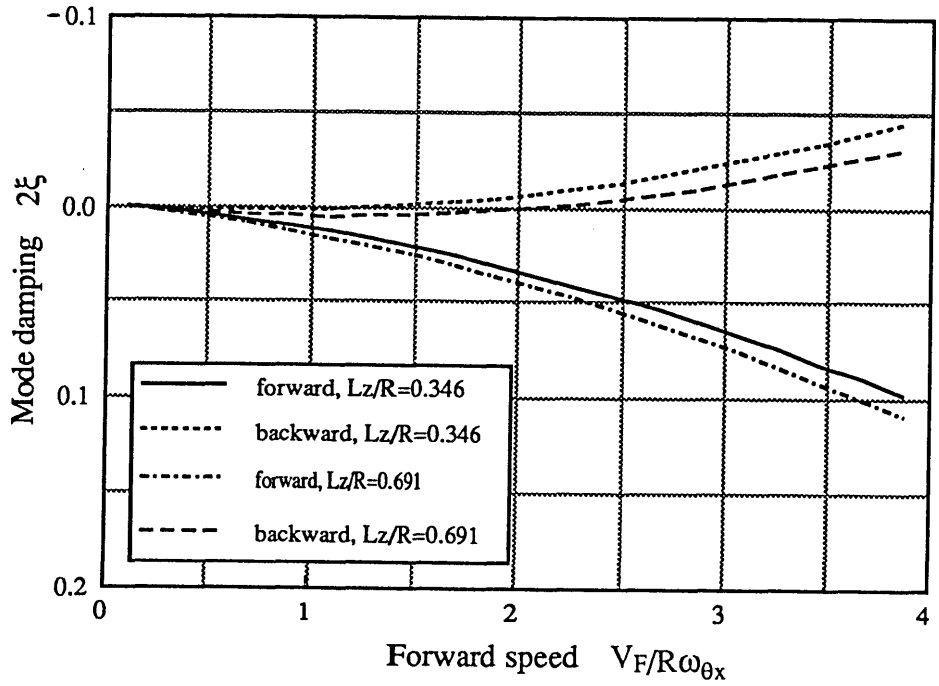

Fig 4.4 Effect of Lz/R on whirl flutter (unsteady aerodynamics model)

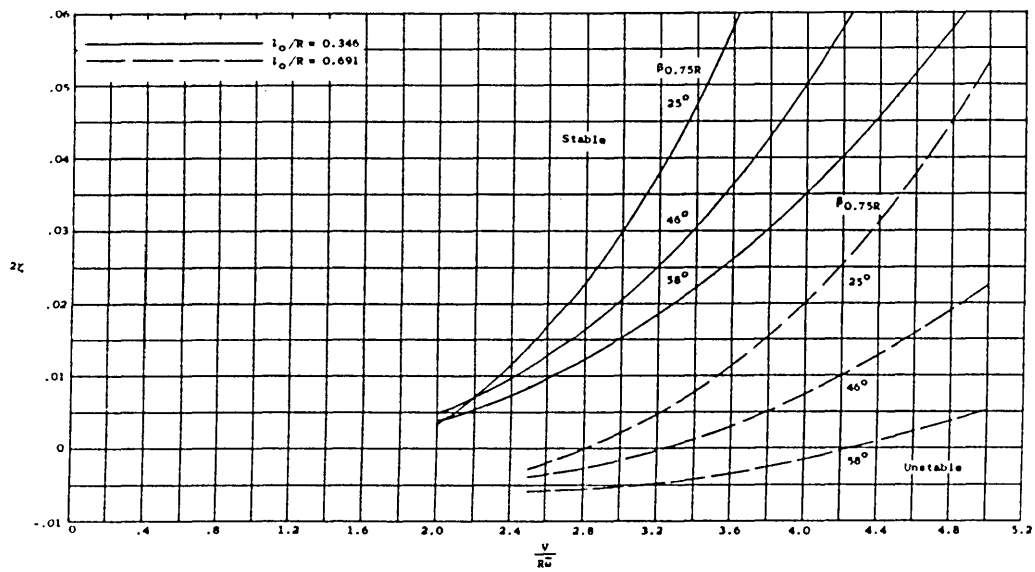

Fig 4.5 Effect of L_z/R on whirl flutter based on experimental static deribatives from Bland & Bennett, 1963

4.4.2 Four Degrees of Freedom Flap-hinged Tilt-rotor Whirl

(Basic Configuration Data Is Listed in Table 4.2)

Table 4.2

A Four Degrees of Freedom Tilt-rotor/pylon Whirl Flutter Model

Rotor: Rotor radius R=0.744 m, Semi-chord b=0.0451 m
Blade mass=0.533 kg, Flap hinge offset e_p/R=0.05
Blade pretwist=-23° root to tip, ρ_a=1.23 kg/m^3
Blade static moment about flapping hinge=0.111 kgm
Blade inertia moment about flapping hinge=0.0493 kgm^2
Distance from pylon pitch axis to rotor hub=0.32 m
Distance from pylon yaw axis to rotor hub=0.277 m
Pylon: Mass effective in pitch and yaw: 3.37 kg and 3.01 kg
Pitch and yaw inertia about gravity centre=0.0496, 0.0343 kgm^2
Distance from pylon pitch axis to gravity centre=0.212 m
Distance from yaw pitch axis to gravity centre=0.193 m

Kvaternik and Kohn [1977] published a group of experimental and analytical investigations of a flap-hinged proprotor. In the present analysis, the flap rotor is equivalent to a universal joint rotor using the relation in Kvaternik and Kohn's work (p30-32). The blade collective angle variation with rotor advance ratio is approximated by the inflow angle at 3/4 rotor radius plus 1 degree,

$$\theta_{0.75} = \mathrm{tg}^{-1}\frac{V_F}{0.75\Omega R} + 1^\circ$$

The computed whirl flutter speeds are listed in Table 4.3 and compared with the experimental and analytical results in Kvaternik and Kohn's work. Good agreements are

obtained. In Table 4.3, the results for theory 1 and theory 2 are two groups of analytical results taken from Kvaternik and Kohn's work [1977]. They correspond to Theory (ref.15) and Theory (ref.1) listed in Table III of that report, respectively.

Table 4.3

Comparison of a Four Degree of Freedom Flap-hinged Tilt-rotor Whirl

		Group 1				Group 2			
δ_3		30				20			
fp(Hz)		5.64				3.72			
fy(Hz)		5.54				3.82			
$2\zeta p$		0.019				0.008			
$2\zeta y$		0.041				0.031			
Ω (rad/sec)		50.27	68.49	86.71	99.27	50.27	63.46	89.22	95.5
	Experiment	0.78	0.55	0.41	0.38	0.68	0.44	0.34^+	0.34^-
Flutter V/ ΩR	Present	0.88	0.56	0.36	0.32	0.58	0.43	0.31	0.30
	Theory 1	0.86	0.54	0.37	0.31	0.74	0.50	0.38	0.36
	Theory 2	0.84	0.53	0.37	0.31	0.72	0.48	0.38	0.36
	Experiment	0.77	0.56	0.46	0.40	0.50	0.37	0.30	0.27
Flutter ω/Ω	Present	0.78	0.59	0.49	0.43	0.53	0.43	0.32	0.30
	Theory 1	0.79	0.58	0.47	0.41	0.50	0.37	0.30	0.28
	Theory 2	0.79	0.59	0.48	0.42	0.51	0.38	0.30	0.28

4.4.3 A Universal Joint Tilt-rotor Whirl Flutter

(Basic Configuration Data for the Universal Joint Tilt-rotor/nacelle and Gimbal Tilt-rotor/nacelle Models Is Listed in Table 4.4)

Table 4.4

A Universal Joint (or a Gimbal) Tilt-rotor/nacelle Configuration

R=5.6 m, b=0.27 m, Blade pitch bearing offset e_p=0.5 m
Blade torsional inertia=1.0 kgm^2, Nacelle G.C. to gimbal centre l_z=1.8 m
I_{xx}=1860 kgm^2, I_{zz}=144 kgm^2, K_ϕ=7.3x10^4 Nm/rad
K_β=2x10^5, K_x=4.1x10^8 N/m, K_y=1.8x10^9 N/m, K_z=2x10^6 N/m
$K_{\theta x}$=4.54x10^6 Nm/rad, $K_{\theta y}$=7.32x10^6 Nm/rad, $K_{\theta z}$=9x10^6 Nm/rad
Blade unit-length mass m=23.7 kg/m, Nacelle mass M=1800 kg
x_A=x_{Gc}=0, β_p=0.1 rad, β_{sw}=0, Rotor operating speed Ω=43.25
Blade pretwist=-40^o root to tip, ρ_a=1.225 kg/m^3

The dynamic characteristics of this universal joint tilt-rotor/nacelle system are shown in Fig 4.6, 4.7, which demonstrate the variation of the system eigenvalues with rotor rotation speed Ω at forward speed V_F=0. A structural damping of about 1.5% critical damping is added to nacelle pitch mode and nacelle x-translational mode in the computation. With the increase of Ω, the progressive flap mode frequency approaches to nacelle axial (z) translational mode, nacelle pitch mode, nacelle roll mode and nacelle vertical (x) translational mode frequencies (the nacelle z-translational mode and roll mode are not plotted). Frequency resonances are produced between the progressive flap mode and nacelle pitch mode, and between the progressive flap mode and nacelle x-translational mode. At resonance there are corresponding decreases in the progressive flap mode damping and increases in nacelle pitch mode and nacelle x-translational mode

dampings. This kind of resonance does not appear for the other two nacelle modes, because they are not coupled with the rotor flapping.

The analysis was initially done for the whole 12 degrees of freedom model. The results obtained were subsequently compared with those of the 6 degrees of freedom model which ignores the 4 blade torsion degrees of freedom, the nacelle axial (z) translational degree of freedom and nacelle roll degree of freedom (θ_z). z and θ_z degrees of freedom have no effect due to no coupling with the retained six degrees of freedom. The torsion degree of freedom is coupled with them and has some effect on the system damping, but its frequency is found to have a very high value in this analysis and blade section gravity centre is assumed to coincide with the elastic centre. Therefore, in subsequent investigation their effects are not considered, and the analyses are carried out for the 6 degrees of freedom model to get a more basic and clear understanding of the whirl flutter characteristics.

Fig 4.8, 4.9 show the variation of the system frequencies and damping with rotor forward speed at an operating rotation speed Ω=43.25 rad/sec. The nacelle side translational (y) mode and vertical translational (x) mode frequencies are not shown graphically because of their high values. Their total damping is very low because no structural damping was added in the computation and all of the damping was aerodynamic. The nacelle yaw mode damping increases with forward speed until a high inflow effect appears at about 280 m/sec, then the damping drops off very quickly and the mode goes unstable. Meanwhile, the regressive flap mode frequency approaches the nacelle yaw mode frequency at high inflow, this causes a damping increase in the former, and a decrease in the latter.

Fig 4.10, 4.11 show the effect of reducing the yaw stiffness to half the previous value. It is observed that the flutter speed is much lower than that in Fig 4.8, 4.9. The computed

results also indicate that the symmetric nacelle restraint stiffnesses are worse than non-symmetric ones. Obviously, the nacelle restraint stiffness has a significant effect on whirl flutter.

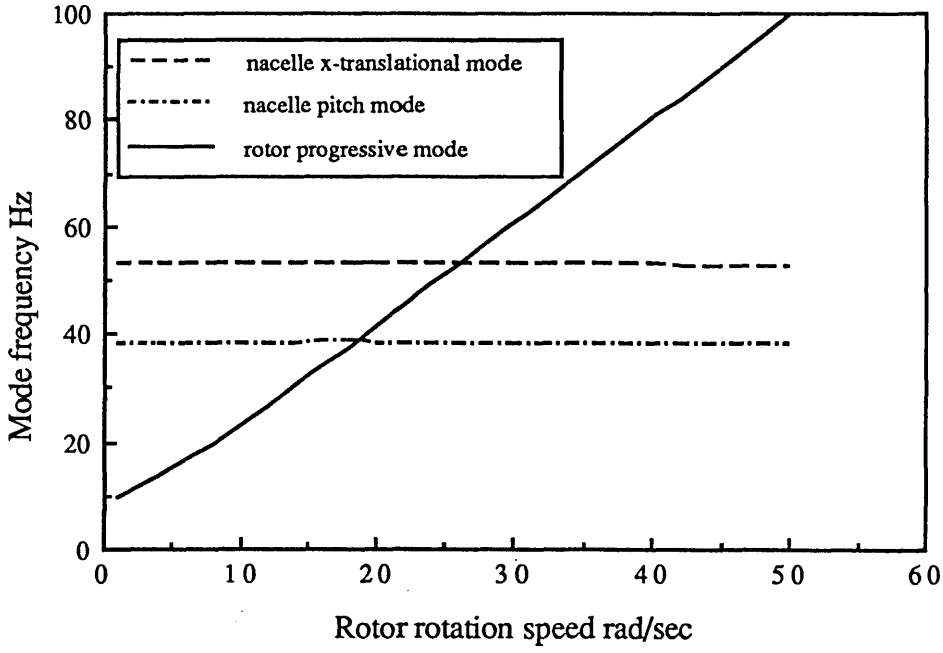

Fig 4.6 Mode frequencies vary with rotor rotation speed at VF=0 for a universal joint rotor

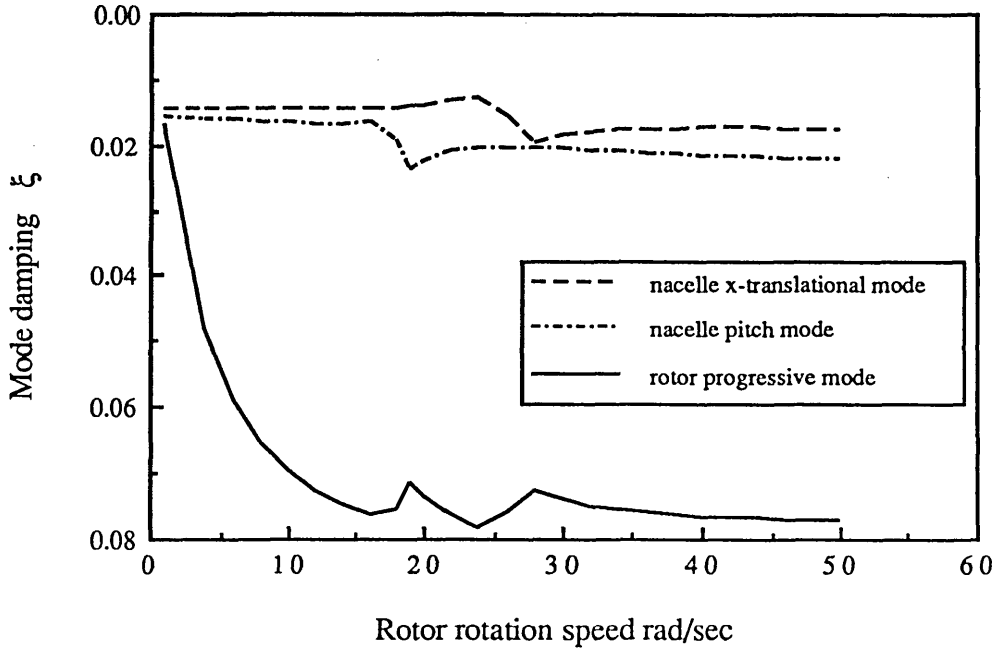

Fig 4.7 Mode dampings vary with rotor rotation speed at VF=0 for a universal joint rotor

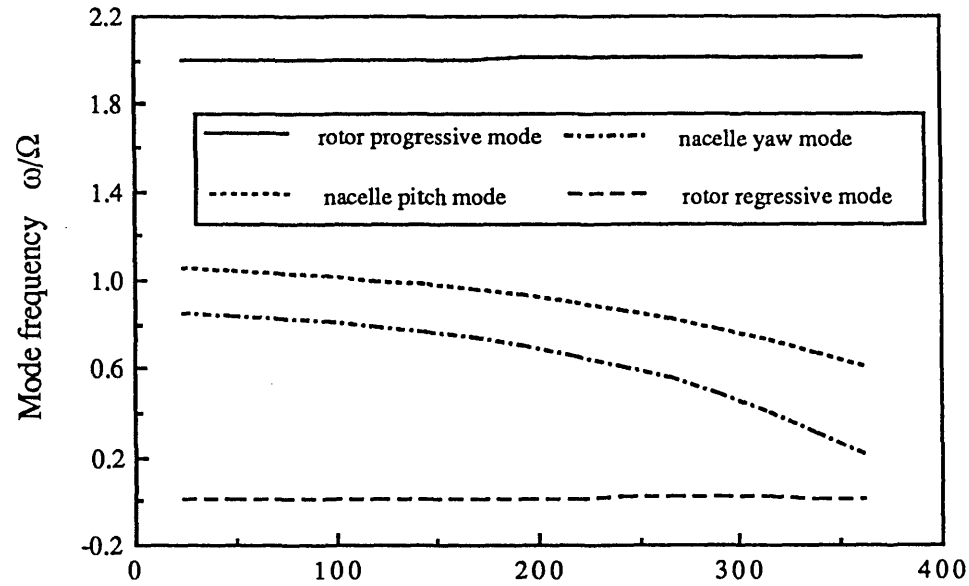

Fig 4.8 Variation of mode frequencies with forward velocity for a universal joint rotor

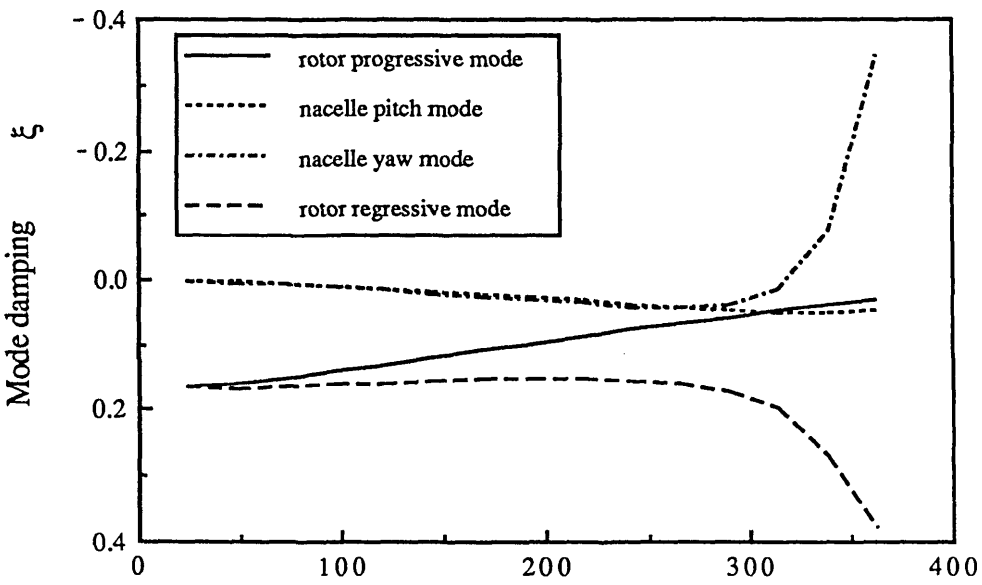

Fig 4.9 Variation of mode dampings with forward speed for a universal joint rotor

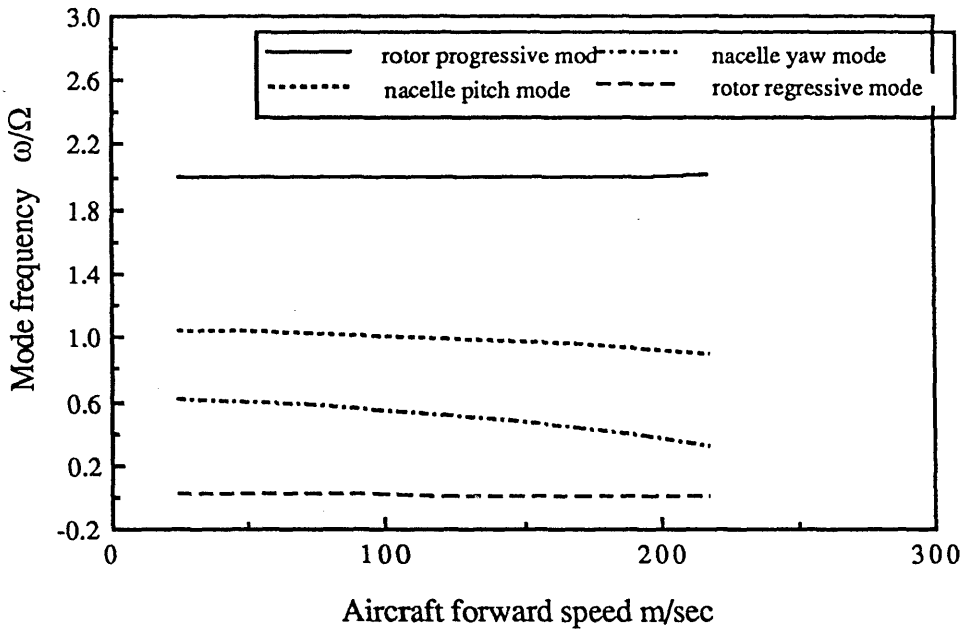

Fig 4.10 Variation of mode frequencies with forward speed
(reducing half nacelle's yaw stiffness of the universal joint rotor)

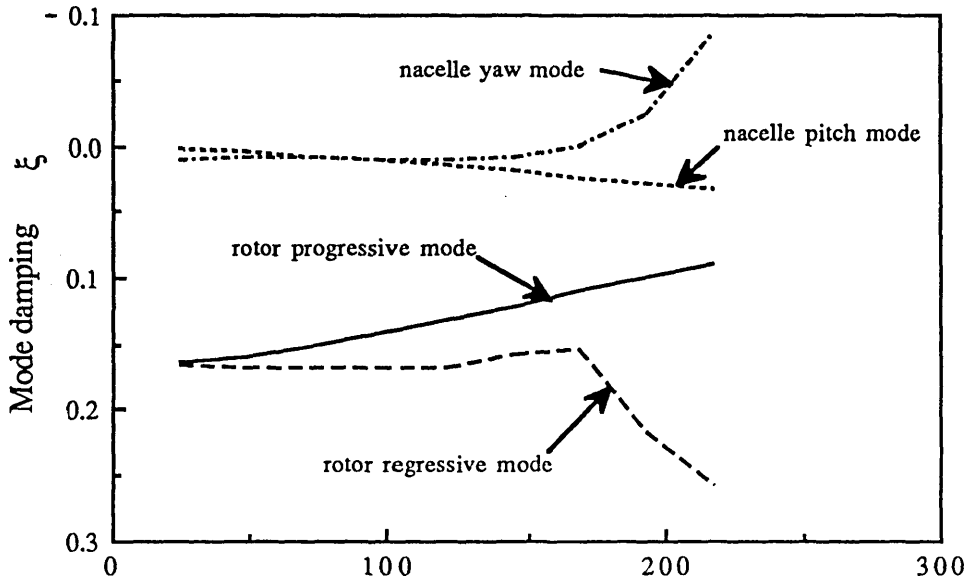

Fig 4.11 Variation of mode dampings with forward speed
(reducing half nacelle's yaw stiffness of the universal joint rotor)

4.4.4 An Ideal Gimbal Tilt-rotor Whirl Flutter

Another possible type of rotor has been proposed for use in the tilt-rotor aircraft. This type of rotor allows the rotation speed vector to tilt following the rotor gimbal motion.It is called a gimbal rotor in this thesis. An ideal gimbal rotor differs from a universal joint rotor in that the rotation speed vector of a gimbal rotor is fixed with the rotor and hence can tilt with the rotor gimbal degrees of freedom. For a universal joint rotor, the rotation speed vector is fixed with the nacelle and therefore can not tilt with the rotor (Fig 4.12).

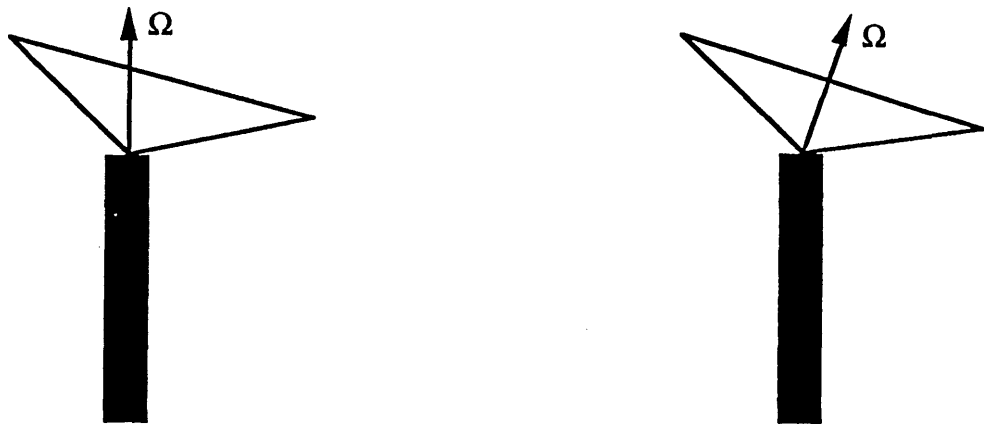

Fig 4.12 Difference between a universal joint rotor and a gimbal rotor

The equations of motion for the gimbal tilt-rotor/nacelle system can be developed following the procedure in chapter 3. It is important to recognise the main difference in the development of the equations of motion for these two systems is the coordinate transformation relation between $x_{1g}y_{1g}z_{1g}$ and $x_hy_hz_h$ systems due to the configuration difference. For the universal joint rotor, $x_hy_hz_h$ is obtained by firstly rotating $\psi=\Omega t$ about z_{1g} axis to $x_{2g}y_{2g}z_{2g}$ and then rotating α_G about x_{2g} and β_G about y_{2g} to $x_hy_hz_h$. While, for the ideal gimbal rotor, $x_hy_hz_h$ is obtained by firstly rotating β_{Gs} about y_{1g} and β_{Gc} about x_{1g} to $x_{2g}y_{2g}z_{2g}$ and then rotating $\psi=\Omega t$ about z_{2g} to $x_hy_hz_h$. Therefore, we can easily obtain the equations of motion for the gimbal tilt-rotor/nacelle system by making use of the equations of motion for the universal joint tilt-rotor/nacelle system obtained in

chapter 3. Replacing $\beta_G = \alpha_G = 0$, $\theta_x = \theta_x + \beta_{Gc}$, $\theta_y = \theta_y + \beta_{Gs}$, and the blade torsion $\phi = \phi + \phi_\Delta$ into the equations of motion obtained in the last chapter, the equations of motion for the gimbal tilt-rotor/nacelle system can be obtained, where ϕ_Δ is caused by the kinematic pitch/gimbal coupling and $\phi_\Delta = -(\beta_{Gs}\sin\psi + \beta_{Gc}\cos\psi)$. The final equations of motion are of the same form as for the universal joint tilt-rotor/nacelle system. The solution procedure introduced in 4.2 can be applied to solve the stability problem.

The whirl flutter problem of a gimbal tilt-rotor/nacelle system is investigated in the following results. The basic configuration data is the same as for the universal joint listed in Table 4.3.

As in Fig 4.6, 4.7, the dynamic characteristics of the ideal gimbal tilt-rotor are shown in Fig 4.13, 4.14, where the same amount of structural damping as in Fig 4.6, 4.7 is given to the nacelle x-translational and pitch mode. Similarly, the frequency resonances occur when the forward flap mode frequency coincides with the nacelle pitch mode and x-translational mode frequencies. This implies the existence of couplings between these modes in the gimbal rotor.

Fig 4.15, 4.16 show the variation of the frequencies and damping with rotor forward speed at the operating rotation speed Ω=43.25 rad/sec. Again, a similar phenomena to the universal joint one (Fig 4.8, 4.9) occurs. The nacelle pitch and yaw mode dampings are increased with forward speed until the high inflow effect appears, then the lower stiffness nacelle mode (yaw) swiftly goes unstable. But the critical forward velocity is a bit higher than that in Fig 4.8, 4.9.

Fig 4.17, 4.18 present the results after reducing half the nacelle yaw stiffness in Fig 4.15, 4.16. The flutter velocity is highly reduced comparing to Fig 4.15, 4.16 because of the stiffness reduction. However, this flutter velocity is still a bit higher than that of

the universal joint rotor under the same case (Fig 4.10, 4.11). Again, this means the nacelle restraint stiffnesses have significant effect on the whirl flutter of an ideal gimbal tilt-rotor.

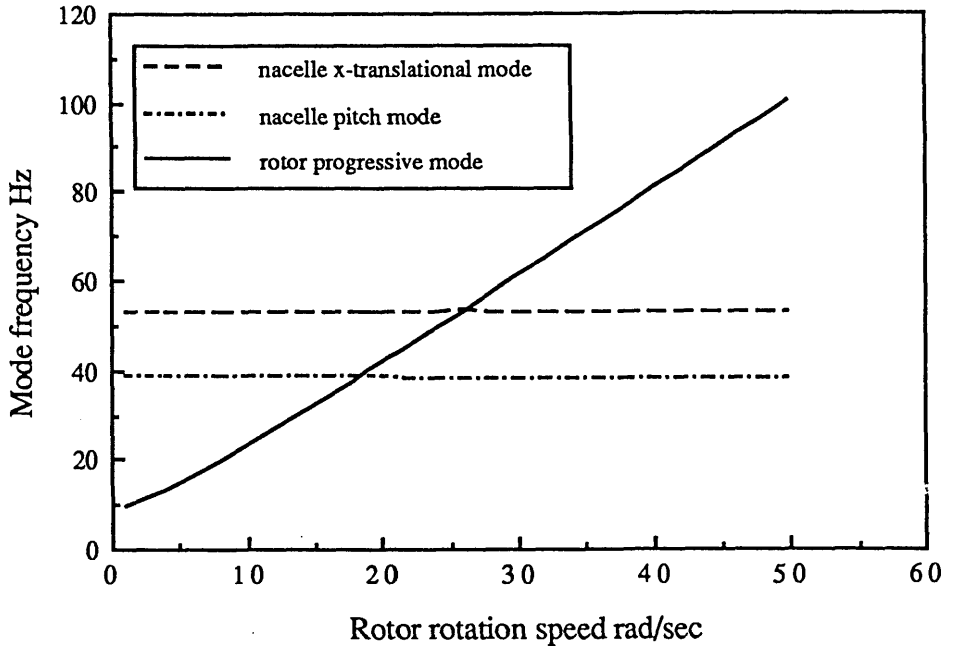

Fig 4.13 Mode frequencies vary with rotor rotation speed at VF=0 for a gimbal rotor

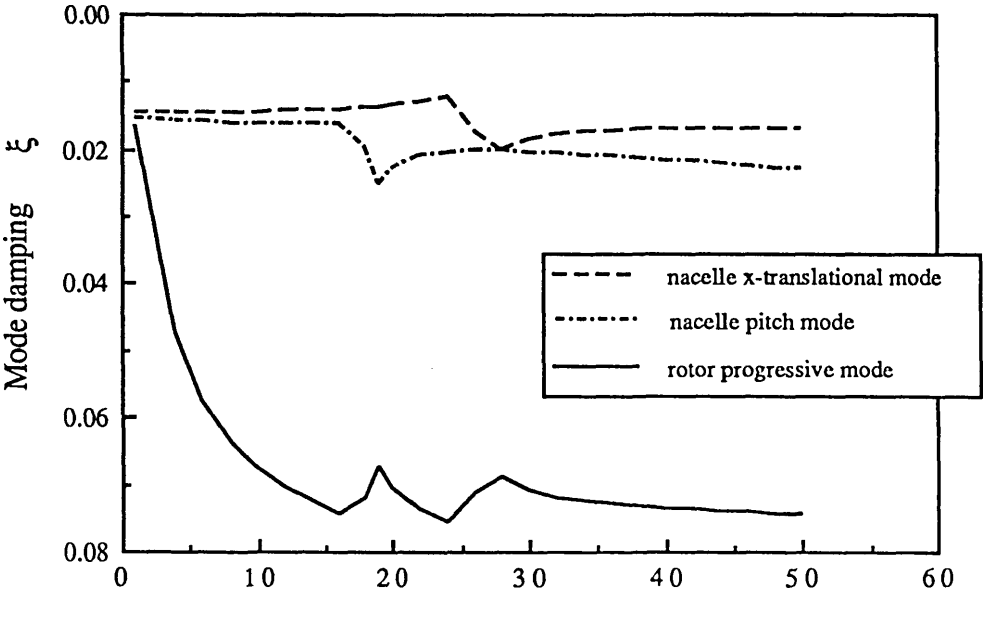

Fig 4.14 Mode dampings vary with rotor rotation speed at VF=0 for a gimbal rotor

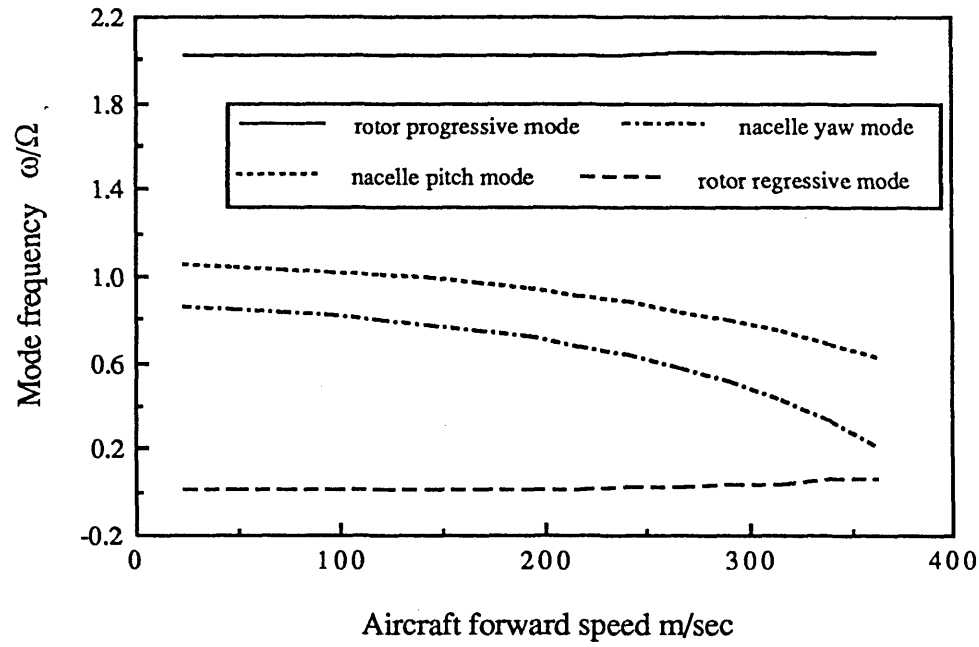

Fig 4.15 Variation of mode frequencies with forward speed for a gimbal rotor

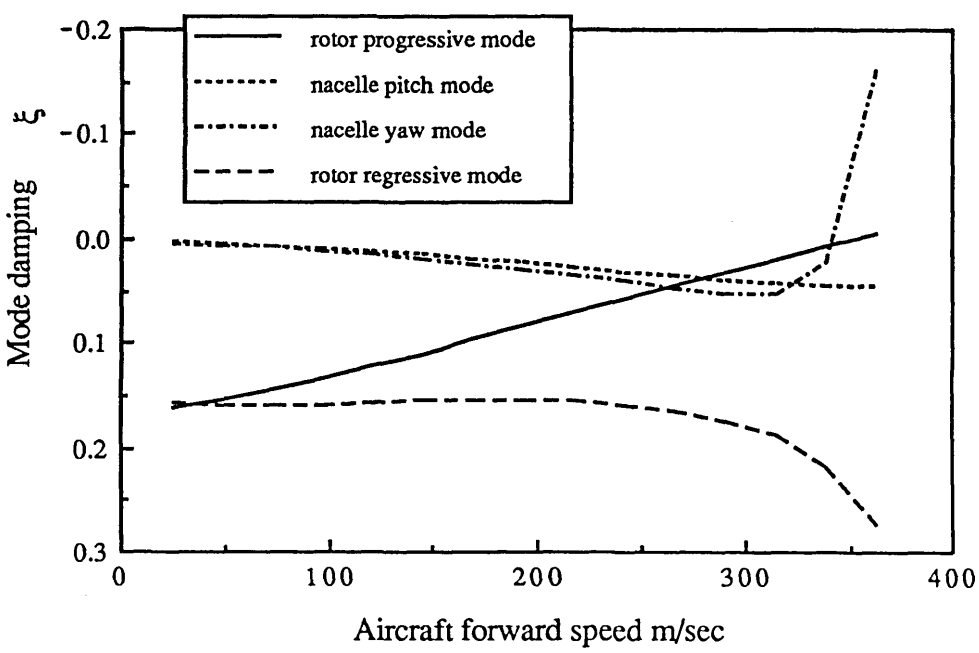

Fig 4.16 Variation of mode dampings with forward speed for a gimbal rotor

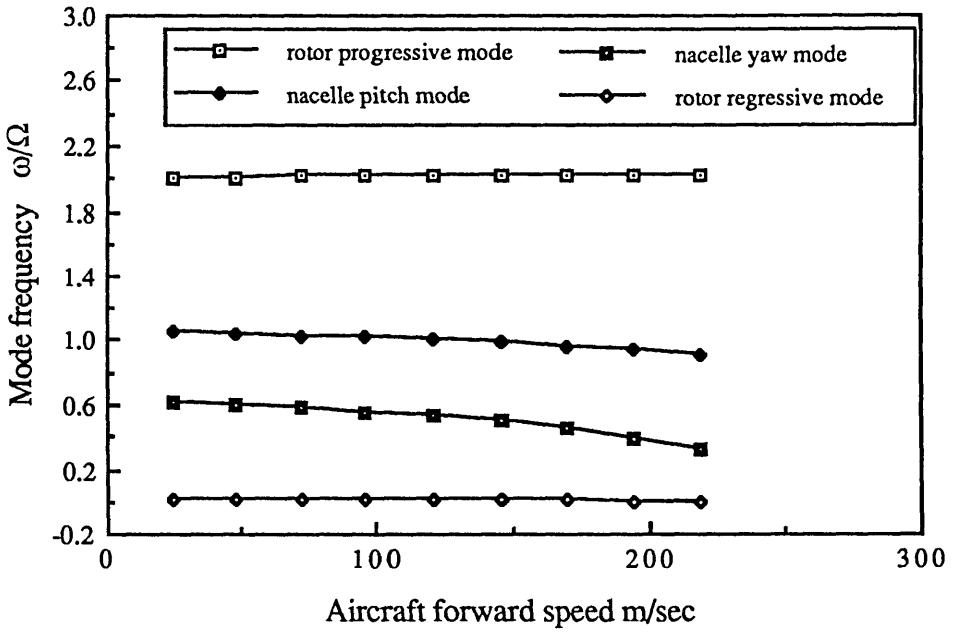

Fig 4.17 Variation of mode frequencies with forward speed
(reducing half nacelle's yaw stiffness of the gimbal rotor)

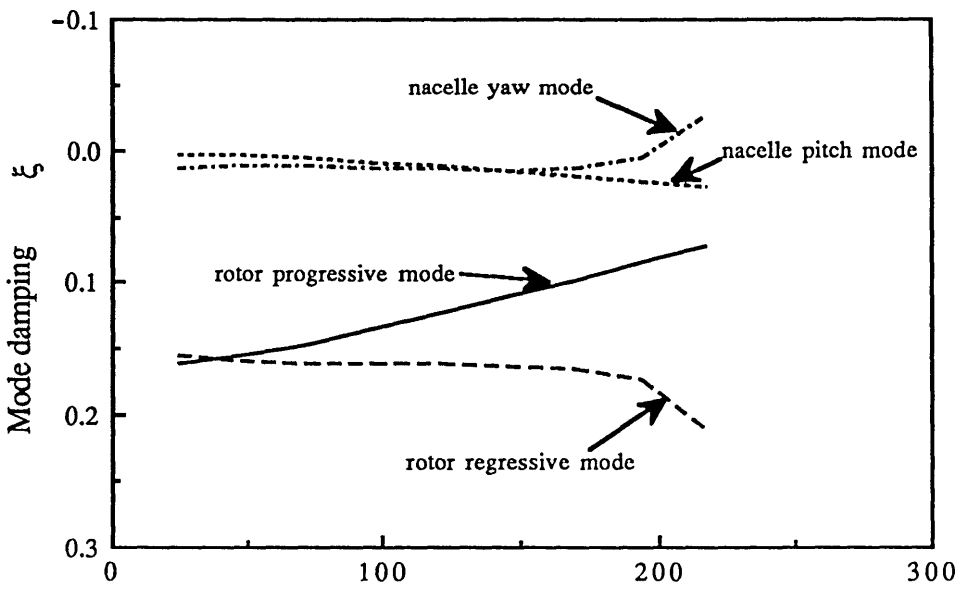

Fig 4.18 Variation of mode dampings with forward speed
(reducing half nacelle's yaw stiffness of the gimbal rotor)

4.5 CONCLUSIONS

A 12 degrees of freedom analytical model has been developed to investigate the coupled tilt-rotor/nacelle whirl flutter problem. The ordering scheme was used to retain the nonlinear terms in formulating the equations of motion for whirl flutter problems. The quasi-steady aerodynamics includes not only the circulatory part, but also the noncirculatory part which was neglected in the previous whirl flutter models. Two different types of connections between rotor and rotor shaft are considered. One is the ordinary universal joint connection. The other is a suggested possible gimbal configuration. Their whirl flutter characteristics are compared. The whirl flutter characteristics of the tilt-rotor of an ideal gimbal configuration is not found in the literature.

This analytical model is applied to the study of a classical propeller whirl flutter, a flap-hinged tilt-rotor/nacelle system whirl flutter. The present analytical results show good agreement with both experimental and analytical results.

Comparative studies were done for a universal joint tilt-rotor /nacelle system and an ideal gimbal tilt-rotor/nacelle system. Their whirl flutter characteristics were evaluated and compared. It is found that the whirl flutter mode in the two tilt-rotor configurations are very similar. In both configurations, the unstable mode appears as the nacelle mode of lowest frequency, and reducing the nacelle support stiffness is highly destabilising. The rotor behaves like a flap-hinged rotor which gives the rotor modes very high damping. The forward rotor mode damping decreases with the forward speed, but the high flapping damping is generally sufficient to maintain its stability until quite high forward velocity is achieved. The gimbal rotor is a bit more stable than the universal joint rotor.

CHAPTER 5 A FINITE ELEMENT STRUCTURAL DYNAMIC MODEL OF A BEAM WITH AN ARBITRARY MOVING BASE

5.1 INTRODUCTION

The previous two chapters develop a rigid body dynamic model to study the whirl flutter problem of a tilt-rotor aircraft. This rigid blade model, like the other rigid blade models in rotorcraft dynamics, can gives us a more direct physical insight into the dynamic behaviour of the system. Such models may be appropriate for some problems of some rotorcraft configurations such as articulated rotor blades. However, It is a fundamental reality that rotor blade flexibility leads to elastic deformations in actual operation. These elastic deformations become important in the dynamic model of many rotorcraft configurations such as those with hingeless and bearingless rotor blades. The lack of hinges results in large bending and torsional deformations of the rotor blades during rotorcraft operation. For these configurations, the rotor blades have to be treated as an elastic beam. Consequently, the fundamental basis for rotor blade dynamics is the structural dynamic behaviour of rotating elastic beams.

A number of suitable dynamic equations have been developed to describe the elastic bending and torsion of rotating beams in the rotorcraft dynamics area over the last 20 years. These models successfully solved the dynamic and aeroelastic problems of a number of rotorcraft configurations and have proven to be very valuable. However, since most of them were developed using the modal method and based on only one specific physical model, they lack the capability as a general analytical model to treat various different configurations. It is desirable to develop a general beam structural dynamics model which can be used as a basic element to couple with the body degrees of freedom or to model the complex blade root geometries instead of developing one dynamic model for each single different configuration. The Finite Element Method provides us an ideal technique suited to modelling the complex geometries in the modern

rotor structures. In recent implementations applying the finite element method to rotorcraft dynamic problems there are several significant efforts to explore the application of the Finite Element Method to this problem [Straub and Friedmann, 1981, Sivaneri and Chopra, 1982]. These models discretize a simple rotating beam, and they are still limited to one configuration. The need to model the general coupling of the beam with the fuselage or blade/root kinematics of an arbitrary configuration is not met by such approaches.

Rotating beam dynamics also have a wide application in a number of other relevant disciplines such as spacecraft dynamics, robotics and machine design. Its investigation is also actively pursued in these fields. A number of publications have dealt with simple spinning beams. Some attempts have been undertaken to construct more comprehensive theories by considering an arbitrary complex base motion of a beam in connection with the multibody dynamics problems. Unfortunately, none of them possess the capability to model the nonlinear elastic equations of motion. Furthermore, as pointed out by Kane et al [1987], the previous models for rotating beams in multibody dynamics have some significant deficiencies. To assess those deficiencies and develop a general dynamic model, Kane et al [1987] recently completed work on multibody dynamics treating the structural dynamics of a beam attached to an arbitrary moving base using a modal method. This is a quite general and comprehensive theory. However, the structural dynamics model is a linear one, and the use of the modal method restricts its application to some beams with complex geometries but with a linear response. Besides, this model does not include some important structural effects of a rotor blade such as the blade pretwist.

Obviously, it is a useful method to consider the motion of a structure in an attached arbitrary moving frame. This can result in a very general dynamic model and is the essence of the multibody dynamics formulation. When this method is combined with the

finite element technique, a very comprehensive and general dynamic model can easily be created. Such a model is not only capable of modelling its coupling effect with other structures, but is also capable of dealing with complex geometries. This chapter is devoted to developing such a new general dynamic model for beam-like structures. This newly developed model is expected to provide a general and fundamental element for solving the dynamic problems of rotating beam-like structures. In the next section a brief introduction to the physical model is given. Subsequently, the equations of motion are derived based on the principle of virtual work. Finally, numerical examples of both the eigenvalue problem and the dynamic response problem are presented to validate the mathematical model that has been developed.

5.2 PHYSICAL MODEL DESCRIPTION

An elastic beam is attached to a rigid body base as shown in Fig 5.1. This base has an arbitrary and large space motion which is defined by the velocity V_A of the connecting point A and the rigid body angular velocity ω_h in an inertial reference xyz. A frame $x_1y_1z_1$ is fixed to the moving base and centred at A. The beam undergoes a three dimensional deformation (Fig 5.2). A frame $x_2y_2z_2$ is fixed with the beam cross section and parallel to $x_1y_1z_1$ before deformation and centred at the cross sectional elasticity centre. The cross sectional mass centre is offset x_{gc} along y_2 and y_{gc} along z_2 (Fig 5.3).

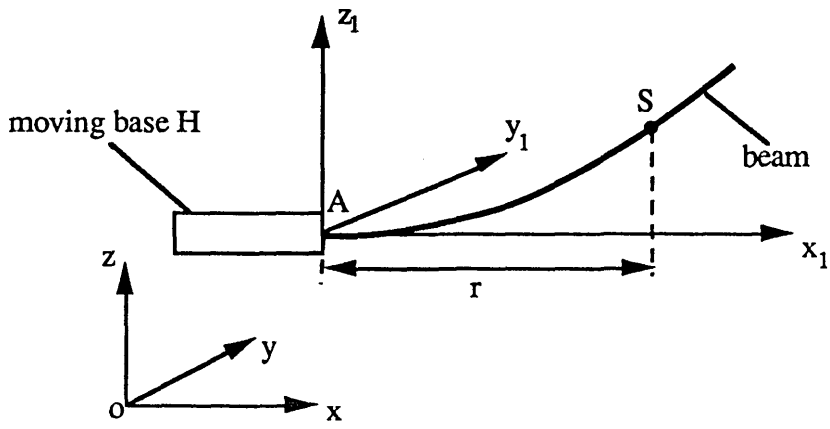

Fig 5.1 A beam attached to a moving base

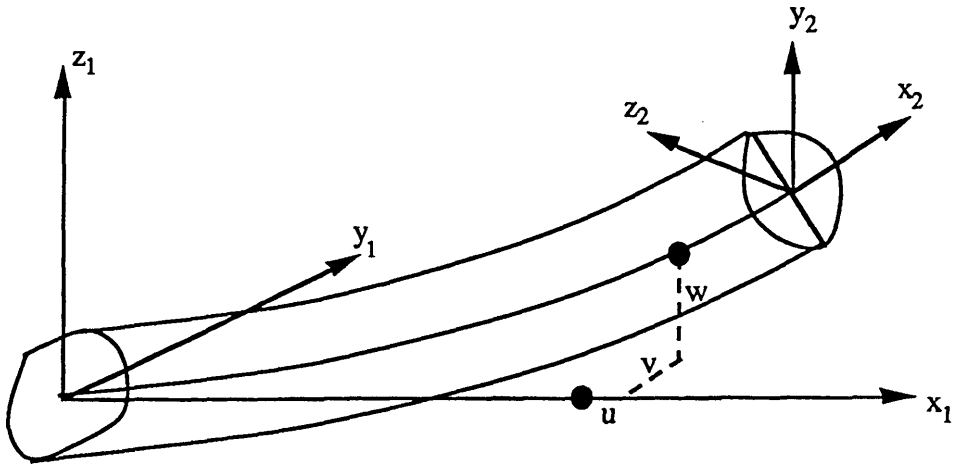

Fig 5.2 Elastic displacements of a beam

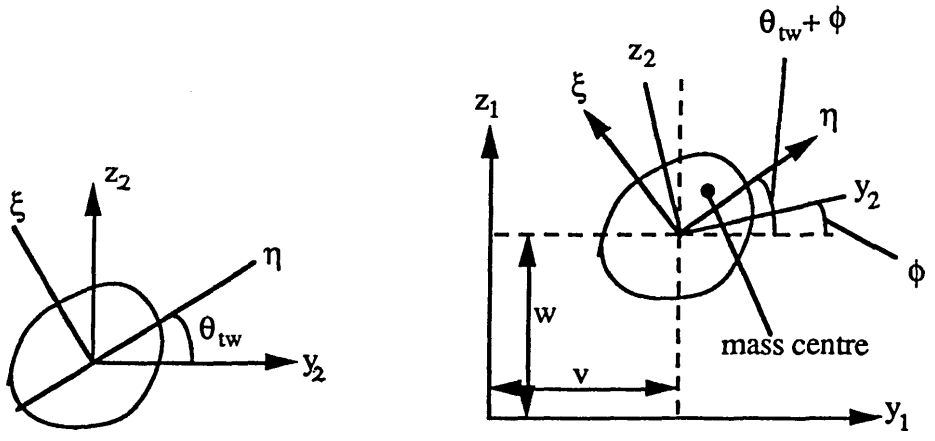

Fig 5.3 Cross-section geometry before the deformation and after the deformation

5.3 FORMULATION OF EQUATIONS OF MOTION

The equations of motion are obtained by using the principle of virtual work. The equations are discretized by the finite element method. Hence, the beam is divided into a number of elements. The beam inertia is lumped at the nodes of each element. This lumped model simplifies the formulation of the generalised inertia forces. As usual, the

lumped rotary inertia of the beam in flexure (flap and lag) are taken as small values. The effect of the cross section warping on the inertial forces are negligible and are not considered.

The system's equations of motion can be obtained from the principle of virtual work as:

$$\delta U - \delta W = 0$$

where δU is the variation of the strain energy of the beam, δW the virtual work done by nonconservative forces.

These equations are discretized using the Finite Element Method. The contributions of an element to the variation of the strain energy and the virtual work are derived in the following sections.

5.3.1 Virtual Work Done by Inertial Loads

Assume the base motion to be described by the following translational velocity and rotational velocity:

$$\vec{V}_A = v_x\vec{i}_1 + v_y\vec{j}_1 + v_z\vec{k}_1 \qquad (3.1.1)$$

$$\vec{\omega}_h = \omega_x\vec{i}_1 + \omega_y\vec{j}_1 + \omega_z\vec{k}_1 \qquad (3.1.2)$$

Considering a differential cross section S of the beam at a distance r from point A (Fig.5.1). After deformation, S is brought to a generic position (Fig 5.2). The sectional Euler rotation sequence is taken as lag-flap-torsion (ζ–(–β)–ϕ). The sectional elasticity centre is displaced u, v, w in x_1, y_1, z_1 directions respectively.

Then, the position vector of the sectional mass centre relative to point A is:

$$\vec{R}_{gc} = (r + u)\vec{i}_1 + v\vec{j}_1 + w\vec{k}_1 + x_{gc}\vec{j}_2 + y_{gc}\vec{k}_2 \qquad (3.1.3)$$

The transformation relationship between $x_1y_1z_1$ and $x_2y_2z_2$ is:

$$\begin{Bmatrix}\vec{i}_2\\ \vec{j}_2\\ \vec{k}_2\end{Bmatrix}=\begin{bmatrix}C_\beta C_\zeta & C_\beta S_\zeta & S_\beta\\ -C_\phi S_\zeta - S_\phi S_\beta C_\zeta & C_\phi C_\zeta - S_\zeta S_\beta S_\phi & C_\beta S_\phi\\ -C_\phi S_\beta C_\zeta + S_\phi S_\zeta & -S_\phi C_\zeta - S_\zeta S_\beta C_\phi & C_\beta C_\phi\end{bmatrix}\begin{Bmatrix}\vec{i}_1\\ \vec{j}_1\\ \vec{k}_1\end{Bmatrix}=[T_{21}]\begin{Bmatrix}\vec{i}_1\\ \vec{j}_1\\ \vec{k}_1\end{Bmatrix} \quad (3.1.4)$$

Where S=sin( ), C=cos( )

The angular velocity of section S in frame $x_1y_1z_1$ is:

$$\vec{\omega}_{p1}=(\dot{\phi}+\dot{\zeta}S_\beta)\vec{i}_2+(-\dot{\beta}C_\phi+\dot{\zeta}C_\beta S_\phi)\vec{j}_2+(\dot{\beta}S_\phi+\dot{\zeta}C_\beta C_\phi)\vec{k}_2$$

$$=\{\vec{E}_1\}^T[T_{21}]^T\begin{Bmatrix}\dot{\phi}+\dot{\zeta}S_\beta\\ -\dot{\beta}C_\phi+\dot{\zeta}C_\beta S_\phi\\ \dot{\beta}S_\phi+\dot{\zeta}C_\beta C_\phi\end{Bmatrix}=\{\vec{E}_1\}^T[M_{p1}]\begin{Bmatrix}\dot{\beta}\\ \dot{\zeta}\\ \dot{\phi}\end{Bmatrix} \quad (3.1.5)$$

where $$[M_{p1}]=[T_{21}]^T\begin{bmatrix}0 & S_\beta & 1\\ -C_\phi & C_\beta S_\phi & 0\\ S_\phi & C_\beta C_\phi & 0\end{bmatrix} \quad (3.1.6)$$

$$\{\vec{E}_1\}=\begin{Bmatrix}\vec{i}_1\\ \vec{j}_1\\ \vec{k}_1\end{Bmatrix} \quad (3.1.7)$$

The absolute angular velocity of S in the inertial frame xyz is:

$$\vec{\omega}=\vec{\omega}_h+\vec{\omega}_{p1}$$

$$=\omega_x\vec{i}_1+\omega_y\vec{j}_1+\omega_z\vec{k}_1+\vec{\omega}_{p1}$$

$$=\omega_{x2}\vec{i}_2+\omega_{y2}\vec{j}_2+\omega_{z2}\vec{k}_2$$

$$=\{\vec{E}_2\}^T[M_\omega][\omega_x,\ \omega_y,\ \omega_z,\ \dot{\beta},\ \dot{\zeta},\ \dot{\phi}]^T \quad (3.1.8)$$

The velocity of the mass centre of S in the inertial frame is obtained from the following equation :

$$\begin{aligned}
\vec{v}_{gc} &= \vec{v}_A + \vec{\omega}_h \times \vec{R}_{gc} + \dot{\vec{R}}_{gc} \\
&= \{v_x + \omega_y[w + x_{gc}C_\beta S_\phi + y_{gc}C_\phi C_\beta] - \omega_z[v + x_{gc}(C_\phi C_\zeta - S_\zeta S_\beta S_\phi) \\
&\quad + y_{gc}(-C_\phi S_\beta S_\zeta - C_\zeta S_\phi)] + \dot{u} + x_{gc}[(-C_\phi S_\beta C_\zeta + S_\zeta S_\phi)\dot{\phi} \\
&\quad - S_\phi C_\beta C_\zeta \dot{\beta} - (-S_\phi S_\beta S_\zeta + C_\zeta C_\phi)\dot{\zeta}] + y_{gc}[(S_\phi S_\beta C_\zeta + S_\zeta C_\phi)\dot{\phi} \\
&\quad - C_\phi C_\beta C_\zeta \dot{\beta} + (C_\phi S_\beta S_\zeta + C_\zeta S_\phi)\dot{\zeta}]\vec{i}_1 \\
&\quad + \{v_y + \omega_z[r + u + x_{gc}(-S_\phi S_\beta C_\zeta - S_\zeta C_\phi) + y_{gc}(-C_\phi S_\beta C_\zeta + S_\zeta S_\phi)] \\
&\quad - \omega_x[w + x_{gc}S_\phi C_\beta + y_{gc}C_\phi C_\beta] + \dot{v} + x_{gc}[(-C_\phi S_\beta S_\zeta - C_\zeta S_\phi)\dot{\phi} \\
&\quad - S_\phi C_\beta S_\zeta \dot{\beta} - (-S_\phi S_\beta C_\zeta - S_\zeta C_\phi)\dot{\zeta}] + y_{gc}[-(-S_\phi S_\beta S_\zeta + C_\zeta C_\phi)\dot{\phi} \\
&\quad - C_\phi C_\beta S_\zeta \dot{\beta} + (-C_\phi S_\beta C_\zeta + S_\zeta S_\phi)\dot{\zeta}]\vec{j}_1 \\
&\quad + \{v_z + \omega_x[v + x_{gc}(-S_\phi S_\beta S_\zeta + C_\zeta C_\phi) + y_{gc}(-C_\phi S_\beta S_\zeta - C_\zeta S_\phi)] \\
&\quad - \omega_y[r + u + x_{gc}(-S_\phi S_\beta C_\zeta - S_\zeta C_\phi) + y_{gc}(-C_\phi S_\beta C_\zeta + S_\zeta S_\phi)] + \dot{w} \\
&\quad + x_{gc}[C_\phi C_\beta \dot{\phi} - S_\phi S_\beta \dot{\beta}] - y_{gc}[S_\phi C_\beta \dot{\phi} + C_\phi S_\beta \dot{\beta}]\}\vec{k}_1 \\
&= [V_x \quad V_y \quad V_z]\{\vec{E}_1\}
\end{aligned} \tag{3.1.9}$$

The acceleration of the mass centre of S is obtained by differentiating $\vec{v}_{gc}$:

$$\vec{a}_{gc} = \vec{a}_A + \vec{\varepsilon}_h \times \vec{R}_{gc} + \vec{\omega}_h \times \dot{\vec{R}}_{gc} + \vec{\omega}_h \times (\vec{\omega}_h \times \vec{R}_{gc}) + \ddot{\vec{R}}_{gc} + \vec{\omega}_h \times \dot{\vec{R}}_{gc} \tag{3.1.10}$$

Where :

$$\begin{aligned}
\vec{a}_A &= a_x\vec{i}_1 + a_y\vec{j}_1 + a_z\vec{k}_1 \\
&= \dot{v}_x\vec{i}_1 + \dot{v}_y\vec{j}_1 + \dot{v}_z\vec{k}_1 + \vec{\omega}_h \times \vec{v}_A \\
&= \dot{v}_x\vec{i}_1 + \dot{v}_y\vec{j}_1 + \dot{v}_z\vec{k}_1 + (\omega_y v_z - \omega_z v_y)\vec{i}_1 \\
&\quad + (\omega_z v_x - \omega_x v_z)\vec{j}_1 + (\omega_x v_y - \omega_y v_x)\vec{k}_1
\end{aligned} \tag{3.1.11}$$

$$\vec{\varepsilon}_h = \varepsilon_x \vec{i}_1 + \varepsilon_y \vec{j}_1 + \varepsilon_z \vec{k}_1$$
$$= \dot{\omega}_x \vec{i}_1 + \dot{\omega}_y \vec{j}_1 + \dot{\omega}_z \vec{k}_1 \qquad (3.1.12)$$

$$\dot{\vec{R}}_{gc} = \dot{r}_x \vec{i}_1 + \dot{r}_y \vec{j}_1 + \dot{r}_z \vec{k}_1 \qquad (3.1.13)$$

$$\ddot{\vec{R}}_{gc} = \ddot{r}_x \vec{i}_1 + \ddot{r}_y \vec{j}_1 + \ddot{r}_z \vec{k}_1 \qquad (3.1.14)$$

And,

$$\dot{r}_x = \dot{u} + x_{gc}[(-C_\phi S_\beta C_\zeta + S_\zeta S_\phi)\dot{\phi} - S_\phi C_\beta C_\zeta \dot{\beta} - (-S_\phi S_\beta S_\zeta + C_\zeta C_\phi)\dot{\zeta}]$$
$$+ y_{gc}[(S_\phi S_\beta C_\zeta + S_\zeta C_\phi)\dot{\phi} - C_\phi C_\beta C_\zeta \dot{\beta} + (C_\phi S_\beta S_\zeta + C_\zeta S_\phi)\dot{\zeta}] \qquad (3.1.15)$$

$$\dot{r}_y = \dot{v} + x_{gc}[(-C_\phi S_\beta S_\zeta - C_\zeta S_\phi)\dot{\phi} - S_\phi C_\beta S_\zeta \dot{\beta} - (-S_\phi S_\beta C_\zeta - S_\zeta C_\phi)\dot{\zeta}]$$
$$+ y_{gc}[-(-S_\phi S_\beta S_\zeta + C_\zeta C_\phi)\dot{\phi} - C_\phi C_\beta S_\zeta \dot{\beta} + (-C_\phi S_\beta C_\zeta + S_\zeta S_\phi)\dot{\zeta}] \qquad (3.1.16)$$

$$\dot{r}_z = \dot{w} + x_{gc}[C_\phi C_\beta \dot{\phi} - S_\phi S_\beta \dot{\beta}] - y_{gc}[S_\phi C_\beta \dot{\phi} + C_\phi S_\beta \dot{\beta}] \qquad (3.1.17)$$

$$\ddot{r}_x = \ddot{u} + x_{gc}\{(-C_\phi S_\beta C_\zeta + S_\zeta S_\phi)\ddot{\phi} - S_\phi C_\beta C_\zeta \ddot{\beta} - (-S_\phi S_\beta S_\zeta + C_\zeta C_\phi)\ddot{\zeta}$$
$$+ \dot{\phi}[(S_\phi S_\beta C_\zeta + S_\zeta C_\phi)\dot{\phi} + (-C_\phi C_\beta C_\zeta)\dot{\beta} + (C_\phi S_\beta S_\zeta + C_\zeta S_\phi)\dot{\zeta}]$$
$$- \dot{\beta}[C_\phi C_\beta C_\zeta \dot{\phi} - S_\phi S_\beta C_\zeta \dot{\beta} - S_\phi C_\beta S_\zeta \dot{\zeta}] - \dot{\zeta}[(-C_\phi S_\beta S_\zeta - C_\zeta S_\phi)\dot{\phi}$$
$$+ (-S_\phi C_\beta S_\zeta)\dot{\beta} + (-S_\phi S_\beta C_\zeta - S_\zeta C_\phi)\dot{\zeta}] + y_{gc}\{(S_\phi S_\beta C_\zeta + S_\zeta C_\phi)\ddot{\phi}$$
$$- C_\phi C_\beta C_\zeta \ddot{\beta} + (C_\phi S_\beta S_\zeta + C_\zeta S_\phi)\ddot{\zeta} + \dot{\phi}[(C_\phi S_\beta C_\zeta - S_\zeta S_\phi)\dot{\phi} + S_\phi C_\beta C_\zeta \dot{\beta}$$
$$+ (-S_\phi S_\beta S_\zeta + C_\zeta C_\phi)\dot{\zeta}] - \dot{\beta}[-S_\phi C_\beta C_\zeta \dot{\phi} - C_\phi S_\beta C_\zeta \dot{\beta} - C_\phi C_\beta S_\zeta \dot{\zeta}]$$
$$+ \dot{\zeta}[(-S_\phi S_\beta S_\zeta + C_\zeta C_\phi)\dot{\phi} + C_\phi C_\beta S_\zeta \dot{\beta} + (C_\phi S_\beta C_\zeta - S_\zeta S_\phi)\dot{\zeta}]\} \qquad (3.1.18)$$

$$\ddot{r}_y = \ddot{v} + x_{gc}\{(-C_\phi S_\beta S_\zeta - C_\zeta S_\phi)\ddot{\phi} - S_\phi C_\beta S_\zeta \ddot{\beta} + (-S_\phi S_\beta C_\zeta - S_\zeta C_\phi)\ddot{\zeta}$$
$$+ \dot{\phi}[(S_\phi S_\beta C_\zeta + S_\zeta C_\phi)\dot{\phi} + (-C_\phi C_\beta C_\zeta)\dot{\beta} + (C_\phi S_\beta S_\zeta + C_\zeta S_\phi)\dot{\zeta}]$$
$$- \dot{\beta}[C_\phi C_\beta C_\zeta \dot{\phi} - S_\phi S_\beta C_\zeta \dot{\beta} - S_\phi C_\beta S_\zeta \dot{\zeta}] - \dot{\zeta}[(-C_\phi S_\beta S_\zeta - C_\zeta S_\phi)\dot{\phi}$$

$$+(-S_\phi C_\beta C_\zeta)\dot{\beta}+(S_\phi S_\beta S_\zeta - C_\zeta C_\phi)\dot{\zeta}] + y_{gc}\{-(-S_\phi S_\beta S_\zeta + C_\zeta C_\phi)\ddot{\phi}$$

$$-C_\phi C_\beta S_\zeta \ddot{\beta}+(-C_\phi S_\beta C_\zeta + S_\zeta S_\phi)\ddot{\zeta} - \dot{\phi}[(-C_\phi S_\beta C_\zeta + C_\zeta S_\phi)\dot{\phi}$$

$$+(-S_\phi C_\beta S_\zeta)\dot{\beta}+(-S_\phi S_\beta C_\zeta + S_\zeta C_\phi)\dot{\zeta}] - \dot{\beta}[-S_\phi C_\beta S_\zeta \dot{\phi} - C_\phi S_\beta S_\zeta \dot{\beta}$$

$$+C_\phi C_\beta C_\zeta \dot{\zeta}] + \dot{\zeta}[(S_\phi S_\beta C_\zeta - S_\zeta C_\phi)\dot{\phi}+(-C_\phi C_\beta C_\zeta)\dot{\beta}$$

$$+(C_\phi S_\beta S_\zeta + C_\zeta S_\phi)\dot{\zeta}]\} \qquad (3.1.19)$$

$$\ddot{r}_z = \ddot{w} + x_{gc}\{C_\phi C_\beta \ddot{\phi} - S_\phi S_\beta \ddot{\beta} + \dot{\phi}[-S_\phi C_\beta \dot{\phi} - C_\phi S_\beta \dot{\beta}] - \dot{\beta}[C_\phi S_\beta \dot{\phi} + S_\phi C_\beta \dot{\beta}]$$

$$-y_{gc}\{S_\phi C_\beta \ddot{\phi} + C_\phi S_\beta \ddot{\beta} + \dot{\phi}[C_\phi C_\beta \dot{\phi} - S_\phi S_\beta \dot{\beta}] + \dot{\beta}[-S_\phi S_\beta \dot{\phi} + C_\phi C_\beta \dot{\beta}]\} \qquad (3.1.20)$$

The acceleration of the lumped mass centre can be written as the following form from (3.1.10)

$$\vec{a}_{gc} = \{\vec{E}_1\}^T \{[A1]\cdot[a_x\, a_y\, a_z\, \varepsilon_x\, \varepsilon_y\, \varepsilon_z\, \ddot{r}_x\, \ddot{r}_y\, \ddot{r}_z]^T$$

$$+[A2]\cdot[\omega_x\, \omega_y\, \omega_z\, \dot{r}_x\, \dot{r}_y\, \dot{r}_z]^T + [A3][r_x\, r_y\, r_z]^T\} \qquad (3.1.21)$$

Replacing $\ddot{r}_x$, $\ddot{r}_y$, $\ddot{r}_z$, $\dot{r}_x$, $\dot{r}_y$, $\dot{r}_z$, and r_x, r_y, r_z in (3.1.15) through (3.1.20) into (3.1.21) :

$$\vec{a}_{gc} = \{\vec{E}_1\}^T \{[Aa][a_x\, a_y\, a_z\, \varepsilon_x\, \varepsilon_y\, \varepsilon_z\, \ddot{u}\, \ddot{v}\, \ddot{w}\, \ddot{\beta}\, \ddot{\zeta}\, \ddot{\phi}]^T$$

$$+[Av][\omega_x\, \omega_y\, \omega_z\, \dot{u}\, \dot{v}\, \dot{w}\, \dot{\beta}\, \dot{\zeta}\, \dot{\phi}]^T$$

$$+[Ad][u\ v\ w]^T + \{Ao\}\} \qquad (3.1.22)$$

The resultant angular acceleration of section S is obtained by differentiating $\vec{\omega}$:

$$\dot{\vec{\omega}} = \vec{\varepsilon}_h + \vec{\omega}_h \times \vec{\omega}_h + \vec{\varepsilon}_{p1} + (\vec{\omega}_h + \vec{\omega}_{p1}) \times \vec{\omega}_{p1}$$

$$= \vec{\varepsilon}_h + \vec{\varepsilon}_{p1} + \vec{\omega}_h \times \vec{\omega}_{p1} \qquad (3.1.23)$$

Where :

$$\vec{\varepsilon}_h = \varepsilon_x \vec{i}_1 + \varepsilon_y \vec{j}_1 + \varepsilon_z \vec{k}_1 \qquad (3.1.24)$$

$$\vec{\varepsilon}_{p1} = \dot{\vec{\omega}}_{p1} = \{\vec{E}_1\}^T \left\{ [M_{\varepsilon a}] \begin{Bmatrix} \ddot{\beta} \\ \ddot{\zeta} \\ \ddot{\phi} \end{Bmatrix} + [M_{\varepsilon v}] \begin{Bmatrix} \dot{\beta} \\ \dot{\zeta} \\ \dot{\phi} \end{Bmatrix} \right\} \qquad (3.1.25)$$

$$\vec{\omega}_h \times \vec{\omega}_{p1} = \{\vec{E}_2\}^T \begin{bmatrix} 0 & -\omega_z & \omega_y \\ \omega_z & 0 & \omega_x \\ -\omega_y & -\omega_x & 0 \end{bmatrix} [T_{21}] [M_{p1}] \begin{Bmatrix} \dot{\beta} \\ \dot{\zeta} \\ \dot{\phi} \end{Bmatrix} \qquad (3.1.26)$$

Applying (3.1.24 through 3.1.26) to (3.1.23), The resultant angular acceleration can be written as:

$$\vec{\varepsilon} = \{\vec{E}_2\}^T \left([Ea] \begin{Bmatrix} \varepsilon_x \\ \varepsilon_y \\ \varepsilon_z \\ \ddot{\beta} \\ \ddot{\zeta} \\ \ddot{\phi} \end{Bmatrix} + [Ev] \begin{Bmatrix} \dot{\beta} \\ \dot{\zeta} \\ \dot{\phi} \end{Bmatrix} \right) = \varepsilon_{x2} \vec{i}_2 + \varepsilon_{y2} \vec{j}_2 + \varepsilon_{z2} \vec{k}_2 \qquad (3.1.27)$$

The inertial loads due to the lumped mass are:

Force : $\vec{F}_I = -m \vec{a}_{gc}$ (3.1.28)

Moment about the mass centre : $\vec{M}_I = -[\vec{\varepsilon} \cdot I + \vec{\omega} \times I \cdot \vec{\omega}]$ (3.1.29)

Where, the inertia dyadic of the lumped mass is written as:

$$I = I_{xx} \vec{i}_2 \vec{i}_2 - 2I_{xy} \vec{i}_2 \vec{j}_2 - 2I_{xz} \vec{i}_2 \vec{k}_2 + I_{yy} \vec{j}_2 \vec{j}_2 - 2I_{yz} \vec{j}_2 \vec{k}_2 + I_{zz} \vec{k}_2 \vec{k}_2 \qquad (3.1.30)$$

The virtual displacement of the mass centre is:

$$\begin{aligned}\delta r_{gc} = {} & \vec{i}_1\delta u + \vec{j}_1\delta v + \vec{k}_1\delta w + \vec{i}_1\delta R_x + \vec{j}_1\delta R_y + \vec{k}_1\delta R_z \\ & + \{x_{gc}[-S_\phi C_\beta C_\zeta \vec{i}_1 - S_\phi C_\beta S_\zeta \vec{j}_1 - S_\phi S_\beta \vec{k}_1] + y_{gc}[-C_\phi C_\beta C_\zeta \vec{i}_1 \\ & - C_\phi C_\beta S_\zeta \vec{j}_1 - C_\phi S_\beta \vec{k}_1]\}\delta_\beta + \{x_{gc}[-(-S_\phi S_\beta C_\zeta + C_\zeta C_\phi)\vec{i}_1 \\ & + (-S_\phi S_\beta C_\zeta - S_\zeta C_\phi)\vec{j}_1] + y_{gc}[(C_\phi S_\beta S_\zeta + C_\zeta S_\phi)\vec{i}_1 \\ & + (-C_\phi S_\beta C_\zeta + S_\zeta S_\phi)\vec{j}_1]\}\delta_\zeta + \{x_{gc}[-(-C_\phi S_\beta C_\zeta + S_\zeta S_\phi)\vec{i}_1 \\ & + (-C_\phi S_\beta S_\zeta - C_\zeta S_\phi)\vec{j}_1 + C_\phi C_\beta \vec{k}_1] + y_{gc}[(S_\phi S_\beta C_\zeta + S_\zeta C_\phi)\vec{i}_1 \\ & - (-S_\phi S_\beta S_\zeta + C_\zeta C_\phi)\vec{j}_1 - S_\phi C_\beta \vec{k}_1]\}\delta_\phi + \{-(w + x_{gc}S_\phi C_\beta + y_{gc}C_\phi C_\beta)\vec{j}_1 \\ & + [v + x_{gc}(-S_\phi S_\beta S_\zeta + C_\zeta C_\phi + y_{gc}(-C_\phi S_\beta S_\zeta - C_\zeta S_\phi]\vec{k}_1\}\delta_{\theta x} \\ & + \{(w + x_{gc}S_\phi C_\beta + y_{gc}C_\phi C_\beta)\vec{i}_1 - [r + u + x_{gc}(-S_\phi S_\beta C_\zeta - S_\zeta C_\phi) \\ & + y_{gc}(-C_\phi S_\beta C_\zeta + S_\zeta S_\phi)]\vec{k}_1\}\delta_{\theta y} + \{-(v + x_{gc}(C_\phi C_\zeta - S_\phi S_\beta S_\zeta) \\ & + y_{gc}(-S_\phi C_\zeta - C_\phi S_\beta S_\zeta))\vec{i}_1 + [r + u + x_{gc}(-S_\phi S_\beta C_\zeta - S_\zeta C_\phi) \\ & + y_{gc}(-C_\phi S_\beta C_\zeta + S_\zeta S_\phi)]\vec{j}_1\}\delta_{\theta z} \end{aligned} \qquad (3.1.31)$$

The virtual rotation of the section S is:

$$\begin{aligned}\delta\gamma = {} & \vec{i}_1\delta\theta_x + \vec{j}_1\delta\theta_y + \vec{k}_1\delta\theta_z + (-C_\phi\vec{j}_2 + S_\phi\vec{k}_2)\delta\beta + (S_\beta\vec{i}_2 + C_\beta S_\phi\vec{j}_2 \\ & + C_\beta C_\phi\vec{k}_2)\delta\zeta + \vec{i}_2\delta\phi \end{aligned} \qquad (3.1.32)$$

The virtual work done by inertial loads is:

$$\delta W_I = \vec{F}_I \bullet \vec{\delta} r_{gc} + \vec{M}_I \bullet \vec{\delta}\gamma \qquad (3.1.33)$$

This can finally be written as:

$$\delta W_I = [\delta u\ \delta v\ \delta w\ \delta\beta\ \delta\zeta\ \delta\phi\ \delta R_x\ \delta R_y\ \delta R_z\ \delta\theta_x\ \delta\theta_y\ \delta\theta_z]\{F^*_I\} \qquad (3.1.34)$$

$\{F_I^*\}$ is the generalised inertial forces

The generalised inertia forces corresponding to the relevant generalised coordinates are as follows:

$$F^*_u = -m\vec{i}_1 \cdot \vec{a}_{gc}$$

$$F^*_v = -m\vec{j}_1 \cdot \vec{a}_{gc}$$

$$F^*_w = -m\vec{k}_1 \cdot \vec{a}_{gc}$$

$$F^*_{vx} = -m\vec{i}_1 \cdot \vec{a}_{gc}$$

$$F^*_{vy} = -m\vec{j}_1 \cdot \vec{a}_{gc}$$

$$F^*_{vz} = -m\vec{k}_1 \cdot \vec{a}_{gc}$$

$$F^*_\beta = -m(b_{11}\vec{i}_1 + b_{12}\vec{j}_1 + b_{13}\vec{k}_1) \cdot \vec{a}_{gc} - (a_{11}\vec{i}_1 + a_{12}\vec{j}_1 + a_{13}\vec{k}_1) \cdot [\vec{\varepsilon} \cdot I + \vec{\omega} \times I \cdot \vec{\omega}]$$

$$F^*_\zeta = -m(b_{21}\vec{i}_1 + b_{22}\vec{j}_1 + b_{23}\vec{k}_1) \cdot \vec{a}_{gc} - (a_{21}\vec{i}_1 + a_{22}\vec{j}_1 + a_{23}\vec{k}_1) \cdot [\vec{\varepsilon} \cdot I + \vec{\omega} \times I \cdot \vec{\omega}]$$

$$F^*_\phi = -m(b_{31}\vec{i}_1 + b_{32}\vec{j}_1 + b_{33}\vec{k}_1) \cdot \vec{a}_{gc} - (a_{31}\vec{i}_1 + a_{32}\vec{j}_1 + a_{33}\vec{k}_1) \cdot [\vec{\varepsilon} \cdot I + \vec{\omega} \times I \cdot \vec{\omega}]$$

$$F^*_{\omega x} = -m(c_{11}\vec{i}_1 + c_{12}\vec{j}_1 + c_{13}\vec{k}_1) \cdot \vec{a}_{gc} - \vec{i}_1 \cdot [\vec{\varepsilon} \cdot I + \vec{\omega} \times I \cdot \vec{\omega}]$$

$$F^*_{\omega y} = -m(c_{21}\vec{i}_1 + c_{22}\vec{j}_1 + c_{23}\vec{k}_1) \cdot \vec{a}_{gc} - \vec{j}_1 \cdot [\vec{\varepsilon} \cdot I + \vec{\omega} \times I \cdot \vec{\omega}]$$

$$F^*_{\omega z} = -m(c_{31}\vec{i}_1 + c_{32}\vec{j}_1 + c_{33}\vec{k}_1) \cdot \vec{a}_{gc} - \vec{k}_1 \cdot [\vec{\varepsilon} \cdot I + \vec{\omega} \times I \cdot \vec{\omega}]$$

.....(3.1.35)

Combining the equations (3.1.30), (3.1.27) and (3.1.8), the following relations can be derived,

$$\vec{\varepsilon} \cdot I = \varepsilon_{x2} I_{xx} \vec{i}_2 + (-2\varepsilon_{x2} I_{xy} + \varepsilon_{y2} I_{yy})\vec{j}_2 + (\varepsilon_{z2} I_{zz} - 2\varepsilon_{x2} I_{xz} - 2\varepsilon_{y2} I_{yz})\vec{k}_2 \quad (3.1.36)$$

$$\begin{aligned}\vec{\omega} \times I \cdot \vec{\omega} = {} & (-\omega_{y2}\omega_{z2} I_{yy} + \omega_{y2}\omega_{z2} I_{zz} - 2\omega^2_{z2} I_{yz})\vec{i}_2 \\ & + (\omega_{x2}\omega_{z2} I_{xx} - 2\omega_{y2}\omega_{z2} I_{xy} - \omega_{x2}\omega_{z2} I_{zz} - 2\omega^2_{z2} I_{xz})\vec{j}_2 \\ & + (-\omega_{x2}\omega_{y2} I_{xx} + \omega_{x2}\omega_{y2} I_{yy} + 2\omega^2_{y2} I_{xy} - 2\omega_{x2}\omega_{z2} I_{yy} + 2\omega_{y2}\omega_{z2} I_{xy})\vec{k}_2\end{aligned}$$

.....(3.1.37)

Replacing $\vec{\varepsilon} \cdot I$, $\vec{\omega} \times I \cdot \vec{\omega}$, $\vec{a}_{gc}$ to the generalised inertial forces in (3.1.35) and using the

expressions for $\vec{a}_{gc}$, $\vec{\varepsilon}$, $\vec{\omega}$ in equations (3.1.22), (3.1.27) and (3.1.8). These generalised inertial forces in (3.1.35) can finally be expressed in the following matrix form:

$$\{F_I^*\} = [Ia]\,[a_x\ a_y\ a_z\ \varepsilon_x\ \varepsilon_y\ \varepsilon_z\ \ddot{u}\ \ddot{v}\ \ddot{w}\ \ddot{\beta}\ \ddot{\zeta}\ \ddot{\phi}]^T + [Iv]\,[\omega_x\ \omega_y\ \omega_z\ \dot{u}\ \dot{v}\ \dot{w}\ \dot{\beta}\ \dot{\zeta}\ \dot{\phi}]^T + [Id]\,[u\ v\ w]^T + \{If\} \qquad (3.1.38)$$

Another method to obtain the generalised forces is widely used in the multibody dynamics formulation [Kane and Levinson, 1985, Kane et al, 1987]. It is called Kane's method. It is more convenient in some cases. Appendix 5A gives the derivation of the above generalised inertial forces using Kane's method to demonstrate its application in rotorcraft dynamics.

5.3.2 Variation of the Strain Energy

The virtual work caused by the internal forces is obtained by the variation of the strain energy. Although the deflections may be large, the strain is assumed to be small. A general nonlinear strain-displacement relation is adopted. The centrifugal stiffness and gyroscopic terms caused by the base motion are specifically treated so that this dynamic model can be conveniently applied to both nonlinear problems and liner problems. The final mathematical models can be readily applied to solve not only an eigenvalue problem but also the dynamic response problem of a beam attached to an arbitrary moving base as in a multibody dynamics algorithm.

The shape functions for the beam element are taken as Hermite polynomials for the bending deformation and linear polynomials for the torsion and axial deformation. They are defined as:

$$H_1 = 2(x_e/l_e)^3 - 3(x_e/l_e)^2 + 1$$
$$H_2 = l_e[(x_e/l_e)^3 - 2(x_e/l_e)^2 + (x_e/l_e)]$$
$$H_3 = -2(x_e/l_e)^3 + 3(x_e/l_e)^2$$
$$H_4 = l_e[(x_e/l_e)^3 - (x_e/l_e)^2]$$
$$L_1 = 1 - (x_e/l_e)$$
$$L_2 = x_e/l_e$$

.....(3.2.1)

Where x_e is the local axial coordinate for the i'th element and l_e is the length of the i'th element.

Therefore, the distribution of the deflections u, v, w, ϕ over an element is represented in terms of the nodal displacements using these shape functions as:

$$w = [H_1 \; H_2 \; H_3 \; H_4] \begin{Bmatrix} w_1 \\ \beta_1 \\ w_2 \\ \beta_2 \end{Bmatrix} \qquad (3.2.2)$$

$$v = [H_1 \; H_2 \; H_3 \; H_4] \begin{Bmatrix} v_1 \\ \zeta_1 \\ v_2 \\ \zeta_2 \end{Bmatrix} \qquad (3.2.3)$$

$$u = [L_1 \quad L_2] \begin{Bmatrix} u_1 \\ u_2 \end{Bmatrix} \qquad (3.2.4)$$

$$\phi = [L_1 \quad L_2] \begin{Bmatrix} \phi_1 \\ \phi_2 \end{Bmatrix} \qquad (3.2.5)$$

To obtain the strain energy of the beam, the strain-displacement relation of the elastic beam must be developed. A general nonlinear strain-displacement relation has been developed based on the Euler-Bernoulli beam assumption (Hodges and Dowell, 1974). This nonlinear relation is widely accepted for rotor blades with moderately large rotation (Ormiston et al, 1987). Therefore, this relation is adopted in the present model. They were expressed as:

$$\begin{aligned}\varepsilon_{xx} = u' + \left(\frac{v'^2}{2} + \frac{w'^2}{2}\right) - \lambda\phi'' + (\eta^2 + \zeta^2)\left(\theta_{tw}'\phi' + \frac{\phi'^2}{2}\right) \\ - v''[\eta\cos(\theta_{tw} + \phi) - \zeta\sin(\theta_{tw} + \phi)] \\ - w''[\eta\sin(\theta_{tw} + \phi) + \zeta\cos(\theta_{tw} + \phi)]\end{aligned} \qquad (3.2.6)$$

$$\varepsilon_{x\eta} \approx -(\zeta + \frac{\partial\lambda}{\partial\eta})\phi' \qquad (3.2.7)$$

$$\varepsilon_{x\zeta} \approx (\eta - \frac{\partial\lambda}{\partial\zeta})\phi' \qquad (3.2.8)$$

where λ is the warping function for the cross section. θ_{tw} is the blade pretwist angle (Fig 5.1-5.3).

The stresses are respectively:

$$\sigma_{xx} = E\varepsilon_{xx} \qquad (3.2.9)$$

$$\sigma_{x\eta} = G\varepsilon_{x\eta} \qquad (3.2.10)$$

$$\sigma_{x\zeta} = G\varepsilon_{x\zeta} \qquad (3.2.11)$$

The strain energy of a beam element is:

$$\begin{aligned}U &= \frac{1}{2}\int_0^{le}\left[\iint_A((\sigma_{xx}\varepsilon_{xx} + \sigma_{x\eta}\varepsilon_{x\eta} + \sigma_{x\zeta}\varepsilon_{x\zeta})\,d_\eta d_\zeta\right]d_x \\ &= \frac{1}{2}\int_0^{le}\left[\iint_A(E\varepsilon_{xx}^2 + G\varepsilon_{x\eta}^2 + G\varepsilon_{x\zeta}^2)\,d_\eta d_\zeta\right]d_x\end{aligned} \qquad (3.2.12)$$

Replacing (3.2.2-3.2.5) into (3.2.6-3.2.8)

$$\varepsilon_{xx} = \varepsilon_{xx}^{linear} + \varepsilon_{xx}^{nonlinear}$$

$$= [L_1', L_2', -(\eta\sin\theta_{tw} + \zeta\cos\theta_{tw})[H_1'', H_2'', H_3'', H_4''],$$

$$-(\eta\cos\theta_{tw} - \zeta\sin\theta_{tw})[H_1'', H_2'', H_3'', H_4''],$$

$$(\eta^2 + \zeta^2)\theta_{tw}'[L_1', L_2']][u_1\ u_2\ w_1\ \beta_1\ w_2\ \beta_2\ v_1\ \zeta_1\ v_2\ \zeta_2\ \phi_1\ \phi_2]^T$$

$$+[0, 0, \frac{1}{2}w'[H_1', H_2', H_3', H_4'] - (\eta\cos\theta_{tw} - \zeta\sin\theta_{tw})\phi[H_1'', H_2'', H_3'', H_4''],$$

$$\frac{1}{2}v'[H_1', H_2', H_3', H_4'] - (-\eta\sin\theta_{tw} - \zeta\cos\theta_{tw})\phi[H_1'', H_2'', H_3'', H_4''],$$

$$\frac{1}{2}\phi'[L_1', L_2']]\{a^e\} \qquad (3.2.13)$$

$$\varepsilon_{x\eta} = -(\zeta + \frac{\partial\lambda}{\partial\eta})[L_1', L_2']\begin{Bmatrix}\phi_1\\ \phi_2\end{Bmatrix} \qquad (3.2.14)$$

$$\varepsilon_{x\zeta} = (\eta - \frac{\partial\lambda}{\partial\zeta})[L_1', L_2']\begin{Bmatrix}\phi_1\\ \phi_2\end{Bmatrix} \qquad (3.2.15)$$

From equation (3.2.12), we can obtain:

$$\frac{\partial U}{\partial u_1} = \int_0^{le}[\iint_A E\varepsilon_{XX}L_1'd_\eta d_\zeta]d_x \qquad (3.2.16)$$

$$\frac{\partial U}{\partial u_2} = \int_0^{le}[\iint_A E\varepsilon_{XX}L_2'd_\eta d_\zeta]d_x \qquad (3.2.17)$$

$$\frac{\partial U}{\partial w_1} = \int_0^{le}\{\iint_A E\varepsilon_{XX}[\underline{w'H_1'} - [\eta\sin(\theta_{tw}+\phi) + \zeta\cos(\theta_{tw}+\phi)]H_1'']d_\eta d_\zeta\}d_x$$

$$\ldots\ldots\ldots (3.2.18)$$

$$\frac{\partial U}{\partial \beta_1} = \int_0^{le}\{\iint_A E\varepsilon_{XX}[\underline{w'H_2'} - [\eta\sin(\theta_{tw}+\phi) + \zeta\cos(\theta_{tw}+\phi)]H_2'']d_\eta d_\zeta\}d_x$$

$$\ldots\ldots\ldots (3.2.19)$$

$$\frac{\partial U}{\partial w_2} = \int_0^{le}\{\iint_A E\varepsilon_{XX}[\underline{w'H_3'} - [\eta\sin(\theta_{tw}+\phi) + \zeta\cos(\theta_{tw}+\phi)]H_3'']d_\eta d_\zeta\}d_x$$

$$\ldots\ldots\ldots (3.2.20)$$

$$\frac{\partial U}{\partial \beta_2} = \int_0^{le} \left\{ \iint_A E\varepsilon_{XX} [\underline{w'H_4'} - [\eta \sin(\theta_{tw} + \phi) + \zeta \cos(\theta_{tw} + \phi)] H_4''] d_\eta d_\zeta \right\} d_x$$

.....(3.2.21)

$$\frac{\partial U}{\partial v_1} = \int_0^{le} \left\{ \iint_A E\varepsilon_{XX} [\underline{v'H_1'} - [\eta \cos(\theta_{tw} + \phi) - \zeta \sin(\theta_{tw} + \phi)] H_1''] d_\eta d_\zeta \right\} d_x$$

.....(3.2.22)

$$\frac{\partial U}{\partial \zeta_1} = \int_0^{le} \left\{ \iint_A E\varepsilon_{XX} [\underline{v'H_2'} - [\eta \cos(\theta_{tw} + \phi) - \zeta \sin(\theta_{tw} + \phi)] H_2''] d_\eta d_\zeta \right\} d_x$$

.....(3.2.23)

$$\frac{\partial U}{\partial v_2} = \int_0^{le} \left\{ \iint_A E\varepsilon_{XX} [\underline{v'H_3'} - [\eta \cos(\theta_{tw} + \phi) - \zeta \sin(\theta_{tw} + \phi)] H_3''] d_\eta d_\zeta \right\} d_x$$

.....(3.2.24)

$$\frac{\partial U}{\partial \zeta_2} = \int_0^{le} \left\{ \iint_A E\varepsilon_{XX} [\underline{v'H_4'} - [\eta \cos(\theta_{tw} + \phi) - \zeta \sin(\theta_{tw} + \phi)] H_4''] d_\eta d_\zeta \right\} d_x$$

.....(3.2.25)

$$\begin{aligned} \frac{\partial U}{\partial \phi_1} = \int_0^{le} \{ \iint_A [& E\varepsilon_{xx} ((\eta^2 + \zeta^2)(\theta_{tw}' L_1' + \underline{\phi' L_1'}) - v''[-\eta \sin(\theta_{tw} + \phi) L_1 \\ & - \zeta \cos(\theta_{tw} + \phi) L_1] - w''[\eta \cos(\theta_{tw} + \phi) L_1 - \zeta \sin(\theta_{tw} + \phi) L_1]) \\ & + G\varepsilon_{x\eta}(-\zeta - \frac{\partial \lambda}{\partial \eta}) L_1' + G\varepsilon_{x\zeta}(\eta - \frac{\partial \lambda}{\partial \zeta}) L_1'] d_\eta d_\zeta \} d_x \end{aligned} \qquad (3.2.26)$$

$$\begin{aligned} \frac{\partial U}{\partial \phi_2} = \int_0^{le} \{ \iint_A & E\varepsilon_{xx} ((\eta^2 + \zeta^2)(\theta_{tw}' L_2' + \underline{\phi' L_2'}) - v''[-\eta \sin(\theta_{tw} + \phi) L_2 \\ & - \zeta \cos(\theta_{tw} + \phi) L_2] - w''[\eta \cos(\theta_{tw} + \phi) L_2 - \zeta \sin(\theta_{tw} + \phi) L_2]) \\ & + G\varepsilon_{x\eta}(-\zeta - \frac{\partial \lambda}{\partial \eta}) L_2' + G\varepsilon_{x\zeta}(\eta - \frac{\partial \lambda}{\partial \zeta}) L_2'] d_\eta d_\zeta \} d_x \end{aligned} \qquad (3.2.27)$$

Note the following relations are applicable to (3.2.16) through (3.2.27):

$$\iint_A E\varepsilon_{xx} d_\eta d_\zeta = [EAL_1',\ EAL_2',\ -EAx_T \sin\theta_{tw} [H''_1\ H''_2\ H''_3\ H''_4],$$

$$-EAx_T \cos\theta_{tw} [H''_1\ H''_2\ H''_3\ H''_4],\ EAk^2_A \theta'_{tw} [L'_1,\ L'_2] \{a^e\}$$

$$+[0,\ 0,\ EA\frac{1}{2}w'[H'_1\ H'_2\ H'_3\ H'_4]-EAx_T\cos\theta_{tw}\phi[H''_1\ H''_2\ H''_3\ H''_4],$$
$$EA\frac{1}{2}v'[H'_1\ H'_2\ H'_3\ H'_4]+EAx_T\sin\theta_{tw}\phi[H''_1\ H''_2\ H''_3\ H''_4],$$
$$EAk_A^2\frac{1}{2}\phi'[L'_1,\ L'_2]\ ]\{a^e\} \qquad (3.2.28)$$

$$\iint_A E\varepsilon_{xx}\eta d_\eta d_\zeta=[EAx_TL_1',\ EAx_TL_2',\ -EI_{ZZ}\sin\theta_{tw}[H''_1\ H''_2\ H''_3\ H''_4],$$
$$-EI_{ZZ}\cos\theta_{tw}[H''_1\ H''_2\ H''_3\ H''_4],\ EB_2^*\theta'_{tw}[L'_1,\ L'_2]\{a^e\}$$
$$+[0,\ 0,\ EAx_T\frac{1}{2}w'[H'_1\ H'_2\ H'_3\ H'_4]-EI_{ZZ}\cos\theta_{tw}\phi[H''_1\ H''_2\ H''_3\ H'$$
$$EAx_T\frac{1}{2}v'[H'_1\ H'_2\ H'_3\ H'_4]+EI_{ZZ}\sin\theta_{tw}\phi[H''_1\ H''_2\ H''_3\ H''_4],$$
$$EAx_T\frac{1}{2}\phi'[L'_1,\ L'_2]\ ]\{a^e\} \qquad (3.2.29)$$

$$\iint_A E\varepsilon_{xx}\zeta d_\eta d_\zeta=[0,\ 0,\ -EI_{yy}\cos\theta_{tw}[H''_1\ H''_2\ H''_3\ H''_4],$$
$$-EI_{yy}\sin\theta_{tw}[H''_1\ H''_2\ H''_3\ H''_4],\ 0,\ 0]\{a^e\}$$
$$+[0,\ 0,\ -EI_{yy}\sin\theta_{tw}\phi[H''_1\ H''_2\ H''_3\ H''_4],$$
$$-EI_{yy}\cos\theta_{tw}\phi[H''_1\ H''_2\ H''_3\ H''_4],\ 0,\ 0]\{a^e\} \qquad (3.2.30)$$

$$\iint_A E\varepsilon_{xx}(\eta^2+\zeta^2)d_\eta d_\zeta=[EAk_A^2L_1',EAk_A^2L_2',-EB_2^*\sin\theta_{tw}[H''_1\ H''_2\ H''_3\ H''_4],$$
$$-EB_2^*\cos\theta_{tw}[H''_1\ H''_2\ H''_3\ H''_4],\ EB_1^*\theta'_{tw}[L'_1\ L'_2]\{a^e\}$$
$$+[0,\ 0,\ EAk_A^2\frac{1}{2}w'[H'_1\ H'_2\ H'_3\ H'_4]$$
$$-EB_2^*\cos\theta_{tw}\phi[H''_1\ H''_2\ H''_3\ H''_4],$$
$$EAk_A^2\frac{1}{2}v'[H'_1\ H'_2\ H'_3\ H'_4]+EB_2^*\sin\theta_{tw}\phi[H''_1\ H''_2\ H''_3\ H''$$
$$EAk_A^2\frac{1}{2}\phi'[L'_1\ L'_2]\ ]\{a^e\} \qquad (3.2.31)$$

$$\iint_A G[\varepsilon_{x\eta}(-\zeta-\frac{\partial\lambda}{\partial\eta})+\varepsilon_{x\zeta}(\eta-\frac{\partial\lambda}{\partial\zeta})]d_\eta d_\zeta=GJ[L'_1,\ L'_2]\begin{Bmatrix}\phi_1\\ \phi_2\end{Bmatrix} \qquad (3.2.32)$$

The symbols related to the section integrals in the above equations are defined as follows:

$$A = \iint_A d\eta d\zeta \qquad x_T = \frac{1}{A}\iint_A \eta d\eta d\zeta$$

$$EI_{yy} = \iint_A E\zeta^2 d\eta d\zeta \qquad EI_{zz} = \iint_A E\eta^2 d\eta d\zeta$$

$$EAk_A^2 = \iint_A E(\zeta^2 + \eta^2) d\eta d\zeta \qquad GJ = \iint_A G[(\zeta + \frac{\partial\lambda}{\partial\eta})^2 + (\eta - \frac{\partial\lambda}{\partial\zeta})^2] d\eta d\zeta$$

$$EB_1^* = \iint_A E(\zeta^2 + \eta^2)^2 d\eta d\zeta \qquad EB_2^* = \iint_A E\eta(\zeta^2 + \eta^2) d\eta d\zeta \quad \text{.....(3.2.33)}$$

The beam section is assumed to have an axis of symmetry η, so the following integrals are zero:

$$\iint_A \zeta d\eta d\zeta = 0 \qquad \iint_A \eta\zeta d\eta d\zeta = 0$$

$$\iint_A \zeta(\zeta^2 + \eta^2) d\eta d\zeta = 0$$

.....(3.2.34)

The variation of the strain energy of a element can be written as:

$$\delta U_j = [\delta u_1,\ \delta v_1,\ \delta w_1,\ \delta\beta_1,\ \delta\zeta_1,\ \delta\phi_1,\ \delta u_2,\ \delta v_2,\ \delta w_2,\ \delta\beta_2,\ \delta\zeta_2,\ \delta\phi_2,$$
$$\delta R_x,\ \delta R_y,\ \delta R_z\ \delta\theta_x,\ \delta\theta_y,\ \delta\theta_z]\{F_s^*\} \qquad (3.2.35)$$

where : $\{F_s^*\}$ is the generalised forces caused by the internal loads. They can be obtained from the following relations.

$$\{F_s^*\} = [\ \frac{\partial U}{\partial u_1},\ \frac{\partial U}{\partial v_1},\ \frac{\partial U}{\partial w_1},\ \frac{\partial U}{\partial\beta_1},\ \frac{\partial U}{\partial\zeta_1},\ \frac{\partial U}{\partial\phi_1},\ \frac{\partial U}{\partial u_2},\ \frac{\partial U}{\partial v_2},$$
$$\frac{\partial U}{\partial w_2},\ \frac{\partial U}{\partial\beta_2},\ \frac{\partial U}{\partial\zeta_2},\ \frac{\partial U}{\partial\phi_2},\ 0,\ 0,\ 0,\ 0,\ 0,\ 0]^T \qquad (3.2.36)$$

They are the generalised forces caused by the internal loads.

Applying Relations (3.2.28-3.2.33) to (3.2.16-3.2.27), then the above generalised force expressions gives the element stiffness matrix. It must be pointed out that the

nonlinear terms in the expressions of the strain energy derivatives are specifically treated here so that the relations can be conveniently applied to a general linear dynamics problem. These terms are related with the centrifugal effect of a rotating beam. They are underlined through equations (3.2.16) to (3.2.27). An approximation is made using the fact that the resultant force of the axial stress on a beam section is roughly equal to the centrifugal force applied on that cross section. That is

$$\iint_A E\varepsilon_{xx} d\eta d\zeta \approx T$$

Where T is the centrifugal force on a section of the beam.

Applying this approximation to the underlined terms in equations (3.2.16) to (3.2.27), we can obtain the generalised forces caused by the internal loads and hence its contribution to the element stiffness matrix. This model can be readily applied to both linear and nonlinear structural dynamics problems.

5.3.3 Equations of Motion of the System

According to the principle of virtual work :

$$\delta U - \delta W_I = 0 \qquad (3.3.1)$$

We use the Finite Element Method to discretize the equations. The beam is divided into a number of beam elements. Therefore, the equations (3.3.1) are discretized as

$$\sum_{j=1}^{Ne} \Delta_j = \sum_{j=1}^{Ne} (\delta U_j - \delta W_{Ij}) = 0 \qquad (3.3.2)$$

$$\Delta_j = \delta U_j - \delta W_{Ij} \qquad (j = 1 \ldots N_e) \qquad (3.3.3)$$

where N_e is the number of elements. Δ_j gives the contribution of the j'th element.

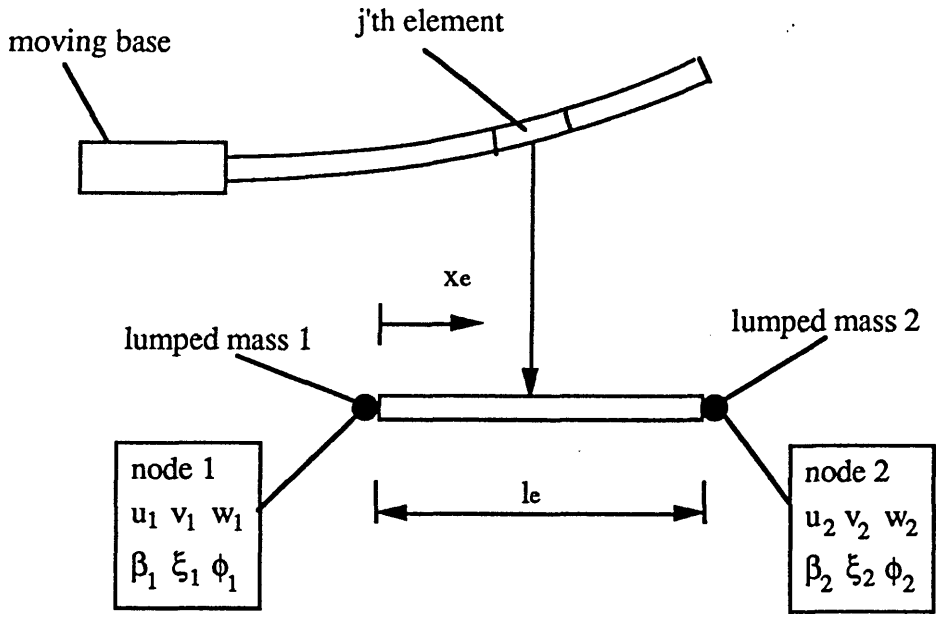

Fig 5.4 Illustration of a general finite element of the beam

Fig 5.4 gives a description of a typical element. The element inertia is lumped to the two nodes of the element. The virtual work done by the inertial loads is:

$$\delta W_{Ij}=\delta W_{Imass1}+\delta W_{Imass2} \qquad (3.3.4)$$

δW_{Imass1}, δW_{Imass2} can be obtained from equation (3.1.34), and utilising the expression (3.1.38), δW_{Ij} can be expressed as :

$$\delta W_{Ij} = [\delta u_1, \delta v_1, \delta w_1, \delta\beta_1, \delta\zeta_1, \delta\phi_1, \delta u_2, \delta v_2, \delta w_2, \delta\beta_2, \delta\zeta_2, \delta\phi_2,$$
$$\delta R_x, \delta R_y, \delta R_z, \delta\theta_x, \delta\theta_y, \delta\theta_z]\{ f(\{\ddot{a}_e\}, \{\dot{a}_e\}, \{a_e\}, \{a_b\}, \{\dot{a}_b\}) \}$$

Where $\{a_e\} = [u_1, u_2, w_1, \beta_1, w_2, \beta_2, v_1, \zeta_1, v_2, \zeta_2, \theta_{e1}, \theta_{e2}]^T$

$\{a_b\} = [v_x, v_y, v_z, \omega_x, \omega_y, \omega_z]^T$

The variation of the strain energy of the element has been obtained in equation (3.2.35), therefore $\Delta_j=\delta U_j-\delta W_{Ij}$ can be written in matrix form as :

$$\Delta_j = [\delta u_1, \delta v_1, \delta w_1, \delta\beta_1, \delta\zeta_1, \delta\phi_1, \delta u_2, \delta v_2, \delta w_2, \delta\beta_2, \delta\zeta_2, \delta\phi_2, \delta R_x, \delta R_y, \delta R_z,$$
$$\delta\theta_x, \delta\theta_y, \delta\theta_z] \{ [M_j]\{\ddot{a}_e\} + [C_j]\{\dot{a}_e\} + [K_j]\{a_e\} - \{Q_j\} \} \qquad (3.4.5)$$

where, $[M_j]$, $[C_j]$, and $[K_j]$ are the element inertia, gyroscopic, and stiffness matrices, respectively and $\{Q_j\}$ is the element load vector for the j'th element. The system global matrices can be obtained by the assembly of the element matrices. The total system degrees of freedom vector is denoted by $\{P\}$ which includes the six base degrees of freedom and all of the nodal degrees of freedom of the beam. The final equations of the beam can be expressed as:

$$\{\delta P\}^T\{[M]\{\ddot{P}_e\} + [C]\{\dot{P}_e\} + [K]\{P_e\} - \{Q\}\} = 0 \qquad (3.4.6)$$

Where $\{P_e\} = [u_1\ v_1\ w_1\ \beta_1\ \zeta_1\ \phi_1 \ldots\ldots u_n\ v_n\ w_n\ \beta_n\ \zeta_n\ \phi_n]$

$$\{\delta P\}^T = [\delta R_x, \delta R_y, \delta R_z\ \delta\theta_x, \delta\theta_y, \delta\theta_z\ \delta u_1, \delta v_1, \delta w_1, \delta\beta_1, \delta\zeta_1, \delta\phi_1,$$
$$\delta u_2, \delta v_2, \delta w_2, \delta\beta_2, \delta\zeta_2, \delta\phi_2, \ldots., \delta u_n, \delta v_n, \delta w_n, \delta\beta_n, \delta\zeta_n, \delta\phi_n]$$

n = number of the nodes of the beam

In equation (3.4.6), [M] is the assembled inertia matrix of the system, [C] is the assembled gyroscopic matrix, [K] is the assembled system stiffness matrix including the centrifugal stiffness effect. {Q} is the load vector.

Equation (3.4.6) is a set of (6n+6) nonlinear differential equations. [C], [K] and {Q} contain the kinematical variables of the beam's moving base, such as the base translational velocities and accelerations, and angular velocities and accelerations. If the coupling problem of a beam with other substructures is considered, a set of kinematical constraint conditions must be used to relate these variables to the relevant degrees of freedom of the other substructures. If we consider a problem with a prescribed base motion, the prescribed motion can be directly included through these kinematical variables.

5.4 COMPUTER SIMULATION

A FORTRAN computer program is developed based on the above model to solve not only eigenvalue problems, but also the dynamic response problem of a beam with arbitrary base motions. To meet the requirement to simulate possible structural coupling or possible complex beam root motions, nine kinematic variables of the beam base are incorporated into the program. They consist of three translational accelerations, three angular velocities and three angular accelerations of the base. In the present code, they are computed by a user supplied subroutine. The elasticity centre, mass centre and tension centre of the beam section may be different. The centrifugal force on a beam section is computed in a single subroutine. For some problems which require the nonlinear integral expressions of the beam deflection to define the centrifugal effects, this subroutine can be replaced by the original nonlinear relations. Again, the numerical integration over an element utilises the four point finite difference formulae [NAG Library].

The problem considered here has a prescribed base movement. Consequently, equation (3.4.6) is reduced to the last 6n equations.

$$[M_1]\{\ddot{P}_e\}+[C_1]\{\dot{P}_e\}+[K_1]\{P_e\}-\{Q_1\}=0 \qquad (4.1)$$

Note that $[M_1]$ is symmetric, but $[C_1]$ is skew symmetric, $[K_1]$ is asymmetric. This means that, although [C] multiplies the velocities like a damping matrix it never dissipates any energy. It serves to transfer energy from one mode to another. The asymmetry of the stiffness matrix $[K_1]$ is caused by the angular acceleration $\vec{\varepsilon}_h$ of the base. The angular acceleration $\vec{\varepsilon}_h$ of the base contributes the term $\vec{\varepsilon}_h x \vec{R}_{gc}$ to the acceleration $\vec{a}_{gc}$ in equation (3.1.10). This leads to an additional skew symmetric matrix to the stiffness matrix, and hence leads to an asymmetric global stiffness matrix $[K_1]$. Most commercial Finite Element programs can not handle a skew-symmetric matrix or an asymmetric matrix. Hence, their use is limited for this type of problem.

The eigenvalue problem associated with a rotating beam, hence, is written as:

$$[M_1]\{\ddot{P}_e\}+[C_1]\{\dot{P}_e\}+[K_1]\{P_e\}=0 \tag{4.2}$$

This is first reduced to the first-order state equation:

$$\begin{bmatrix} 0 & M_1 \\ M_1 & C_1 \end{bmatrix}\begin{Bmatrix} \ddot{P}_e \\ \dot{P}_e \end{Bmatrix} + \begin{bmatrix} -M_1 & 0 \\ 0 & K_1 \end{bmatrix}\begin{Bmatrix} \dot{P}_e \\ P_e \end{Bmatrix} = \begin{Bmatrix} 0 \\ 0 \end{Bmatrix} \tag{4.3}$$

The eigenvalue problem associated with (4.3) is then solved using the QZ algorithm [NAG Library].

We derived the equations of equilibrium (4.1) governing the nonlinear dynamic response of a finite element beam with an arbitrary base movement. The solution of this system of differential equations can be obtained by either the direct time integration or the mode superposition method [Bathe, 1982]. In direct integration the equations in (4.1) are integrated using a numerical step-by-step procedure. In mode superposition, before the temporal solution is performed, the equations of motion (4.1) has to be transformed into the modal coordinate system. Then the equations of motion in modal coordinates can be solved using the direct numerical integration procedure. The mode superposition method is usually much more economic than the direct integration method especially when a linear solution is required, because only a small portion of the total modes of the finite element system usually need be considered. This implies a great reduction of the system degree of freedom and hence, a great saving of the computing cost.

The mode superposition method is incorporated into the present computer program to solve the dynamic equations (4.1). The nonrotating natural modes are found first and used to reduce the size of the differential equations. Therefore, setting all of the base

kinematical variables in (4.1) to zero, the equations of motion for the natural vibration of the nonrotating beam become:

$$[M_2]\{\ddot{P}_e\}+[K_2]\{P_e\}=0 \tag{4.4}$$

Solving the eigenvalue problem associated with (4.4) and taking the first M modes $\{x_1\}$, $\{x_2\}$.....$\{x_M\}$, we can approximately express the nodal coordinates $\{P_e\}$ in terms of the linear combination of these M modes. That is:

$$\{P_e\}=\eta_1\{x_1\}+\eta_2\{x_2\}+.....+\eta_M\{x_M\}=[\Lambda]\{\eta\} \tag{4.5}$$

Replacing (4.5) into (4.1) and premultiplying (4.1) by $[\Lambda]^T$, we can obtain M differential equations of motion expressed by the modal coordinates $\{\eta\}$:

$$[M^*]\{\ddot{\eta}\}+[C^*]\{\dot{\eta}\}+[K^*]\{\eta\}-\{Q^*\}=0 \tag{4.6}$$

Writing (4.6) in the form of first-order state equation:

$$\begin{bmatrix} M^* & 0 \\ 0 & I \end{bmatrix}\begin{Bmatrix} \ddot{\eta} \\ \dot{\eta} \end{Bmatrix}=\begin{Bmatrix} Q^* \\ 0 \end{Bmatrix}-\begin{bmatrix} C^* & K^* \\ -I & 0 \end{bmatrix}\begin{Bmatrix} \dot{\eta} \\ \eta \end{Bmatrix} \tag{4.7}$$

The time history solution of (4.7) at a given initial conditions is subsequently obtained using the Runge Kutta step-by-step integration. The fourth order Runge Kutta formula is selected for its simplicity and good accuracy. The truncation error of the fourth order Runge Kutta method is of $(\Delta t)^5$. The modal solution is then transformed back to the physical coordinates according to the equation (4.5). The time step Δt for the integration can be decided approximately by observing the natural frequencies of the system. The outputs include the axial deflection, flap-wise deflection, lead-lag wise deflection, torsion deformation and the flapwise, lag-wise rotations of the beam section. The flow chart of the program is illustrated at the end of this section.

The modal reduction mentioned above can also be conducted using the rotating natural modes. Writing (4.1) in the first-order state form:

$$\begin{bmatrix} 0 & M_1 \\ M_1 & C_1 \end{bmatrix} \begin{Bmatrix} \ddot{P}_e \\ \dot{P}_e \end{Bmatrix} + \begin{bmatrix} -M_1 & 0 \\ 0 & K_1 \end{bmatrix} \begin{Bmatrix} \dot{P}_e \\ P_e \end{Bmatrix} = \begin{Bmatrix} 0 \\ Q_1 \end{Bmatrix} \tag{4.8}$$

or $$[A]\{\dot{x}\}+[B]\{x\}=\{F\} \tag{4.9}$$

To solve (4.9), we consider first the eigenvalue problem

$$[A]\{\dot{x}\}+[B]\{x\}=0 \tag{4.10}$$

Taking the first N modes of the eigensolution of (4.10), again, we approximate the state variable $\{x\}$ in terms of the linear combination of the N modes

$$\{x\}=\eta_1\{x_1\}+\eta_2\{x_2\}+.....+\eta_N\{x_N\}=[\Lambda]\{\eta\} \tag{4.11}$$

Substituting (4.11) into (4.10) and premultiplying (4.10) by $[\Lambda]^T$, we can obtain N first-order state equations:

$$[A^*]\{\dot{\eta}\}+[B^*]\{\eta\}=\{F^*\} \tag{4.12}$$

The time response solution of (4.12) can also obtained using the step-by-step integration. The solution for the state variable $\{x\}$ can be obtained from relation (4.11). The time history of the displacements $\{P_e\}$ can be extracted from the solution $\{x\}$. However, a significant fact must be pointed out that the component $\{\dot{P}_e\}$ of $\{x\}$ is not equal to the derivative of $\{P_e\}$ relative to the time t. That is : $\{\dot{P}_e\} \neq \frac{d\{P_e\}}{dt}$. This condition is only satisfied if all of the modes of equation (4.10) are used in solving (4.12). Care must be taken to avoid possible misunderstandying when this method is used.

As stated above, we could also obtain the dynamic response solution by directly integrating the finite element equations of motion (4.1). The modal reduction stated above is unnecessary in this case. It should be pointed out, however, that this will lead to many more degrees of freedom in the equations, and inevitably, much more computing time. Furthermore, more degrees of freedom will bring about much higher characteristic frequencies of the system. This usually implies that a smaller integration time step is required for numerical stability. Consequently, more computing time is needed to obtain the response at the required time. Nevertheless, when the nonlinear solution is required it is particularly desirable to directly apply the step-by-step integration technique to the finite element equations of motion (4.1). This task can be accomplished in the present code by simply abandoning the modal reduction procedure.

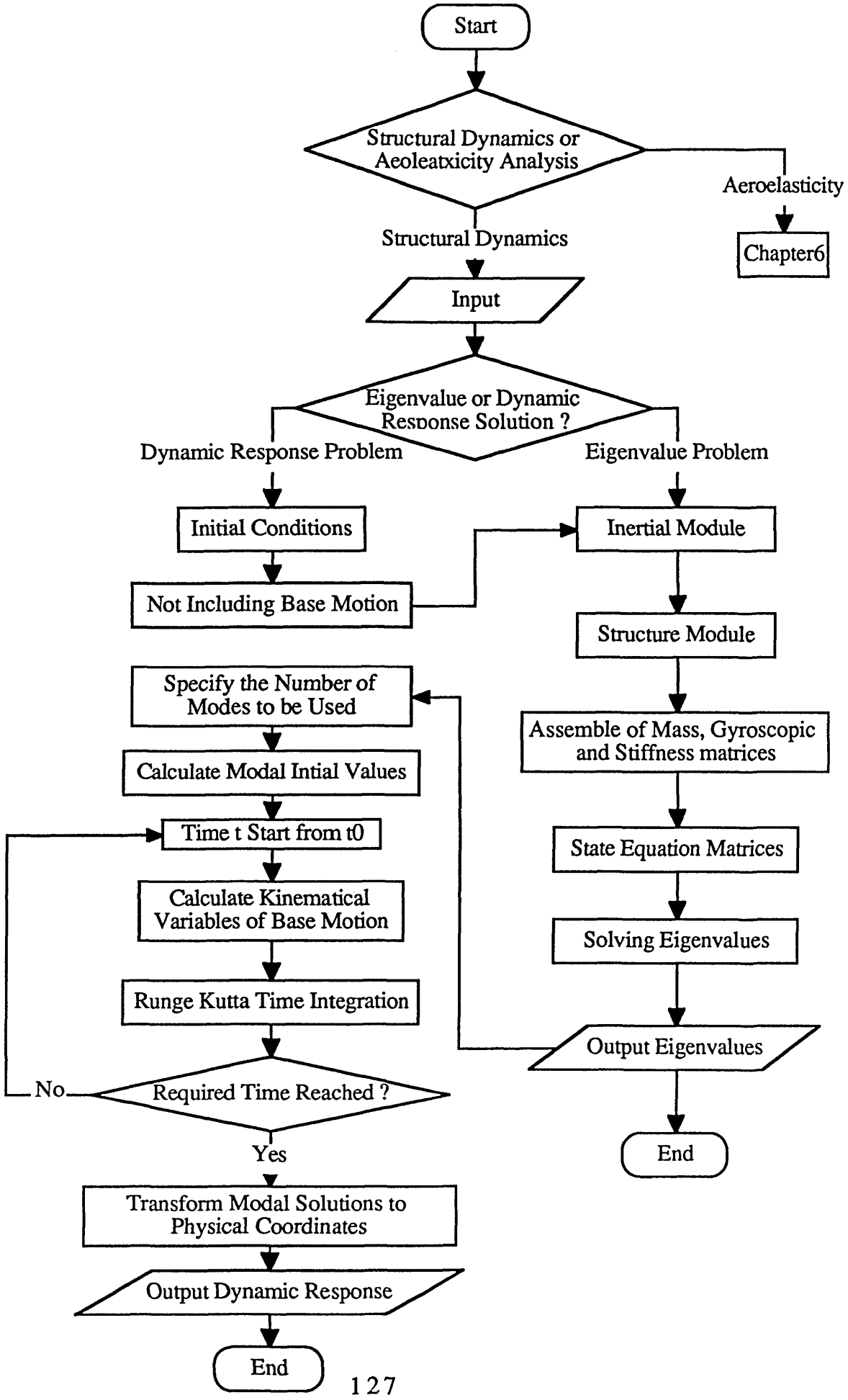
Start
Structural Dynamics or Aeoleatxicity Analysis
Aeroelasticity
Chapter6
Structural Dynamics
Input
Eigenvalue or Dynamic Response Solution ?
Dynamic Response Problem
Eigenvalue Problem
Initial Conditions
Not Including Base Motion
Inertial Module
Structure Module
Specify the Number of Modes to be Used
Assemble of Mass, Gyroscopic and Stiffness matrices
Calculate Modal Intial Values
Time t Start from t0
State Equation Matrices
Calculate Kinematical Variables of Base Motion
Solving Eigenvalues
Runge Kutta Time Integration
Output Eigenvalues
No
Required Time Reached ?
End
Yes
Transform Modal Solutions to Physical Coordinates
Output Dynamic Response
End

5.5 NUMERICAL EXAMPLES

Two groups of numerical examples are studied to validate the model and to show its application to the general dynamic simulation of a complex rotating beam. The first group is for a simple spinning beam and has an analytical solution to compare with. The second group is simulating the behaviour of a robotic manipulator which has a complex base motion. Results of this problem from a modal method specifically developed for a general multibody code are available for comparison.

5.5.1 An Example of a Simple Spinning Beam

A simple centrifugally stiffened beam is illustrated in Fig 5.5. The beam spins about a fixed axis at a constant angular velocity Ω. The beam is free to vibrate in the vertical direction. Wright et al [1982] developed an exact analytical model for this system.

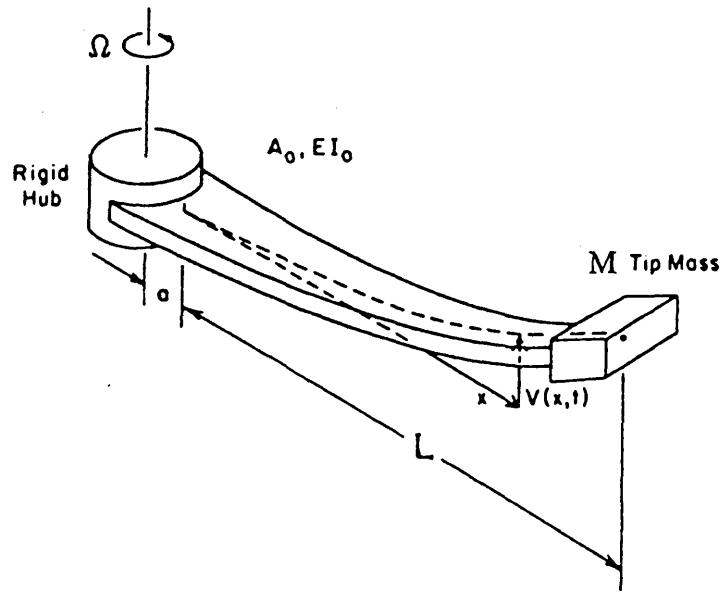

Fig 5.5 A simple centrifugally stiffened beam

The convergence of the modal frequencies, using different numbers of finite elements is presented first. Table 5.1 shows the values of the first five modal frequencies as the total number of elements is varied from 2 to 8. The value of η ($=\sqrt{\rho AL^4\Omega^2/EI}$) is 6.0. The results show, for the case considered, that eight elements are sufficient for reasonably good convergence.

Table 5.1 Convergence of Finite Element

Number of Elements	ω_1	ω_2	ω_3	ω_4	ω_5
2	7.1958	20.846			
3	7.2773	23.415	51.620		
4	7.3113	24.692	57.711	97.468	
5	7.3282	25.387	60.587	109.08	157.82
6	7.3377	25.795	62.280	114.30	176.75
7	7.3436	26.053	63.368	117.30	185.52
8	7.3475	26.224	64.105	119.27	190.38

Subsequently, two groups of analytical results from Wright et al [1982] are tabled in Table 5.2 and Table 5.3 for a cantilever beam and a hinged beam respectively. The results from the present finite element model are also given in the two Tables, where 8 elements are used. A good agreement between these two models is observed for all the first five mode frequencies and especially the first four modes. The symbols in the tables are introduced as: $\eta=\sqrt{\rho AL^4\Omega^2/EI}$, ρA: mass per unit length of beam, EI: flexural rigidity of beam, L: length of beam, Ω: rotating speed of beam. ω_1 to ω_5 represent the first five modal frequencies of the spinning beam.

Table 5.2 Frequency Ratios of a Uniform Cantilever Beam

η		ω_1	ω_2	ω_3	ω_4	ω_5
0.0	Exact	3.5160	22.0345	61.6972	120.902	199.860
	Present	3.4910	21.501	59.276	114.28	185.37
1.0	Exact	3.6817	22.1810	61.8418	121.051	200.012
	Present	3.6577	21.646	59.416	114.43	185.51
2.0	Exact	4.1373	22.6149	62.2732	121.497	200.467
	Present	4.1159	22.076	59.835	114.85	185.93
3.0	Exact	4.7973	23.3203	62.9850	122.236	201.223
	Present	4.7787	22.775	60.524	115.55	186.64
4.0	Exact	5.5850	24.2734	63.9668	123.261	202.277
	Present	5.5688	23.718	61.476	116.53	187.62
5.0	Exact	6.4495	25.4461	65.2050	124.566	203.622
	Present	6.4352	24.877	62.674	117.77	188.86
6.0	Exact	7.3604	26.8091	66.6840	126.140	205.253
	Present	7.3475	26.224	64.105	119.27	190.38
7.0	Exact	8.2996	28.3341	68.3860	127.972	207.161
	Present	8.2878	27.730	65.750	121.00	192.15
8.0	Exact	9.2568	29.9954	70.2930	130.049	209.338
	Present	9.2459	29.369	67.591	122.98	194.17
9.0	Exact	10.2257	31.7705	72.3867	132.358	211.775
	Present	10.216	31.119	69.611	125.16	196.43
10.0	Exact	11.2023	33.6404	74.6493	134.884	214.461
	Present	11.193	32.962	71.791	127.56	198.92
11.0	Exact	12.1843	35.5890	77.0638	137.614	217.385
	Present	12.175	34.881	74.114	130.14	201.62
12.0	Exact	13.1702	37.6031	79.6145	140.534	220.536
	Present	13.162	36.863	76.566	132.90	204.54

Table 5.3 Frequency Ratios of a Uniform Hinged Beam

η		ω_1	ω_2	ω_3	ω_4	ω_5
0.0	Exact	0.0000	15.4182	49.9649	104.248	178.270
	Present	0.0000	15.1100	48.1971	98.9931	166.483
1.0	Exact	1.0000	15.6242	50.1537	104.420	178.440
	Present	1.0000	15.3148	48.3717	99.1587	166.643
2.0	Exact	2.0000	16.2261	50.6760	104.936	178.949
	Present	2.0000	15.9127	48.8914	99.6535	167.122
3.0	Exact	3.0000	17.1807	51.5498	105.789	179.794
	Present	3.0000	16.8604	49.7441	100.472	167.916
4.0	Exact	4.0000	18.4313	52.7463	106.971	180.970
	Present	4.0000	18.1004	50.9108	101.606	169.022
5.0	Exact	5.0000	19.9197	54.2419	108.469	182.469
	Present	5.0000	19.5746	52.3678	103.042	170.431
6.0	Exact	6.0000	21.5944	56.0099	110.270	184.283
	Present	6.0000	21.2314	54.0880	104.766	172.134
7.0	Exact	7.0000	23.4133	58.0223	112.356	186.401
	Present	7.0000	23.0290	56.0436	106.762	174.123
8.0	Exact	8.0000	25.3436	60.2513	114.709	188.812
	Present	8.0000	24.9347	58.2067	109.012	176.385
9.0	Exact	9.0000	27.3601	62.6705	117.313	191.504
	Present	9.0000	26.9239	60.5511	111.497	178.908
10.0	Exact	10.0000	29.4439	65.2554	120.146	194.462
	Present	10.0000	28.9780	63.0525	114.200	181.678
11.0	Exact	11.0000	31.5809	67.9842	123.193	197.673
	Present	11.0000	31.0830	65.6890	117.101	184.683
12.0	Exact	12.0000	33.7603	70.8373	126.431	201.122
	Present	12.0000	33.2285	68.4416	120.182	187.909

5.5.2 An Example for a Robotic Manipulator

Fig 5.6 shows the structure of this problem. The manipulator consists of three links L1, L2, L3 connected by revolute joints. The outboard link L3 consists of a base A and two distinct segments B1 and B2. Segment B1 is 2.6667 meters long and has a symmetric box cross section, while B2 is a 5.3333 meter-long channel. Both segments are made of a material for which $E=6.895X10^{10}$ N/m^2, $G=2.6519X10^{10}$ N/m^2 and $\rho/A=2766.67$ kg/m^3. The section properties for B1 are: $A=3.84x10^{-4}$ m^2, $I_{yy}=I_{zz}=1.5x10^{-7}$ m^4, the torsion constant $J=2.2x10^{-7}$ m^4, sectional mass centre offset $x_{gc}=0$, while the corresponding properties of B2 are: $A=7.3x10^{-5}$ m^2, $I_{yy}=8.2181x10^{-9}$ m^4, $I_{zz}=4.8746x10^{-9}$ m^4, the torsion constant $J=2.433x10^{-11}$ m^4, sectional mass centre offset $x_{gc}=0.01875$ m.

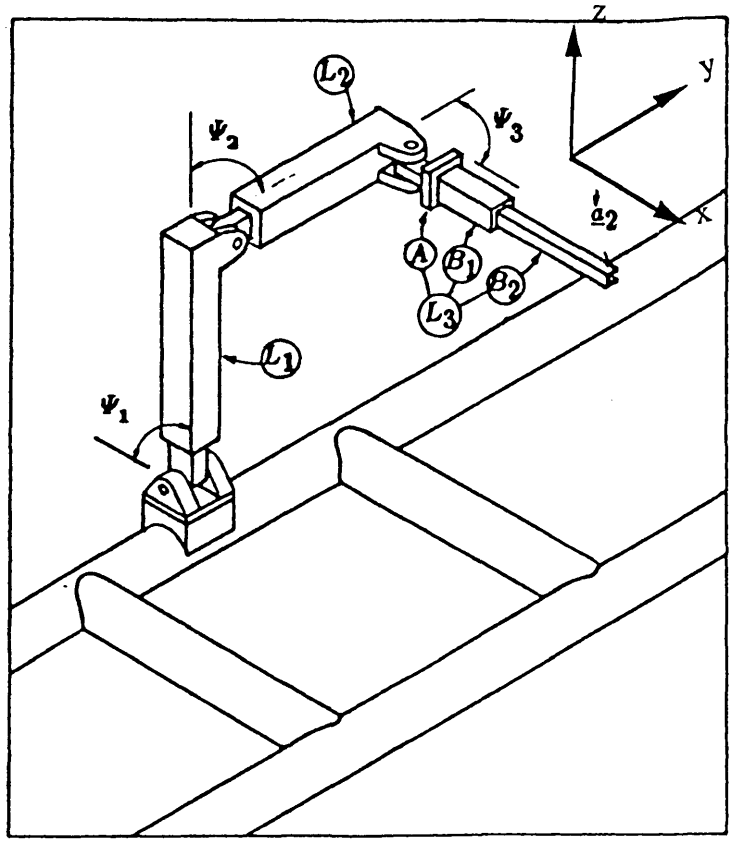

Fig 5.6 Illustration of a space-based robotic manipulator

The behaviour of L3 during two different base movement cases are simulated by Kane et al [1987]. These two cases are investigated using the present structural dynamics model and are compared with the simulation results from Kane et al [1987]. In order to save the computing time and be consistent when comparing with the reference, the nonlinear terms are set to zero in the computation for this problem. The nonlinear terms are thoroughly verified in the aeroelasticity model in the next chapter.

If the two inboard links L1 and L2, each of length l=8 m, are treated as rigid, the motion of the base A of the outboard link is characterised by the following kinematical functions:

$$v_x = l(1+c_2)s_3\dot{\Psi}_1, \qquad v_y = -l(1+c_2)c_3\dot{\Psi}_1, \qquad v_z = -l\dot{\Psi}_2$$

$$\omega_x = \dot{\Psi}_1 s_2 c_3 - \dot{\Psi}_2 s_3, \qquad \omega_y = \dot{\Psi}_1 s_2 s_3 + \dot{\Psi}_2 c_3, \qquad \omega_z = -\dot{\Psi}_1 c_2 - \dot{\Psi}_3$$

where: $c_i=\cos\Psi_i$, $s_i=\sin\Psi_i$ (i=1,2,3)

The first base movement case is the deployment process of the manipulator from a stowed configuration to a fully operational configuration. This process is presumed to last for 15 seconds (T=15 secs). The changes of the angles Ψ_1, Ψ_2, Ψ_3 are given as following.

$$\Psi_1 = \begin{cases} \pi - \frac{\pi}{2T}\left(t - \frac{T}{2\pi}\sin\frac{2\pi t}{T}\right) \text{ rad} & 0 < t \le T \\ \frac{\pi}{2} \text{ rad} & t > T \end{cases}$$

$$\Psi_2 = \begin{cases} \pi - \frac{3\pi}{4T}\left(t - \frac{T}{2\pi}\sin\frac{2\pi t}{T}\right) \text{ rad} & 0 < t \le T \\ \frac{\pi}{4} \text{ rad} & t > T \end{cases}$$

$$\Psi_3 = \begin{cases} \pi - \frac{\pi}{T}\left(t - \frac{T}{2\pi}\sin\frac{2\pi t}{T}\right) \text{ rad} & 0 < t \le T \\ 0 \text{ rad} & t > T \end{cases}$$

* *In the dynamic response analysis for the manipulator, 9 elements were used to obtain the eigen modes of the non-rotating and non-translating cantilever manipulator arm. Then, the first 10 modes are used in the computation of the dynamic responses.*

Fig 5.7, 9, 11 present the simulation results from the present algorithm. Fig 5.7, 5.9 and 5.11 give the displacement of the manipulator's tip during the deployment process in the flapping (z), lead-lag (y) and torsion respectively. Fig 5.8, 5.10, 5.12 show the corresponding results published by Kane et al [1987]. Comparing Fig 5.7 and 5.9 to Fig 5.8 and 5.10, it is found that the present simulation results are identical to the results from Kane et al [1987] but with a slightly larger amplitude. This difference is caused by the exclusion of the effect of the warping on the beam torsion stiffness (GJ) in the present computation. This simplification implies a smaller effective torsional constant (J) than in Kane's calculation and hence a larger response amplitude of the torsion deflection. Consequently, the flapping deflection is also increased by the strong flap-torsion coupling.

Comparing Fig 5.11 to Fig 5.12, a relatively large discrepancy is observed in the two curves. Especially interesting is that this discrepancy is obvious from time 0 second to about 12 seconds, while the discrepancy becomes much smaller from then on. This difference is due to the approximation of the beam's axial extension deflection introduced by the linear Kane's model. That is analysed in detail as follows.

In Kane's model, the stretch s(x) in the beam along the elastic axis is taken as axial degree of freedom (Fig 5.13). Therefore, the following relation exists:

$$s(x)=\int_0^x \varepsilon_{xx} dx \qquad (5.1)$$

where ε_{xx} is the axial strain at the elastic axis.

In the present model, the displacement u(x) of beam sectional elasticity centre in the x direction is taken as axial degree of freedom (Fig 5.13). From the nonlinear strain-displacement relation (3.2.6), we can obtain:

$$\varepsilon_{xx}=u'+\frac{v'^2}{2}+\frac{w'^2}{2} \qquad (5.2)$$

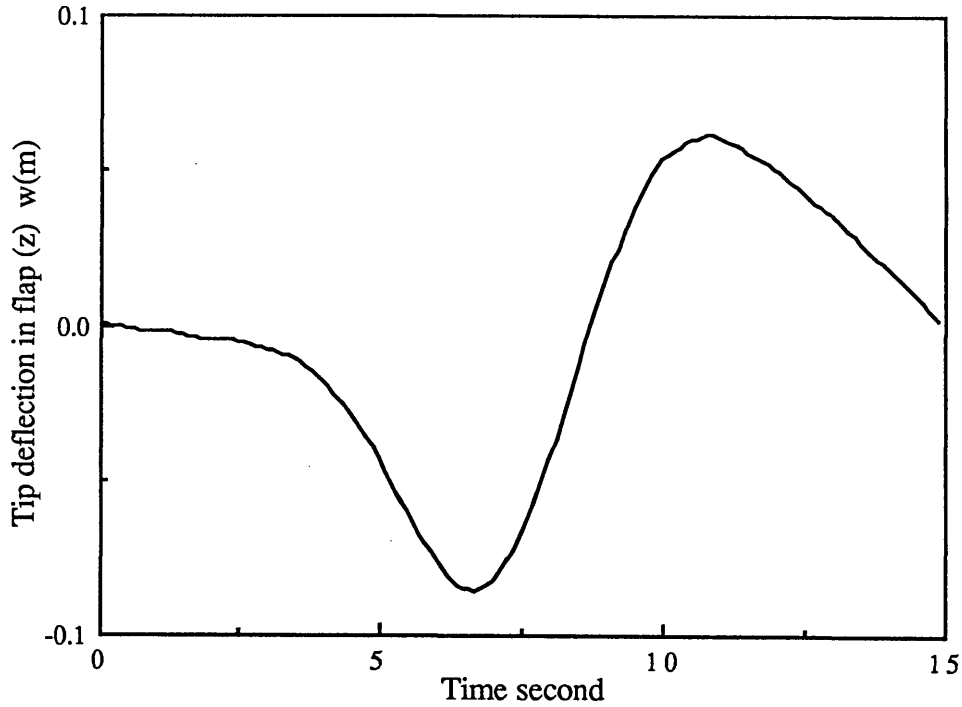

Fig 5.7 Simulation of the deployment of the robotic manipulator (in flap)

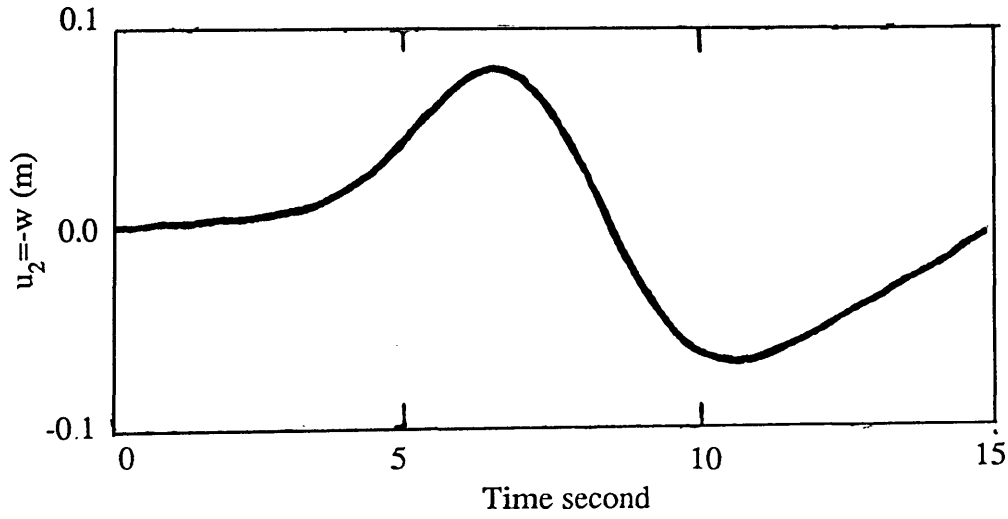

Fig 5.8 Simulation of the deployment of the robotic manipulator (in flap) from Kane et al, 1987

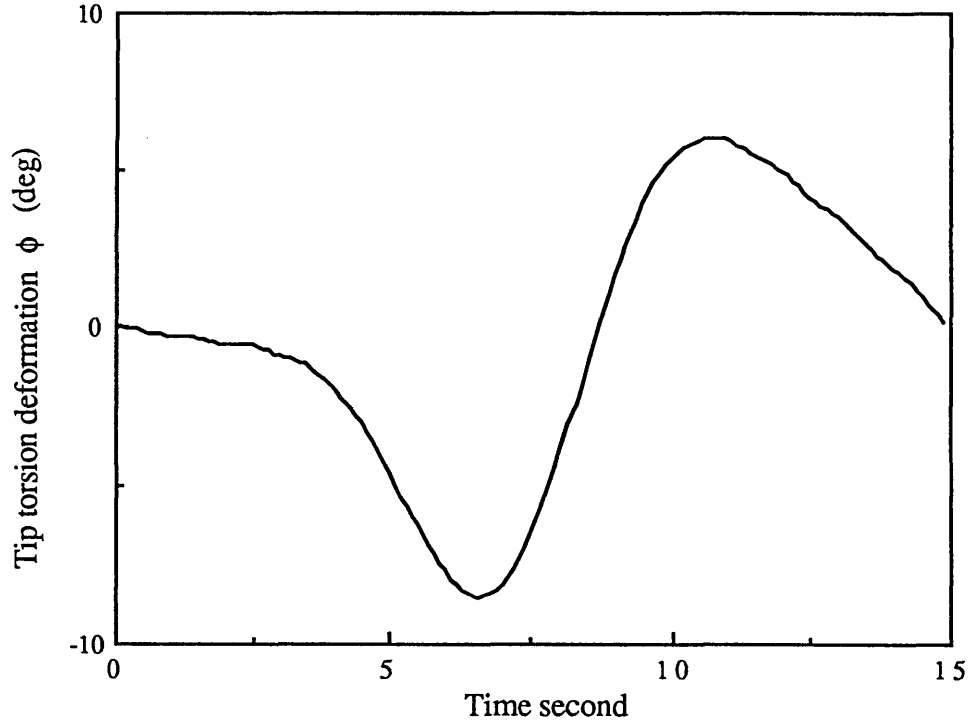

Fig 5.9 Simulation of the deployment of the robotic manipulator (in torsion)

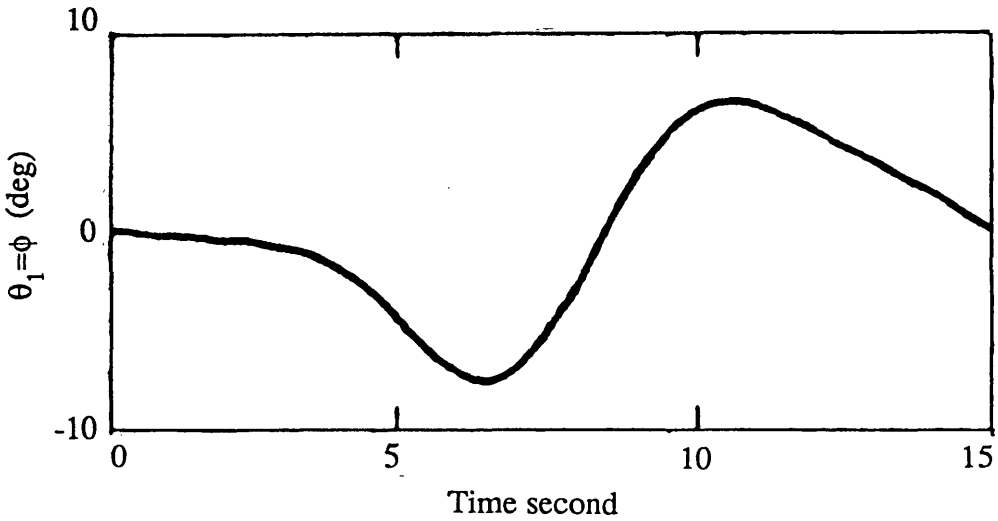

Fig 5.10 Simulation of the deployment of the robotic manipulator (in torsion) from Kane et al, 1987

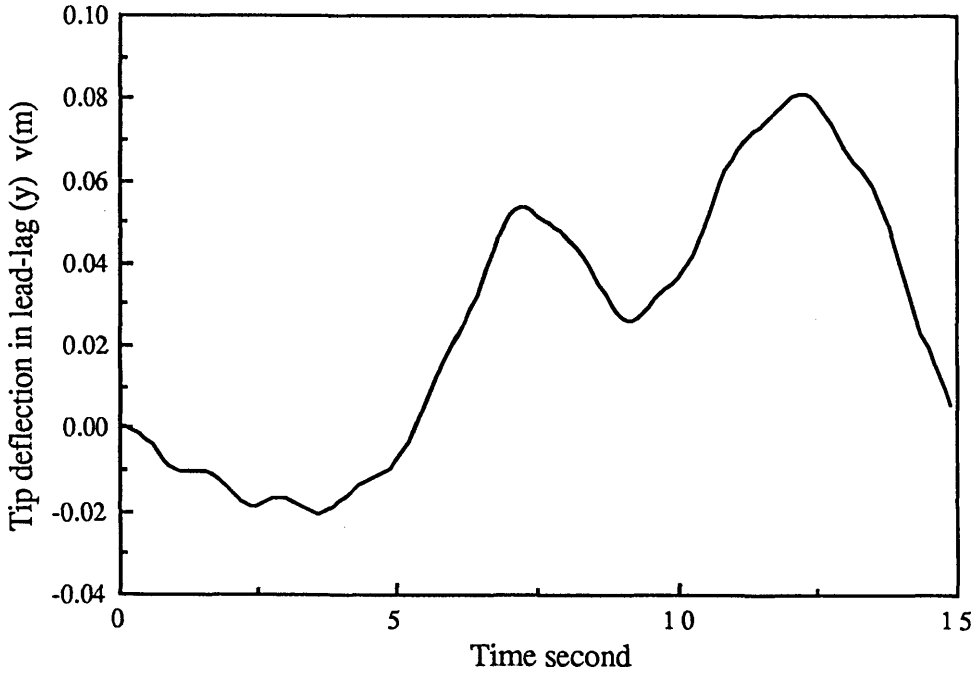

Fig 5.11 Simulation of the deployment of the robotic manipulator (in lead-lag)

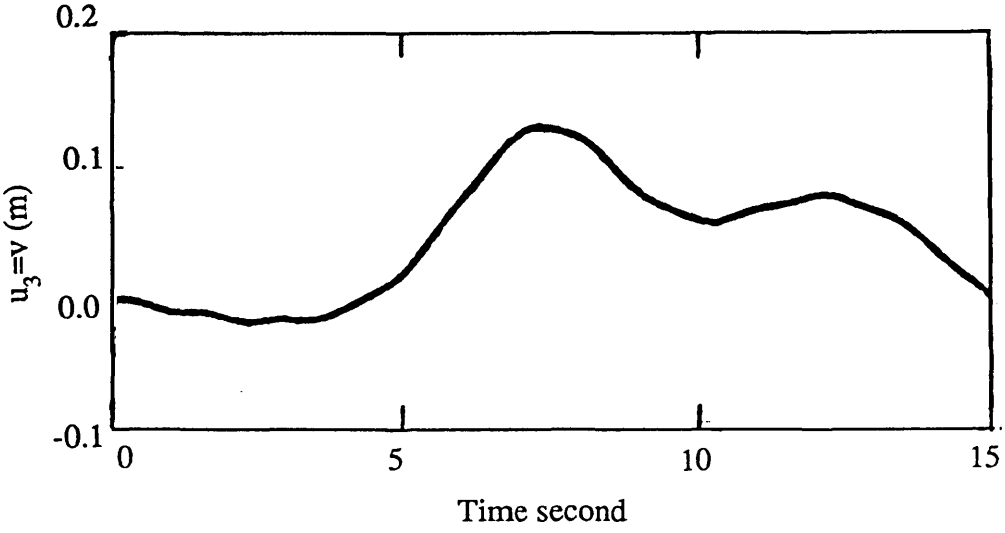

Fig 5.12 Simulation of the deployment of the robotic manipulator (in lead-lag) from Kane et al, 1987

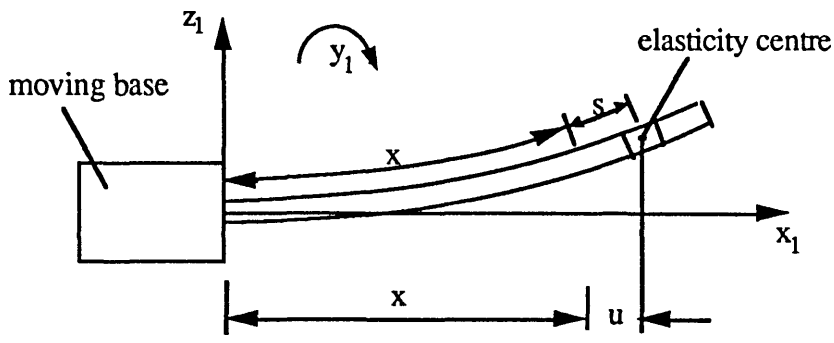

Fig 5.13 Illustration of displacement u and stretch s of the beam

Combining (5.1) and (5.2), we have:

$$s'(x)=u'+\frac{v'^2}{2}+\frac{w'^2}{2} \tag{5.3}$$

Then,
$$u=s(x)-\int_0^x(\frac{v'^2}{2}+\frac{w'^2}{2})dx \tag{5.4}$$

Differentiating (5.4) with respect to time gives:

$$\dot{u}=\dot{s}-\int_0^x(v'\dot{v}'+w'\dot{w}')dx \tag{5.5}$$

$$\ddot{u}=\ddot{s}-\int_0^x(\dot{v}'^2+v'\ddot{v}'+\dot{w}'^2+w'\ddot{w}')dx \tag{5.6}$$

In Kane's model, s(x) is taken as degree of freedom. Consequently, the displacement u(x) must be expressed in terms of s(x) and v, w. Therefore, (5.6) should be used for u(x) to be more accurately considered. However, Kane's model used the approximate relation $\ddot{u}=\ddot{s}$ since that model is a linear one. By contrast, such an approximation was not made in the present model. This approximation gives Kane's results an approximate axial inertial load ($m\ddot{u}$) inconsistent with that of the present model. This inconsistency could cause the solution difference for the axial deflection between these two models and

therefore, cause the solution difference for the lead-lag deflection due to the strong extension--lead-lag coupling. Obviously, such a difference depends on the values of $\dot{v}'^2$, $v'\dot{v}'$, $\dot{w}'^2$, $w'\dot{w}'$ from (5.6). That is the reason why the discrepancy between the present model and Kane's model is larger in some time ranges and is smaller in others. It is believed that the values of $\dot{v}'$, $\ddot{v}'$, $\dot{w}'$, $\ddot{w}'$ are relatively large from time 0 second to about 12 seconds, while they are relatively small from the last peak of Fig 5.11 to 15 seconds. Fig 5.14 shows the time history of the axial extensional deflection u of the manipulator's tip. Fig 5.15, 5.16 illustrate the variations of v' and w' of the manipulator's tip with the time.

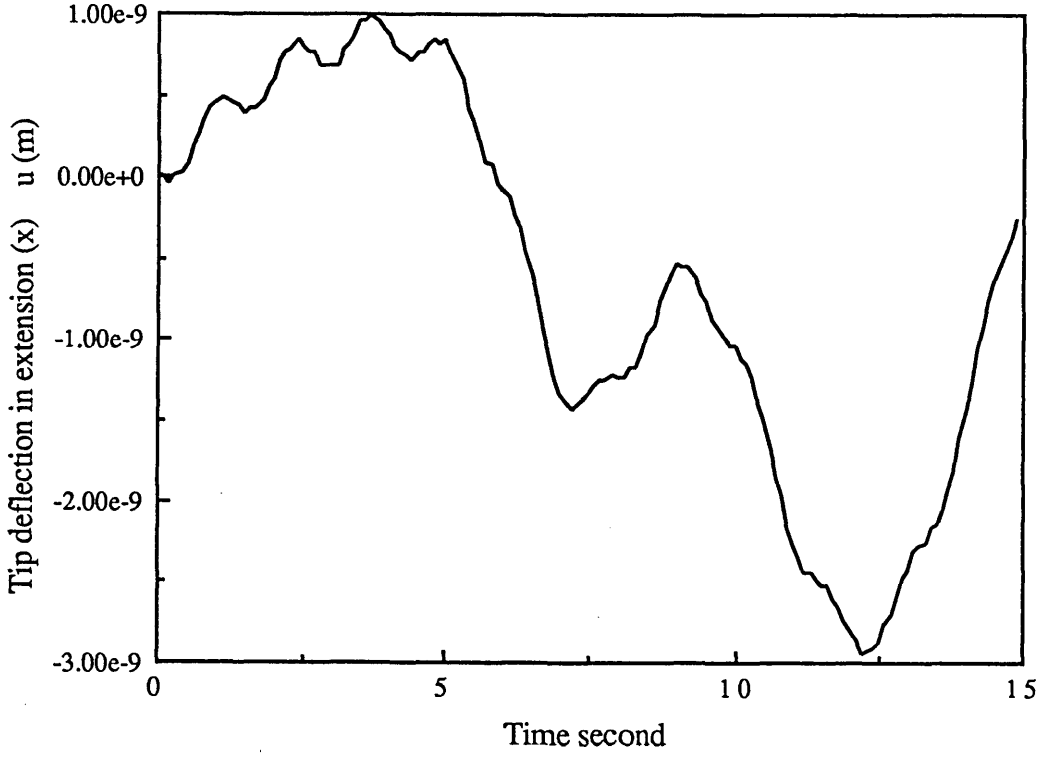

Fig 5.14 Simulation of the deployment of the robotic manipulator (in extension)

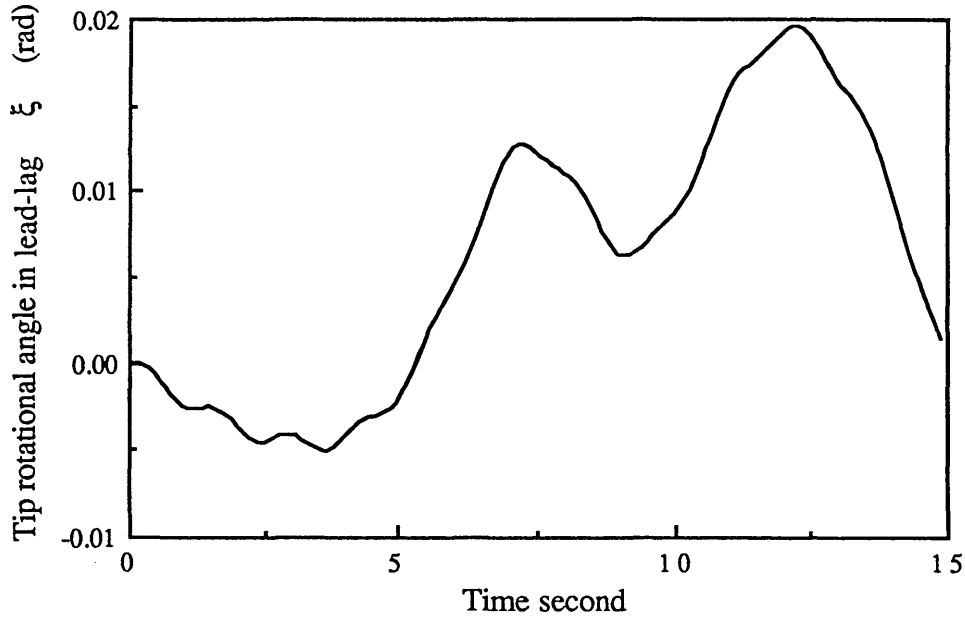

Fig 5.15 Simulation of the deployment of the robotic manipulator (lead-lag rotatio

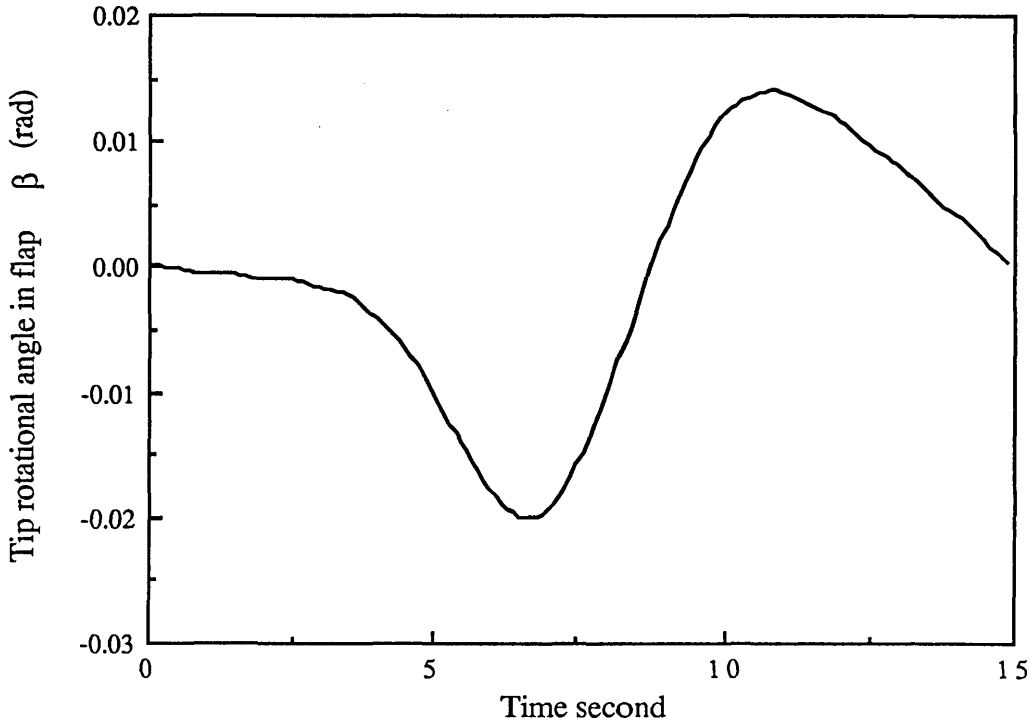

Fig 5.16 Simulation of the deployment of the robotic manipulator (flap rotation)

The second base movement case is for the so-called spin-up manoeuvre. The link L1 remains at rest, L2 and A remain at rest relative to each other, and the angular speed of A increases from zero to 6 rad/sec in a time interval of 15 seconds. This, therefore, is a simple case of centrifugal stiffening. The base motion description is:

$$\Psi_1 = \frac{\pi}{2} \quad \text{rad} \qquad t > 0$$

$$\Psi_2 = \begin{cases} \frac{6}{15}\left[\frac{t^2}{2} + \left(\frac{15}{2\pi}\right)^2\left(\cos\frac{2\pi t}{15} - 1\right)\right] & \text{rad} \qquad 0 < t \le T \\ (6t - 45) \quad \text{rad} & \qquad t > T \end{cases}$$

$\Psi_3 = 0$ rad $\qquad t > 0$

Fig 5.17, 19, 21 present the dynamic responses of the manipulator's tip in this process. They are obtained from the present algorithm. Fig 5.18, 20, 22 are taken from Kane et al [1987]. In Fig 5.18, 20, 22, the solid lines are obtained using the theory of Kane et al [1987], while the dashed lines are from a conventional multibody dynamics program. As pointed out by Kane et al [1987], the previous conventional approach lacks some significant terms in modelling and hence leads to some significant deficiencies in the dynamic simulation. Comparing Fig 5.17 and 5.19 to Fig 5.18 and 5.20, the present simulation is found to be identical to those from Kane's model but, again, with a slightly larger amplitude. As explained before, that is due to ignoring of the effect of warping on the effective torsional constant (J) in the present computation.

Comparing Fig 5.21 to Fig 5.22, this time, it is found that the discrepancy in the lead-lag deflection between the present model and Kane's model is small. Such a result is expected since the current lead-lag deflection is very small and has a very small variation with the time. This results in very small values of v', $\dot{v}'$, $\ddot{v}'$. Meanwhile, the variation of the flap deflection with the time is also relatively small. Consequently, the values of $\dot{w}'$, $\ddot{w}'$ are also relatively small. Therefore, as pointed out in the last example, the

approximation $\ddot{u}=\ddot{s}$ made in Kane's model leads to much smaller difference in the extension and lead-lag deflection. Consequently, the result agree better with the present model. The response of the manipulator's tip in extension (u) is also presented in Fig 5.23.

5.6 CONCLUSIONS

A new general Finite Element structural dynamics model is developed for a three dimensional elastic beam with an arbitrary and large moving base with six degrees of freedom. The six degrees of freedom of the beam base can incorporate either a prescribed arbitrary motion of the base or the coupling of the beam with other substructures. The beam can be pretwisted and has a mass centre offset from the elasticity centre. The equation of motion are derived using the virtual work principle. Large deflections and small strains of the beam are assumed so that the geometrical nonlinearities are included. The equations are discretised using the finite element method. The beam inertia is lumped at the end nodes of each element and this simplifies the analysis. The axial and torsional deflections of the beam element are represented by linear polynomials, while the bending deflections are represented by cubic polynomials. The centrifugal stiffness and gyroscopic terms caused by the large base motion are specifically considered so that this dynamic model is applicable for both nonlinear and linear problems.

This dynamic model was coded into a computer program and applied to both solve the eigenvalue problem of a spinning beam and to simulate a dynamic response of a robotic manipulator with a complex time-varying base motion. The former has a precise analytical solution to compare with, and the latter has an numerical solution based on a modal method to compare with. The results show:

1) Six to eight elements are sufficient for determining natural frequencies of a rotating beam.

2) The present Finite Element model can successfully solve the eigenvalue problems of a rotating beam.
3) The present model has been shown to be an appropriate and general tool for treating the dynamic response problem of a beam with complex and large base motion. This model is of a great modelling generality due to the combination of the Finite Element method and the arbitrary base motion variables which is widely used in Multibody Dynamics.
4) An approximation introduced by a linear dynamics model is found to have relatively large effect on the dynamic response in some cases. That approximation and effect are discussed in detail. Some significant deficiencies existing in previous multibody dynamics models are confirmed.

Results show that the newly developed model can appropriately model a complex rotating beam system and is of great modelling flexibility.

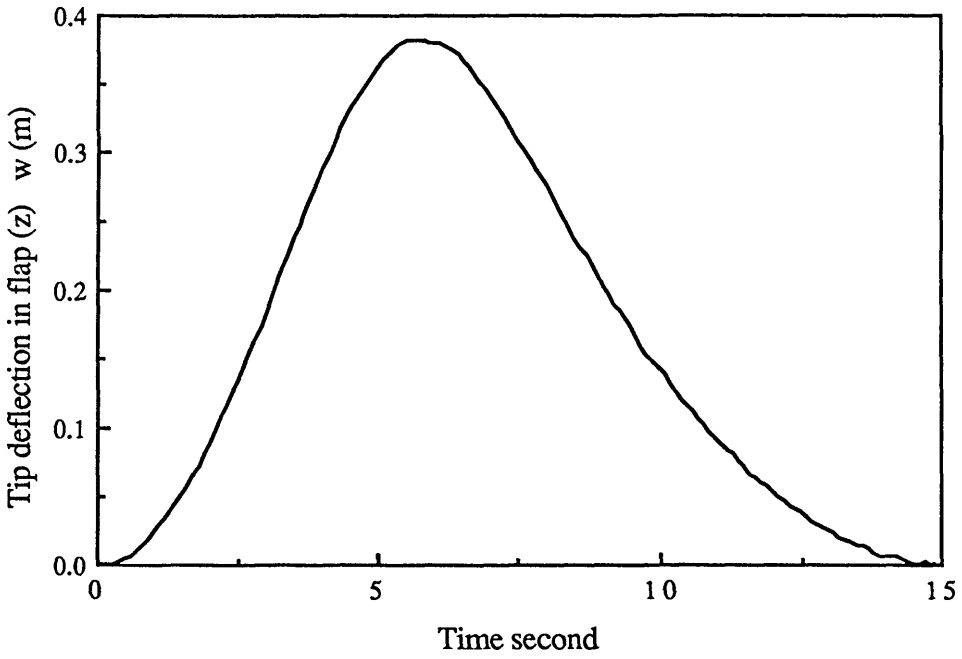

Fig 5.17 Simulation of the spin-up manoeuvre of the robotic manipulator (in flap)

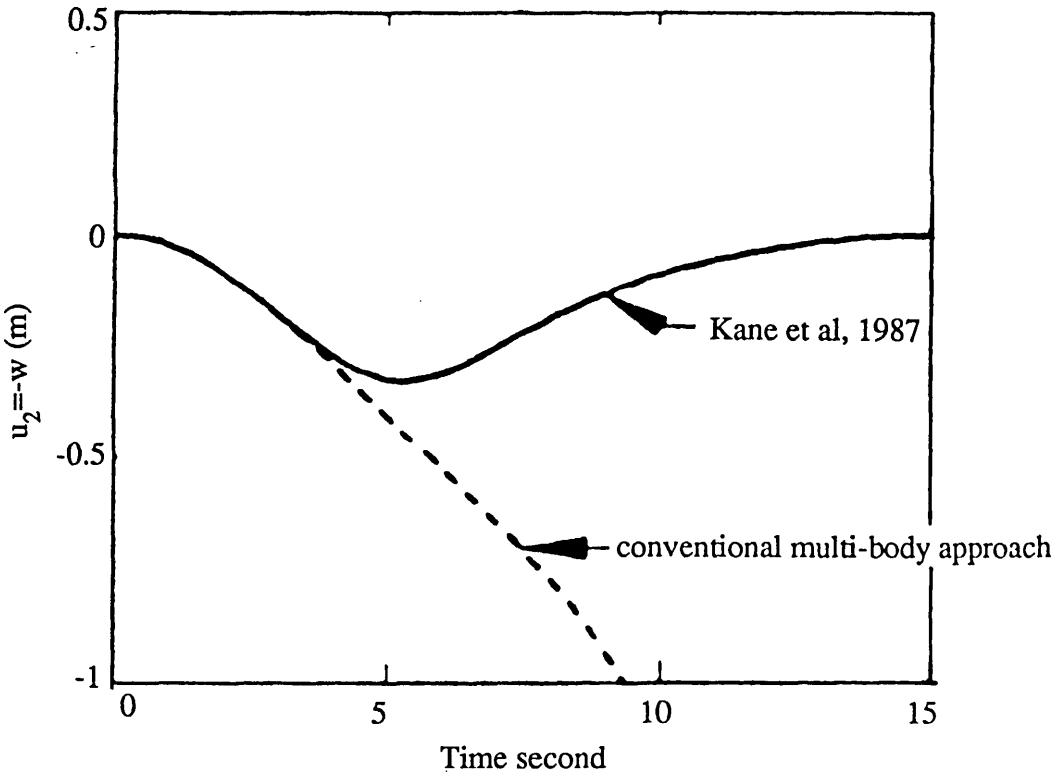

Fig 5.18 Simulation of the spin-up manoeuvre of the robotic manipulator (in flap) from Kane et al, 1987

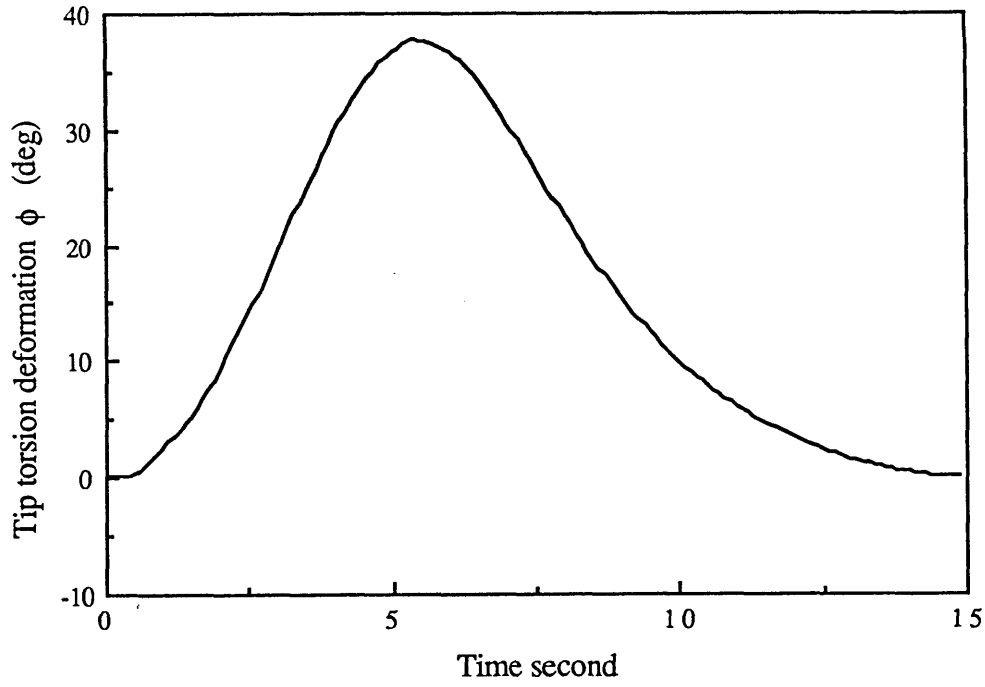

Fig 5.19 Simulation of the spin-up manoeuvre of the robotic manipulator (in torsic

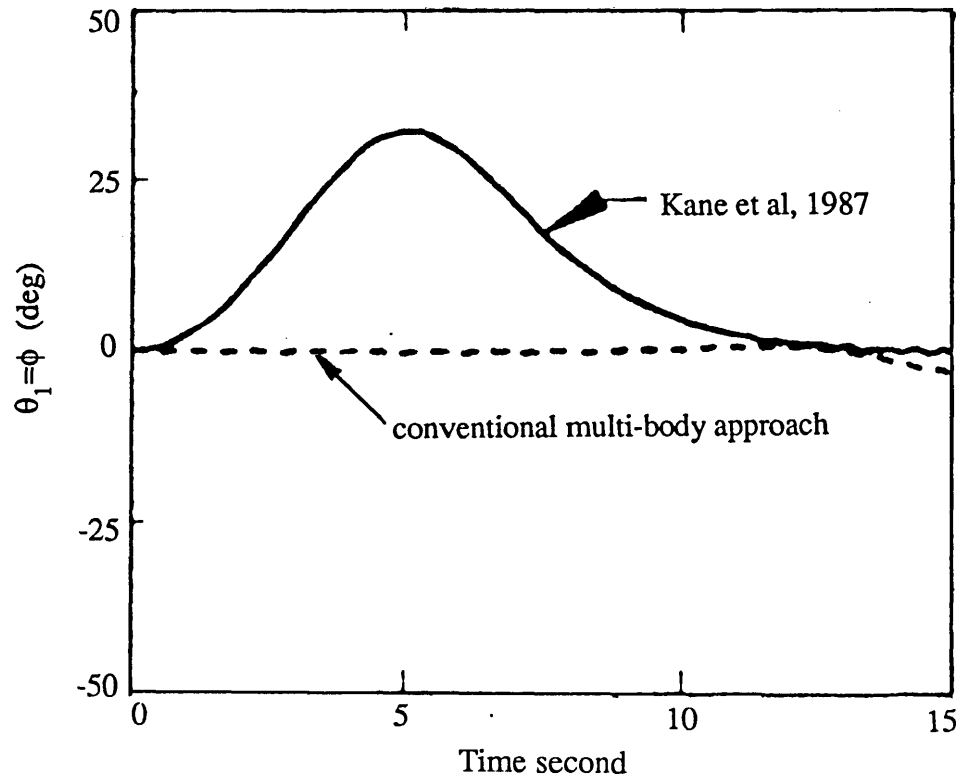

Fig 5.20 Simulation of the spin-up manoeuvre of the robotic manipulator (in torsion) from Kane et al, 1987

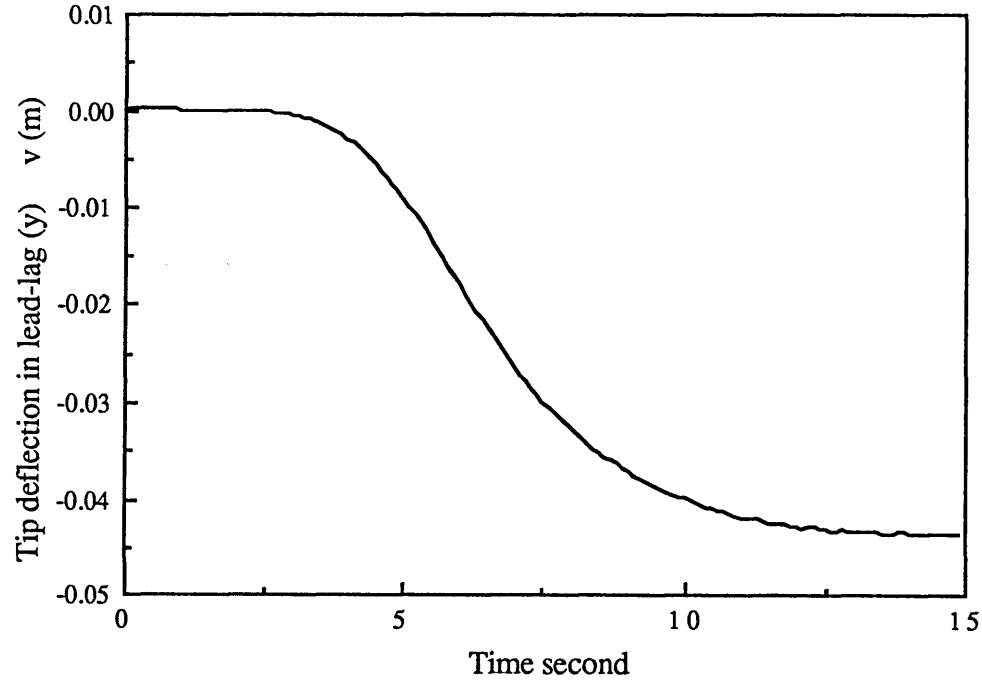

Fig 5.21 Simulation of the spin-up manoeuvre of the robotic manipulator (in lead-lag)

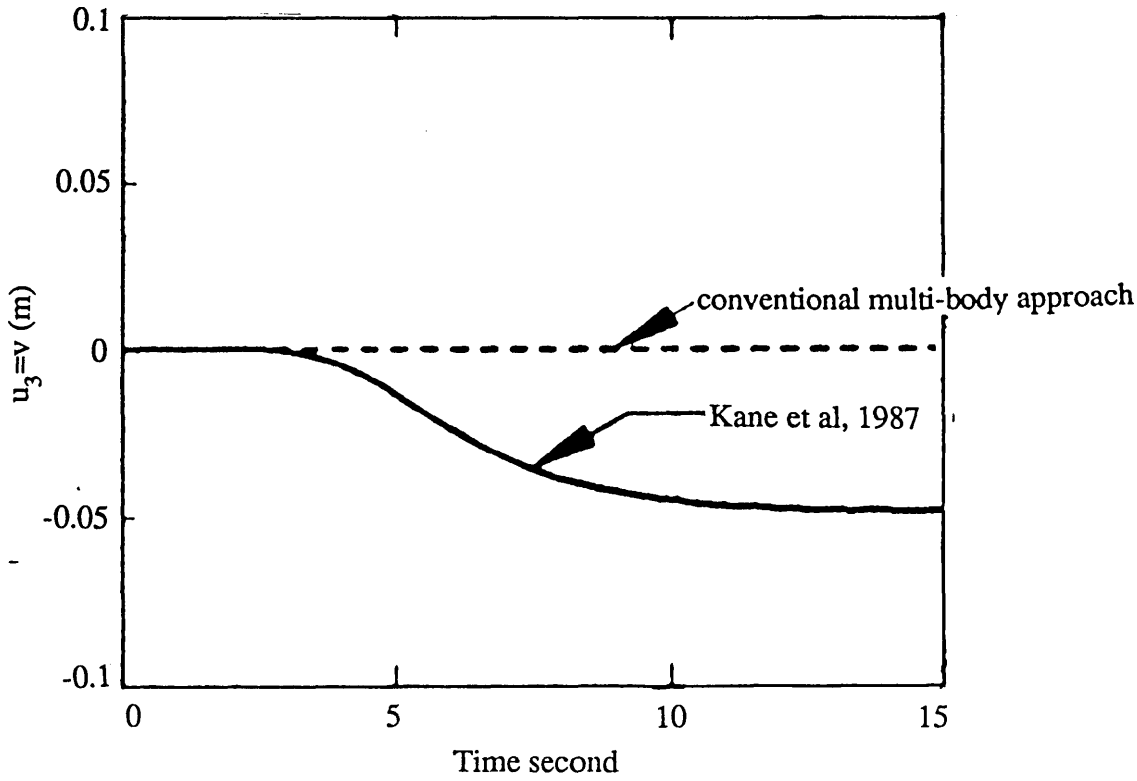

Fig 5.22 Simulation of the spin-up manoeuvre of the robotic manipulator (in lead-lag) from Kane et al, 1987

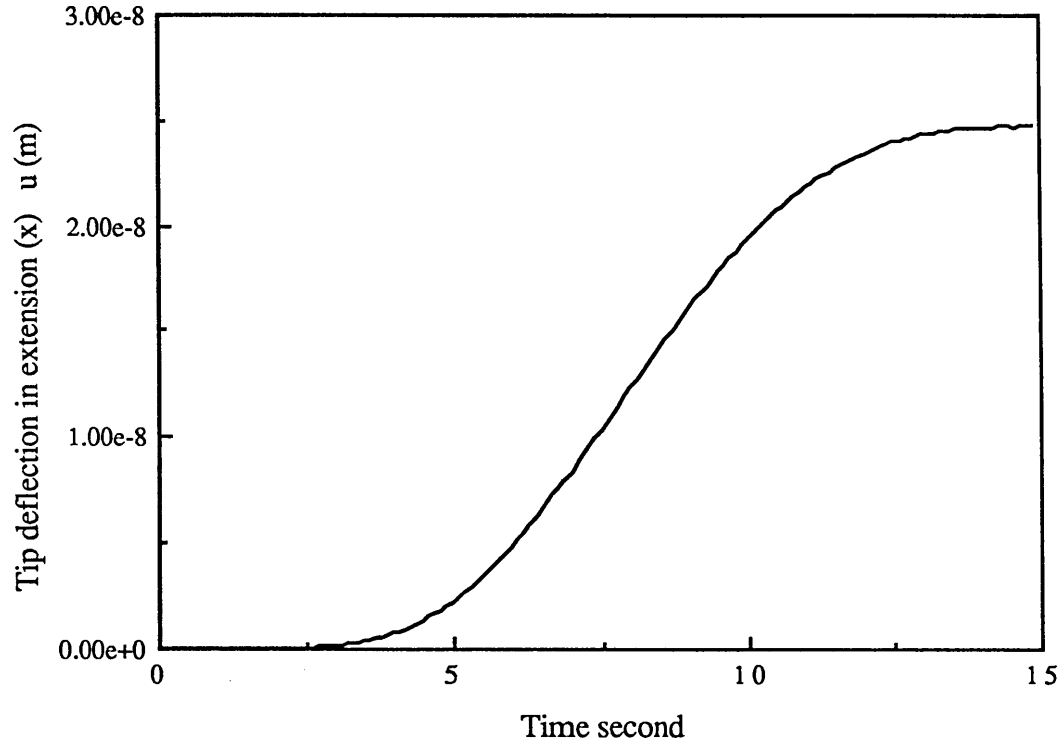

Fig 5.23 Simulation of the spin-up manoeuvre of the robotic manipulator (in extension)

CHAPTER 6 A FINITE ELEMENT AEROELASTICITY BEAM MODEL

6.1 INTRODUCTION

Rotorcraft blade dynamics represents the most actively investigated example of rotating beam dynamics. One of the principal dynamic problems associated with rotorcraft is their aeroelasticity stability. Extensive studies have been conducted on this during the last four decades, and especially in the last twenty years. As one of the aims of this thesis, a new general finite element model is developed in this chapter based on the structural dynamics model in the last chapter. It is then used to analyse aeroelasticity stability problems of rotorcraft.

The structural dynamics model for an arbitrary rotating beam has been developed in the previous chapter. As pointed out there, the structural dynamics model is aimed at developing a general dynamics model for a beam with an arbitrary base motion and hence having sufficient modelling flexibility to represent complex geometries and the structural coupling effects of a complex structure such as a rotorcraft. Obviously, this structural dynamics model can be directly applied to obtain the present rotorcraft blade aeroelasticity model by adding the aerodynamic loads to the system. We only consider the axial flow case of a rotorcraft, such as the tilt-rotor aircraft in forward flight in an aeroplane mode, helicopter hovering, and vertical flight.

In section 2, the distributed aerodynamic loads on a blade are derived using a two dimensional quasi steady thin airfoil aerodynamic theory. The virtual work done by these loads is derived and discretized using the same shape functions as in the last chapter. Section 3 combines the structural dynamic model from the previous chapter with the aerodynamics operator to obtain the equations of motion for the aeroelastic system. Subsequently, section 4 presents the solution procedures for the aeroelasticity stability

problem. Section 5 gives a brief introduction to the computer coding. Following that, extensive numerical examples are given in section 6. Both equilibrium solutions and eigenvalue solutions are compared with an existing reliable results. Finally, some conclusions are drawn in section 7.

6.2 AERODYNAMIC LOADS ON A BLADE

The aerodynamic loads are calculated using a two dimensional quasi steady thin airfoil theory. The aerodynamic loads consist of circulatory forces and noncirculatory forces. The rotor is assumed to work in an axial flow state. The induced velocity is assumed to be uniform over the rotor. The formulation is specially treated so that the aerodynamics model can be applied to both low inflow case (helicopter hovering and vertical flight) and high inflow case (tilt-rotor aircraft forward flight in aeroplane mode).

Considering a blade section, the aerodynamic flow and aerodynamics loads acted on the blade section is shown in Fig 6.1

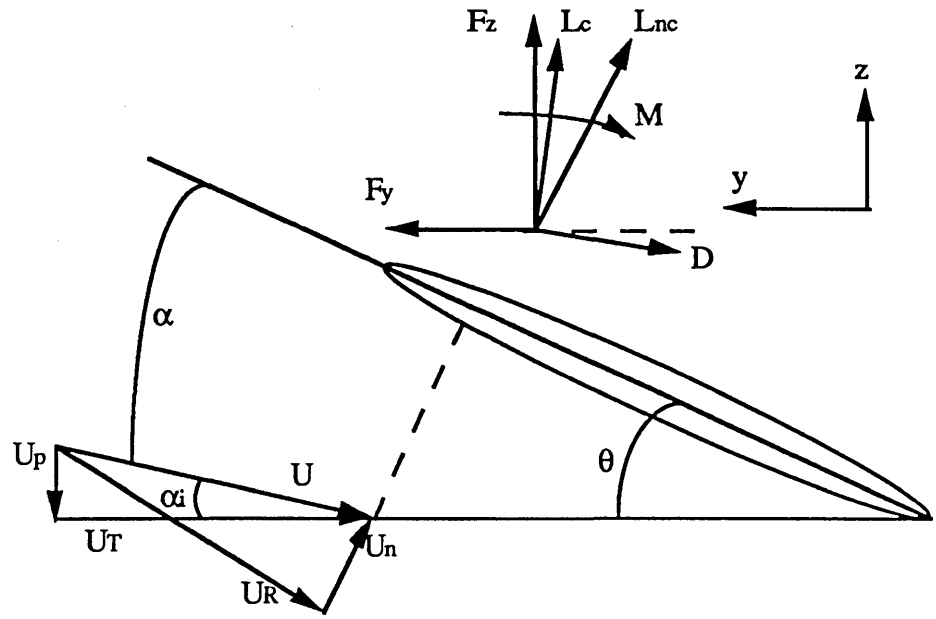

Fig 6.1 Blade section aerodynamics

The resultant air velocity is U, where U_T, U_P are its components in y and z directions, and U_R and U_n are its components parallel to the chord line and perpendicular to the chord line respectively. The angle of attack of the blade section is α. The pitch angle of the blade section is θ. F_y, F_z are the components of resultant aerodynamic forces on the section in the y and z directions. M is the resultant aerodynamic moment on the section, $M=M_c+M_{nc}$. L_c and L_{nc} are the circulatory part and noncirculatory part of the aerodynamic forces, respectively. D is the blade section aerodynamic drag.

The circulatory forces are:

$$\text{Lift}: \qquad L_c = \rho b C_l U^2 \qquad (2.1)$$

This is perpendicular to the resultant velocity U .

$$\text{Drag}: \qquad D = \rho b C_d U^2 \qquad (2.2)$$

This is parallel to the resultant velocity U .

The pitch moment about the elasticity centre is:

$$M_c = 2\rho b^2 C_{mac} U^2 + x_A L_c \qquad (2.3)$$

and is positive nosing up .

Where, C_l, C_d, C_{mac} are section lift, drag and moment coefficient.

The noncirculatory forces are :

$$\text{Lift}: \qquad L_{nc} = \pi\rho b^2[\dot{U}_n + (\frac{1}{2}b - x_A)\ddot{\varepsilon}] \qquad (2.4)$$

$$\text{Pitch monent} \quad M_{nc} = \pi\rho b^2[-(\frac{1}{2}b - x_A)\dot{U}_n - \frac{b}{2}U_R\dot{\varepsilon} + (\frac{3b^2}{8} - x_A b + x_A^2)\ddot{\varepsilon}] \qquad (2.5)$$

Where, U_n is the velocity component vertical to the chord line of the blade cross-section,

U_R is the velocity component parallel to chord line of the blade cross-section,

ε is the change of the angle of attack.

They can be expressed as :

$$U_n = U_T \sin\theta - U_P \cos\theta \qquad (2.6)$$

$$U_R = U_T \cos\theta + U_P \sin\theta \qquad (2.7)$$

$$\dot{\varepsilon} = \dot{\theta} + \omega_x + \omega_z w' + \omega_y v' \qquad (2.8)$$

$$\text{And hence , } \quad \dot{U}_n = (U_T \cos\theta + U_P \sin\theta)\dot{\theta} + \dot{U}_T \sin\theta - \dot{U}_P \cos\theta \qquad (2.9)$$

The aerodynamic force components in the y and z directions are obtained as:

$$F_y = -D_c \cos\alpha_i - L_c \sin\alpha_i - L_{nc} \sin\theta \qquad (2.10)$$

$$F_z = L_c \cos\alpha_i - D_c \sin\alpha_i + L_{nc} \cos\theta \qquad (2.11)$$

where α_i is the inflow angle, as shown in Fig 6.1,

$$\sin\alpha_i = \frac{U_P}{U}, \quad \cos\alpha_i = \frac{U_T}{U} \qquad (2.12)$$

Replacing (2.1), (2.2) and (2.12) into (2.10) and (2.11), we have:

$$F_y = -\rho b C_d U_T U - \rho b C_l U_p U - L_{nc} \sin\theta \qquad (2.13)$$

$$F_z = \rho b C_l U_T U - \rho b C_d U_p U + L_{nc} \cos\theta \qquad (2.14)$$

The resultant aerodynamic pitch moment is:

$$M = 2\rho b^2 C_{mac} U^2 + x_A L_c + \pi \rho b^2 [-(\frac{1}{2}b - x_A)\dot{U}_n - \frac{b}{2} U_R \dot{\varepsilon}$$

$$+ (\frac{3b^2}{8} - x_A b + x_A^2)\ddot{\varepsilon}] \qquad (2.15)$$

The expressions for U_T, U_P and U are obtained by considering the relative velocity of the blade section elasticity centre to the air.

$$\vec{v}_{EC} = \dot{\vec{R}}_{EC} + \vec{v}_A + \vec{\omega}_h \times \vec{R}_{EC} \qquad (2.16)$$

$$\vec{R}_{EC} = (r+u)\vec{i}_1 + v\vec{j}_1 + w\vec{k}_1 \qquad (2.17)$$

$$\vec{v}_A = v_x\vec{i}_1 + v_y\vec{j}_1 + v_z\vec{k}_1 \qquad (2.18)$$

$$\vec{\omega}_h = \omega_x\vec{i}_1 + \omega_y\vec{j}_1 + \omega_z\vec{k}_1 \qquad (2.19)$$

Applying relations (2.17) through (2.19), We have:

$$\vec{v}_{EC} = [v_x + \omega_y w - \omega_z v + \dot{u}]\vec{i}_1 + [v_y + \omega_z(r+u) - \omega_x w + \dot{v}]\vec{j}_1 + [v_z + \omega_x v - \omega_y(r+u) + \dot{w}]\vec{k}_1 \qquad (2.20)$$

Let v_F be the axial free air flow velocity and v_i be the induced velocity , then the relative on-coming airflow velocity can be written as :

$$\vec{v} = -(v_F + v_i)\vec{k}_0 - \vec{v}_{EC} \qquad (2.21)$$

Giving $$\vec{k}_0 = t_1\vec{i}_1 + t_2\vec{j}_1 + t_3\vec{k}_1 \qquad (2.22)$$

(2.21) is written as after replacing (2.20) and (2.22) into (2.21):

$$\vec{v} = \{-(v_F + v_i)t_1 - [v_x + \omega_y w - \omega_z v + \dot{u}]\}\vec{i}_1 + \{-(v_F + v_i)t_2 - [v_y + \omega_z(r+u) - \omega_x w + \dot{v}]\}\vec{j}_1 + \{-(v_F + v_i)t_3 - [v_z - \omega_y(r+u) + \omega_x v + \dot{w}]\}\vec{k}_1 = v_{ax}\vec{i}_1 + v_{ay}\vec{j}_1 + v_{az}\vec{k}_1 \qquad (2.23)$$

U_T, U_p are the y and z components of $\vec{v}$ in xyz frame. The coordinate system xyz is obtained from $x_1y_1z_1$ by including the blade lead-lag and flap deflections (v, w) but without the torsion deformation (ϕ). The transformation relation is:

$$\begin{Bmatrix} i \\ j \\ k \end{Bmatrix} = \begin{bmatrix} 1-\frac{v'^2}{2}-\frac{w'^2}{2} & v' & w' \\ -v' & 1-\frac{v'^2}{2} & 0 \\ -w' & 0 & 1-\frac{w'^2}{2} \end{bmatrix} \begin{Bmatrix} i_1 \\ j_1 \\ k_1 \end{Bmatrix}$$

We write $\vec{v}$ in xyz coordinates:

$$\vec{v} = [(1-\frac{v'^2}{2}-\frac{w'^2}{2})v_{ax} + v_{ay}v' + v_{az}w')\vec{i} + (v_{ay} - v_{ax}v')\vec{j} + (v_{az} - v_{ax}w')\vec{k} \quad (2.24)$$

From (2.23) and (2.24), we obtain :

$$U_T = -(v_{ay} - v_{ax}v') \qquad (2.24)$$

$$U_P = -(v_{az} - v_{ax}w') \qquad (2.25)$$

From Fig. 6.1, we can derive :

$$U_R = U\cos\alpha \qquad (2.26)$$

Where, α is instant angle of attack of the blade section and is generally a small quantity, therefore,

$$U = \frac{U_R}{\cos\alpha} = \frac{U_T\cos\theta + U_P\sin\theta}{\cos\alpha} \approx U_T\cos\theta + U_P\sin\theta \qquad (2.27)$$

Where , $\theta = \theta_G + \hat{\phi}$ $\hat{\phi} = \phi - \int_0^r v''w'dx$ (2.28)

θ_G is the pretwist angle of the blade, $\hat{\phi}$ is the geometric twist angle, and ϕ is the elastic twist.

Replacing (2.27) into (2.13) and (2.14), we have

$$F_y = -\rho bC_d[U_T^2\cos\theta + U_TU_P\sin\theta] - \rho bC_l[U_P^2\sin\theta + U_TU_P\cos\theta] - L_{nc}\sin\theta \qquad .....(2.29)$$

$$F_z = -\rho b C_d[U_p^2 \sin\theta + U_T U_p \cos\theta] + \rho b C_l[U_T^2 \cos\theta + U_T U_p \sin\theta] + L_{nc}\cos\theta$$

.....(2.30)

From (2.24), (2.25), we can obtain the expressions for U_T^2 , U_p^2 etc. They are:

$$\begin{aligned}
U_T^2 = {} & v_\lambda^2 t_2^2 + 2[v_\lambda t_2 v_y + v_\lambda t_2 \omega_z (r+u) - v_\lambda t_2 \omega_x w + v_\lambda t_2 \dot{v}] \\
& + v_y^2 + \omega_z^2 (r+u)^2 + \omega_x^2 w^2 + \dot{v}^2 + 2v_y \omega_z (r+u) - 2v_y \omega_x w \\
& + 2v_y \dot{v} - 2\omega_z \omega_x (r+u) w + 2\omega_z (r+u)\dot{v} - 2\omega_x w \dot{v} \\
& -2\{v_\lambda^2 t_1 t_2 + v_\lambda t_1 [v_y + \omega_z (r+u) - \omega_x w] + v_\lambda t_2 [v_x + \omega_y w - \omega_z v] \\
& + [v_x + \omega_y w - \omega_z v][v_y + \omega_z (r+u) - \omega_x w] + v_\lambda t_1 \dot{v} + v_\lambda t_2 \dot{u} \\
& + [v_y + \omega_z (r+u) - \omega_x w]\dot{u} + [v_x + \omega_y w - \omega_z v]\dot{v} + \dot{u}\dot{v}\} v' \\
& + \{v_\lambda^2 t_1^2 + [v_x + \omega_y w - \omega_z v]^2 + 2v_\lambda t_1 [v_x + \omega_y w - \omega_z v] + 2v_\lambda t_1 \dot{u} \\
& + 2[v_x + \omega_y w - \omega_z v]\dot{u} + \dot{u}^2\} v'^2
\end{aligned} \qquad (2.31)$$

$$\begin{aligned}
U_P^2 = {} & v_\lambda^2 t_3^2 + 2v_\lambda t_3 v_z - 2v_\lambda t_3 \omega_y (r+u) + 2v_\lambda t_3 \omega_x v + 2v_\lambda t_3 \dot{w} \\
& + v_z^2 + \omega_y^2 (r+u)^2 + \omega_x^2 v^2 + \dot{w}^2 - 2v_z \omega_y (r+u) + 2v_z \omega_x v \\
& + 2v_z \dot{w} - 2\omega_x \omega_y (r+u) v - 2\omega_y (r+u)\dot{w} + 2\omega_x v \dot{w} \\
& -2\{v_\lambda^2 t_1 t_3 + v_\lambda t_1 [v_z - \omega_y (r+u) + \omega_x v] + v_\lambda t_3 [v_x + \omega_y w - \omega_z v] \\
& + [v_x + \omega_y w - \omega_z v][v_z - \omega_y (r+u) + \omega_x v] + v_\lambda t_1 \dot{w} + v_\lambda t_3 \dot{u} \\
& + [v_z - \omega_y (r+u) + \omega_x v]\dot{u} + [v_x + \omega_y w - \omega_z v]\dot{w} + \dot{u}\dot{v}\} w' \\
& + \{v_\lambda^2 t_1^2 + [v_x + \omega_y w - \omega_z v]^2 + 2v_\lambda t_1 [v_x + \omega_y w - \omega_z v] + 2v_\lambda t_1 \dot{u} \\
& + 2[v_x + \omega_y w - \omega_z v]\dot{u} + \dot{u}^2\} w'^2
\end{aligned} \qquad (2.32)$$

$$\begin{aligned}
U_T U_P = {} & v_\lambda^2 t_2 t_3 + v_\lambda t_2 v_z + v_\lambda t_2 \omega_x v - v_\lambda t_2 \omega_y (r+u) + v_\lambda t_2 \dot{w} \\
& + v_\lambda t_3 v_y + v_\lambda t_3 \omega_z (r+u) - v_\lambda t_3 \omega_x w + v_\lambda t_3 \dot{v} + v_y v_z \\
& + v_y \omega_x v - v_y \omega_y (r+u) + v_y \dot{w} + v_z \omega_z (r+u) + \omega_x \omega_z v (r+u)
\end{aligned}$$

$$
\begin{aligned}
&-\omega_y\omega_z(r+u)^2+\omega_z(r+u)\dot{w}-\omega_x v_z w-\omega_x^2 vw\\
&+\omega_x\omega_y w(r+u)-\omega_x w\dot{w}+v_z\dot{v}+\omega_x v\dot{v}-\omega_y(r+u)\dot{v}+\dot{v}\dot{w}\\
&-\{v_\lambda^2 t_1 t_3+v_\lambda t_1[v_z-\omega_y(r+u)+\omega_x v]+v_\lambda t_3[v_x+\omega_y w-\omega_z v]\\
&+[v_x+\omega_y w-\omega_z v][v_z-\omega_y(r+u)+\omega_x v]+v_\lambda t_1\dot{w}+v_\lambda t_3\dot{u}\\
&+[v_z-\omega_y(r+u)+\omega_x v]\dot{u}+[v_x+\omega_y w-\omega_z v]\dot{w}+\dot{u}\dot{v}\}v'\\
&-\{v_\lambda^2 t_1 t_2+v_\lambda t_1[v_y+\omega_z(r+u)-\omega_x w]+v_\lambda t_2[v_x+\omega_y w-\omega_z v]\\
&+[v_x+\omega_y w-\omega_z v][v_y+\omega_z(r+u)-\omega_x w]+v_\lambda t_1\dot{v}+v_\lambda t_2\dot{u}\\
&+[v_y+\omega_z(r+u)-\omega_x w]\dot{u}+[v_x+\omega_y w-\omega_z v]\dot{v}+\dot{u}\dot{v}\}w'\\
&+\{v_\lambda^2 t_1^2+[v_x+\omega_y w-\omega_z v]^2+2v_\lambda t_1[v_x+\omega_y w-\omega_z v]+2v_\lambda t_1\dot{u}\\
&+2[v_x+\omega_y w-\omega_z v]\dot{u}+\dot{u}^2\}v'w' \qquad (2.33)
\end{aligned}
$$

$$U^2=U_T^2+U_P^2 \qquad (2.34)$$

where : $v_\lambda=v_F+v_i$ (2.35)

From equation (2.28), sinθ and cosθ are:

$$\sin\theta=\sin(\theta_G+\hat{\phi})=\sin\theta_G+\hat{\phi}\cos\theta_G \qquad (3.36)$$

$$\cos\theta=\cos(\theta_G+\hat{\phi})=\cos\theta_G-\hat{\phi}\sin\theta_G \qquad (3.37)$$

Writing (2.31) through (2.33) in matrix form :

$$U_T^2=U_{T0}+[U_{Tv}]\begin{Bmatrix}\dot{u}\\ \dot{v}\\ \dot{w}\end{Bmatrix}+[U_{Td}]\begin{Bmatrix}u\\ v\\ w\end{Bmatrix} \qquad (2.38)$$

$$U_P^2=U_{P0}+[U_{Pv}]\begin{Bmatrix}\dot{u}\\ \dot{v}\\ \dot{w}\end{Bmatrix}+[U_{Pd}]\begin{Bmatrix}u\\ v\\ w\end{Bmatrix} \qquad (2.39)$$

$$U_T U_P = U_{TP0} + [U_{TPv}]\begin{Bmatrix}\dot{u}\\ \dot{v}\\ \dot{w}\end{Bmatrix} + [U_{TPd}]\begin{Bmatrix}u\\ v\\ w\end{Bmatrix} \qquad (2.40)$$

The expressions of U_{T0}, $[U_{Tv}]$, $[U_{Td}]$, U_{p0}, $[U_{pv}]$, $[U_{pd}]$, U_{Tp0}, $[U_{Tpv}]$ and $[U_{Tpd}]$ are listed in Appendix 6A.

From (2.24) and (2.25), the derivatives of U_T and U_p are found:

$$\dot{U}_T = v_\lambda \dot{t}_2 + \dot{v}_y + \dot{\omega}_z(r+u) + \omega_z \cdot \dot{u} - \dot{\omega}_x w - \omega_x \dot{w} + \ddot{v} + \{-v_\lambda \dot{t}_1 - \dot{v}_x - \dot{\omega}_y w - \omega_y \dot{w} + \dot{\omega}_z v + \omega_z \dot{v} - \ddot{u}\}v' + \{-v_\lambda t_1 - v_x - \omega_y w + \omega_z v - \dot{u}\}\dot{v}' \qquad (2.41)$$

$$\dot{U}_P = v_\lambda \dot{t}_3 + \dot{v}_z - \dot{\omega}_y(r+u) - \omega_y \cdot \dot{u} + \dot{\omega}_x v + \omega_x \dot{v} + \ddot{w} + \{-v_\lambda \dot{t}_1 - \dot{v}_x - \dot{\omega}_y w - \omega_y \dot{w} + \dot{\omega}_z v + \omega_z \dot{v} - \ddot{u}\}w' + \{-v_\lambda t_1 - v_x - \omega_y w + \omega_z v - \dot{u}\}\dot{w}' \qquad (2.42)$$

Replacing (2.41), (2.42), (2.24) and (2.25) into (2.9), we can obtain U_n. Then, replacing U_n and (2.8) into (2.4) and (2.5), we can write L_{nc} and M_{nc} in the following forms :

$$L_{nc} = [L_{nca}]\{\ddot{q}\} + [L_{ncv}]\{\dot{q}\} + [L_{ncd}]\{q\} \qquad (2.43)$$

$$M_{nc} = [M_{nca}]\{\ddot{q}\} + [M_{ncv}]\{\dot{q}\} + [M_{ncd}]\{q\} \qquad (2.44)$$

Where $$\{q\} = \begin{Bmatrix}u\\ v\\ w\\ \phi\end{Bmatrix} \qquad (2.45)$$

Applying (2.38) through (2.40), (2.43) and (2.44) to (2.29) and (2.30), and noting the relationships in (2.36) and (2.37), then finally, F_y, F_z can be expressed as :

$$F_y = F_{y0} + [F_{yd}]\{q\} + [F_{yv}]\{\dot{q}\} + [F_{ya}]\{\ddot{q}\} \quad (2.46)$$

$$F_z = F_{z0} + [F_{zd}]\{q\} + [F_{zv}]\{\dot{q}\} + [F_{za}]\{\ddot{q}\} \quad (2.47)$$

From (2.15), The aerodynamic pitch moment M is:

$$M = 2\rho b^2 C_{mac}(U_T^2 + U_p^2) + x_A \rho b C_l (U_T^2 + U_p^2) + M_{nc} \quad (2.48)$$

Again, applying (2.38) , (2.39) and (2.44), M can also be expressed as:

$$M = M_0 + [M_d]\{q\} + [M_v]\{\dot{q}\} + [M_a]\{\ddot{q}\} \quad (2.49)$$

This implementation is undertaken in the computer code. These loads are the distributed aerodynamic loads acting on a unit-length of blade.

6.3 EQUATIONS OF MOTION FOR THE AEROELASTICITY SYSTEM

Now, we can obtain the equations of motion for a rotor blade which is subject to the above aerodynamic loads. We apply the virtual work principal to the rotor blade and discretize the blade into a number of elements. This can be expressed as:

$$\delta U - \delta W_I - \delta W_A = \sum_{j=1}^{Ne} \Delta_j = \sum_{j=1}^{Ne} (\delta U_j - \delta W_{Ij} - \delta W_{Aj}) = 0 \quad (3.1)$$

Where U is the strain energy of the blade, W_I is the virtual work done by the inertial loads, W_A is the work done by the aerodynamic loads. Δ_j is the contribution of the j'th element to $\delta U - \delta W_I - \delta W_A$. The first two terms of (3.1) give the structural operator which has been obtained in the previous chapter. We shall derive the aerodynamic operator through the principle of virtual work.

Considering a general element, the kinematical variables u , v, w, ϕ, are represented by the same shape functions as in the last chapter. They are:

$$u = [L_1 \quad L_2]\begin{Bmatrix} u_1 \\ u_2 \end{Bmatrix} \quad (3.2)$$

$$v = [H_1 \quad H_2 \quad H_3 \quad H_4]\begin{Bmatrix} v_1 \\ \zeta_1 \\ v_2 \\ \zeta_2 \end{Bmatrix} \tag{3.3}$$

$$w = [H_1 \quad H_2 \quad H_3 \quad H_4]\begin{Bmatrix} w_1 \\ \beta_1 \\ w_2 \\ \beta_2 \end{Bmatrix} \tag{3.4}$$

$$\phi = [L_1 \quad L_2]\begin{Bmatrix} \phi_1 \\ \phi_2 \end{Bmatrix} \tag{3.5}$$

The aerodynamic loads F_y, F_z, M act on the elastic axis so that the virtual work done by the aerodynamic loads of the j'th element is:

$$\delta W_{Aj} = \int_0^{le} [(F_y \vec{j}_1 + F_z \vec{k}_1) \cdot \delta r_{EC} + M\vec{i}_2 \cdot \delta_\gamma] d\chi \tag{3.6}$$

Where : the virtual rotation $\delta\gamma = \vec{i}_1\delta\theta_x + \vec{j}_1\delta\theta_y + \vec{k}_1\delta\theta_z + \vec{i}_2\delta\psi$

and $\delta_\psi = \delta_\phi + w'\delta v'$ [Hodges etal. 1980] (3.7)

$$\delta r_{EC} = [\delta R_x + w\delta\theta_y - v\delta\theta_z + \delta u]\vec{i}_1 + [\delta R_y + (r+u)\delta\theta_z - w\delta\theta_x + \delta v]\vec{j}_1 + [\delta R_z + v\delta\theta_x - (r+u)\delta\theta_y + \delta w]\vec{k}_1 \tag{3.8}$$

Applying (3.2) through (3.5) , we have ,

$$\{q\} = \begin{bmatrix} L_1 & & & & & & & & L_2 & \\ & H_1 & & H_2 & & H_3 & & H_4 & & \\ & & H_1 & & H_2 & & H_3 & & H_4 & \\ & & & & & & & & & L_1 \quad L_2 \end{bmatrix} \{a_e\} \tag{3.9}$$

Where $\{a_e\} = [u_1 \; u_2 \; v_1 \; \zeta_1 \; v_2 \; \zeta_2 \; w_1 \; \beta_1 \; w_2 \; \beta_2 \; \phi_1 \; \phi_2]^T$ (3.10)

that is, the node variables of an element .

Similarly , the virtual displacement can be discretized as :

$$\delta u = [L_1 \quad L_2]\begin{Bmatrix}\delta u_1 \\ \delta u_2\end{Bmatrix} \tag{3.11}$$

$$\delta v = [H_1 \; H_2 \; H_3 \; H_4]\begin{Bmatrix}\delta v_1 \\ \delta \zeta_1 \\ \delta v_2 \\ \delta \zeta_2\end{Bmatrix} \tag{3.12}$$

$$\delta w = [H_1 \; H_2 \; H_3 \; H_4]\begin{Bmatrix}\delta w_1 \\ \delta \beta_1 \\ \delta w_2 \\ \delta \beta_2\end{Bmatrix} \tag{3.13}$$

$$\delta \phi = [L_1 \quad L_2]\begin{Bmatrix}\delta \phi_1 \\ \delta \phi_2\end{Bmatrix} \tag{3.14}$$

Replacing (3.11) through (3.14) into (3.7) and (3.8), we obtain:

$$\delta r_{EC} = [i_1 \; j_1 \; k_1][A1][\, \delta u_1 \; \delta v_1 \; \delta w_1 \; \delta \beta_1 \; \delta \zeta_1 \; \delta \phi_1 \; \delta u_2 \; \delta v_2 \; \delta w_2 \; \delta \beta_2 \; \delta \zeta_2 \; \delta \phi_2 \; \delta R_x \; \delta R_y \; \delta R_z \; \delta \theta_x \; \delta \theta_y \; \delta \theta_z]^T$$

$$\delta \gamma = [i_1 \; j_1 \; k_1][A2][\, \delta u_1 \; \delta v_1 \; \delta w_1 \; \delta \beta_1 \; \delta \zeta_1 \; \delta \phi_1 \; \delta u_2 \; \delta v_2 \; \delta w_2 \; \delta \beta_2 \; \delta \zeta_2 \; \delta \phi_2 \; \delta R_x \; \delta R_y \; \delta R_z \; \delta \theta_x \; \delta \theta_y \; \delta \theta_z]^T \tag{3.15}$$

Replacing (3.9) into (2.46), (2.47) and (2.49), then applying (3.6),We can obtain,

$$\delta W_{Aj} = \{\delta a_i\}^T [M_A]\{\ddot{a}_e\} + \{\delta a_i\}^T [C_A]\{\dot{a}_e\} + \{\delta a_i\}^T [K_A]\{a_e\} - \{\delta a_i\}^T [Q_A] \tag{3.16}$$

where $$\{\delta a_i\}^T = [\, \delta R_x \; \delta R_y \; \delta R_z \; \delta \theta_x \; \delta \theta_y \; \delta \theta_z \; \delta u_1 \; \delta v_1 \; \delta w_1 \; \delta \beta_1 \; \delta \zeta_1 \; \delta \phi_1 \; \delta u_2 \; \delta v_2 \; \delta w_2 \; \delta \beta_2 \; \delta \zeta_2 \; \delta \phi_2 \,]^T \tag{3.17}$$

Replacing (3.16) into (3.1) and utilising the structural dynamics results from the last chapter [Eq(3.3.3),ch5], we can obtain the mass, damping and stiffness matrices of the blade element. Therefore, $[M_A]$, $[C_A]$, $[K_A]$ are the aerodynamic contributions to the element mass, damping and stiffness matrices respectively. $\{Q_A\}$ is the aerodynamic contribution to the element load vector. Adding these element matrices and load vector to the respective element matrices and load vector in the last chapter, we obtain the total element mass matrix $[M_i]$, damping matrix $[C_i]$, stiffness matrix $[K_i]$ and load vector $[Q_i]$. Finally, the global system matrices and load vector are obtained by appropriate assembly of these total element matrices and load vector. Consequently, the assembly of the element matrix $[M_i]$ leads to the global mass matrix [M], the assembly of the element damping matrix $[C_i]$ results in the global damping matrix [C]. Similarly, the global stiffness matrix [K] and load vector [Q] are obtained. We can write the final equations of motion as :

$$\{\delta P\}^T\{[M]\{\ddot{P}_e\} + [C]\{\dot{P}_e\} + [K]\{P_e\} - \{Q\}\} = 0 \qquad (3.18)$$

Where $\{\delta P\}$ are the variation of all the generalised coordinates, which consists of the six independent base degrees of freedom and all the node degrees of freedom of the blade elements.

$$\{\delta P\}^T = [\delta R_x\ \delta R_y\ \delta R_z\ \delta\theta_x\ \delta\theta_y\ \delta\theta_z\ \delta u_1\ \delta v_1\ \delta w_1\ \delta\beta_1\ \delta\zeta_1\ \delta\phi_1$$
$$\delta u_2\ \delta v_2\ \delta w_2\ \delta\beta_2\ \delta\zeta_2\ \delta\phi_2 \ldots \delta u_n\ \delta v_n\ \delta w_n\ \delta\beta_n\ \delta\zeta_n\ \delta\phi_n] \qquad (3.19)$$

While $\{P_e\}$ only consists of the nodal degrees of freedom of the blade elements and hence does not include the six base coordinates.

Therefore, (3.18) represents 6n+6 equations. These equations are nonlinear. [C], [K], and [Q] contain the kinematical variables of the moving blade base, such as the base translational velocities and accelerations, and angular velocities and accelerations. However, they are not explicitly written out in the vector $\{P_e\}$. If the coupling problem

of a blade with other substructures, such as a rotorcraft fuselage, is considered, a set of kinematical constraint conditions must be used to relate these variables to the relevant degrees of freedom of the other substructures. In principal, an arbitrary coupling can be modelled with the help of this dynamics model. If we consider a problem with a prescribed base motion, we only need the last 6n differential equations. The prescribed motion can be directly included in the kinematical variables related with the base motion

6.4 SOLUTION PROCEDURES OF AEROELASTICITY STABILITY

We shall apply the equation (3.18) to solve the aeroelasticity stability problem of a rotorcraft blade. As pointed out in the previous section, the differential equations are nonlinear. To obtain the stability solution, one normally uses the small perturbation method to linearise the nonlinear equations. For simplicity, we assume that the problem to be solved has prescribed base motions. Therefore, (3.18) reduces to a set of 6n nonlinear differential equations and can be expressed as:

$$[M]\{\ddot{P}_e\} + [C]\{\dot{P}_e\} + [K]\{P_e\} = \{Q\} \qquad (4.1)$$

The global mass matrix [M] is still symmetric. The global damping matrix [C] and stiffness matrix [K] are asymmetric. The damping matrix [C] includes both the aerodynamic component and the structural gyroscopic forces. It could also include any structural damping description if this is required.

The linearising procedure is conducted by assuming the motion of the system is a small perturbation around a equilibrium values of the system.

That is $\{P_e\} = \{\tilde{P}\} + \{P_0\}$ (4.2)

Where $\{\tilde{P}\}$ are the perturbational variables, $\{P_0\}$ are the steady state values.

Replacing (4.2) into (4.1), then this leads to two groups of equations. One group contains only the steady state quantities and constants. This group represents the trim or

equilibrium equations. The second group contains the time dependent perturbational quantities and represent the linearised equations of motion about the equilibrium position.

The steady state equations are obtained by dropping all time dependent terms in (4.1) and can be written as :

$$[K_0]\{P_0\} = \{Q_0\} \qquad (4.3)$$

This is a set of nonlinear algebraic equations. This set of equations can be iteratively solved using an existing algorithm [NAG Library].

After obtaining the steady state solution, we can apply (4.2) to (4.1), then subtract (4.3) from (4.1) and neglect higher order perturbation terms, the linearised dynamics equations are obtained as:

$$[M(P_0)]\{\ddot{\tilde{P}}\} + [C(P_0)]\{\dot{\tilde{P}}\} + [K(P_0)]\{\tilde{P}\} = 0 \qquad (4.4)$$

The stability of the system can be obtained by solving the eigenvalue problem represented by (4.4). For convenience, (4.4) can be written in state equation form:

$$[A]\{\dot{x}\} = [B]\{x\} \qquad (4.5)$$

Where
$$\{x\} = \begin{Bmatrix} \dot{\tilde{P}} \\ \tilde{P} \end{Bmatrix} \qquad (4.6)$$

The eigenvalues obtained from (4.5) can be either real or complex conjugate pairs:

$$\lambda_i = \sigma_i \pm i\omega_i \qquad (4.7)$$

The complex parts of the eigenvalues ω_i represents the modal frequency and the real part σ_i reflects the modal damping. When $\sigma_i<0$, the system is stable.

6.5 PROGRAM CODING

The program for the structural dynamics model is subsequently further developed to analyse the aeroelastic stability of rotor blades based on the above theory. The structural dynamics component is the same as in the structural dynamics code discussed in the previous chapter but the step-by-step time integration is not required. The aerodynamic centre may be different from the elasticity centre. The nine kinematical quantities of the beam base are also assigned to the aerodynamics part and are implemented as prescribed variables in the current code. When the aeroelastic analysis of a coupled rotor/support system is required, then kinematical constraint relations must be used through these base variables to obtain the coupled dynamics model.

The first step of the aeroelasticity program consists of computing the nonlinear steady equilibrium values of the elastic blades under the action of aerodynamic loads. The nonlinear solution is obtained using the Powell method [NAG Library]. The initial values are taken as the solution of the linear equations. The linear algebraic equations are solved using the LU decomposition method. The equilibrium values that are so obtained are used in the linearised ordinary differential equations and subsequently in the associated eigenvalue problem. This is solved by the QZ algorithm [NAG Library]. Finally, the aeroelasticity stability of the system can be analysed from the computed eigenvalues. The flow chart of the computer code is presented below.

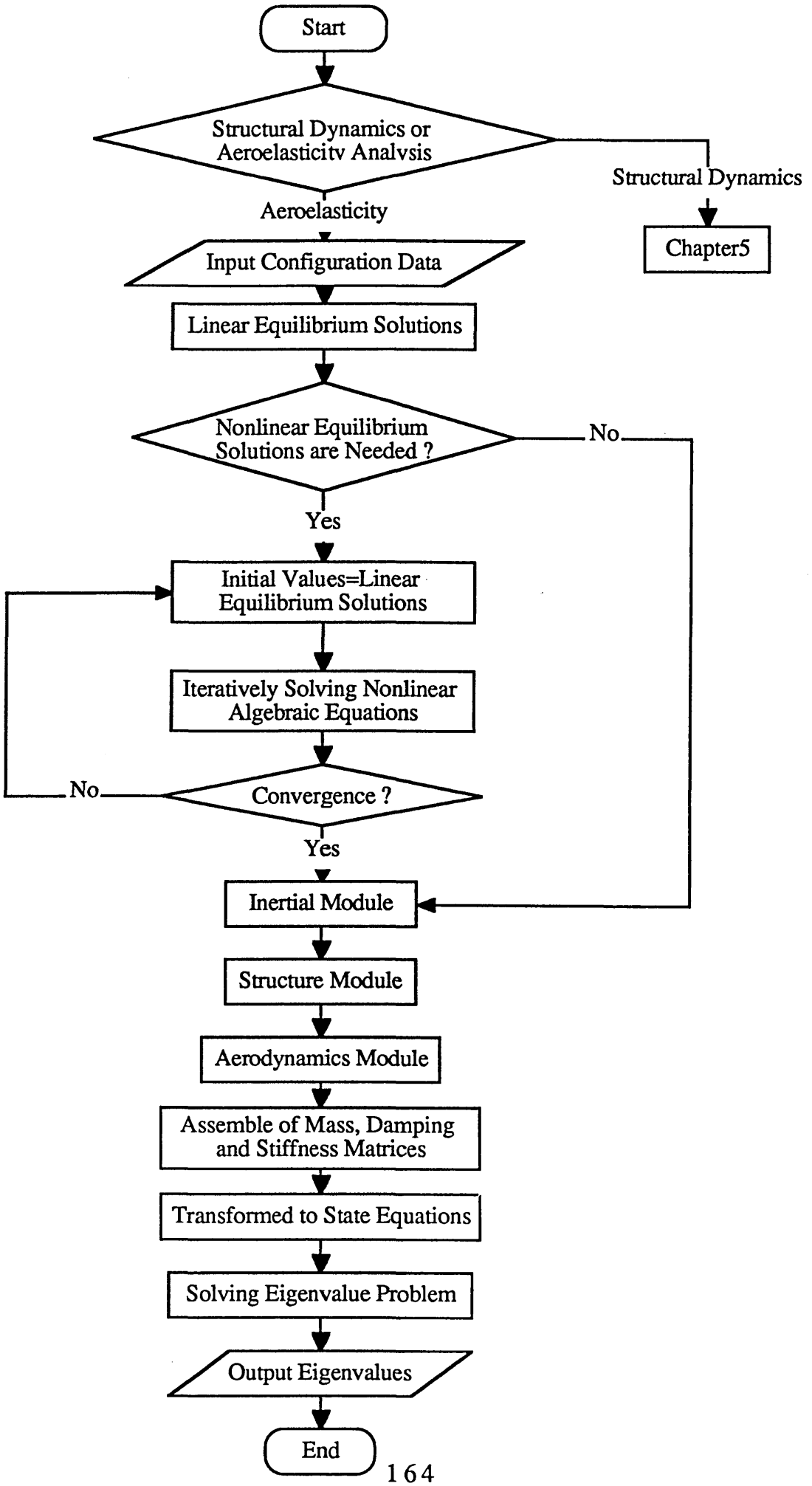
Start
Structural Dynamics or Aeroelasticity Analysis
Structural Dynamics
Chapter5
Aeroelasticity
Input Configuration Data
Linear Equilibrium Solutions
Nonlinear Equilibrium Solutions are Needed ?
No
Yes
Initial Values=Linear Equilibrium Solutions
Iteratively Solving Nonlinear Algebraic Equations
No
Convergence ?
Yes
Inertial Module
Structure Module
Aerodynamics Module
Assemble of Mass, Damping and Stiffness Matrices
Transformed to State Equations
Solving Eigenvalue Problem
Output Eigenvalues
End

6.6 NUMERICAL EXAMPLES AND DISCUSSIONS

Having established the aeroelasticity model, extensive numerical examples have been solved to validate the developed model and to illustrate the solution of the aeroelastic stability problem of rotorcraft blades. These numerical examples are divided into two groups. Some of the significant parameters are varied in each group, and their effects on the system stability are identified. The first group is concerned with investigating the aeroelasticity stability of hingeless rotor blades without a precone angle. Complete analytical results are available to compare with in the literature [Hodges and Ormiston, 1976]. The second group is for rotor blades with a precone angle. The purpose of these examples is to demonstrate the modelling flexibility of the present model by modelling the blade precone angle through the degrees of freedom of the blade base. The past traditional treatment includes the structural configurations at the root of rotor blades in the formulation from the start and hence the modelling generality is restricted [Hodges and Ormiston,1976, Friedmann and Straub,1980, Sivaneri and Chopra, 1982]. The present model introduces six arbitrary base degrees of freedom which, theoretically, can model arbitrary blade root geometries or motions or coupling with other substructures. Therefore, this gives a greater modelling flexibility to the present model when compared to existing ones.

6.6.1 Results for Rotor Blades without Precone Angle

A classical study of the aeroelasticity stability of hingeless rotor blades was conducted by Hodges and Ormiston [1976]. The global modal method was used there. A wide range of parametric investigations was performed. Both equilibrium values and stability solutions are available to compare with. The basic blade properties are given in Table 6.1. All blades properties are assumed to be uniform along the span of the blade. The rotor blade is rotating about the shaft with a constant rotating speed Ω. Fig 6.2 is a simple illustration of the configuration.

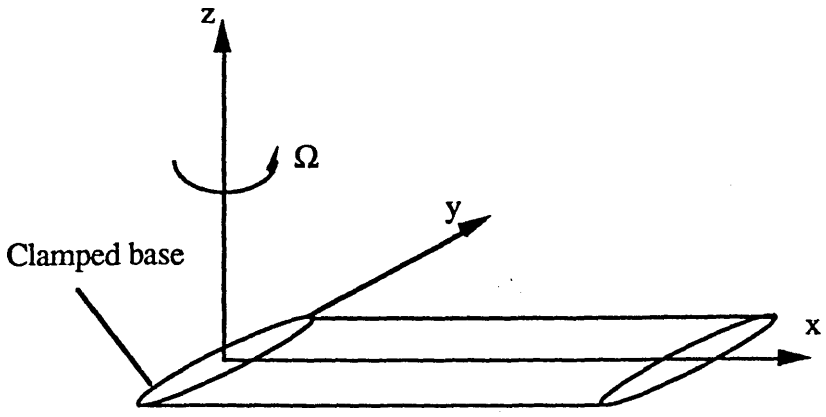

Fig 6.2 A hingeless rotor blade without precone angle

Table 6.1 Values of Configuration Parameters of a Hingeless Rotor Blades for Numerical Results

ω_v	0.7, or 1.5 (corresponding to $EI_z/m\Omega^2R^4$ =0.0291359, 0.166908 respectively)
ω_w	1.15 (corresponding to $EI_y/m\Omega^2R^4$= 0.014486)
ω_ϕ	2.5, or 5.0 (corresponding to $GJ/m\Omega^2R^4$=0.000925, 0.005661 respectively)
k_A/k_m	1.5
β_p	0.0 or 0.05 rad
k_m/R	0.025
k_{m_1}/k_{m_2}	0.0
$\gamma=3\rho acR/m$	5
σ	0.1
c/R	$\pi/40$
C_d	0.0095
C_{mac}	0
a	6

Where: k_m is the blade cross-section mass radius of gyration. k_{m_1} and k_{m_2} are the blade cross-section principal mass radii of gyration (flapwise and chordwise respectively). σ is the solidity and equal to $\frac{kc}{\pi R}$ (k=number of blades).

The convergence of the finite element method is considered first. The steady-state deflections of the blade and the eigenvalues for the blade aeroelasticity system are calculated using different numbers of finite elements. Table 6.2 presents the steady-state blade tip deflections in flap (w0), lead-lag (v0) and torsion (ϕ0) as the number of elements is varied from 2 to 9. The blade properties are ω_v=1.5, ω_ϕ=5.0 and β_p=0. The collective pitch angle of the blade is θ_0=0.2 rad. It can be observed from Table 6.2 that eight to nine elements gives a reasonably good convergence for the equilibrium solutions. Table 6.3 presents the eigenvalues for the first flap, the first lead-lag and the first torsion modes associated with the blade aeroelasticity equations under the same case as in Table 6.2. Each eigenvalue consists of a real part and a imaginary part, which represents the damping and the frequency of the mode, respectively. The results show, for the case considered, that 8 or 9 elements can give a reasonably good convergence. Therefore, 9 elements are adopted in the subsequent computations.

Table 6.2 Equilibrium Blade Tip Deflections using Various Number of Elements (ω_v=1.5, ω_ϕ=5.0, β_p=0.0 rad, θ_0=0.2 rad)

Number of element	Equilibrium blade tip deflection in lead-lag	Equilibrium blade tip deflection in flap	Equilibrium blade tip deflection in torsion
2	-0.023574	0.11482	-0.0073984
3	-0.017576	0.081974	-0.0075046
4	-0.015287	0.069460	-0.0079041
5	-0.014118	0.063072	-0.0082414
6	-0.013719	0.060933	-0.0085116
7	-0.013241	0.058320	-0.0087017
8	-0.012890	0.056401	-0.0088500
9	-0.012622	0.054936	-0.0089686

Table 6.3 Eigenvalues using Various Number of Elements
ω_v=1.5, ω_ϕ=5.0, β_p=0.0 rad, θ_0=0.2 rad

	First lead-lag mode		First flap mode		First torsion mode	
Number of elements	Real part	Imaginary part	Real part	Imaginary part	Real part	Imaginary part
2	-0.11976	2.23958	-0.78228	0.88850	-0.46652	5.99133
3	-0.05774	1.88164	-0.49782	0.99292	-0.41367	5.50313
4	-0.04555	1.73690	-0.41505	1.00743	-0.38878	5.30436
5	-0.04062	1.66017	-0.37543	1.01266	-0.37365	5.19057
6	-0.03844	1.61457	-0.35215	1.01391	-0.36354	5.11635
7	-0.03692	1.58234	-0.33674	1.01539	-0.35664	5.06468
8	-0.03594	1.55900	-0.32580	1.01636	-0.35155	5.02649
9	-0.03528	1.54131	-0.31762	1.01703	-0.34764	4.99711

Subsequently, the following cases are investigated using the code developed based on the present algorithm. Some significant parameters such as lead-lag and torsion stiffness are varied and their effects on stability are assessed.

Case I (ω_v=1.5, ω_ϕ=5.0)

The first case is for the blade configuration of ω_v=1.5, ω_ϕ=5.0 (lead-lag and torsion dimensionless natural frequency respectively). The blade is the so-called stiff in-plane blade configuration (ω_v>1). The nonlinear equilibrium deflections of the blade tip are shown in Fig 6.3 to 6.5 at various pitch angles θ. v0, w0, ϕ0 represent the lead-lag, flap and torsion equilibrium deflections of the blade tip respectively. v0 and w0 are nondimensionlized by the rotor blade radius R. The results of Hodges and Ormiston [1976] are also presented in the figures. The agreement between the two results is good.

A slight deviation appears at high collective pitch angle θ in v0 and w0. The biggest relative error is less than 6%. This difference is due to the approximation by Hodges and Ormiston that $\sin\theta=\theta$, $\cos\theta=1$ in the aerodynamics and $\sin(\theta+\phi)=\sin\theta$, $\cos(\theta+\phi)=\cos\theta$ in the structural analysis. These assumptions are not very accurate at high values of θ. This approximation is not assumed in the present model. In the equilibrium torsion deflection, the torsion deflection is caused by the inertial moment (or the so-called tennis racket effect [Hodges and Ormiston,1976, Hodges and Dowell,1974]) rather than aerodynamics. Consequently, the agreement is still good at high pitch angles. This inertial moment term is equal to $2\omega_z^2 I_{yz}=2\omega_z^2(I_1-I_f)\sin(\theta+\phi)\cos(\theta+\phi)$ in this case, where

I_1, I_f are the principal moments of inertia of the lumped mass, respectively.

Fig 6.6 presents the locus of roots of the first flap, lead-lag and torsion modes. As the pitch angle increases, the flap mode damping does not change much, the lead-lag mode damping rises, and the torsion mode damping decreases slightly. This is identical to the trend presented by Hodges and Ormiston (Fig 6.19). Obviously, the system is stable over the practical range of collective angle. This leads to the same conclusion as drawn by Hodges and Ormiston.

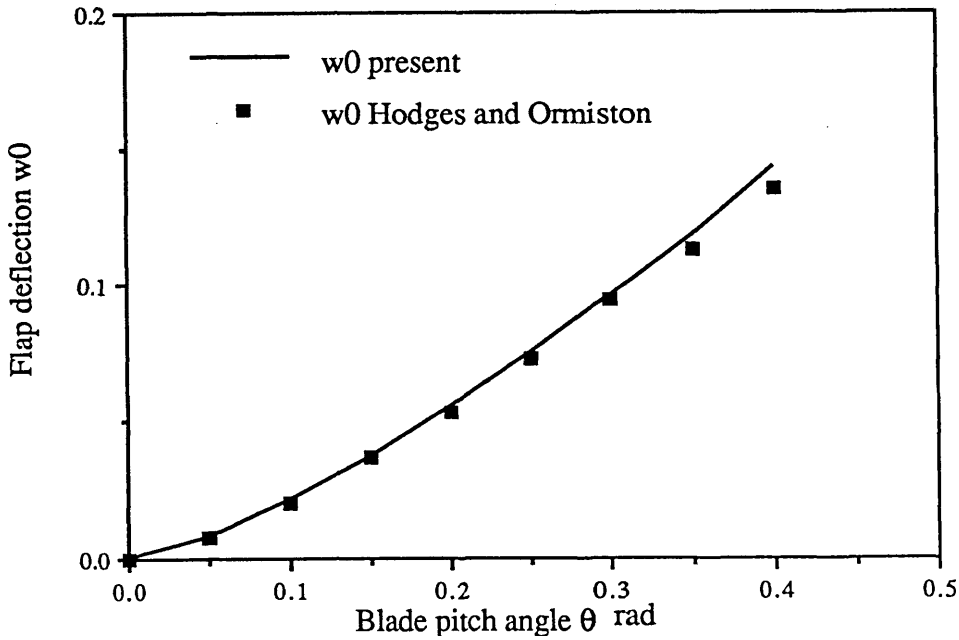

Fig 6.3 Equilibrium flap deflection of a blade tip at various pitch angles

$\omega_v=1.5$, $\omega_\phi=5.0$, $\beta_{pc}=0.0$ rad

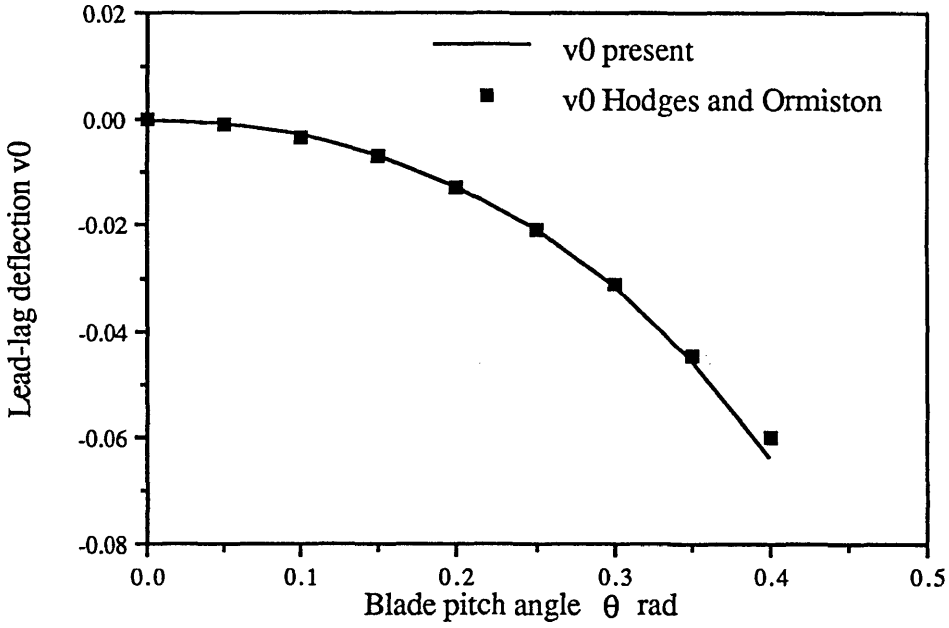

Fig 6.4 Equilibrium lag deflection of a rotor blade tip at various pitch angles

ω_v=1.5, ω_ϕ=5.0, β_{pc}=0.0 rad

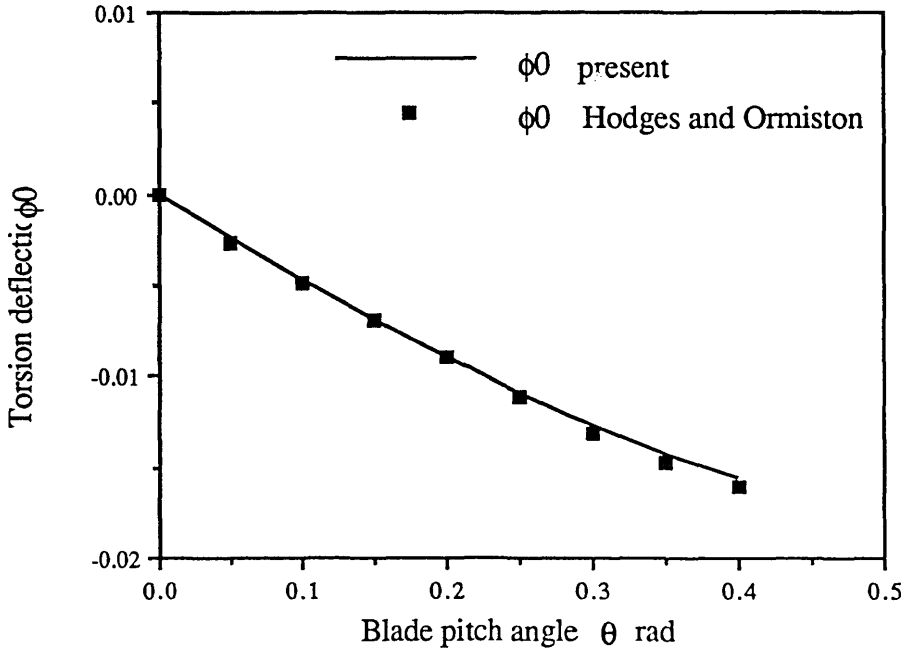

Fig 6.5 Equilibrium torsion deflection of a rotor blade tip at various pitch angles

ω_v=1.5, ω_ϕ=5.0, β_{pc}=0.0 rad

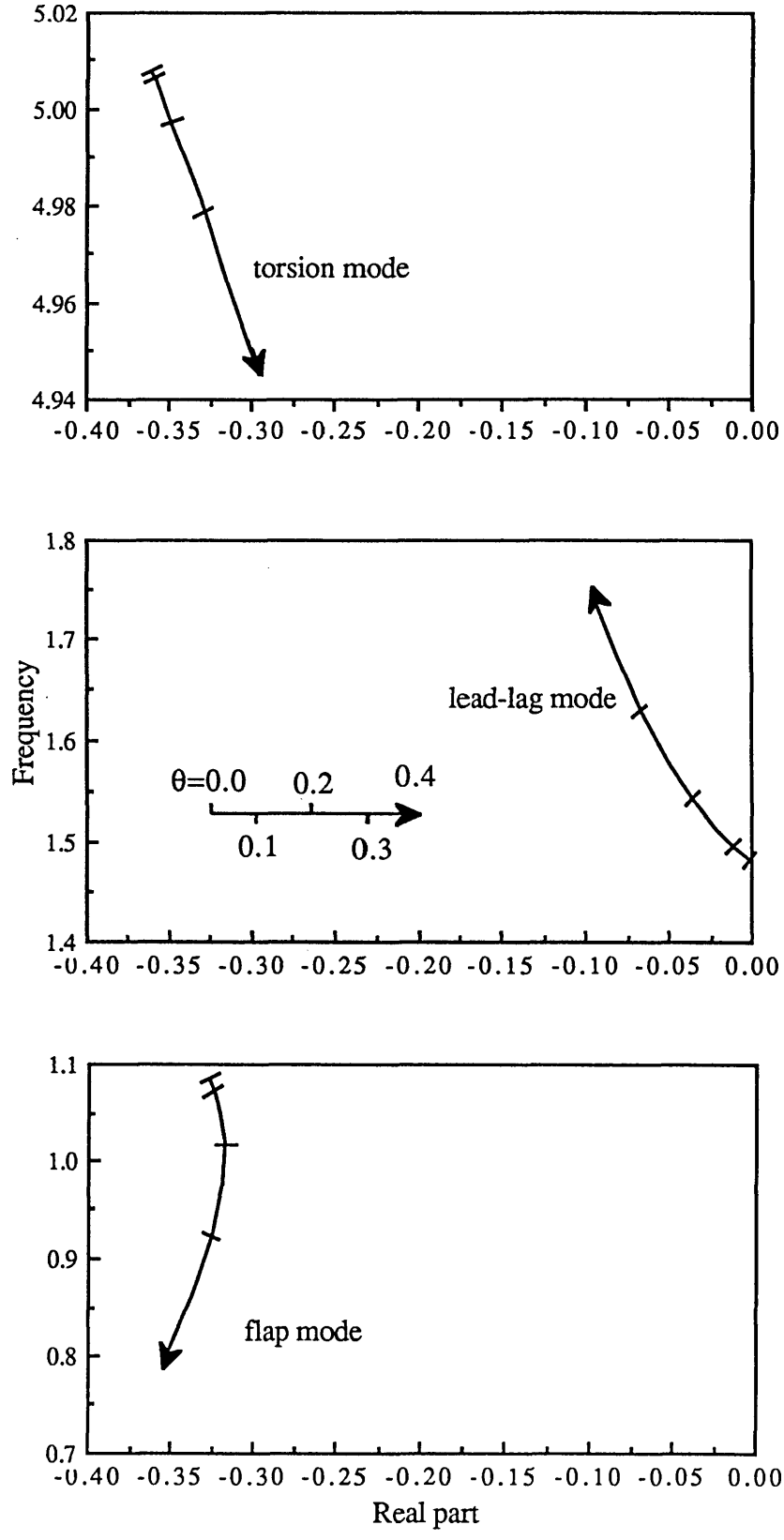

Fig 6.6 Locus of roots of blade modes

ω_v=1.5, ω_ϕ=5.0, β_{pc}=0.0 rad

Case II (ω_v=1.5, ω_ϕ=2.5)

The second case is for the configuration of ω_v=1.5, ω_ϕ=2.5. Comparing with case I, the torsional rigidity is reduced. The equilibrium values of the blade tip are shown in Fig 6.7 to 6.9 at various pitch angles. The equilibrium solution for this case is not given by Hodges and Ormiston. Comparing Fig 6.9 with fig 6.5, the decreased torsional rigidity increases the torsional deflection. As a result of the increase of the torsional deflection, the real blade collective angle ($\theta+\phi$) decreases and hence this reduces the aerodynamic loads. Consequently, as expected, the flap and lag deflections in Fig 6.7 and 6.8 are smaller than those in Fig 6.3, 6.4.

Fig 6.10 gives the locus of roots of the first flap, lag and torsion modes with the variation of blade pitch angle. As shown, there is a lead-lag mode instability when the pitch angle reaches a certain value. This instability is a feature of the coupling between the lead-lag mode and the torsion mode. The same conclusion was drawn by Hodges and Ormiston (Fig 6.19). Therefore, for the stiff inplane blade configuration, a low torsion stiffness can leads to a lead-lag instability.

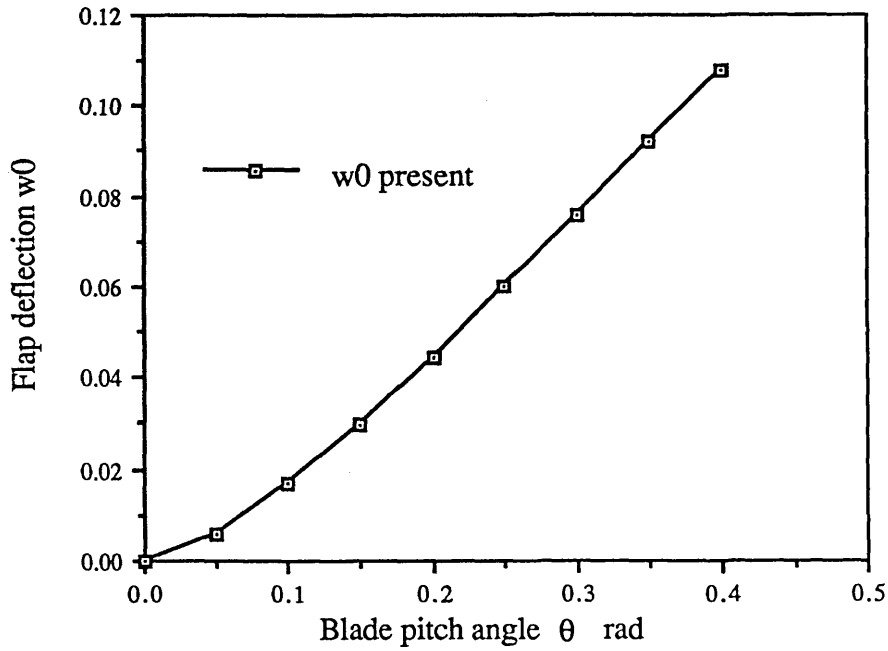

Fig 6.7 Equilibrium flap deflection of a rotor blade tip at various pitch angles

ω_v=1.5, ω_ϕ=2.5, β_{pc}=0.0 rad

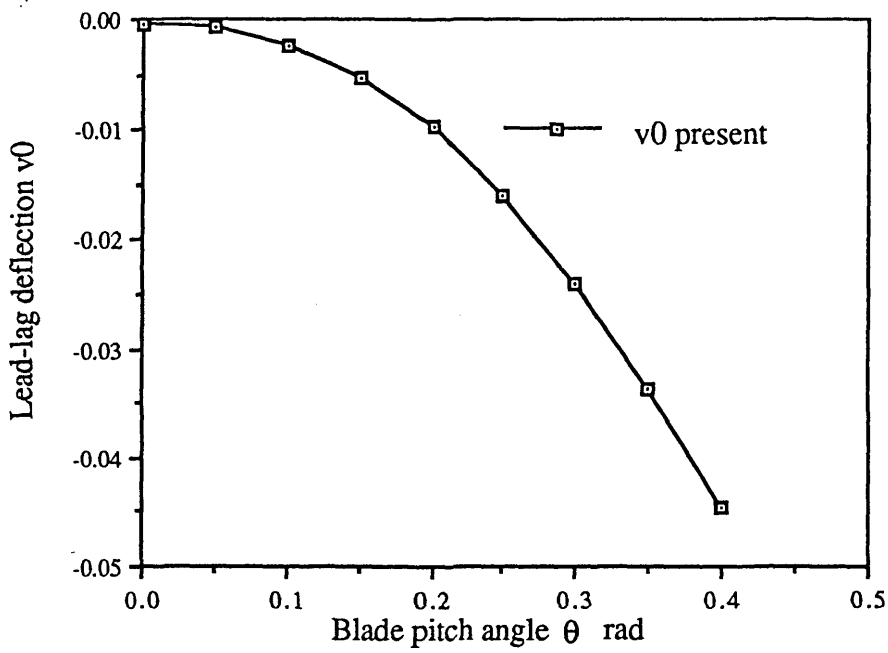

Fig 6.8 Equilibrium lag deflection of a rotor blade tip at various pitch angles

ω_v=1.5, ω_ϕ=2.5, β_{pc}=0.0 rad

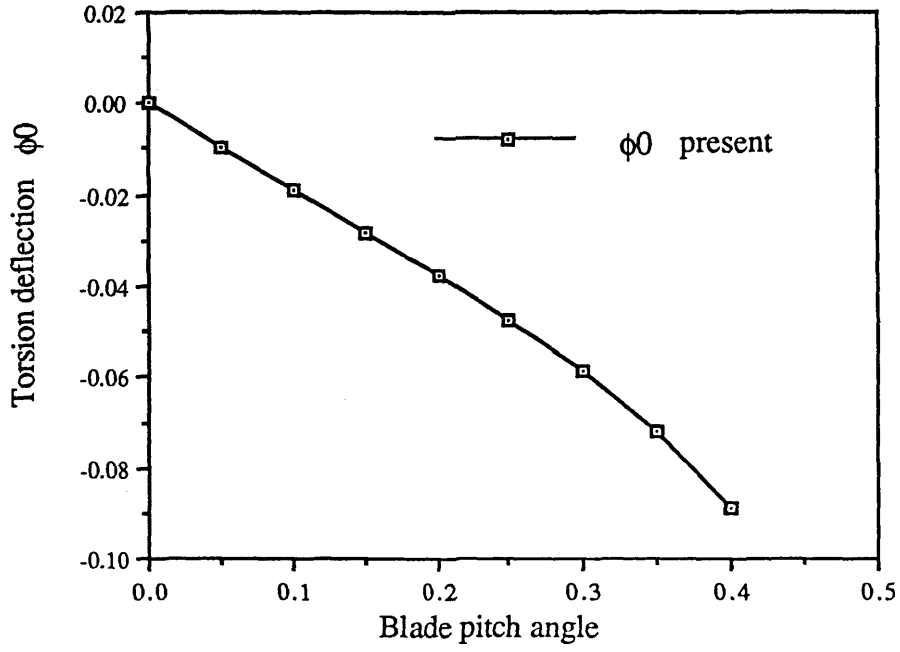

Fig 6.9 Equilibrium torsion deflection of a rotor blade tip at various pitch angles

ω_v=1.5, ω_ϕ=2.5, β_{pc}=0.0 rad

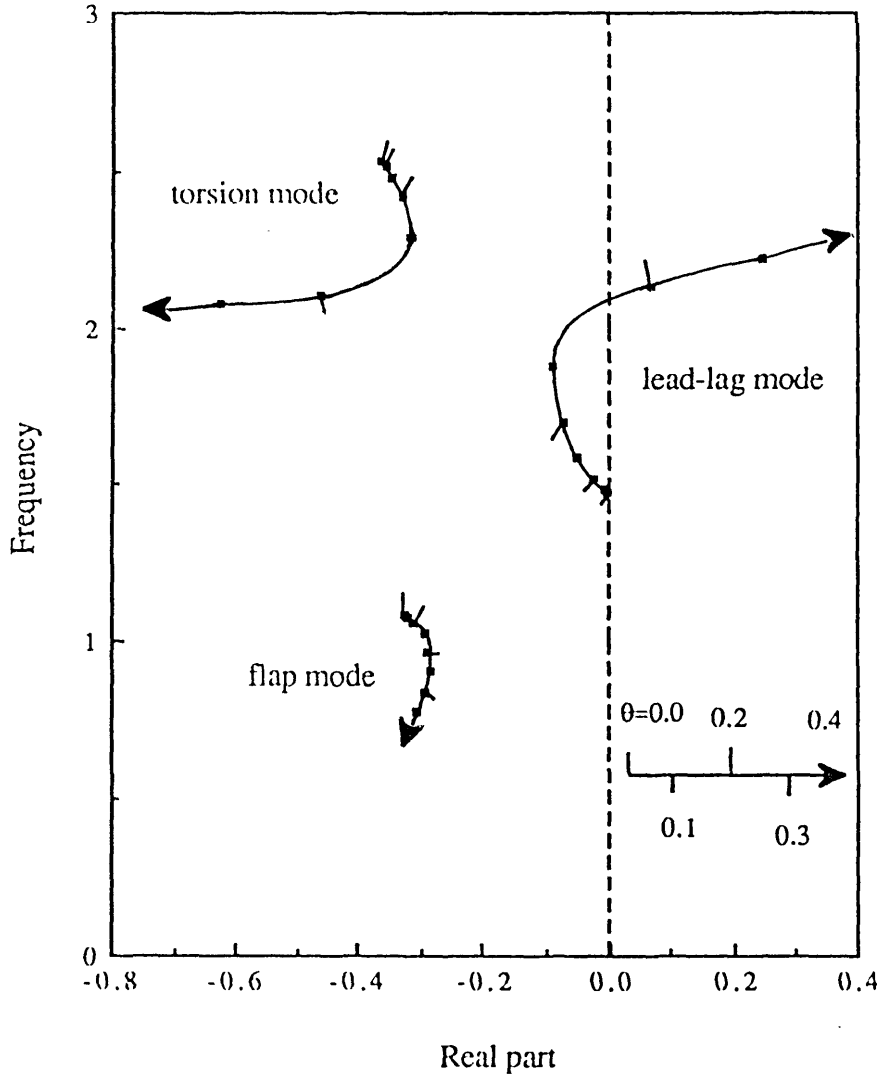

Fig 6.10 Locus of roots of blade modes

ω_v=1.5, ω_ϕ=2.5, β_{pc}=0.0 rad

Case III (ω_v=0.7, ω_ϕ=5.0)

Case III is for the configuration of ω_v=0.7, ω_ϕ=5.0. That is the so-called soft inplane blade configuration (ω_v<1). The lead-lag stiffness is reduced relative to case I. Fig 6.11 to 6.13 present the equilibrium values of the blade tip for lag, flap and torsion deformation respectively. The solid line is obtained from the present model, while the square points are taken from Hodges and Ormiston's work. Again, the results show a good agreement between the two models. A slight discrepancy appears at very high pitch angle θ in v0 and w0. However, the biggest relative error is about 7%. As pointed out before, the slight difference is due to the approximation of $\sin\theta$, $\cos\theta$ and $\sin(\theta+\phi)$, $\cos(\theta+\phi)$ made in the reference.

Fig 6.14 demonstrates the locus of roots of the first flap, lead-lag and torsion mode with the variation of the pitch angle θ. The lead-lag mode damping increases with θ. The flap mode damping reduces, while the torsion mode damping is little changed. Fig 6.20 presents the stability results for the soft inplane rotor blades from Hodges and Ormiston. Identical trend is observed between Fig 6.14 and 6.20. Over the practical range of the pitch angle θ, the system is stable. This gives the same conclusion as obtained by Hodges and Ormiston.

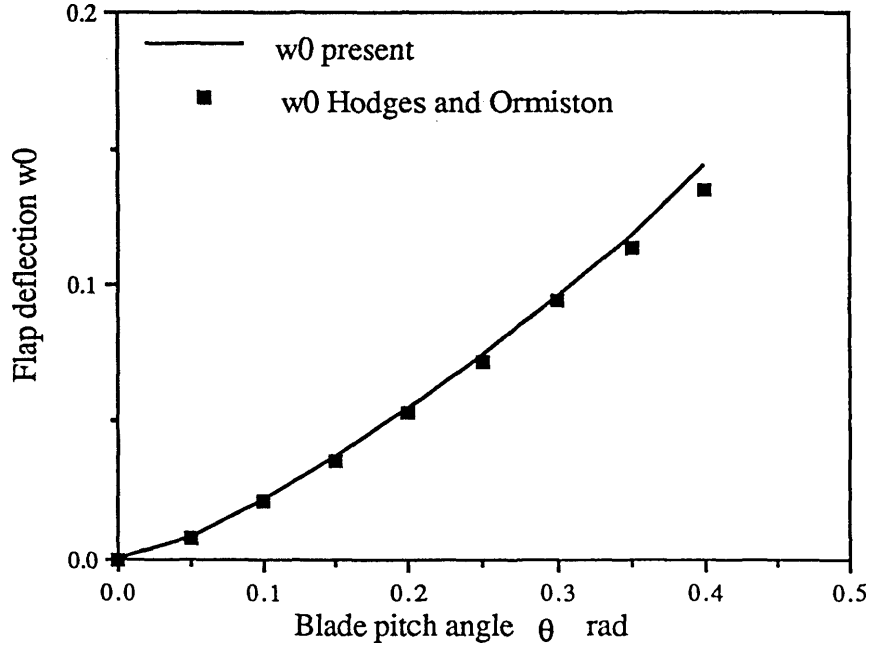

Fig 6.11 Equilibrium flap deflection of a rotor blade tip at various pitch angles ω_v=0.7, ω_ϕ=5.0, β_{pc}=0.0 rad

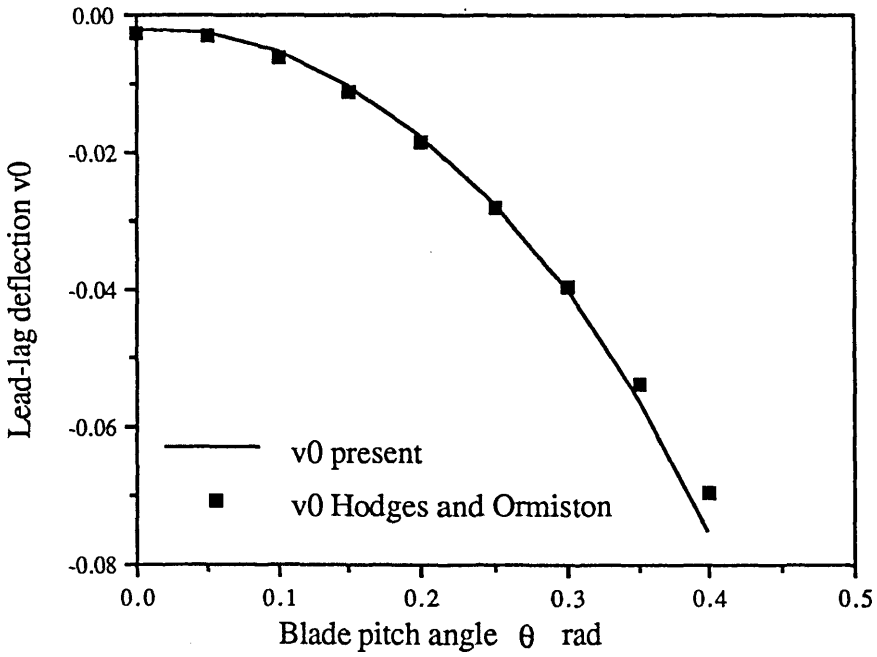

Fig 6.12 Equilibrium lag deflection of a rotor blade tip at various pitch angles

ω_v=0.7, ω_ϕ=5.0, β_{pc}=0.0 rad

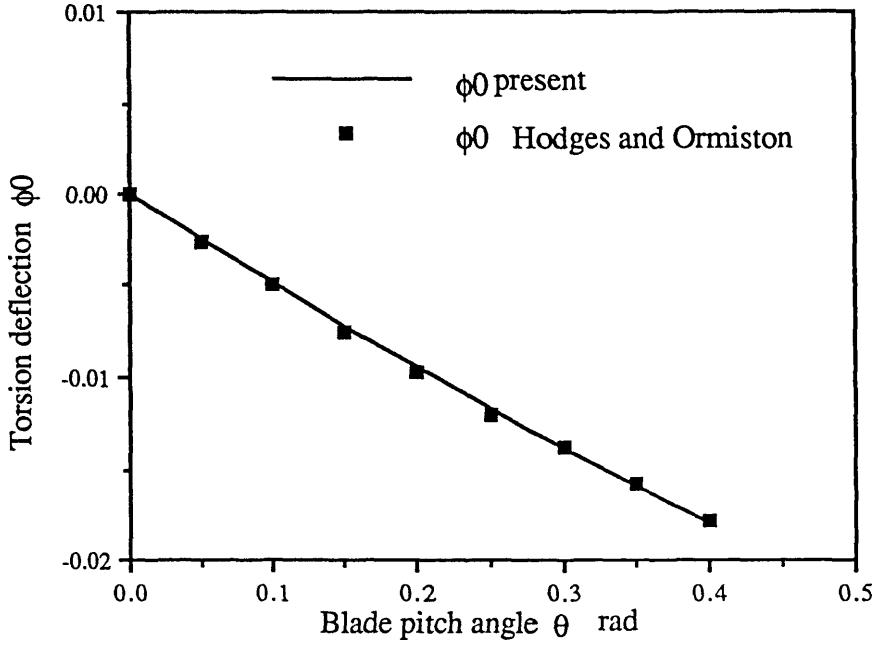

Fig 6.13 Equilibrium torsion deflection of a rotor blade tip at various pitch angles

ω_v=0.7, ω_ϕ=5.0, β_{pc}=0.0 rad

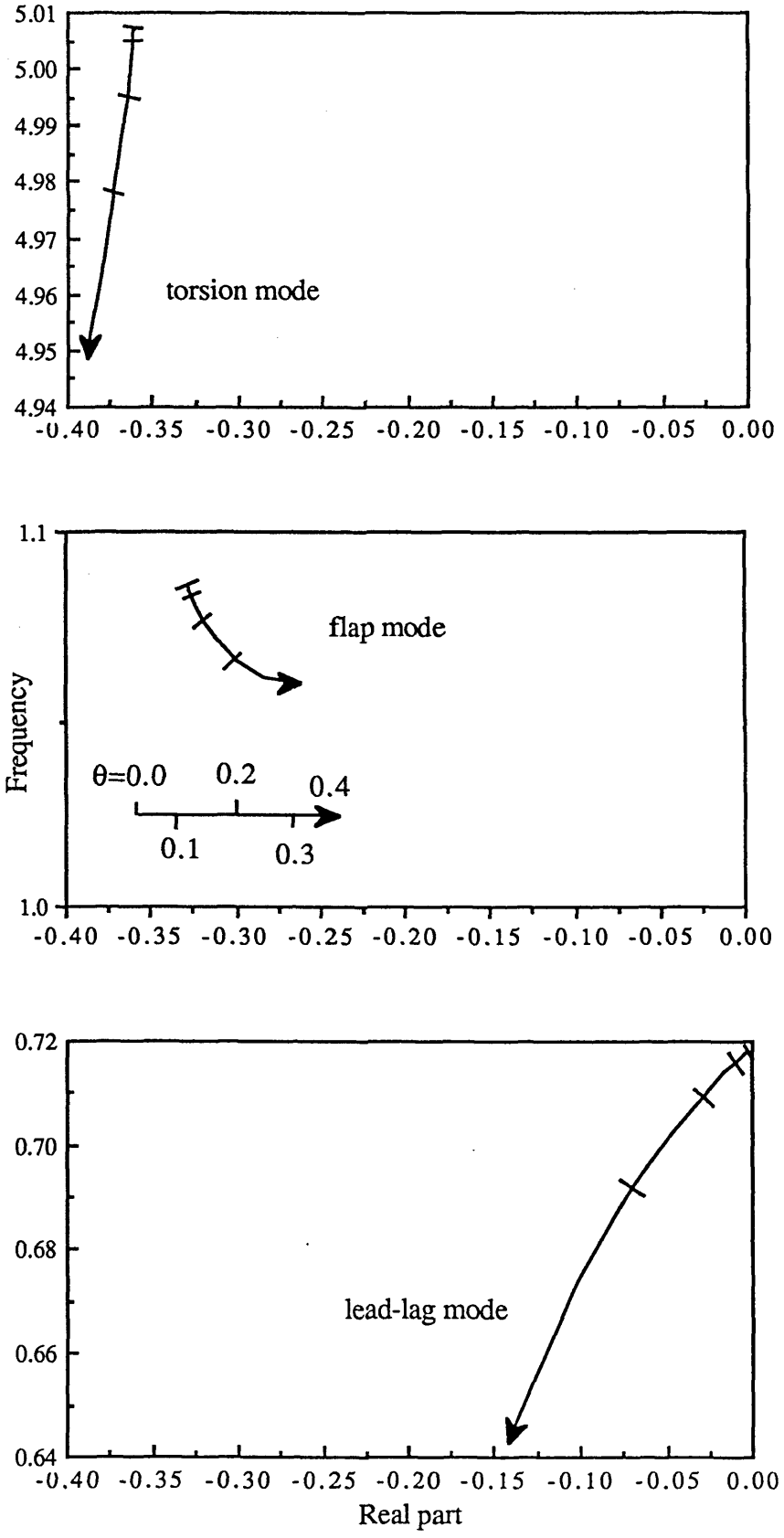

Fig 6.14 Locus of roots of blade modes

ω_v=0.7, ω_ϕ=5.0, β_{pc}=0.0 rad

Case IV (ω_v=0.7, ω_ϕ=2.5)

This case is for the configuration of ω_v=0.7, ω_ϕ=2.5. Compared with case III, the torsion frequency is reduced. Fig 6.15 to 6.17 present the equilibrium values of the blade tip deflections at various pitch angles. Only the results from the present model are shown because the equilibrium solution of this configuration is not given by Hodges and Ormiston. Comparing Fig 6.15-6.17 with Fig 6.11-6.13, the torsion deflection is largely increased due to the reduction of the torsional stiffness. Again, this increase leads to smaller real pitch angle ($\theta+\phi$), and hence smaller flap and lead-lag deflections are produced in Fig 6.15-6.16 than in Fig 6.11 to 12.

The locus of roots of the first flap mode, first lag mode and first torsion mode are plotted in Fig 6.18. The flap mode damping is decreased with the increase of pitch angle θ. The lead-lag mode damping is increased with θ. The torsion mode damping is little changed. The result from Hodges and Ormiston is also shown in Fig 6.20. The system is stable over the practical range of pitch angles θ. Comparing this case to case II, it should be noted that for a stiff inplane blade, a low torsion stiffness can result in a lag-torsion type instability as in Fig 6.10, but for a soft inplane blade, the stability is maintained for a low torsion stiffness. There is a significant difference between a stiff inplane configuration and a soft inplane configuration.

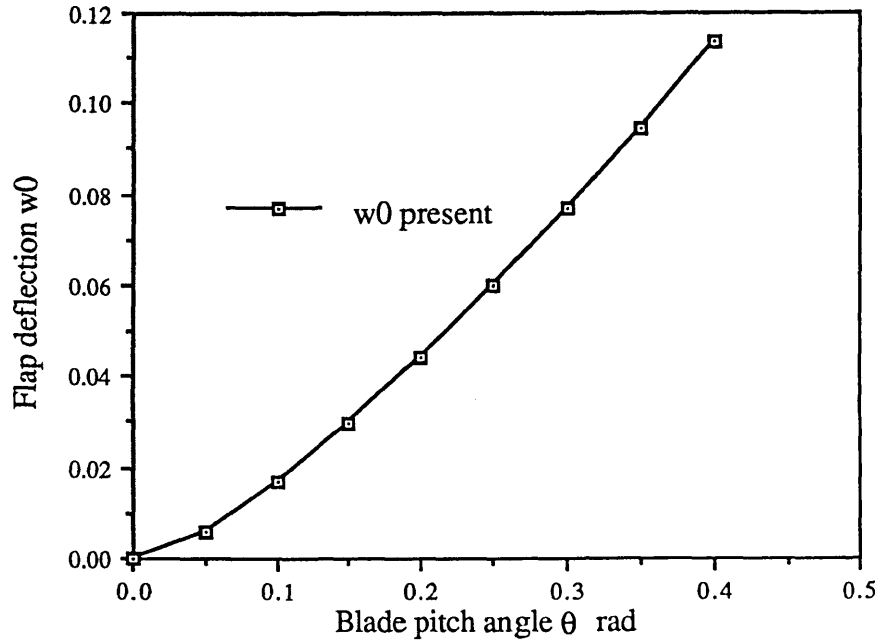

Fig 6.15 Equilibrium flap deflection of a rotor blade tip at various pitch angles

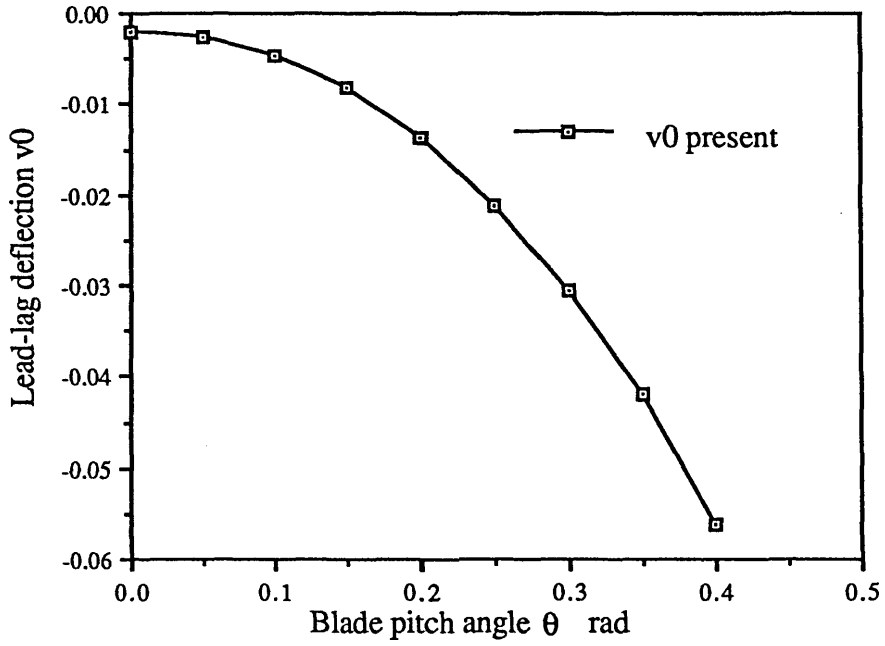

Fig 6.16 Equilibrium lag deflection of a rotor blade tip at various pitch angles
ω_v=0.7, ω_ϕ=2.5, β_{pc}=0.0 rad

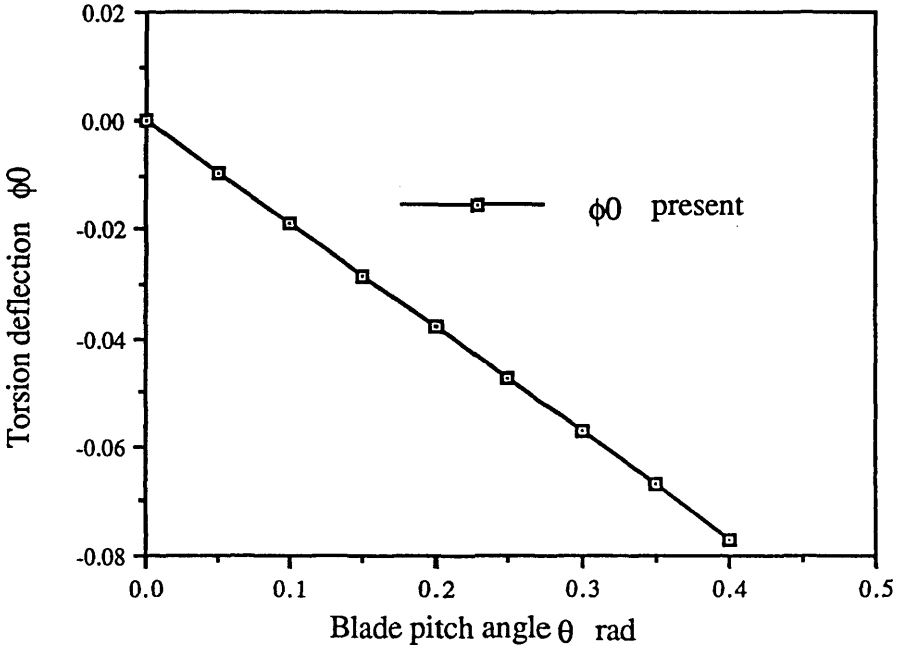

Fig 6.17 Equilibrium torsion deflection of a rotor blade tip at various pitch angles
ω_v=0.7, ω_ϕ=2.5, β_{pc}=0.0 rad

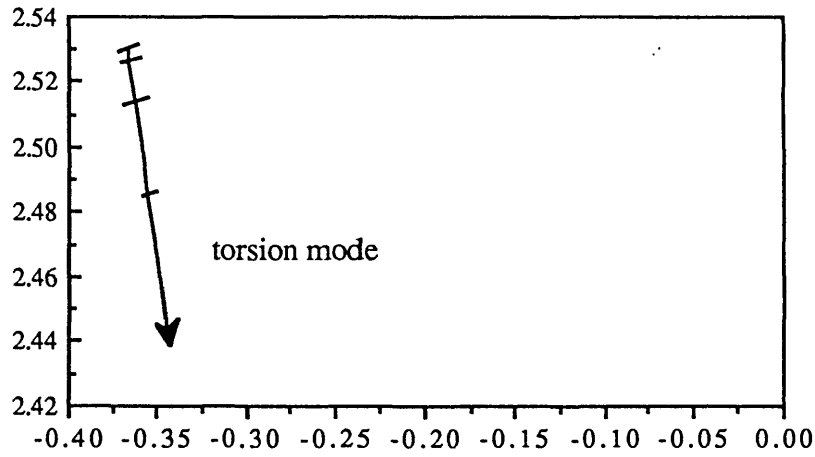

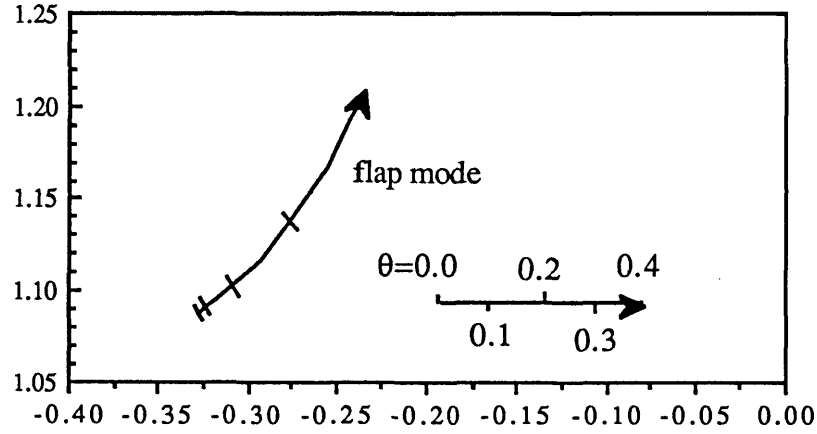

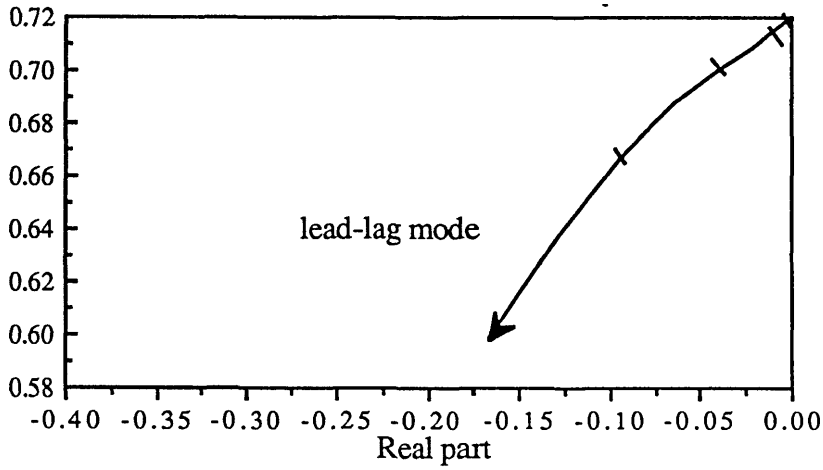

Fig 6.18 Locus of roots of blade modes

ω_v=0.7, ω_ϕ=2.5, β_{pc}=0.0 rad

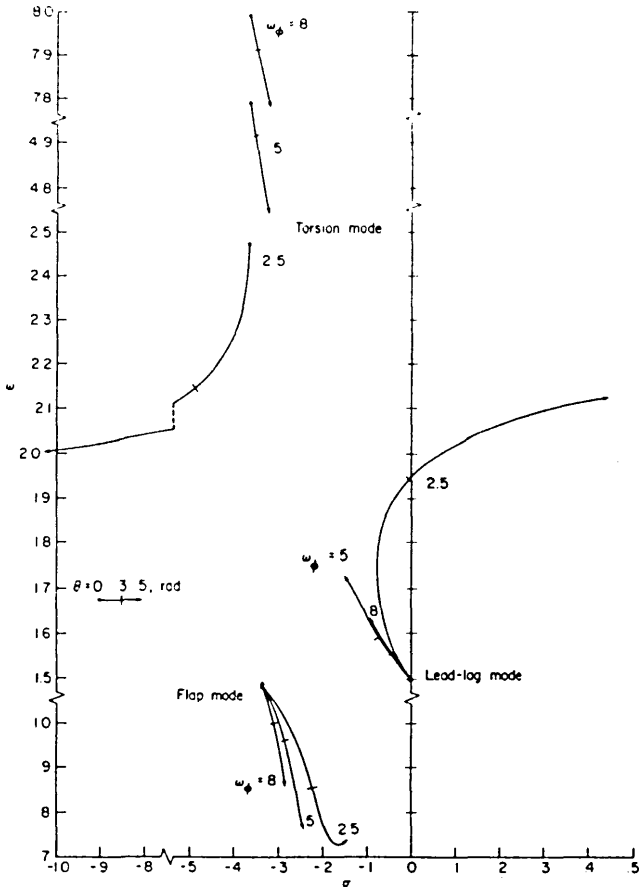

Fig 6.19 Locus of roots for stiff inplane rotor blade from Hodges and Ormiston, 1976 (ω_v=1.5, β_{pc}=0.0 rad)

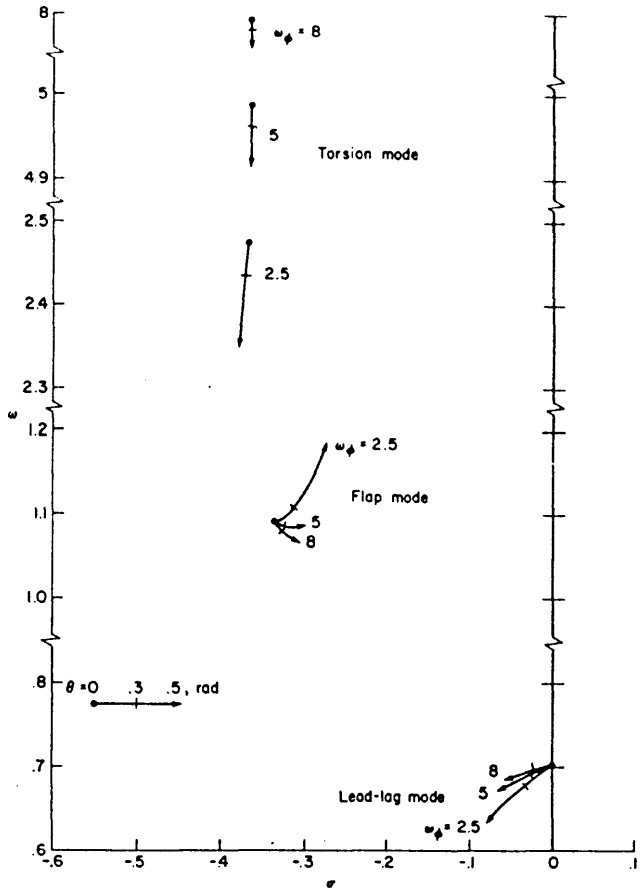

Fig 6.20 Locus of roots for soft inplane rotor blade from Hodges and Ormiston, 1976 (ω_v=0.7, β_{pc}=0.0 rad)

6.6.2 Results for Rotor Blades with Precone Angle

The present model is subsequently used to analyse the aeroelasticity stability of hingeless rotor blades with a precone angle β_p. This group of numerical examples is used to demonstrate the generality and flexibility of the present model. The blade root geometries can be easily modelled by making use of the blade base motion variables. According to the developed model, the translational velocity of the blade base can be obtained as $v_x=v_y=v_z=0$, the angular velocity of the base is $\omega_x=\Omega\sin\beta_p$, $\omega_y=0$, $\omega_z=\Omega\cos\beta_p$ from Fig 6.19. The other properties of the blade are the same as in the previous section. Applying these kinematical variables of the base to the program, we can analyse the aeroelastic stability of the rotor blades. The following four cases correspond to the case I to case IV respectively, but also has an 0.05 rad precone angle.

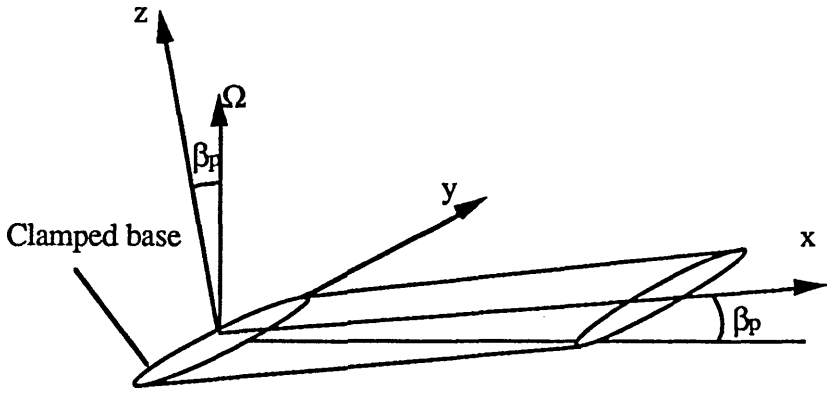

Fig 6.21 A hingeless rotor blade with precone angle β_p

Case V (ω_v=1.5, ω_ϕ=5.0, β_p=0.05 rad)

This case is for the configuration of ω_v=1.5, ω_ϕ=5.0, β_p=0.05 rad. Again, the configuration is the so-called stiff inplane blade. Fig 6.22 to 6.24 give the equilibrium values of the blade tip deflections in flap, lag and torsion together with the results from Hodges and Ormiston. These two groups of results have a good agreement. The slight discrepancies at high pitch angle θ are less than 6%. Again that is attributed to the

approximation of $\sin\theta$, $\cos\theta$ and $\sin(\theta+\phi)$, $\cos(\theta+\phi)$ in the reference. As expected, the blade tip flap deflection at zero pitch angle is negative due to the positive precone angle rather than zero as for zero precone angle. This is caused by the centrifugal force. Comparing Fig 6.23 to 6.4, the positive precone angle generates a positive lead-lag deflection increment. This is caused by the negative increment of the flap deflection through the flap-lag structural coupling.

Fig 6.25 gives the locus of the roots of the first flap, lead-lag and torsion modes with the variation of the pitch angle θ. The lead-lag mode damping is increased with the increase of the pitch angle, while the flap and torsion mode dampings are slightly decreased. The system is stable over the practical range of pitch angle.

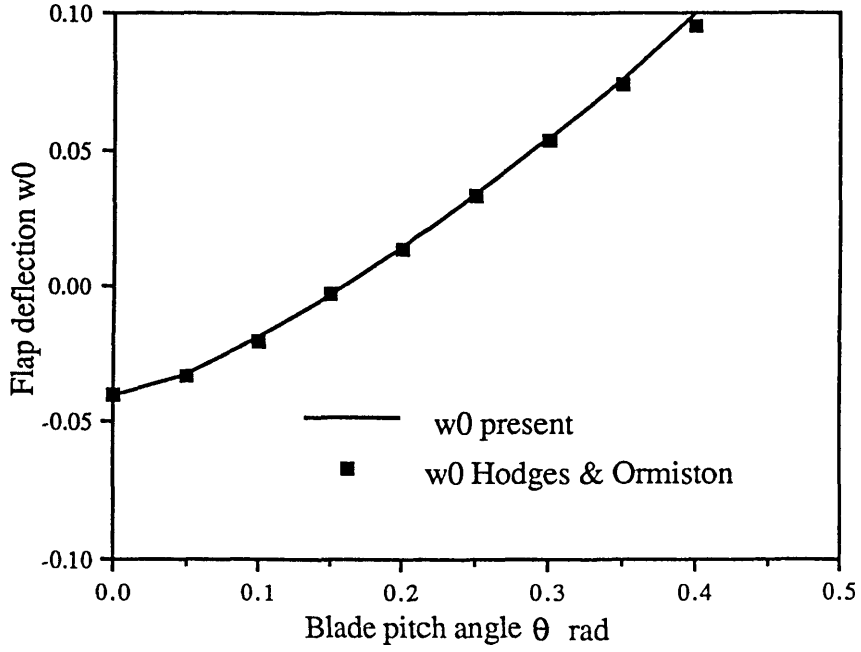

Fig 6.22 Equilibrium flap deflection of a rotor blade tip at various pitch angles

ω_ν=1.5, ω_ϕ=5.0, $\beta_{precone}$=0.05 rad

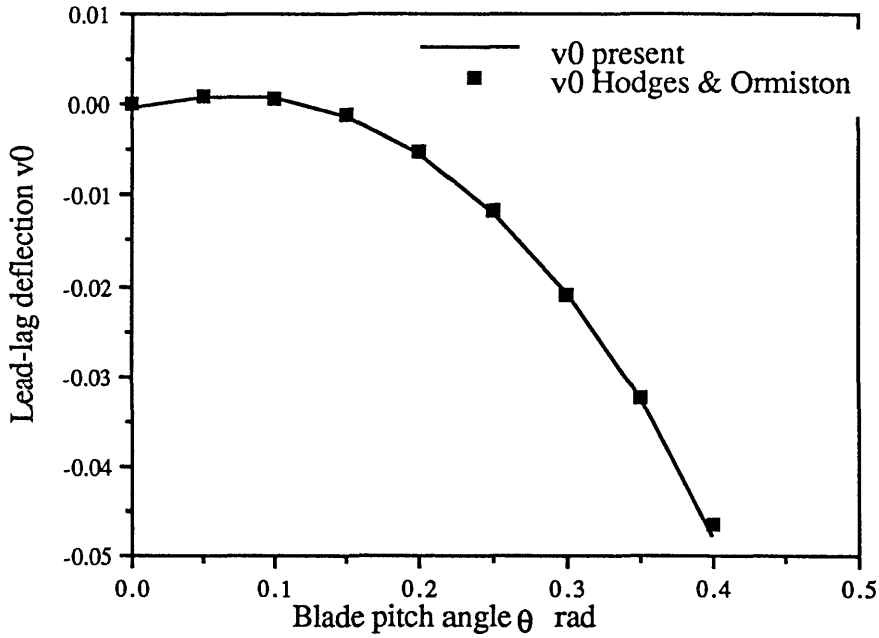

Fig 6.23 Equilibrium lag deflection of a rotor blade tip at various pitch angles

ω_v=1.5, ω_ϕ=5.0, β_{pc}=0.05 rad

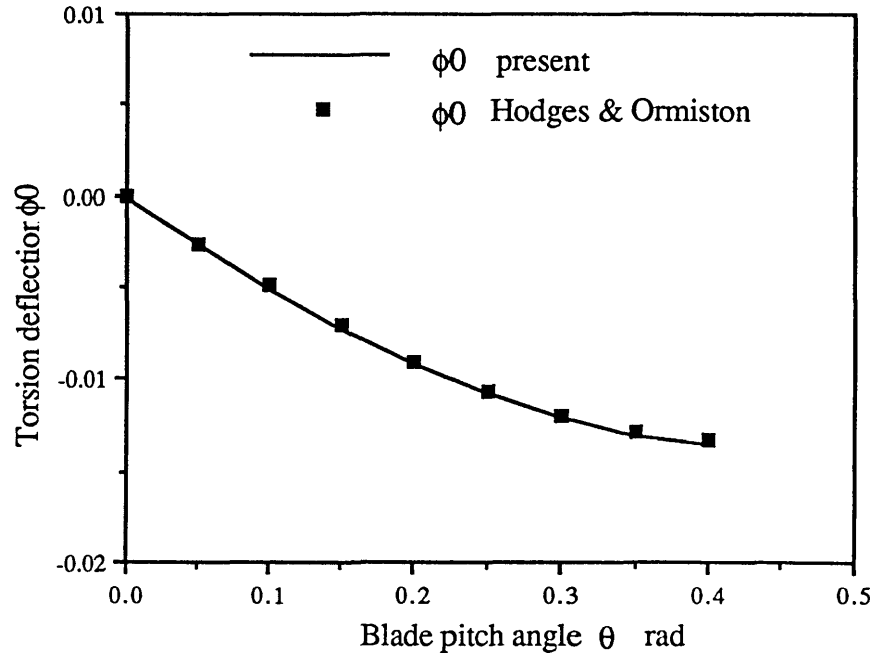

Fig 6.24 Equilibrium torsion deflection of a rotor blade tip at various pitch angles

ω_v=1.5, ω_ϕ=5.0, β_{pc}=0.05 rad

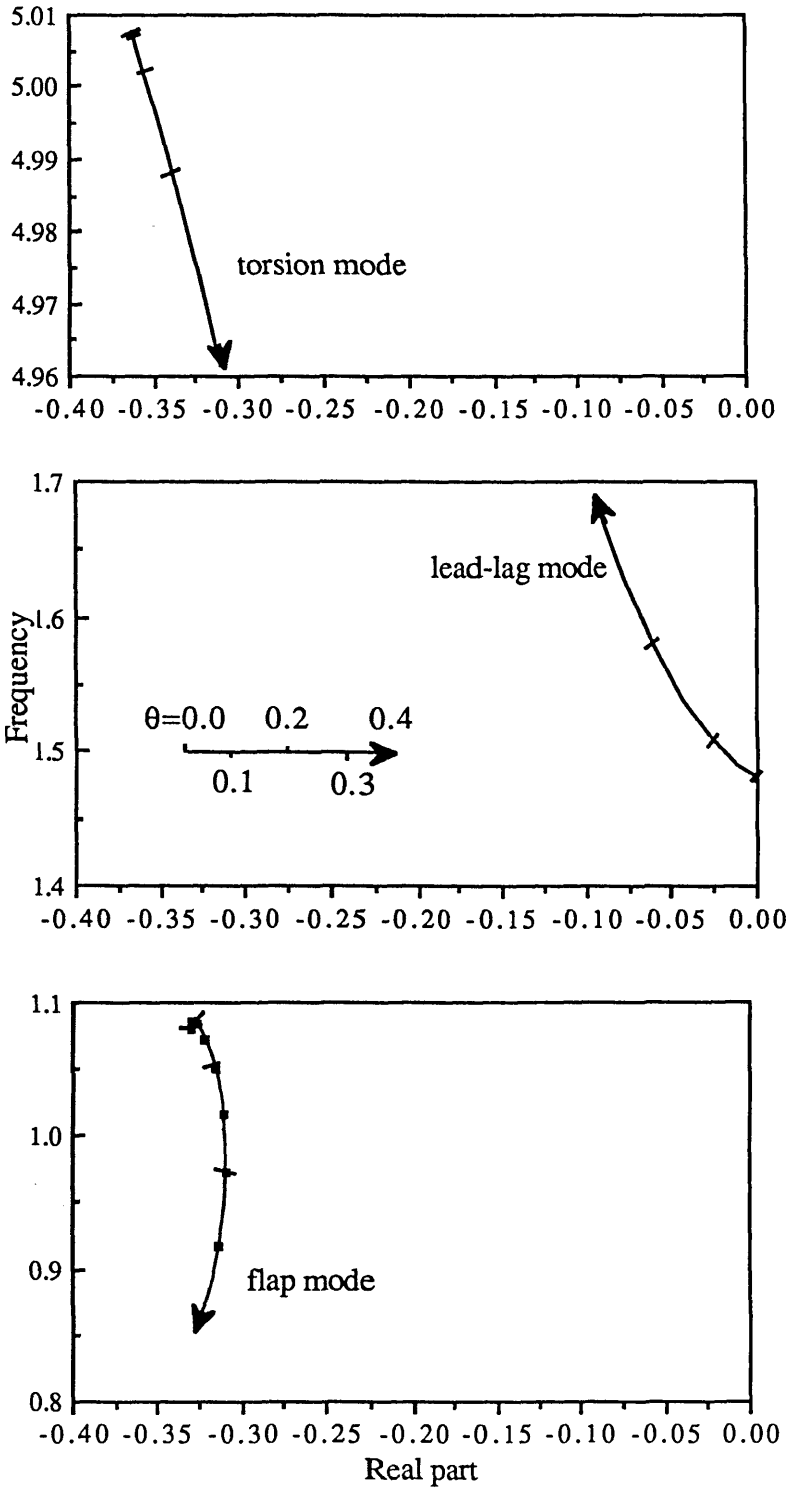

Fig 6.25 Locus of roots of blade modes

ω_v=1.5, ω_ϕ=5.0, β_{pc}=0.05 rad

Case VI (ω_v=1.5, ω_ϕ=2.5, β_p=0.05 rad)

The torsion frequency of the blade in case V is subsequently reduced to a low value 2.5 (ω_v=1.5, ω_ϕ=2.5, β_p=0.05 rad). The equilibrium values obtained for the blade tip are given in Fig 6.26 to 6.28. Compared with Fig 6.7 to 6.9, the positive precone angle produces a negative increment in flap deflection and a positive increment in the lead-lag deflection. The reason is the same as that stated in case V.

The locus of the roots of the flap, lag and torsion modes are plotted in Fig 6.29. As observed in Fig 6.10, the stiff inplane configuration at low torsion stiffness leads to the lag-torsion type instability at higher pitch angle. Furthermore, in this case, an instability occurs at quite low pitch angles due to the effect of the precone angle. This is another significant feature of a stiff inplane blade configuration. That is: for a low torsion stiffness, a stiff inplane configuration with a precone angle can result the lead-lag instability both at very low pitch angle and at a certain high pitch angle.

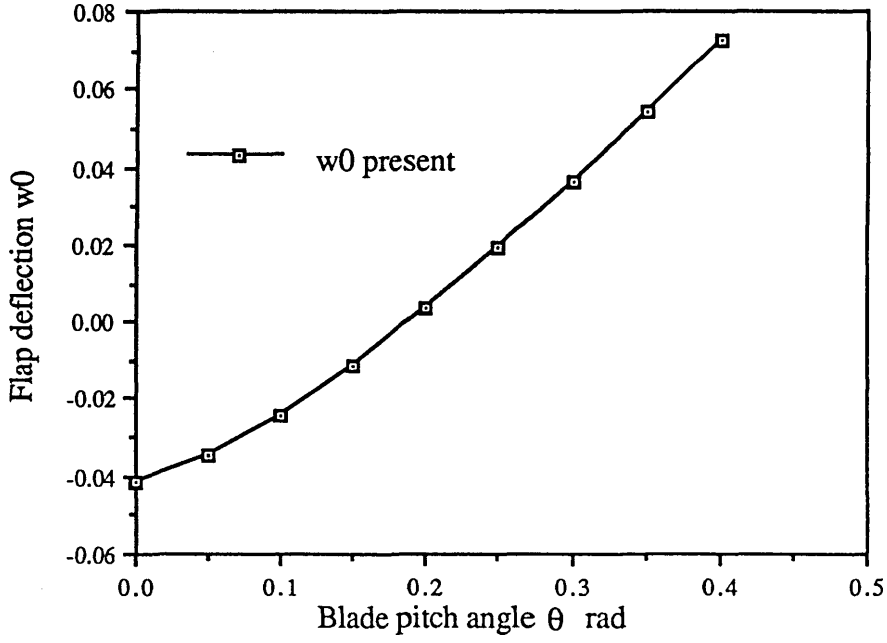

Fig 6.26 Equilibrium flap deflection of a rotor balde tip at various pitch angles ω_v=1.5, ω_ϕ=2.5, β_{pc}=0.05 rad

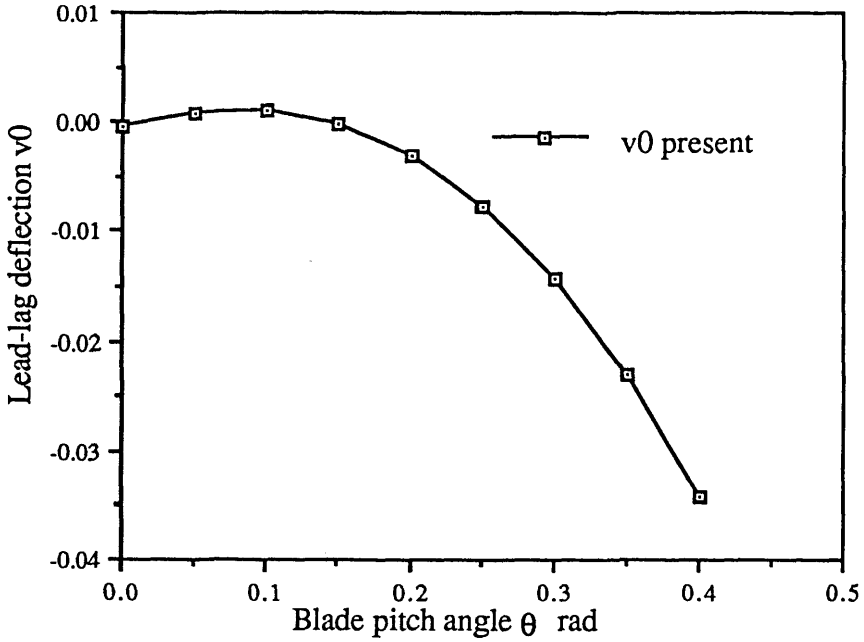

Fig 6.27 Equilibrium lag deflection of a rotor blade tip at various pitch angles

ω_v=1.5, ω_ϕ=2.5, β_{pc}=0.05 rad

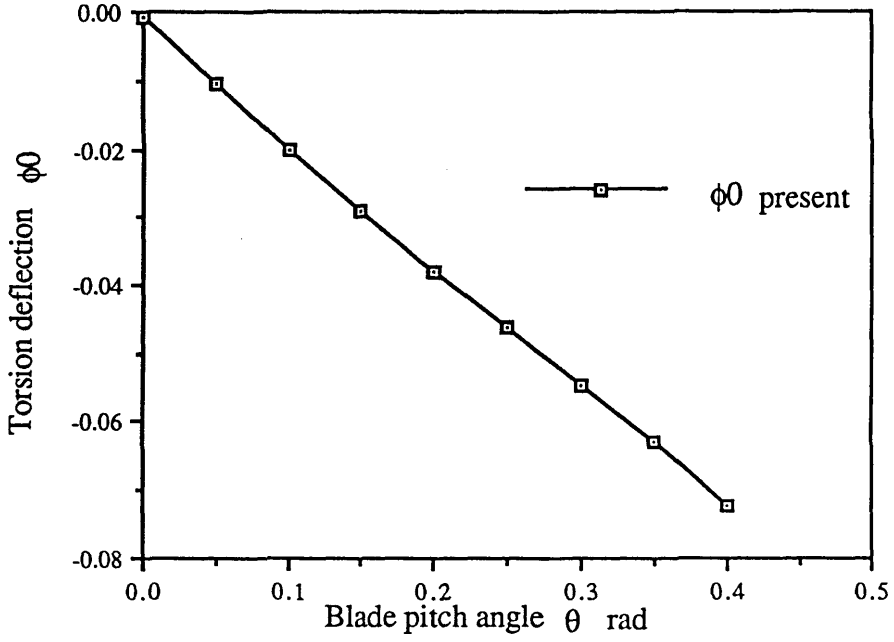

Fig 6.28 Equilibrium torsion deflection of a rotor blade tip at various pitch angles

ω_v=1.5, ω_ϕ=2.5, β_{pc}=0.05 rad

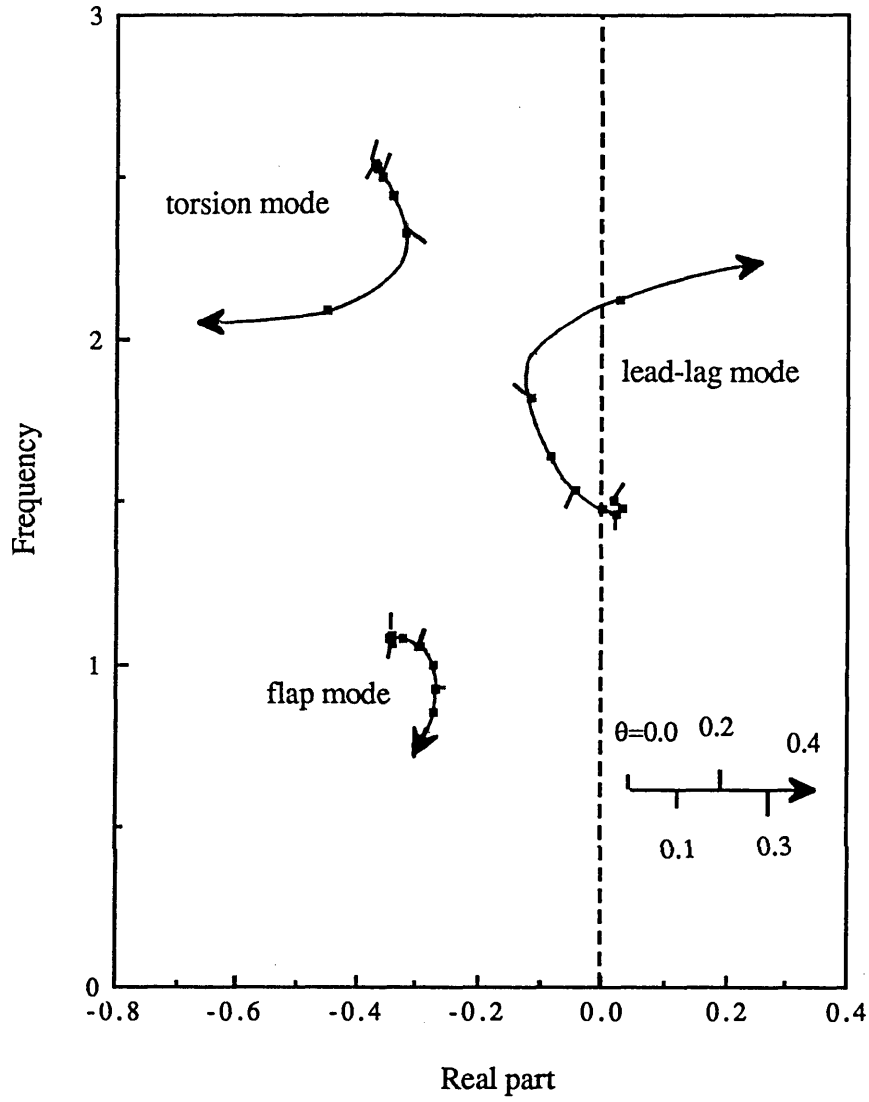

Fig 6.29 Locus of roots of blade modes

ω_v=1.5, ω_ϕ=2.5, β_{pc}=0.05 rad

Case VII (ω_v=0.7, ω_ϕ=5.0, β_p=0.05)

Case VII analyses the stability of a soft inplane blade configuration of ω_v=0.7, ω_ϕ=5.0, β_p=0.05 rad. Fig 6.30 to 6.32 present the equilibrium values of the blade tip deflections in flap, lag and torsion respectively. In Fig 6.30, the results from the current analysis and those from Hodges and Ormiston are plotted together. They agree with each other very well. The equilibrium solution for the lag and torsion is unavailable for this precone angle from the reference. However, the results for β_p=0.1 and 0.0 rad are given by Hodges and Ormiston. They give a good indication as to the accuracy of the present results.

Fig 6.33 plots the locus of roots of the flap, lag and torsion modes with the variation of pitch angle. The lead-lag mode damping increases with the pitch angle. The flap mode damping slightly decreases with the pitch angle. The torsion mode damping has a very small change. The system is stable over the practical range of pitch angles.

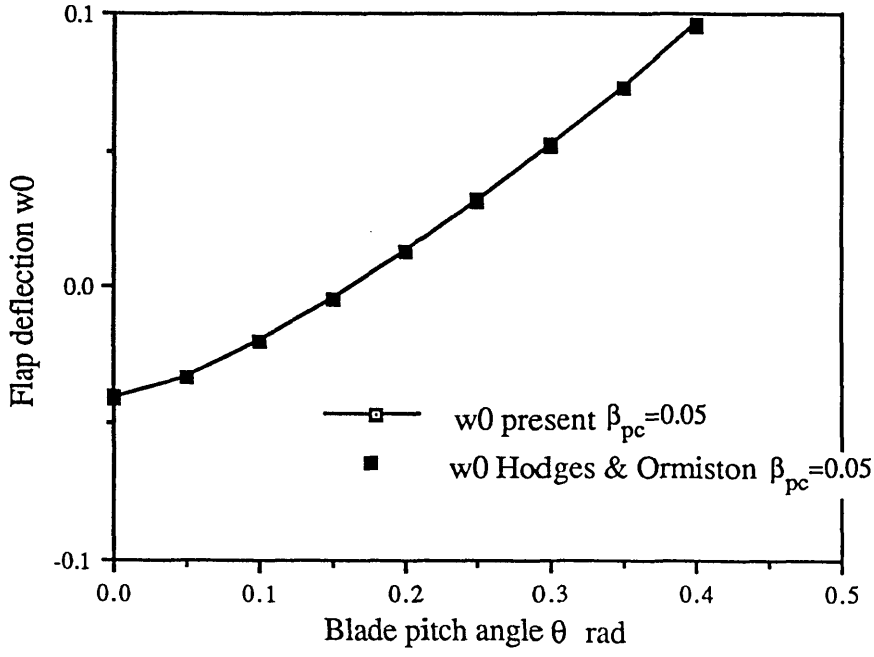

Fig 6.30 Equilibrium flap deflection of a rotor blade at various pitch angles
ω_v=0.7, ω_ϕ=5.0, β_{pc}=0.05 rad

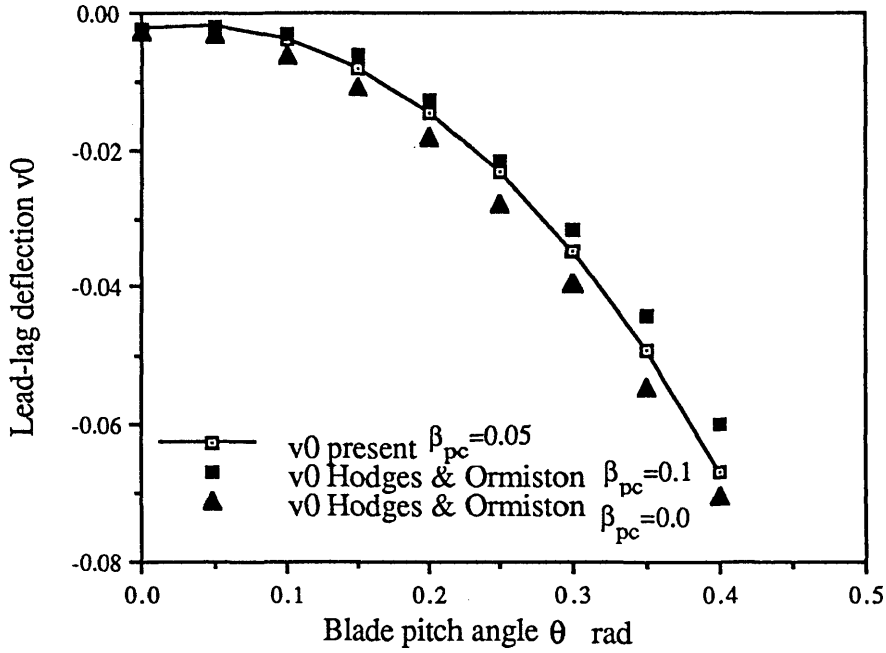

Fig 6.31 Equilibrium lag deflection of a rotor blade tip at various pitch angles

ω_v=0.7, ω_ϕ=5.0, β_{pc}=0.05 rad

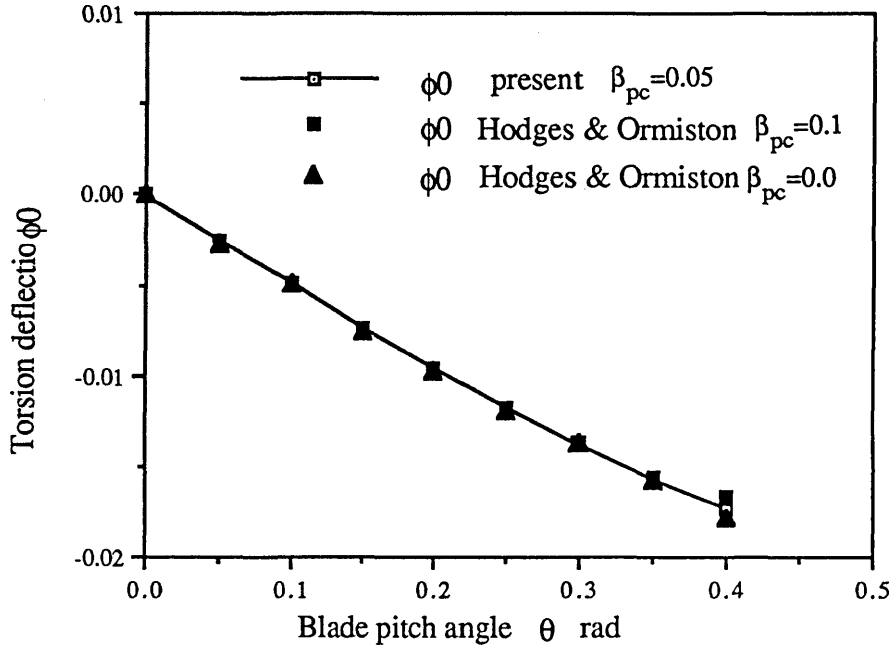

Fig 6.32 Equilibrium torsion deflection of a rotor blade tip at various pitch angles

ω_v=0.7, ω_ϕ=5.0, β_{pc}=0.05 rad

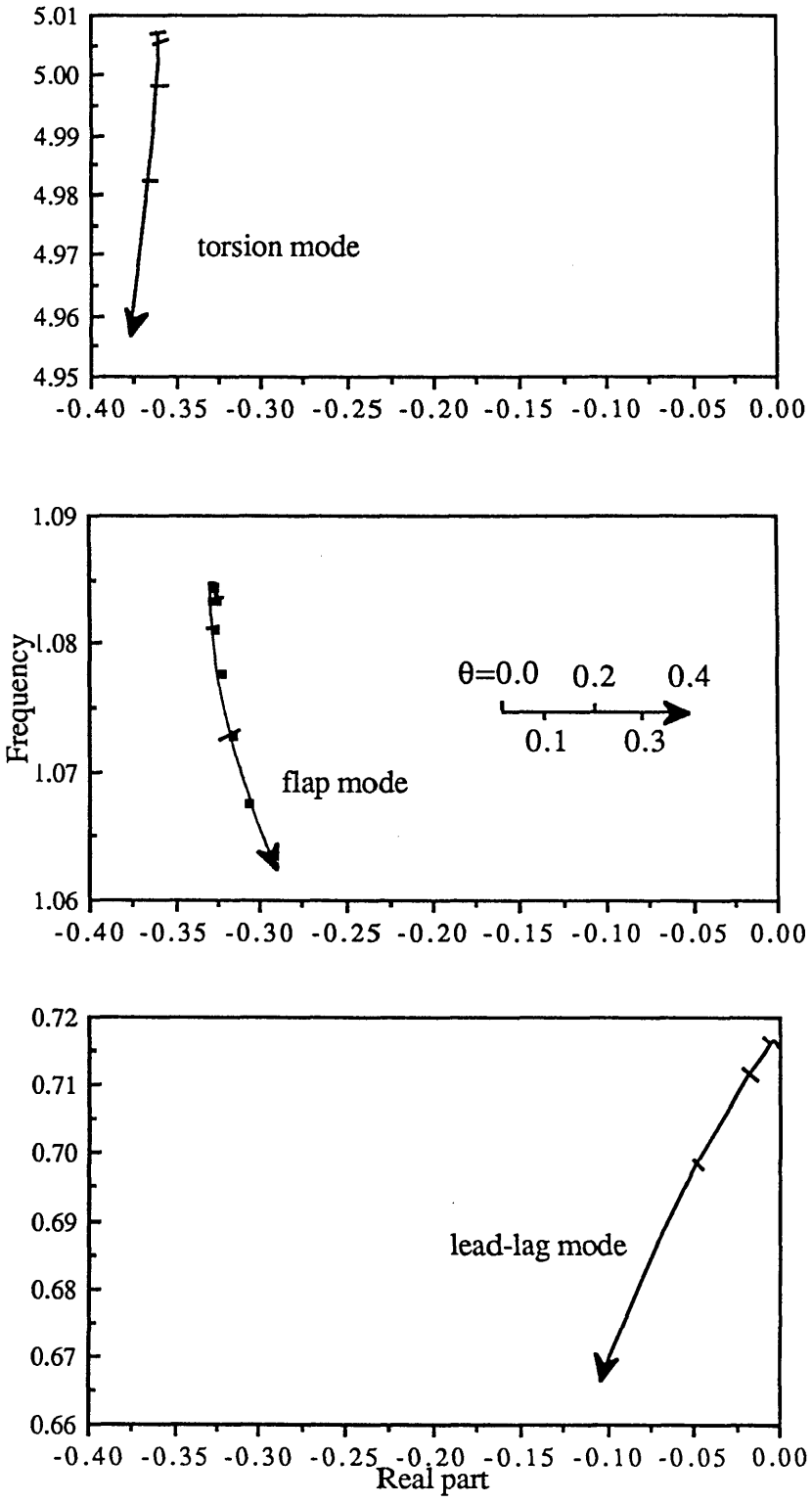

Fig 6.33 Locus of roots of blade modes

ω_v=0.7, ω_ϕ=5.0, β_{pc}=0.05 rad

Case VIII (ω_v=0.7, ω_ϕ=2.5, β_p=0.05)

This case is for the configuration of ω_v=0.7, ω_ϕ=2.5, β_p=0.05 rad. That is a soft inplane blade with a low torsion stiffness. The equilibrium solutions are given in Fig 6.34 to 6.36. They represent the blade tip deflections in flap, lag and torsion respectively. Comparing Fig 6.36 to 6.32, the present torsion deflection is largely increased due to the reduced torsional stiffness. In this case, the flap and lag deflections are also reduced by a small amount. This, again, is indirectly influenced by the effective blade pitch angle ($\theta+\phi$). As expected, the flap deflection at zero pitch angle is negative rather than zero due to the precone angle effect.

The locus of roots of the first flap, lead-lag and torsion modes are plotted in Fig 6.37. The lead-lag mode damping is increased with the increase of the pitch angle. The flap mode damping is decreased with the increase of pitch angle. The change of the torsion mode damping is quite small. The system is stable over the practical pitch angle values.

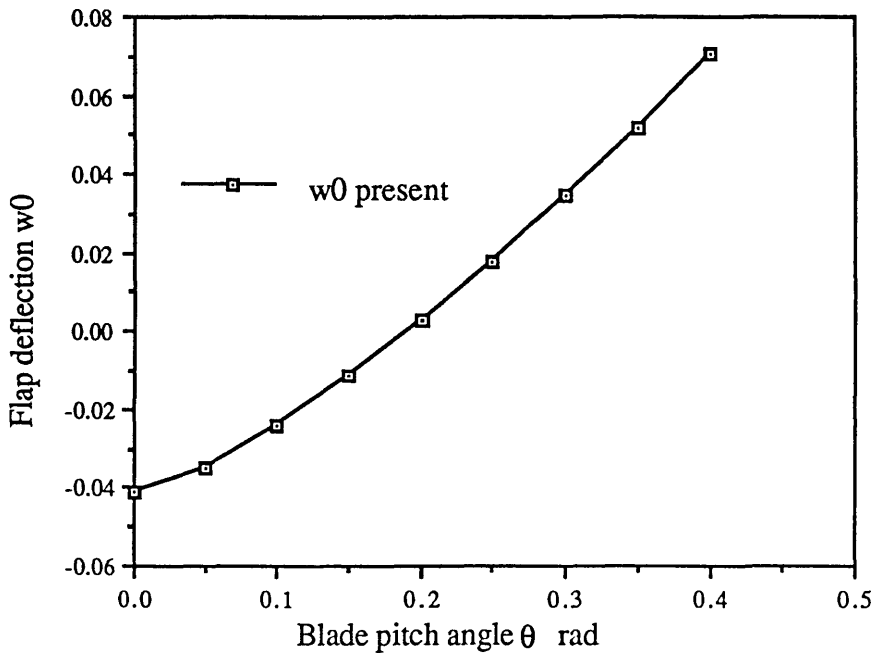

Fig 6.34 Equilibrium flap deflection of a rotor blade tip at various pitch angles

ω_v=0.7, ω_ϕ=2.5, β_{pc}=0.05 rad

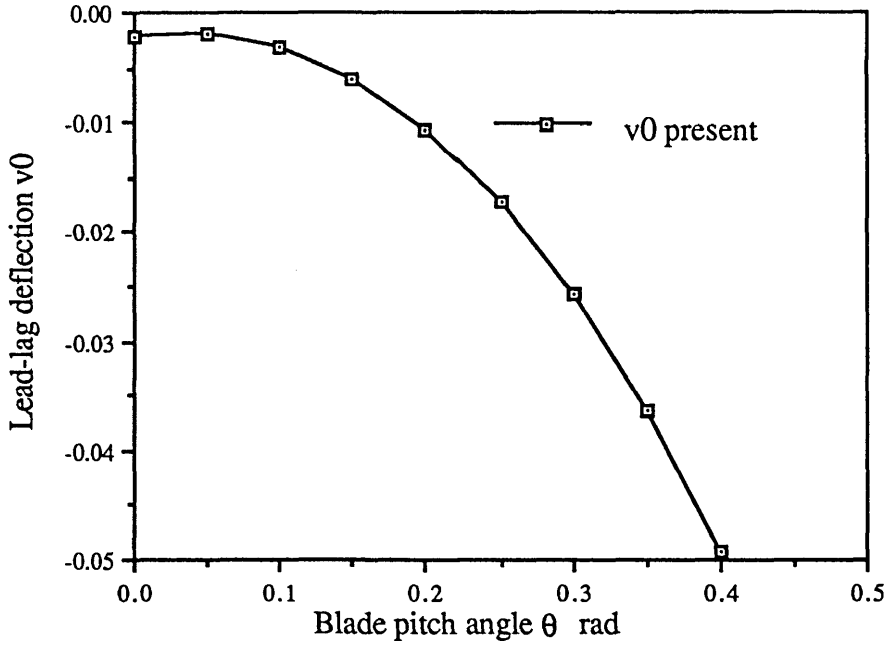

Fig 6.35 Equilibrium lag deflection of a rotor blade tip at various pitch angles

ω_v=0.7, ω_ϕ=2.5, β_{pc}=0.05 rad

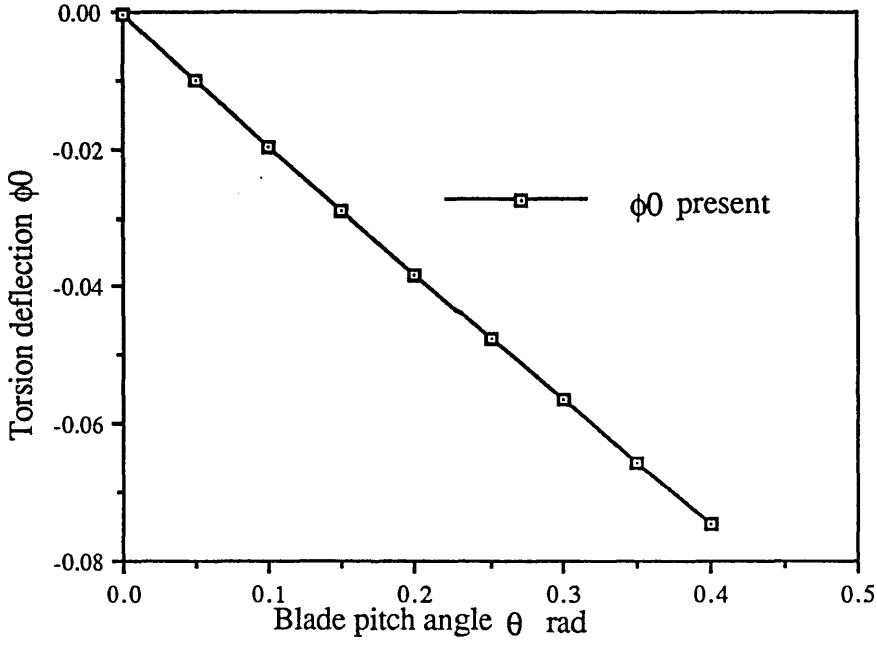

Fig 6.36 Equilibrium torsion deflection of a rotor blade tip at various pitch angles

ω_v=0.7, ω_ϕ=2.5, β_{pc}=0.05 rad

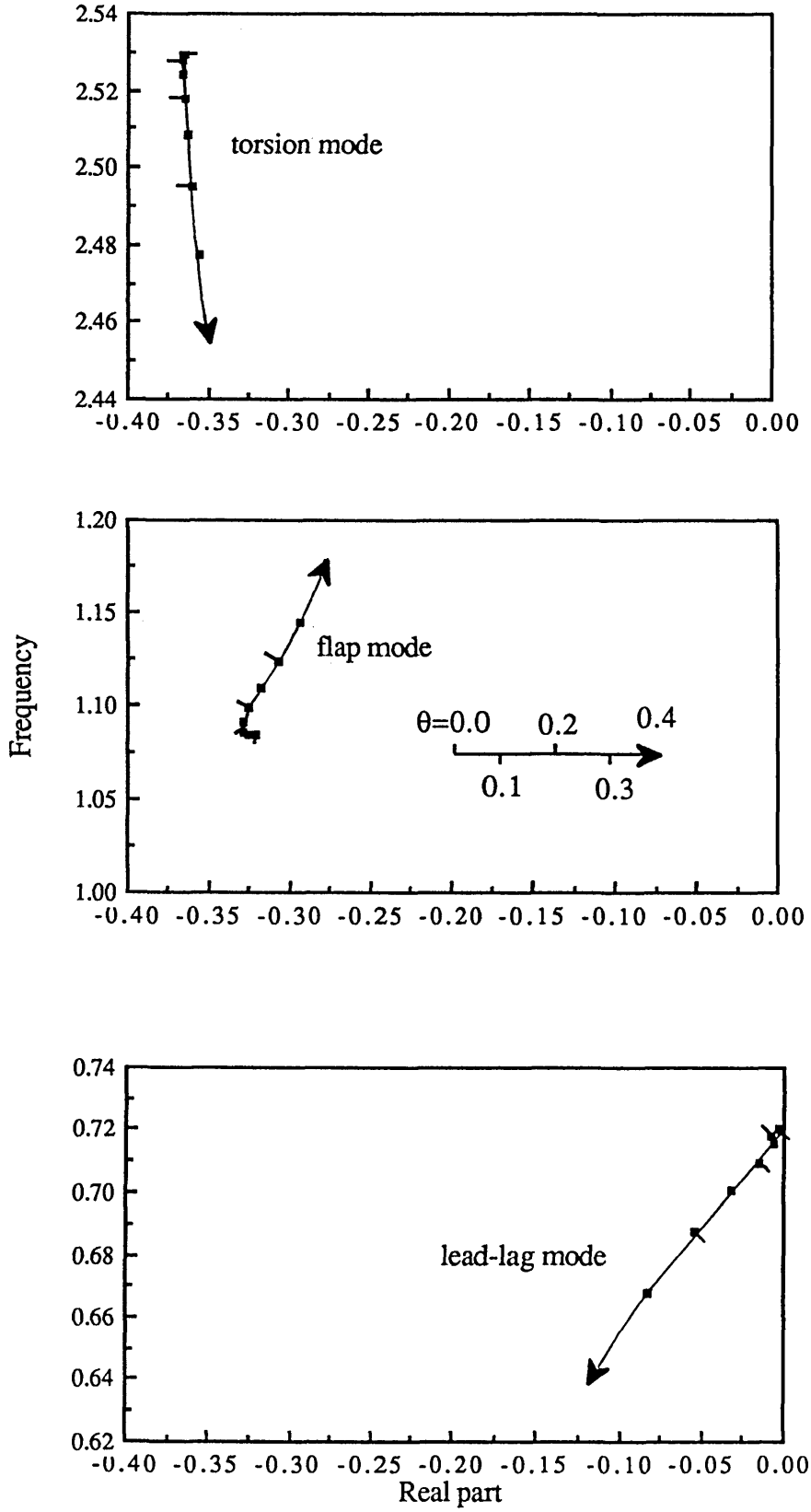

Fig 6.37 Locus of roots of blade modes

ω_v=0.7, ω_ϕ=2.5, β_{pc}=0.05 rad

6.7 SOME CONCLUSIONS

Some significant conclusions can be drawn from the above analyses. It is shown that the newly developed model presented here and the code based upon this is an appropriate and powerful tool to analyse the rotorcraft aeroelasticity stability. The Finite Element Method combined with the multibody dynamics approach creates a quite general model to model a complex structure with complex geometries and complicated couplings between substructures. It is a promising method. The combination produces great modelling flexibility and generality. The extensive parametric investigations of the aeroelasticity stability of hingeless rotor blades show:

1) Usually in the coupled blade flap-lag-torsion aeroelasticity system, the flap mode damping and torsion mode dampings are quite high, while the lead-lad mode damping is low.
2) Soft inplane blade configurations are stable over the practical range of pitch angles.
3) Stiff inplane blade configurations may be destabilised depending upon the torsion stiffness. Low torsion stiffness can lead to lag-torsion type instability.
4) Positive precone angle is destabilising for the stiff inplane configurations and can lead to lead-lag mode instability at quite low pitch angles.

CHAPTER 7 CONCLUSIONS AND FURTHER WORK

7.1 CONCLUSIONS

In the first part of this work, the whirl flutter of the tilt-rotor aircraft was studied. A particular endeavour was made in the second part to develop a general model of great modelling flexibility for rotorcraft aeroelasticity analysis and the dynamic analysis of rotating beam-like structures.

Whirl Flutter Model of a Tilt-rotor Aircraft

Firstly, an aeroelastic model is developed to study the whirl flutter problem of a tilt-rotor aircraft. In order to obtain a clear physical insight into the whirl flutter characteristics of a tilt-rotor aircraft, it is simplified as a coupled rotor/nacelle system. The aircraft is assumed to be in stable forward flight. The flexibility of the fuselage and wing are excluded. The nacelle is considered to be a rigid body supported on springs and dampers. The rotor of N blades are assumed to be rigid in flap and lead-lag. Each blade is set to a pitch bearing with a torque spring and hence has a rigid torsion degree of freedom. The rotor is connected to the nacelle through either a universal joint or a gimbal. Both have two degrees of freedom one each in pitch and yaw with spring and damping restraints. Rotor configurations include the gimbal undersling, blade pitch bearing offset, blade precone angle, blade pitch bearing sweep angle, blade sectional mass centre offset and aerodynamic centre offset from the pitch axis. The total degrees of freedom is 12 for each configuration.

The equations of motion for these two systems are derived using the Newton method. The nonlinear terms that are retained are based upon an ordering scheme. The aerodynamic loads are included based upon a two dimensional quasi-steady thin airfoil theory and are valid for both high inflow and low inflow cases. The multi-blade

coordinate transformation is used for blade torsion degrees of freedom to eliminate the periodic coefficients in the equations of motion. The nonlinear differential equations of motion are linearised using the perturbation method. The eigenvalue problem associated with the linearised differential equations are then solved to analyse the system stability.

A computer program was developed for this model. It was first applied to the investigation of the classical propeller whirl flutter problem and a coupled flap-hinged tilt-rotor/nacelle whirl flutter problem. The present numerical results show good agreement with available experimental and analytical results. Subsequently, the present model was applied to analyse the whirl flutter characteristics of a universal joint tilt-rotor aircraft and an ideal gimbal tilt-rotor aircraft. Their whirl flutter characteristics are evaluated and compared. The following conclusions are drawn:

1) The developed model can adequately model the whirl flutter of propeller and tilt-rotor aeroplanes.
2) The whirl flutter modes of of the universal joint rotor configuration and the ideal gimbal rotor configuration are very similar. The gimbal rotor whirls at a slightly higher velocity than the universal joint rotor.
3) In both configurations, the unstable mode appears as the nacelle mode of lower frequency.
4) The stiffness of the nacelle support springs in pitch and yaw are significant for the whirl flutter of both configurations. A reduction of the stiffness is highly destablising.
5) The rotor modes are highly damped because the rotor behaves like a flap blade. The forward rotor mode damping decreases with the forward speed, but its high damping is generally sufficient to maintain the stability until quite a high forward speed.

A General Finite Element Model for Beams Attached to an Arbitrary Moving Base

In the second part, an endeavour was made to develop a general Finite Element model for rotating beam-like structures and especially for modelling the rotorcraft aeroelasticity problems. This model has a great modelling flexibility and can deal with complex beam geometries, arbitrary blade root kinematics and the coupling between the beam and other substructures, such as the fuselage. The model was developed in two stages.

The structural dynamics model

As the first step, a general Finite Element structural dynamics model was developed for a three dimensional elastic beam with an arbitrary and large moving base of six degrees of freedom. The six degrees of freedom of the beam base can incorporate either a prescribed arbitrary motion of the base or the coupling of the beam with other substructures. The beam can be pretwisted and have a mass centre offset from the elasticity centre. The equations of motion were derived using the virtual work principle. Large deflections and small strains of the beam were assumed so that the geometrical nonlinearities are included. The equations are discretised using the finite element method. The beam inertia is lumped at the end nodes of each element and this simplifies the analysis. The axial and torsional deflections of the beam element are represented by linear polynomials, while the bending deflections are represented by cubic polynomials. The centrifugal stiffness and gyroscopic terms caused by the large base motion were specifically considered so that this dynamics model is applicable for both nonlinear and linear problems.

This dynamics model was coded into a computer program and applied to solve both an eigenvalue problem of a spinning beam and to simulate the dynamic response of a space-based robotic manipulator arm with a complex time-varying base motions. The former has a precise analytical solution to compare with, and the latter has a numerical solution based on a modal method to compare with. The results show:

1) Six to eight elements are sufficient for determining natural frequencies of a rotating beam.
2) The present Finite Element model can successfully solve the eigenvalue problems of a rotating beam.
3) The present model was shown to be an appropriate and general tool to treat the dynamic response problem of a beam with complex and large base motion. This model has a great modelling generality due to the combination of the Finite Element method and the arbitrary base motion variables which is widely used in Multibody Dynamics.
4) The significant deficiencies of the previous multibody dynamics models, which were pointed out by Kane et al [1987], were confirmed by the present model.
5) A minor deficiency is believed to exist in the simulation of the extension and lead-lag deflections in the multibody dynamics model recently developed [Kane et al, 1987]. It is believed to be caused by the linearisation of that model and was eliminated in the current model.

The aeroelasticity model

The structural dynamics model that was developed was further extended to a finite element aeroelastic beam model for rotorcraft blades in an axial flow. The virtual work done by the aerodynamic loads was formulated. The aerodynamic loads are computed using a two dimensional quasi-steady thin airfoil theory, and is discretised by the Finite Element Method. The aerodynamic model was specifically considered such that it is valid for both high inflow rotors and low inflow rotors. The arbitrary base motion and the aerodynamic centre offset from the elasticity centre were included in the aerodynamic formulation. The nonlinear differential equations of motion were obtained by combining the structural dynamics model with the virtual work done by the aerodynamic loads. Again the nonlinear differential equations were linearised using the perturbation method to analyse the aeroelastic stability of rotorcraft. This results in a set of nonlinear algebraic

equations for the steady equilibrium values and a set of linear differential equations for the dynamic component. The nonlinear algebraic equations are solved iteratively to obtain the equilibrium values. The equilibrium values are then used to obtain the coefficient matrices for the linearised differential dynamic equations. The associated eigenvalue problem is finally solved to analyse the aeroelastic stability of rotorcraft. The algorithm is incorporated into a computer program to evaluate the aeroelasticity stability of rotor blades. This general model can be used as a basic element to analyse the isolated blade aeroelastic stability and the coupled rotor/body system aeroelastic stability by making use of the six rigid body degrees of freedom of the blade base.

This developed model was applied to solve a number of numerical examples to validate it and to illustrate the solution of the aeroelastic stability of rotor blades. The first example was an isolated hingeless rotor blade without precone angle. The second example demonstrates the modelling flexibility of the present model by modelling the blade precone angle through the degrees of freedom of the base which are essential for the modelling generality and flexibility of the present model. A wide range of parametric variations were made in both examples. Comparison of the present results with the existing results allows the following conclusions to be reached:

1) The present model is an appropriate and powerful tool for analysing rotor blade aeroelastic stability.
2) This model has a great modelling flexibility and generality. The Finite Element Method combined with the Multibody Dynamics approach creates a quite general model to model a complex structure with complex geometries and complicated couplings between substructures. It is a promising method. The method developed is of great potential as a general model for rotating beams dynamics and rotorcraft aeroelasticity.

3) Usually, the flap mode damping and torsion mode damping are quite high in the coupled hingeless blade flap-lag-torsion aeroelasticity system, while the lead-lag mode damping is low.
4) Stiff inplane blade configurations with low torsional stiffness may give rise to lead-lag instability due to the pitch-lag coupling.
5) A positive blade precone angle is destablising and may give rise to a lead-lag instability at quite low pitch angles.

7.2 FURTHER WORK

Further work is needed to develop a comprehensive and general model for rotorcraft aeroelasticity problems. Some of the items for this are suggested in follows.

Application to Coupled Rotor/body Aeroelasticity

The analysis of coupled rotor/body aeroelastic stability is a complex and important part of rotorcraft aeroelasticity problems. One of the aims in developing the present general model was to provide a significant basic element for the analysis of such coupled systems. Some further work is required to combine the present model with a supporting body dynamics model in the nonrotating frame. The coupling can be realised by the kinematical restraint relation on the interface. The six degrees of freedom of the blade base can be used to advantage for this. Since the blade generalised coordinates are defined in the rotating frame,while the body coordinates are in the non-rotating frame, the so-called multi-blade coordinate transformation needs to be used.

Inclusion of Dynamic Inflow Model in the Aerodynamics

The present model utilises the two dimensional quasi-steady thin airfoil theory. A logical improvement is to add the dynamic inflow model to the quasi-steady aerodynamics. The dynamic inflow model is an efficient approximation for low frequency unsteady aerodynamics.

Composites Blades

The present structural dynamics model is based on the Euler-Bernoulli assumption. This is invalid for anisotropic composites blades. Modifications have to be made to consider the transverse shear deformations and cross-sectional warping effects in the structural model.

Forward Flight in Helicopter Mode

The present aerodynamics model is only developed for axial flow rotors. When a rotorcraft flies forward in a helicopter mode the air flow through the airfoil is periodic in nature. Further developments are needed to include the effect of the forward flight in the aerodynamics model. This leads to much more complex unsteady aerodynamics and to time-varying periodic coefficients in the equations of motion.

APPENDIX 3A

COORDINATE TRANSFORMATION MATRICES

1. "$x_0y_0z_0$" system $\Leftrightarrow$ "$x_gy_gz_g$" system

Parallel systems and hence

$$\begin{Bmatrix} i_g \\ j_g \\ k_g \end{Bmatrix} = \begin{bmatrix} 1 & 0 & 0 \\ 0 & 1 & 0 \\ 0 & 0 & 1 \end{bmatrix} \begin{Bmatrix} i_0 \\ j_0 \\ k_0 \end{Bmatrix} = [E] \begin{Bmatrix} i_0 \\ j_0 \\ k_0 \end{Bmatrix}$$

[E] is a unit matrix

2. "$x_gy_gz_g$" system $\Leftrightarrow$ "$x_{1g}y_{1g}z_{1g}$" system

Euler angle (θ_x,θ_y,θ_z,) rigid body rotations, undergoing the series roll, pitch, yawing motion of nacelle.

$$\begin{Bmatrix} i_{1g} \\ j_{1g} \\ k_{1g} \end{Bmatrix} \approx \begin{bmatrix} 1 & \theta_z & -\theta_y \\ \theta_x\theta_y-\theta_z & 1 & \theta_x \\ \theta_y+\theta_x\theta_z & \theta_y\theta_z-\theta_x & 1 \end{bmatrix} \begin{Bmatrix} i_g \\ j_g \\ k_g \end{Bmatrix}$$

3. "$x_{1g}y_{1g}z_{1g}$" system $\Leftrightarrow$ "$x_{2g}y_{2g}z_{2g}$" system

Rotating $\psi=\Omega t$ about z_{1g} axis

$$\begin{Bmatrix} i_{2g} \\ j_{2g} \\ k_{2g} \end{Bmatrix} = \begin{bmatrix} \cos\psi & \sin\psi & 0 \\ -\sin\psi & \cos\psi & 0 \\ 0 & 0 & 1 \end{bmatrix} \begin{Bmatrix} i_{1g} \\ j_{1g} \\ k_{1g} \end{Bmatrix}$$

4. "$x_{2g}y_{2g}z_{2g}$" system $\Leftrightarrow$ "$x_hy_hz_h$" system

The gimball degrees of freedom α_G about $\vec{i}_{2g}$ and β_G about $\vec{j}_{2g}$

$$\begin{Bmatrix} i_h \\ j_h \\ k_h \end{Bmatrix} \approx \begin{bmatrix} 1 & 0 & -\beta_G \\ 0 & 1 & \alpha_G \\ \beta_G & -\alpha_G & 1 \end{bmatrix} \begin{Bmatrix} i_{2g} \\ j_{2g} \\ k_{2g} \end{Bmatrix}$$

5."$x_{2g}y_{2g}z_{2g}$" system $\Leftrightarrow$ "$x_by_bz_b$" system

The blade pitch angle θ is defined with respect to the hub plane, so the blade outboard of the pitch bearing doesn't undergo the α_G rotation about $\vec{i}_{2g}$ due to the gimball motion. Therfore remove rotation α_G about $\vec{i}_{2g}$ from "H" system and include the blade precone angle β_p and

sweep angle β_{sw} to obtain "$x_b y_b z_b$" system.

$$\begin{Bmatrix} i_b \\ j_b \\ k_b \end{Bmatrix} \approx \begin{bmatrix} 1 & -\beta_{sw} & \beta_p-\beta_G \\ \beta_{sw} & 1 & \beta_{sw}(\beta_p-\beta_G) \\ \beta_G-\beta_p & 0 & 1 \end{bmatrix} \begin{Bmatrix} i_{2g} \\ j_{2g} \\ k_{2g} \end{Bmatrix}$$

6. "$x_b y_b z_b$" system $\Leftrightarrow$ "$x_{cs} y_{cs} z_{cs}$" system

Including blade pitch degree of freedom ϕ about i_b

$$\begin{Bmatrix} i_{cs} \\ j_{cs} \\ k_{cs} \end{Bmatrix} \approx \begin{bmatrix} 1 & 0 & 0 \\ 0 & 1 & \phi \\ 0 & -\phi & 1 \end{bmatrix} \begin{Bmatrix} i_b \\ j_b \\ k_b \end{Bmatrix}$$

7. "$x_{cs} y_{cs} z_{cs}$" system $\Leftrightarrow$ "$x_{pA} y_{pA} z_{pA}$" system

Including geometry torsion angle θ_G rotation about $\vec{i}_{cs}$

$$\begin{Bmatrix} i_{pA} \\ j_{pA} \\ k_{pA} \end{Bmatrix} = \begin{bmatrix} 1 & 0 & 0 \\ 0 & \cos\theta_G & \sin\theta_G \\ 0 & -\sin\theta_G & \cos\theta_G \end{bmatrix} \begin{Bmatrix} i_{cs} \\ j_{cs} \\ k_{cs} \end{Bmatrix}$$

θ_G is blade geometry torsion angle

$$\theta_G = \theta_{\text{collective pitch}} + \theta_{\text{pretwist}} + \theta_{1c}\cos\psi + \theta_{1s}\sin\psi - K_{pG}\beta_G$$

* *The transformation matrices in this appendix are for the universal joint rotor configuration. The difference between the ideal gimbal rotor configuration and the universal joint configuration is introduced in section 4.4.4.*

APPENDIX 3B

RESULTANT LOADS

RESULTANT AERODYNAMIC LOADS

It should be pointed out that c_l, c_d, c_{mac} in F_y and F_z etc. have a trim value c_{l0}, c_{d0}, c_{mac0} and a perturbation Δc_l, Δc_d, Δc_{mac} about the trim value due to the system perturbation motions, and hence

$$c_l = c_{l0} + \Delta c_l \qquad \text{etc.}$$

Assuming c_d, c_{mac} is constant without perturbation effect to simplify the analysis.

$$c_{l0} = a\left[\theta_{trim} - \tan^{-1}\left(\frac{U_p}{U_T}\right)_{trim}\right]$$

$$= a\left[\theta_G - \tan^{-1}\left(\frac{(v_F+v_i)R}{e_p+x}\right)\right]$$

$$\Delta c_l = \frac{\partial c_l}{\partial \alpha}\Delta\alpha = a\cdot\Delta\alpha$$

Where, $\Delta\alpha = \Delta\theta - \dfrac{U_{T\,trim}\Delta U_p - U_{p\,trim}\Delta U_T}{U_{trim}^2}$

$$= \phi - \frac{e_p+x}{\Omega[(e_p+x)^2+(v_F+v_i)^2R^2]}\Delta U_p + \frac{(v_F+v_i)}{\Omega[(e_p+x)^2+(v_F+v_i)^2R^2]}\Delta U_T$$

$$= \phi - \alpha_{Up}\Delta U_p + \alpha_{UT}\Delta U_T$$

The expressions of ΔU_p and ΔU_T are

$$\Delta U_p = \Omega\{\dot{z}_g - x\dot{\beta}_G - \sin\psi[-\beta_G\dot{y}_g + \beta_p\dot{y}_g + x\beta_{sw}\dot{\theta}_y - (e_p+x)\dot{\theta}_x]$$
$$-\cos\psi[-\beta_G\dot{x}_g + \beta_p\dot{x}_g + x\beta_{sw}\dot{\theta}_x + (e_p+x)\dot{\theta}_y]\}$$
$$= M_1\dot{z}_g + M_2\dot{\beta}_G + M_3\beta_G\dot{y}_g\sin\psi + M_4\dot{y}_g\sin\psi + M_5\theta_y\sin\psi + M_6\dot{\theta}_x\sin\psi$$
$$+M_7\beta_G\dot{x}_g\cos\psi + M_8\dot{x}_g\cos\psi + M_9\dot{\theta}_x\cos\psi + M_{10}\dot{\theta}_y\cos\psi$$

$$\Delta U_T = \Omega\{-(v_F+v_i)R\beta_{sw}\beta_G + x\dot{\theta}_z - \sin\psi[-(v_F+v_i)R(\theta_y+\beta_{sw}\theta_x) + \dot{x}_g - \beta_{sw}\dot{y}_g]$$
$$-\cos\psi[-(v_F+v_i)R(\theta_x-\beta_{sw}\theta_y) - \beta_{sw}\dot{x}_g - \dot{y}_g]\}$$
$$= N1\beta_G + N_2\dot{\theta}_z + N_3\theta_y\sin\psi + N_4\theta_x\sin\psi + N_5\dot{x}_g\sin\psi + N_6\dot{y}_g\sin\psi$$

$$+N_7\theta_x\cos\psi+N_8\theta_y\cos\psi+N_9x_g\cos\psi+N_{10}y_g\cos\psi$$

After neglecting higher order terms,

$$F_{AR}^x=\int_0^{R-e_p}\{\beta_{sw}[-\rho bc_{l0}\sin\theta_G\Omega^2(v_F+v_i)^2R^2-\rho ab(\phi-\alpha_{Up}\Delta U_p+\alpha_{UT}\Delta U_T)$$

$$\sin\theta_G\Omega^2(v_F+v_i)^2R^2-\rho bc_{l0}\cos\theta_G\Omega^2x(v_F+v_i)R$$

$$-\rho ab(\phi-\alpha_{Up}\Delta U_p+\alpha_{UT}\Delta U_T)\cos\theta_G\Omega^2x(v_F+v_i)R]+(\beta_G-\beta_p)$$

$$[\rho bc_{l0}\cos\theta_G\Omega^2x^2+\rho ab(\phi-\alpha_{Up}\Delta U_p+\alpha_{UT}\Delta U_T)\cos\theta_G\Omega^2x^2$$

$$+\rho bc_{l0}\sin\theta_G\Omega^2(v_F+v_i)Rx+\rho ab(\phi-\alpha_{Up}\Delta U_p+\alpha_{UT}\Delta U_T)$$

$$\sin\theta_G\Omega^2(v_F+v_i)Rx]\}d_x$$

$$=A_1+A_2\phi+A_3\Delta U_p+A_4\Delta U_T+A_8\beta_G+A_5\phi\beta_G+A_6\beta_G\Delta U_p+A_7\beta_G\Delta U_T$$

$$F_{AR}^y=\int_0^{R-e_p}-\rho bc_d\Omega^2x^2\cos\theta_G-\rho bc_{l0}\cos\theta_G\Omega^2\{(v_F+v_i)^2R^2\phi$$

$$-\rho bc_{l0}\sin\theta_G\Omega^2\{(v_F+v_i)^2R^2+2(v_F+v_i)R\dot{z}_g$$

$$-2(v_F+v_i)Rx\dot{\beta}_G+\sin\psi<2(v_F+v_i)Rx\dot{\theta}_x>+\cos\psi<-2(v_F+v_i)Rx\dot{\theta}_y>\}$$

$$-\rho ab\sin\theta_G\Omega^2(\phi-\alpha_{Up}\Delta U_p+\alpha_{UT}\Delta U_T)\{(v_F+v_i)^2R^2+2(v_F+v_i)R\dot{z}_g$$

$$-2(v_F+v_i)Rx\dot{\beta}_G+\sin\psi<2(v_F+v_i)Rx\dot{\theta}_x>+\cos\psi<-2(v_F+v_i)Rx\dot{\theta}_y>\}$$

$$-\rho ab\cos\theta_G\Omega^2\phi(\phi-\alpha_{Up}\Delta U_p+\alpha_{UT}\Delta U_T)(v_F+v_i)^2R^2$$

$$-\rho bc_{l0}\cos\theta_G\Omega^2\{(e_p+x)(v_F+v_i)R+x(v_F+v_i)R\dot{\theta}_z+x\dot{z}_g-x^2\dot{\beta}_G$$

$$+\sin\psi[-(v_F+v_i)R\theta_y+\dot{x}_g][-(v_F+v_i)R]+\cos\psi[-(v_F+v_i)R\theta_x-\dot{y}_g][-(v_F+v_i)R]$$

$$+\sin\psi[x(e_p+x)\dot{\theta}_x]+\cos\psi[-x(e_p+x)\dot{\theta}_y]\}+\rho bc_{l0}\sin\theta_G\Omega^2x(v_F+v_i)R\phi$$

$$-\rho ab\cos\theta_G\Omega^2(\phi-\alpha_{Up}\Delta U_p+\alpha_{UT}\Delta U_T)\{(e_p+x)(v_F+v_i)R$$

$$+x(v_F+v_i)R\dot{\theta}_z+x\dot{z}_g-x^2\dot{\beta}_G+\sin\psi[-(v_F+v_i)R\theta_y+\dot{x}_g][-(v_F+v_i)R]$$

$$+\cos\psi[-(v_F+v_i)R\theta_x-\dot{y}_g][-(v_F+v_i)R]+\sin\psi[x^2\dot{\theta}_x]+\cos\psi[-x^2\dot{\theta}_y]\}$$

$$+\rho ab\sin\theta_G\Omega^2(\phi-\alpha_{Up}\Delta U_p+\alpha_{UT}\Delta U_T)\phi x(v_F+v_i)R+\rho ab\sin\theta_G\times$$

$$\{\frac{b}{2}[\Omega^2\dot{\theta}\cos\theta_G x+\Omega^2\dot{\theta}\sin\theta_G(v_F+v_i)R+\Omega^2\sin\theta_G x\ddot{\theta}_z-\Omega^2\cos\theta_G$$

$$(\ddot{z}_g-x\ddot{\beta}_G)]$$

$$+\sin\psi<\frac{b}{2}\{-\Omega^2\sin\theta_G[-(v_F+v_i)R(\dot{\theta}_y-\theta_x)+\ddot{x}_g+\dot{y}_g]+\Omega^2\cos\theta_G x$$

$$(-\ddot{\theta}_x-\dot{\theta}_y)\}>+\cos\psi<\frac{b}{2}\{-\Omega^2\sin\theta_G[-(v_F+v_i)R(\theta_y+\dot{\theta}_x)+\dot{x}_g-\ddot{y}_g]$$

$$+\Omega^2\cos\theta_G x(\ddot{\theta}_y-\dot{\theta}_x)\}>\}\,d_x$$

$$=\int_0^{R-e_p}(B0+B1\dot{z}_g+B2\dot{\beta}_G+B3\dot{\theta}_x\sin\psi+B4\dot{\theta}_y\cos\psi+(\phi-\alpha_{Up}\Delta U_p+\alpha_{UT}\Delta U_T)$$

$$(O1+O2\dot{z}_g+O3\dot{\beta}_G+O4\dot{\theta}_x\sin\psi+O5\dot{\theta}_y\cos\psi+O6\dot{\theta}_z+O7\theta_y\sin\psi$$

$$+O8\dot{x}_g\sin\psi+O9\theta_x\cos\psi+O10\dot{y}_g\cos\psi)+B6\phi^2+B7\phi\Delta U_p$$

$$+B8\phi\Delta U_T+B9\dot{\theta}_z+B10\theta_y\sin\psi+B11\dot{x}_g\sin\psi+B12\theta_x\cos\psi+B13\dot{y}_g\cos\psi$$

$$+B14\phi+B15\ddot{z}_g+B16\beta_G+B17\dot{\theta}+B18\ddot{\theta}_z+B19\dot{\theta}_y\sin\psi+B20\theta_x\sin\psi$$

$$+B21\ddot{x}_g\sin\psi+B22\dot{y}_g\sin\psi+B23\ddot{\theta}_x\sin\psi+B24\theta_y\cos\psi+B25\theta_x\cos\psi$$

$$+B26\dot{x}_g\cos\psi+B27\ddot{y}_g\cos+B28\ddot{\theta}_y\cos\psi)d_x$$

$$F_{AR}^z=\int_0^{R-e_p}\rho bc_{l0}\cos\theta_G\Omega^2\{x^2+2e_px+2x^2\dot{\theta}_z+\sin\psi<-2(e_p+x)$$

$$[-(v_F+v_i)R\theta_y+\dot{x}_g]>+\cos\psi<-2(e_p+x)[-(v_F+v_i)R\theta_x-\dot{y}_g]>\}$$

$$+\rho abc\cos\theta_G\Omega^2(\phi-\alpha_{Up}\Delta U_p+\alpha_{UT}\Delta U_T)\{x^2+2e_px+2x^2\dot{\theta}_z+\sin\psi$$

$$<-2(e_p+x)[-(v_F+v_i)R\theta_y+\dot{x}_g]>+\cos\psi<-2(e_p+x)$$

$$[-(v_F+v_i)R\theta_x-\dot{y}_g]>\}-\rho bc_{l0}\sin\theta_G\Omega^2x^2\phi-\rho ab\sin\theta_G\Omega^2\phi$$

$$(\phi-\alpha_{Up}\Delta U_p+\alpha_{UT}\Delta U_T)x^2-\rho bc_d\sin\theta_G\Omega^2\{(v_F+v_i)^2R^2$$

$$+\rho bc_{l0}\sin\theta_G\Omega^2\{(e_p+x)(v_F+v_i)R+x(v_F+v_i)R\dot{\theta}_z+(e_p+x)\dot{z}_g-x(e_p+x)\dot{\beta}_G$$

$$+\sin\psi[-(v_F+v_i)R\theta_y+\dot{x}_g][-(v_F+v_i)R]+\cos\psi[-(v_F+v_i)R\theta_x-\dot{y}_g][-(v_F+v_i)R]$$

$$+\sin\psi[x(e_p+x)\dot{\theta}_x]+\cos\psi[-x(e_p+x)\dot{\theta}_y]\}+\rho ab\sin\theta_G\Omega^2\times$$

$$(\phi-\alpha_{Up}\Delta U_p+\alpha_{UT}\Delta U_T)\{(e_p+x)(v_F+v_i)R+x(v_F+v_i)R\dot{\theta}_z+(e_p+x)\dot{z}_g-x(e_p+x)\dot{\beta}_G$$

$$+\sin\psi[-(v_F+v_i)R\theta_y+\dot{x}_g][-(v_F+v_i)R]+\cos\psi[-(v_F+v_i)R\theta_x-\dot{y}_g][-(v_F+v_i)R]$$

$$+\sin\psi[x(e_p+x)\dot{\theta}_x]+\cos\psi[-x(e_p+x)\dot{\theta}_y]\}+\rho bc_{l0}\cos\theta_G\Omega^2$$

$$x(v_F+v_i)R\phi+\rho abc\cos\theta_G\Omega^2\phi(\phi-\alpha_{Up}\Delta U_p+\alpha_{UT}\Delta U_T)x(v_F+v_i)R$$

$$-\rho bc_d\cos\theta_G\Omega^2x(v_F+v_i)R+\rho abc\cos\theta_G$$

$$\left\{\frac{b}{2}[\Omega^2\dot{\theta}\cos\theta_Gx+\Omega^2\dot{\theta}\sin\theta_G(v_F+v_i)R+\Omega^2\sin\theta_Gx\ddot{\theta}_z-\Omega^2\cos\theta_G\right.$$

$$(\ddot{z}_g-x\ddot{\beta}_G)]$$

$$+\sin\psi<\frac{b}{2}\{-\Omega^2\sin\theta_G[-(v_F+v_i)R(\dot{\theta}_y-\theta_x)+\ddot{x}_g+\dot{y}_g]+\Omega^2\cos\theta_Gx$$

$$(-\ddot{\theta}_x-\dot{\theta}_y)\}>+\cos\psi<\frac{b}{2}\{-\Omega^2\sin\theta_G[-(v_F+v_i)R(\theta_y+\dot{\theta}_x)+\dot{x}_g-\ddot{y}_g]$$

$$+\Omega^2\cos\theta_Gx(\ddot{\theta}_y-\dot{\theta}_x)\}>\}d_x$$

$$=\int_0^{R-e_p}(C0+C1\dot{\theta}_z+C2\theta_y\sin\psi+C3\dot{x}_g\sin\psi+C4\theta_x\cos\psi+C5\dot{y}_g\cos\psi$$

$$+(\phi-\alpha_{Up}\Delta U_p+\alpha_{UT}\Delta U_T)(P1+P2\dot{\theta}_z+P3\theta_y\sin\psi+P4\dot{x}_g\sin\psi+P5\theta_x\cos\psi$$

$$+P6\dot{y}_g\cos\psi+P7\dot{z}_g+P8\dot{\beta}_G+P9\dot{\theta}_x\sin\psi+P10\dot{\theta}_y\cos\psi)+C7\phi+C8\phi^2$$

$$+C9\Delta U_p+C10\Delta U_T+C11\dot{z}_g+C12\dot{\beta}_G+C13\dot{\theta}_x\sin\psi+C14\dot{\theta}_y\cos\psi$$

$$+C15\dot{\theta}+C16\ddot{\theta}_z+C17\ddot{z}_g+C18\beta_G+C19\dot{\theta}_y\sin\psi+C20\theta_x\sin\psi+C21\ddot{x}_g\sin\psi$$

$$+C22\dot{y}_g\sin\psi+C23\ddot{\theta}_x\sin\psi+C24\theta_y\cos\psi+C25\dot{\theta}_x\cos\psi+C26\dot{x}_g\cos\psi$$

$$+C27\ddot{y}_g\cos\psi+C28\ddot{\theta}_y\cos\psi)d_x$$

$$M_{AR}^x=\int_0^{R-e_p}\{-x\beta_{sw}F_{AR}^z-[-z_h+x(\beta_p-\beta_G)]F_{AR}^y$$

$$+z_h\alpha_G[\rho bc_{l0}\cos\theta_G\Omega^2x^2+\rho abc\cos\theta_G\Omega^2$$

$$(\phi-\alpha_{Up}\Delta U_p+\alpha_{UT}\Delta U_T)x^2+\rho bc_{l0}\sin\theta_G\Omega^2x(v_F+v_i)R+\rho absin\theta_G\Omega^2$$

$$(\phi-\alpha_{Up}\Delta U_p+\alpha_{UT}\Delta U_T)x(v_F+v_i)R]$$

$$+e_p(\beta_G-\beta_p)[-\rho bc_{l0}\sin\theta_G\Omega^2\{(v_F+v_i)^2R^2-\rho absin\theta_G\Omega^2(\phi-\alpha_{Up}\Delta U_p+\alpha_{UT}\Delta U_T)$$

$$(v_F+v_i)^2R^2-\rho bc_{l0}\cos\theta_G\Omega^2\{(e_p+x)(v_F+v_i)R$$

$$-\rho abc\cos\theta_G\Omega^2(\phi-\alpha_{Up}\Delta U_p+\alpha_{UT}\Delta U_T)\{(e_p+x)(v_F+v_i)R]$$

$$+(2\rho b^2c_{mac}+\rho bc_{l0}x_A)\Omega^2[x^2+(v_F+v_i)^2R^2]+\rho ab\left\{\frac{b}{2}\left(x_A-\frac{b}{2}\right)\right.$$

$$[\Omega^2\dot{\theta}\cos\theta_Gx+\Omega^2\dot{\theta}\sin\theta_G(v_F+v_i)R+\Omega^2\sin\theta_Gx\ddot{\theta}_z-\Omega^2\cos\theta_G$$

$$(\ddot{z}_g - x\ddot{\beta}_G)] + \left(-\frac{b^2}{4}\right)(\dot{\theta} - \beta_G + \beta_p)\Omega^2[\cos\theta_G x + \sin\theta_G(v_F + v_i)R]$$

$$+\sin\psi < \frac{b}{2}\left(x_A - \frac{b}{2}\right)\{-\Omega^2\sin\theta_G[-(v_F + v_i)R(\dot{\theta}_y - \theta_x) + \ddot{x}_g + \dot{y}_g] + \Omega^2\cos\theta_G x$$

$$(-\ddot{\theta}_x - \dot{\theta}_y)\} > + \cos\psi < \frac{b}{2}\left(x_A - \frac{b}{2}\right)\{-\Omega^2\sin\theta_G[-(v_F + v_i)R(\theta_y + \dot{\theta}_x) + \dot{x}_g - \ddot{y}_g]$$

$$+\Omega^2\cos\theta_G x(\ddot{\theta}_y - \dot{\theta}_x)\} > \Big\} dx$$

$$= \int_0^{R-e_p} \{-x\beta_{sw}F_{AR}^z - [-z_h + x\beta_p - x\beta_G]F_{AR}^y$$

$$+D0 + D1\alpha_G + D2\phi\alpha_G + D3\alpha_G\Delta U_p + D4\alpha_G\Delta U_T$$

$$+D5\phi + D6\Delta U_p + D7\Delta U_T + \beta_G(D9 + D10\phi + D11\Delta U_p + D12\Delta U_T)$$

$$+D8\dot{\theta} + D17\ddot{\theta}_z + D18\ddot{z}_g + D19\ddot{\beta}_G + D20\beta_G + D21\dot{\theta}_y\sin\psi + D22\theta_x\sin\psi$$

$$+D23\ddot{x}_g\sin\psi + D24\dot{y}_g\sin\psi + D25\ddot{\theta}_x\sin\psi + D26\theta_y\cos\psi + D27\dot{\theta}_x\cos\psi$$

$$+D28\dot{x}_g\cos\psi + D29\ddot{y}_g\cos\psi + D30\ddot{\theta}_y\cos\psi\}d_x$$

$$M_{AR}^y = -\int_0^{R-e_p}(e_p + x)F_z d_x$$

$$= -\int_0^{R-e_p}(e_p + x)(C0 + C1\dot{\theta}_z + C2\theta_y\sin\psi + C3\dot{x}_g\sin\psi + C4\theta_x\cos\psi + C5\dot{y}_g\cos\psi$$

$$+(\phi - \alpha_{Up}\Delta U_p + \alpha_{UT}\Delta U_T)(P1 + P2\dot{\theta}_z + P3\theta_y\sin\psi + P4\dot{x}_g\sin\psi + P5\theta_x\cos\psi$$

$$+P6\dot{y}_g\cos\psi + P7\dot{z}_g + P8\dot{\beta}_G + P9\dot{\theta}_x\sin\psi + P10\dot{\theta}_y\cos\psi) + C7\phi + C8\phi^2$$

$$+C9\Delta U_p + C10\Delta U_T + C11\dot{z}_g + C12\dot{\beta}_G + C13\dot{\theta}_x\sin\psi + C14\dot{\theta}_y\cos\psi$$

$$+C15\dot{\theta} + C16\ddot{\theta}_z + C17\ddot{z}_g + C18\beta_G + C19\dot{\theta}_y\sin\psi + C20\theta_x\sin\psi + C21\ddot{x}_g\sin\psi$$

$$+C22\dot{y}_g\sin\psi + C23\ddot{\theta}_x\sin\psi + C24\theta_y\cos\psi + C25\dot{\theta}_x\cos\psi + C26\dot{x}_g\cos\psi$$

$$+C27\ddot{y}_g\cos\psi + C28\ddot{\theta}_y\cos\psi)d_x$$

$$M_{AR}^z = \int_0^{R-e_p}(e_p + x)F_y d_x$$

$$= \int_0^{R-e_p}(e_p + x)(B0 + B1\dot{z}_g + B2\dot{\beta}_G + B3\dot{\theta}_x\sin\psi + B4\dot{\theta}_y\cos\psi + (\phi - \alpha_{Up}\Delta U_p + \alpha_{UT}\Delta U_T)$$

$$(O1 + O2\dot{z}_g + O3\dot{\beta}_G + O4\dot{\theta}_x\sin\psi + O5\dot{\theta}_y\cos\psi + O6\dot{\theta}_z + O7\theta_y\sin\psi$$

$$+O8\dot{x}_g\sin\psi + O9\theta_x\cos\psi + O10\dot{y}_g\cos\psi) + B6\phi^2 + B7\phi\Delta U_p$$

$$+B8\phi\Delta U_T+B9\dot{\theta}_z+B10\theta_y\sin\psi+B11\dot{x}_g\sin\psi+B12\theta_x\cos\psi+B13\dot{y}_g\cos\psi$$

$$+B14\phi+B15\ddot{z}_g+B16\beta_G+B17\dot{\theta}+B18\ddot{\theta}_z+B19\dot{\theta}_y\sin\psi+B20\theta_x\sin\psi$$
$$+B21\ddot{x}_g\sin\psi+B22\dot{y}_g\sin\psi+B23\ddot{\theta}_x\sin\psi+B24\theta_y\cos\psi+B25\theta_x\cos$$
$$+B26\dot{x}_g\cos\psi+B27\ddot{y}_g\cos\psi+B28\ddot{\theta}_y\cos\psi)d_x$$

Noting where,

$$(\phi-\alpha_{Up}\Delta U_p+\alpha_{UT}\Delta U_T)(O1+O2\dot{z}_g+O3\dot{\beta}_G+O4\dot{\theta}_x\sin\psi+O5\dot{\theta}_y\cos\psi$$
$$+O6\dot{\theta}_z+O7\theta_y\sin\psi+O8\dot{x}_g\sin\psi+O9\theta_x\cos\psi+O10\dot{y}_g\cos\psi)$$
$$=\phi(O1+O2\dot{z}_g+O3\dot{\beta}_G+O4\dot{\theta}_x\sin\psi+O5\dot{\theta}_y\cos\psi+O6\dot{\theta}_z+O7\theta_y\sin\psi$$
$$+O8\dot{x}_g\sin\psi+O9\theta_x\cos\psi+O10\dot{y}_g\cos\psi)+Q1\dot{z}_g+Q2\dot{\beta}_G+Q3\beta_G\dot{y}_g\sin\psi$$
$$+Q4\dot{y}_g\sin\psi+Q5\dot{\theta}_y\sin\psi+Q6\dot{\theta}_x\sin\psi+Q7\beta_G\dot{x}_g\cos\psi+Q8\dot{x}_g\cos\psi$$
$$+Q9\dot{\theta}_x\cos\psi+Q10\dot{\theta}_y\cos\psi+Q11\beta_G+Q12\dot{\theta}_z+Q13\theta_y\sin\psi+Q14\theta_x\sin\psi$$
$$+Q15\dot{x}_g\sin\psi+Q16\theta_x\cos\psi+Q17\theta_y\cos\psi+Q18\dot{y}_g\cos\psi$$

And

$$(\phi-\alpha_{Up}\Delta U_p+\alpha_{UT}\Delta U_T)(P1+P2\dot{\theta}_z+P3\theta_y\sin\psi+P4\dot{x}_g\sin\psi+P5\theta_x\cos\psi$$
$$+P6\dot{y}_g\cos\psi+P7\dot{z}_g+P8\dot{\beta}_G+P9\dot{\theta}_x\sin\psi+P10\dot{\theta}_y\cos\psi)$$
$$=\phi(P1+P2\dot{\theta}_z+P3\theta_y\sin\psi+P4\dot{x}_g\sin\psi+P5\theta_x\cos\psi+P6\dot{y}_g\cos\psi+P7\dot{z}_g$$
$$+P8\dot{\beta}_G+P9\dot{\theta}_x\sin\psi+P10\dot{\theta}_y\cos\psi)+Qp1\dot{z}_g+Qp2\dot{\beta}_G+Qp3\beta_G\dot{y}_g\sin\psi$$
$$+Qp4\dot{y}_g\sin\psi+Qp5\dot{\theta}_y\sin\psi+Qp6\dot{\theta}_x\sin\psi+Qp7\beta_G\dot{x}_g\cos\psi+Qp8\dot{x}_g\cos\psi$$
$$+Qp9\dot{\theta}_x\cos\psi+Qp10\dot{\theta}_y\cos\psi+Qp11\beta_G+Qp12\dot{\theta}_z+Qp13\theta_y\sin\psi+Qp14\theta_x\sin\psi$$
$$+Qp15\dot{x}_g\sin\psi+Qp16\theta_x\cos\psi+Qp17\theta_y\cos\psi+Qp18\dot{y}_g\cos\psi$$

RESULTANT INERTIAL LOADS

$$F_{IR}^{x}=-\Omega^2\left\{\int_0^{R-e_p} m[\ddot{x}_g\cos\psi+\ddot{y}_g\sin\psi-(e_p+x)-2x\dot{\theta}_z]d_x\right\}$$

$$=\int_0^{R-e_p}(h1+h2\ddot{x}_g\cos\psi+h3\ddot{y}_g\sin\psi+h4\dot{\theta}_z)d_x$$

$$F_{IR}^{y}=-\Omega^2\left\{\int_0^{R-e_p} m[x\beta_{sw}+\ddot{\theta}_z x-\sin\psi\ddot{x}_g+\cos\psi\ddot{y}_g]d_x\right\}$$

$$=\int_0^{R-e_p}(i1+i2\ddot{\theta}_z+i3\sin\psi\ddot{x}_g+i4\cos\psi\ddot{y}_g)d_x$$

$$F_{IR}^{z}=-\Omega^2\left\{\int_0^{R-e_p} m[\ddot{z}_g-e_p\ddot{\beta}_G-x\ddot{\beta}_G+\sin\psi x(\ddot{\theta}_x+2\dot{\theta}_y)\right.$$

$$+\cos\psi\,[-x(\ddot{\theta}_y-2\dot{\theta}_x)]d_x$$

$$=\int_0^{R-e_p}(j1\ddot{z}_g+j2\ddot{\beta}_G+j3\dot{\theta}_y\sin\psi+j4\ddot{\theta}_x\sin\psi+j5\dot{\theta}_x\cos\psi+j6\ddot{\theta}_y\cos\psi)d_x$$

$$M_{IR}^{x}=\Omega^2\left\{\int_0^{R-e_p} m[x\beta_{sw}\ddot{z}_g-x^2\beta_{sw}\ddot{\beta}_G+x^2\beta_{sw}\dot{\theta}_y\sin\psi\right.$$

$$+x^2\beta_{sw}(\ddot{\theta}_x+\dot{\theta}_y)\sin\psi+x^2\beta_{sw}\dot{\theta}_x\cos\psi-x^2\beta_{sw}(\ddot{\theta}_y-\dot{\theta}_x)\cos\psi$$

$$\left.+[-z_h+x(\beta_p-\beta_G)][x\beta_{sw}+\ddot{\theta}_z x-\sin\psi\ddot{x}_g+\cos\psi\ddot{y}_g]\}-(I_3-I_2)\sin\theta_G\cos\theta_G\right\}d_x$$

$$=\int_0^{R-e_p}(E0+E1\ddot{z}_g+E2\ddot{\beta}_G+E3\dot{\theta}_y\sin\psi+E4\ddot{\theta}_x\sin\psi+E5\dot{\theta}_y\sin\psi$$

$$+E6\dot{\theta}_x\cos\psi+E7\ddot{\theta}_y\cos\psi+E8\dot{\theta}_x\cos\psi+E9\ddot{\theta}_z+E10\sin\psi\ddot{x}_g$$

$$+E11\cos\psi\ddot{y}_g+E12\beta_G+E13\beta_G\ddot{\theta}_z+E14\beta_G\sin\psi\ddot{x}_g+E15\beta_G\cos\psi\ddot{y}_g)d_x$$

$$M_{IR}^{y}=\Omega^2\int_0^{R-e_p} m\{[-z_h+x(\beta_p-\beta_G)]x+(e_p+x)\ddot{z}_g-x(e_p+x)\ddot{\beta}_G$$

$$+\sin\psi x(e_p+x)(\ddot{\theta}_x+2\dot{\theta}_y)+\cos\psi\,[-x(e_p+x)(\ddot{\theta}_y-2\dot{\theta}_x)]\}d_x$$

$$=\int_0^{R-e_p}(F0+F1\beta_G+F2\ddot{z}_g+F3\ddot{\beta}_G+F4\dot{\theta}_y\sin\psi+F5\ddot{\theta}_x\sin\psi+F6\dot{\theta}_x\cos\psi$$

$$+F7\ddot{\theta}_y\cos\psi)d_x$$

$$M_{IR}^z=\Omega^2\int_0^{R-e_p}m\{-x(e_p+x)\beta_{sw}-x(e_p+x)\ddot{\theta}_z+(e_p+x)\sin\psi\ddot{x}_g$$

$$-(e_p+x)\cos\psi\ddot{y}_g+x^2\beta_{sw}\}d_x$$

$$=\int_0^{R-e_p}(G0+G1\ddot{\theta}_z+G2\ddot{x}_g\sin\psi+G3\ddot{y}_g\cos\psi)d_x$$

APPENDIX 3C

RESULTANT LOADS TRANSMITTED TO NACELLE FROM THE WHOLE ROTOR

$$P_R^x=\sum_{k=1}^{4}(F_R^x\cos\psi_k-F_R^y\sin\psi_k)$$

$$=\sum_{k=1}^{4}[(F_{IR}^x+F_{AR}^x)\cos\psi_k-(F_{IR}^y+F_{AR}^y)\sin\psi_k]$$

$$=\int_0^{R-e_p}[\ddot{x}_g(2h2-2i3-2B21)+\ddot{\theta}_x(-2B23)+\dot{x}_g(2A3\times M8+2A4\times N9-2B8\times N5\phi_0$$

$$-2B11-2O8\phi_0-2Q15)+\dot{\theta}_x(2A3\times M9-2B3-2B7\times M6\phi_0-2O4\times\phi_0-2Q6)$$

$$+\dot{\theta}_y(2A3\times M10-2B7\times M5\phi_0-2B19-2Q5)+\dot{y}_g(2A4\times N10-2B7\times M4\phi_0$$

$$-2B8\times N6\phi_0-2B22-2Q4)+\dot{\phi}_{1s}(-2B17)+\phi_{1c}(2A2+2B17)+\beta_{Gs}(2A8+2A5\phi_0$$

$$+2B17K_{\beta G}+2A3\times M2+2A4\times N1+2B2+2B7\times M2\phi_0+2O3\phi_0+2Q2)$$

$$+\beta_{Gc}(-2A3\times M2+2B16+2(B14+B6\phi_0)K_{\beta G}+2B8\times N1\phi_0+2Q11)$$

$$+\theta_x(2A4\times N7-2B8\times N4\phi_0-2B20-2Q14)+\theta_y(2A4\times N8-2B8\times N3\phi_0$$

$$-2B10-2O7\phi_0-2Q13)+\phi_{1s}(-2B14-2B6\phi_0)+\dot{\beta}_{Gs}(2A3\times M2)$$

$$+\dot{\beta}_{Gc}(2B2+2B17K_{\beta G}+2B7\times M2\phi_0+2O3\phi_0+2Q2)]d_x$$

$$P_R^y=\sum_{k=1}^{4}(F_R^x\sin\psi_k+F_R^y\cos\psi_k)$$

$$=\sum_{k=1}^{4}[(F_{IR}^x+F_{AR}^x)\sin\psi_k+(F_{IR}^y+F_{AR}^y)\cos\psi_k]$$

$$=\int_0^{R-e_p}[\ddot{y}_g(2h3+2i4+2B27)+\ddot{\theta}_y(2B28)+\dot{y}_g(2A3\times M4+2A4\times N6+2B8\times N10\phi_0$$

$$+2B13+2O10\phi_0+2Q18)+\dot{x}_g(2A4\times N5+2B7\times M8\phi_0+2B8\times N9\phi_0+2B26+2Q8)$$

$$+\dot{\theta}_y(2A3\times M5+2B4+2B7\times M10\phi_0+2O5\phi_0+2Q10)+\dot{\theta}_x(2A3\times M6+2B7\times M9\phi_0$$

$$+2B25+2Q9)+\dot{\phi}_{1c}(2B17)+\phi_{1s}(2A2+2B17)+\phi_{1c}(2B6\phi_0+2O1+2B14)$$
$$+\beta_{Gc}(-2A8-2A5\phi_0-2A4\times N1-2B7\times M2\phi_0-2B2-2O3\phi_0-2Q2)+\beta_{Gs}(-2A3\times M2$$
$$+2B16+2B8\times N1\phi_0+2Q11)+\theta_y(2A4\times N3+2B8\times N8\phi_0+2B24+2Q17)+\theta_x(2A4\times N4$$
$$+2B8\times N7\phi_0+2B12+2O9\phi_0+2Q16)+\dot{\beta}_{Gs}(2B2-B17K_{\beta G}+2B7\times M2\phi_0+2O3\phi_0$$
$$+2Q2)+\dot{\beta}_{Gc}(-2A3\times M2)]d_x$$

$$P_R^z=\sum_{k=1}^{4}F_R^z$$

$$=\sum_{k=1}^{4}(F_{IR}^z+F_{AR}^z)$$

$$=\int_0^{R-e_p}[\ddot{z}_g(4j2+4C17)+\ddot{\theta}_z(4C16)+\dot{\theta}_z(4C1+4C10\times N2+4P2\phi_0+4Qp12)$$
$$+\dot{z}_g(4C9\times M1+4C11+4P7\phi_0+4Qp1)+\dot{\phi}_c(4C15)+\phi_c(4C7+4C8\phi_0+4P1)$$
$$+4C0]d_x$$

$$Q_R^x=\sum_{k=1}^{4}(M_R^x\cos\psi_k-M_R^y\sin\psi_k)$$

$$=\sum_{k=1}^{4}[(M_{IR}^x+M_{AR}^x)\cos\psi_k-(M_{IR}^y+M_{AR}^y)\sin\psi_k]$$

$$=\int_0^{R-e_p}\{\ddot{\theta}_x[-2F5+(e_p+x)\times 2C23]+\ddot{x}_g[(e_p+x)\times 2C21]+\dot{\theta}_y[-2F4+(e_p+x)\times$$
$$(2C9\times M5+2C19+2Qp5)]+\dot{x}_g[(e_p+x)\times(2C3+2C10\times N5+2P4\phi_0+2Qp15)]$$
$$+\dot{y}_g[(e_p+x)\times(2C9\times M4+2C10\times N6+2C22+2Qp4)]+\dot{\theta}_x[(e_p+x)\times(2C9\times M6$$
$$+2E6+2E8+2C13+2P9\phi_0+2Q6)]+\dot{\phi}_{1s}[(e_p+x)\times 2C15)]+\beta_{Gs}[2xB0$$
$$-2E2+2E12+(e_p+x)\times(-2C9\times M2-2C12+2C15K_{\beta G}-2Q2-2P8\phi_0)]$$
$$+\beta_{Gc}[2F1-2F3+(e_p+x)\times(-2C10\times N1-2C18-2Q11)]+\theta_y[(e_p+x)\times(2C2$$
$$+2C10\times N3+2P3\phi_0+2Q13)]+\theta_x[(e_p+x)\times(2C10\times N4+2C20+2Q14)]$$

$$+\phi_{1s}[(e_p+x)\times(2C7+2C8\phi_0+2P1)]+\phi_{1c}[(e_p+x)\times(-2C15)]+\ddot{\beta}_{Gs}(2E2)+\ddot{\beta}_{Gc}(2F3)$$
$$+\dot{\beta}_{Gs}(4F3)+\dot{\beta}_{Gc}[-4E2+(e_p+x)(-2C9\times M2-2C12-2P8\phi_0-2Qp2)]$$
$$+\ddot{\theta}_y(2E7)+\ddot{y}_g(2E11)]d_x$$

$$Q_R^y=\sum_{k=1}^{4}(M_R^x\sin\psi_k+M_R^y\cos\psi_k)$$

$$=\sum_{k=1}^{4}[(M_{IR}^x+M_{AR}^x)\sin\psi_k+(M_{IR}^y+M_{AR}^y)\cos\psi_k]$$

$$=\int_0^{R-e_p}\{\ddot{\theta}_y[2F7-(e_p+x)\times 2C28]+\ddot{y}_g[-(e_p+x)\times 2C27]+\dot{\theta}_x[2F6-(e_p+x)\times(2C9\times M9$$
$$+2C25+2Qp9)]+\dot{y}_g[-(e_p+x)\times(2C5+2C10\times N10+2P6\phi_0+2Qp18)]+\dot{x}_g[-(e_p+x)$$
$$\times(2C9\times M8+2C10\times N9+2C26+2Qp8)]+\dot{\theta}_y[2E3+2E5-(e_p+x)\times(2C9\times M10$$
$$+2C14+2P10\phi_0+2Qp10)]+\dot{\phi}_{1c}[-(e_p+x)\times 2C15]+\beta_{Gc}[2E2-2E12-2B0x$$
$$-(e_p+x)\times(-2C9\times M2-2C12-2P8\phi_0-2Qp2)]+\beta_{Gs}[2F1-2F3-(e_p+x)$$
$$\times(2C10\times N1+2C18+2Qp11)]+\theta_x[-(e_p+x)\times(2C4+2C10\times N7+2P5\phi_0+2Qp16)]$$
$$+\theta_y[-(e_p+x)\times(2C10\times N8+2C24+2Qp17)]+\phi_{1c}[-(e_p+x)\times(2C8\phi_0+2C7+2P1)]$$
$$+\phi_{1s}[-(e_p+x)\times 2C15]+\ddot{\beta}_{Gs}(2F3)+\ddot{\beta}_{Gc}(-2E2)+\ddot{\theta}_x(2E4)+\ddot{x}_g(2E10)+\dot{\beta}_{Gs}[-4E2$$
$$-(e_p+x)\times(2C9\times M2+2C12-2C15K_{\beta G}+2P8\phi_0+2Qp2)]+\dot{\beta}_{Gc}(-4F3)]\}d_x$$

$$Q_R^z=\sum_{k=1}^{4}(M_{IR}^z+M_{AR}^z)$$

$$=\int_0^{R-e_p}\{\ddot{\theta}_z[4G2+(e_p+x)\times 4B18]+\ddot{z}_g 4B15(e_p+x)+\dot{z}_g[(e_p+x)\times(4B1+4B7\times M1\phi_0+4O2\phi_0+4Q1)]$$
$$+\dot{\theta}_z[(e_p+x)\times(4B8\times N2\phi_0+4B9+4O6\phi_0+4Q12)]+\dot{\phi}_c[(e_p+x)\times 4B17]$$
$$+\phi_c[(e_p+x)\times(4B6\phi_0+4B14+4O1)]+4G1+4G5+(e_p+x)\times 4B0\}d_x$$

APPENDIX 3D

$$U_T^0 = \Omega(e_p+x+x\dot{\theta}_z)$$

$$U_T^s = -\Omega[-(v_F+v_i)R\theta_y+\dot{x}_g]$$

$$U_T^c = -\Omega[-(v_F+v_i)R\theta_x-\dot{y}_g]$$

$$U_p^0 = \Omega[(v_F+v_i)R+\dot{z}_g-x\dot{\beta}_G]$$

$$U_p^s = \Omega x\dot{\theta}_x$$

$$U_p^c = -\Omega x\dot{\theta}_y$$

$$\dot{U}_T^0 = \Omega^2[-(v_F+v_i)R\beta_{sw}\dot{\beta}_G+x\ddot{\theta}_z]=T1\dot{\beta}_G+T2\ddot{\theta}_z$$

$$\dot{U}_T^s = -\Omega^2[-(v_F+v_i)R(\dot{\theta}_y+\beta_{sw}\dot{\theta}_x-\theta_x+\beta_{sw}\theta_y)+\ddot{x}_g+\beta_{sw}\dot{x}_g-\beta_{sw}\ddot{y}_g+\dot{y}_g]$$
$$= Ts1\dot{\theta}_y+Ts2\dot{\theta}_x+Ts3\theta_x+Ts4\theta_y$$
$$+Ts5\ddot{x}_g+Ts6\dot{x}_g+Ts7\ddot{y}_g+Ts8\dot{y}_g$$

$$\dot{U}_T^c = -\Omega^2[-(v_F+v_i)R(\theta_y+\beta_{sw}\theta_x+\dot{\theta}_x-\beta_{sw}\dot{\theta}_y)+\dot{x}_g-\beta_{sw}\ddot{x}_g-\beta_{sw}\dot{y}_g-\ddot{y}_g]$$
$$= Tc1\dot{\theta}_y+Tc2\dot{\theta}_x+Tc3\theta_x+Tc4\theta_y+Tc5\ddot{x}_g+Tc6\dot{x}_g+Tc7\ddot{y}_g+Tc8\dot{y}_g$$

$$\dot{U}_p^0 = \Omega^2[\ddot{z}_g-x(e_p+x)\ddot{\beta}_G+x\beta_{sw}\dot{\beta}_G]$$
$$= P1\ddot{z}_g+P2\ddot{\beta}_G+p3\dot{\beta}_G$$

$$\dot{U}_p^s = -\Omega^2[-(\beta_G-\beta_p)(-\ddot{y}_g-\dot{x}_g)+x\beta_{sw}\ddot{\theta}_y-x\beta_{sw}\dot{\theta}_x-(e_p+x)\ddot{\theta}_x$$
$$-(e_p+x)\dot{\theta}_y-\dot{\beta}_G\dot{y}_g]$$
$$= Ps1\ddot{y}_g+Ps2\dot{x}_g+Ps3\beta_G\ddot{y}_g+Ps4\beta_G\dot{x}_g+Ps5\ddot{\theta}_y+Ps6\dot{\theta}_x+Ps7\ddot{\theta}_x$$
$$+Ps8\dot{\theta}_y+Ps9\beta_G\dot{y}_g$$

$$\dot{U}_p^c = -\Omega^2[-(\beta_G-\beta_p)(\ddot{x}_g+\dot{y}_g)+x\beta_{sw}\ddot{\theta}_x++x\beta_{sw}\dot{\theta}_y+(e_p+x)\ddot{\theta}_y$$
$$-(e_p+x)\dot{\theta}_x-\dot{\beta}_G\dot{x}_g]$$
$$= Pc1\ddot{x}_g+Pc2\dot{y}_g+Pc3\beta_G\ddot{x}_g+Pc4\beta_G\dot{y}_g+Pc5\ddot{\theta}_x+Pc6\dot{\theta}_y+Pc7\ddot{\theta}_y$$
$$+Pc8\dot{\theta}_x+Pc9\beta_G\dot{x}_g$$

$$U_R^0=U_T^0\cos\theta+U_p^0\sin\theta$$

$$U_R^s=U_T^s\cos\theta+U_p^s\sin\theta$$

$$U_R^c=U_T^c\cos\theta+U_p^c\sin\theta$$

$$\dot{U}_n^0=\Omega\dot{\theta}(U_T^0\cos\theta+U_p^0\sin\theta)+\dot{U}_T^0\sin\theta-\dot{U}_p^0\cos\theta$$

$$\dot{U}_n^s=\Omega\dot{\theta}(U_T^s\cos\theta+U_p^s\sin\theta)+\dot{U}_T^s\sin\theta-\dot{U}_p^s\cos\theta$$

$$\dot{U}_n^c=\Omega\dot{\theta}(U_T^c\cos\theta+U_p^c\sin\theta)+\dot{U}_T^c\sin\theta-\dot{U}_p^c\cos\theta$$

APPENDIX 3E

PITCH MOMENTS ABOUT PITCH BEARING

THE INERTIA PITCH MOMENT ABOUT PITCH BEARING

$$M_I^{pitch}=\int_0^{R-e_p}[q_I^x+(\beta_p-\beta_G)q_I^z-\beta_{sw}q_I^y]d_x$$

$$=\int_0^{R-e_p}\{<-m\Omega^2\{x_{Gc}\cos\theta_G[\ddot{z}_g-e_p\ddot{\beta}_G-x\ddot{\beta}_G-\phi x\beta_{sw}-\phi x\ddot{\theta}_z+\sin\psi[-x\beta_{sw}\,(\ddot{\theta}_y-2\dot{\theta}_x)$$

$$-(e_p+x)(-\ddot{\theta}_x-2\dot{\theta}_y)+\phi\ddot{x}_g]+\cos\psi[-x\beta_{sw}\,(\ddot{\theta}_x+2\dot{\theta}_y)-(e_p+x)\,(\ddot{\theta}_y-2\dot{\theta}_x)-\phi\ddot{y}_g]$$

$$+x_{Gc}\sin\theta_G[-x\beta_{sw}-\ddot{\theta}_z(e_p+x)-z_h\ddot{\alpha}_G+2z_h\dot{\beta}_G-2x\dot{\theta}_z\beta_{sw}-2x\beta_p\dot{\beta}_G-\phi\ddot{z}_g$$

$$+x\phi\ddot{\beta}_G+\sin\psi[\ddot{x}_g+\ddot{\theta}_y(-z_h+x(\beta_p-\beta_G))-2x\dot{\theta}_y\dot{\beta}_G]+\phi x\,(-\ddot{\theta}_x-2\dot{\theta}_y)]$$

$$+\cos\psi[-\ddot{y}_g+\ddot{\theta}_x(-z_h+x(\beta_p-\beta_G))-2x\dot{\theta}_x\dot{\beta}_G+\phi x(\ddot{\theta}_y-2\dot{\theta}_x)]\}$$

$$+\Omega^2(I_3\sin\theta_G^2+I_2\cos\theta_G^2)\{\phi+(-\beta_p+\beta_G)\ddot{\theta}_z-\ddot{\theta}_G-\ddot{\phi}+2\dot{\beta}_G-2\beta_{sw}\dot{\theta}_G-2\beta_{sw}\dot{\phi}$$

$$+2\dot{\theta}_z\dot{\theta}_G+2\phi\dot{\theta}_z-\ddot{\theta}_y\sin\psi-\ddot{\theta}_x\cos\psi\}+\Omega^2(I_3-I_2)\sin\theta_G\cos\theta_G(-1-2\dot{\theta}_z)$$

$$-\Omega^2(I_3\cos\theta_G^2+I_2\sin\theta_G^2)\{-\beta_{sw}\ddot{\beta}_G+\ddot{\phi}+\ddot{\theta}_G+\phi(1+2\dot{\theta}_z)+\sin\psi[\ddot{\theta}_y-2\dot{\theta}_x$$

$$-\beta_{sw}(-\ddot{\theta}_x-2\dot{\theta}_y)]+\cos\psi[\ddot{\theta}_x+2\dot{\theta}_y-\beta_{sw}(\ddot{\theta}_y-2\dot{\theta}_x)]\}>+(\beta_p-\beta_G)$$

$$<-m\Omega^2\{x_{Gc}\cos\theta_G[\ddot{x}_g\cos\psi+\ddot{y}_g\sin\psi-(e_p+x)-2x\dot{\theta}_z]$$

$$+x_{Gc}\sin\theta_G\phi x\}>-\beta_{sw}<-m\Omega^2\{x_{Gc}\cos\theta_G[-x\phi]$$

$$+x_{Gc}\sin\theta_G[-(e_p+x)-2x\dot{\theta}_z+\ddot{x}_g\cos\psi+\ddot{y}_g\sin\psi]\}>\}d_x$$

THE AERODYNAMIC MOMENT ABOUT PITCH BEARING

$$M_A^{pitch}=\int_0^{R-e_p} M d_x$$

$$=\int_0^{R-e_p}(2\rho b^2 c_{mac}+x_A\rho b c_l)\Omega^2\{x^2+(v_F+v_i)^2R^2+2e_p x+2x^2\dot{\theta}_z+2(v_F+v_i)R\dot{z}_g$$

$$-2x(v_F+v_i)R\dot{\beta}_g+\sin\psi<-2(e_p+x)[-(v_F+v_i)R\theta_y+\dot{x}_g]+2(v_F+v_i)Rx\dot{\theta}_x>$$

$$+\cos\psi<-2(e_p+x)[-(v_F+v_i)R\theta_x-\dot{y}_g]-2(v_F+v_i)Rx\dot{\theta}_y>\}$$

$$+\rho ab\Omega^2\{\frac{b}{2}\left(x_A-\frac{b}{2}\right)[\dot{\theta}(\cos\theta(e_p+x+x\dot{\theta}_z)+\sin\theta[(v_F+v_i)R+\dot{z}_g-x\dot{\beta}_G])$$

$$+\sin\theta[-(v_F+v_i)R\beta_{sw}\dot{\beta}_G+x\ddot{\theta}_z]-\cos\theta[\ddot{z}_g-x(e_p+x)\ddot{\beta}_G+x\beta_{sw}\dot{\beta}_G]]$$

$$+\frac{b}{2}\left(x_A^2-x_Ab+\frac{3b^2}{8}\right)(\ddot{\theta}-\dot{\beta}_G)+(\dot{\theta}-\beta_G+\beta_p)\left(-\frac{b^2}{4}\right)[\cos\theta(e_p+x+x\dot{\theta}_z)$$

$$+\sin\theta[(v_F+v_i)R+\dot{z}_g-x\dot{\beta}_G]]+\sin\psi\left[\frac{b}{2}\left(x_A-\frac{b}{2}\right)[\dot{\theta}(\cos\theta[-(v_F+v_i)R\theta_y+\dot{x}_g]\right.$$

$$+\sin\theta x\dot{\theta}_x]+\sin\theta(-[-(v_F+v_i)R(\dot{\theta}_y+\beta_{sw}\dot{\theta}_x-\theta_x+\beta_{sw}\theta_y)+\ddot{x}_g+\beta_{sw}\dot{x}_g-\beta_{sw}\ddot{y}_g$$

$$+\dot{y}_g])-\cos\theta(-[-(\beta_G-\beta_p)(-\ddot{y}_g-\dot{x}_g)+x\beta_{sw}\ddot{\theta}_y-x\beta_{sw}\dot{\theta}_x-(e_p+x)\ddot{\theta}_x$$

$$-(e_p+x)\dot{\theta}_y-\dot{\beta}_G\dot{y}_g])]+(\dot{\theta}-\beta_G+\beta_p)\left(-\frac{b^2}{4}\right)(\cos\theta[-(v_F+v_i)R\theta_y+\dot{x}_g]$$

$$\left.+\sin\theta x\dot{\theta}_x]\right]+\cos\psi\left[\frac{b}{2}\left(x_A-\frac{b}{2}\right)\left[\dot{\theta}(\cos\theta(-[-(v_F+v_i)R\theta_x-\dot{y}_g])\right.\right.$$

$$+\sin\theta(-x\dot{\theta}_y))+\sin\theta(-\Omega^2[-(v_F+v_i)R(\theta_y+\beta_{sw}\theta_x+\dot{\theta}_x-\beta_{sw}\dot{\theta}_y)+\dot{x}_g$$

$$-\beta_{sw}\ddot{x}_g-\beta_{sw}\dot{y}_g-\ddot{y}_g])-\cos\theta(-\Omega^2[-(\beta_G-\beta_p)(\ddot{x}_g+\dot{y}_g)+x\beta_{sw}\ddot{\theta}_x$$

$$+x\beta_{sw}\dot{\theta}_y+(e_p+x)\ddot{\theta}_y-(e_p+x)\dot{\theta}_x-\dot{\beta}_G\dot{x}_g])+(\dot{\theta}-\beta_G+\beta_p)\left(-\frac{b^2}{4}\right)$$

$$\left.\left.(\cos\theta(-[-(v_F+v_i)R\theta_x-\dot{y}_g])+\sin\theta(-x\dot{\theta}_y))\right]\right\}d_x$$

APPENDIX 4A
MULTI-BLADE COORDINATE TRANSFORMATION

$$\phi_0 = \frac{1}{N}\sum_{k=1}^{N}\phi^{(k)}$$

$$\phi_{nc} = \frac{2}{N}\sum_{k=1}^{N}\phi^{(k)}\cos n\psi_k$$

$$\phi_{ns} = \frac{2}{N}\sum_{k=1}^{N}\phi^{(k)}\sin n\psi_k$$

$$\phi_{N/2} = \frac{1}{N}\sum_{k=1}^{N}\phi^{(k)}(-1)^k$$

$$\dot{\phi}_0 = \frac{1}{N}\sum_{k=1}^{N}\dot{\phi}^{(k)}$$

$$\dot{\phi}_{nc}+n\phi_{ns} = \frac{2}{N}\sum_{k=1}^{N}\dot{\phi}^{(k)}\cos n\psi_k$$

$$\dot{\phi}_{ns}-n\phi_{nc} = \frac{2}{N}\sum_{k=1}^{N}\dot{\phi}^{(k)}\sin n\psi_k$$

$$\dot{\phi}_{N/2} = \frac{1}{N}\sum_{k=1}^{N}\dot{\phi}^{(k)}(-1)^k$$

$$\ddot{\phi}_0 = \frac{1}{N}\sum_{k=1}^{N}\ddot{\phi}^{(k)}$$

$$\ddot{\phi}_{nc}+2n\dot{\phi}_{ns}-n^2\phi_{nc} = \frac{2}{N}\sum_{k=1}^{N}\ddot{\phi}^{(k)}\cos n\psi_k$$

$$\ddot{\phi}_{ns} - 2n\dot{\phi}_{nc} - n^2\phi_{ns} = \frac{2}{N}\sum_{k=1}^{N}\ddot{\phi}^{(k)}\sin n\psi_k$$

$$\ddot{\phi}_{N/2} = \frac{1}{N}\sum_{k=1}^{N}\ddot{\phi}^{(k)}(-1)^k$$

where $\phi^{(k)}$ is the k'th blade coordinate in the rotating frame, ψ_k is the azimuth angle of the k'th blade, N is the number of blades, and the following relations exist:

$$\frac{1}{N}\sum_{k=1}^{N}\cos n\psi_k = \begin{cases}\cos n\psi & \text{if } n=pN \\ 0 & \text{otherwise}\end{cases}$$

$$\frac{1}{N}\sum_{k=1}^{N}\sin n\psi_k = \begin{cases}\sin n\psi & \text{if } n=pN \\ 0 & \text{otherwise}\end{cases}$$

APPENDIX 5A
KANE'S METHOD TO OBTAIN THE GENERALISED FORCES

In the formulation of equations of motion in chapter 5, the essence is to obtain the generalised forces. Kane's method is widely used in multibody dynamics formulation to compute the generalised forces [Kane and Levinson, 1985]. It is quite convenient in some cases. According to Kane's method, the generalised forces can be obtained by summing the dot product of the force and respective partial velocity. We shall derive the generalised inertial forces using Kane's method in follows.

The partial velocities of the lumped mass centre and partial angular velocities of the lumped mass can be obtained using the expression of $\vec{v}_{gc}$ in (3.1.9) in chapter 5.

The partial velocities:

$$\vec{v}_{gc/u} = \vec{i}_1, \quad \vec{v}_{gc/v} = \vec{j}_1, \quad \vec{v}_{gc/w} = \vec{k}_1$$

$$\vec{v}_{gc/\beta} = x_{gc}[-S_\phi C_\beta C_\zeta \vec{i}_1 - S_\phi C_\beta S_\zeta \vec{j}_1 - S_\phi S_\beta \vec{k}_1]$$

$$= [b_{11}\ b_{12}\ b_{13}]\ \{\vec{E}_1\}$$

$$\vec{v}_{gc/\zeta} = x_{gc}[-(-S_\phi S_\beta S_\zeta + C_\zeta C_\phi)\vec{i}_1 + (-S_\phi S_\beta C_\zeta - S_\zeta C_\phi)\vec{j}_1]$$

$$= [b_{21}\ b_{22}\ b_{23}]\ \{\vec{E}_1\}$$

$$\vec{v}_{gc/\phi} = x_{gc}[-(-C_\phi S_\beta C_\zeta + S_\zeta S_\phi)\vec{i}_1 + (-C_\phi S_\beta S_\zeta - C_\zeta S_\phi)\vec{j}_1 + C_\phi C_\beta \vec{k}_1]$$

$$= [b_{31}\ b_{32}\ b_{33}]\ \{\vec{E}_1\}$$

$$\vec{v}_{gc/vx} = \vec{i}_1, \quad \vec{v}_{gc/vy} = \vec{j}_1, \quad \vec{v}_{gc/vz} = \vec{k}_1$$

$$\vec{v}_{gc/wx} = -(w + x_{gc} S_\phi C_\beta)\vec{j}_1 + [v + x_{gc}(-S_\phi S_\beta S_\zeta + C_\zeta C_\phi)]\vec{k}_1 = [C_{11}\ C_{12}\ C_{13}]\ \{\vec{E}_1\}$$

$$\vec{v}_{gc/wy} = (w + x_{gc} S_\phi C_\beta)\vec{i}_1 - [r + u + x_{gc}(-S_\phi S_\beta C_\zeta - S_\zeta C_\phi)]\vec{k}_1 = [C_{21}\ C_{22}\ C_{23}]\ \{\vec{E}_1\}$$

$$\vec{v}_{gc/wz} = -[v + x_{gc}(C_\phi C_\zeta - S_\phi S_\beta S_\zeta)]\vec{I}_1 + [r + u + x_{gc}(-S_\phi S_\beta C_\zeta - S_\zeta C_\phi)]\vec{J}_1$$

$$= [C_{31}\ C_{32}\ C_{33}]\ \{\vec{E}_1\}$$

.....(1)

The partial angular velocities:

$$\vec{\omega}_u = \vec{\omega}_v = \vec{\omega}_w = 0$$

$$\vec{\omega}_\beta = -C_\varepsilon \vec{J}_2 + S_\phi \vec{k}_2 = [a_{11}\ a_{12}\ a_{13}]\ \{\vec{E}_2\}$$

$$\vec{\omega}_\zeta = S_\varepsilon \vec{I}_2 + C_\beta S_\phi \vec{J}_2 + C_\beta C_\phi \vec{k}_2 = [a_{21}\ a_{22}\ a_{23}]\ \{\vec{E}_2\}$$

$$\vec{\omega}_\phi = \vec{I}_2 = [a_{31}\ a_{32}\ a_{33}]\ \{\vec{E}_2\}$$

$$\vec{\omega}_{vx} = \vec{\omega}_{vy} = \vec{\omega}_{vz} = 0$$

$$\vec{\omega}_{wx} = \vec{I}_1$$

$$\vec{\omega}_{wy} = \vec{J}_1$$

$$\vec{\omega}_{wz} = \vec{k}_1$$

.....(2)

The generalised inertia forces due to a lumped mass are according to Kane's method:

$$\tilde{F}_i^* = -m\vec{v}_{gc/i} \cdot \vec{a}_{gc} - \vec{\omega}_i \cdot [\vec{\varepsilon} \cdot I + \vec{\omega} \times I \cdot \vec{\omega}] \qquad (i = 1, 2, ...12) \qquad (3)$$

where $\tilde{F}_i^*$ means the i'th generalised inertial forces corresponding to the i'th generalised coordinate, one of u, v, w, β, ξ, ϕ, v_x, v_y, v_z, ω_x, ω_y, ω_z

Where, the inertia dyadic of the lumped mass is written as:

$$I = I_{xx}\vec{I}_2\vec{I}_2 - 2I_{xy}\vec{I}_2\vec{J}_2 - 2I_{xz}\vec{I}_2\vec{k}_2 + I_{yy}\vec{J}_2\vec{J}_2 - 2I_{yz}\vec{J}_2\vec{k}_2 + I_{zz}\vec{k}_2\vec{k}_2$$

Replacing (1) and(2) into (3), the generalised inertia forces corresponding to the relevant generalised velocities are, therefore, obtained from Kane's method as:

$$\tilde{F}^*_u = -m\vec{i}_1 \cdot \vec{a}_{gc}$$

$$\tilde{F}^*_v = -m\vec{j}_1 \cdot \vec{a}_{gc}$$

$$\tilde{F}^*_w = -m\vec{k}_1 \cdot \vec{a}_{gc}$$

$$\tilde{F}^*_{vx} = -m\vec{i}_1 \cdot \vec{a}_{gc}$$

$$\tilde{F}^*_{vy} = -m\vec{j}_1 \cdot \vec{a}_{gc}$$

$$\tilde{F}^*_{vz} = -m\vec{k}_1 \cdot \vec{a}_{gc}$$

$$\tilde{F}^*_\beta = -m(b_{11}\vec{i}_1 + b_{12}\vec{j}_1 + b_{13}\vec{k}_1) \cdot \vec{a}_{gc} - (a_{11}\vec{i}_1 + a_{12}\vec{j}_1 + a_{13}\vec{k}_1) \cdot [\vec{\varepsilon} \cdot I + \vec{\omega} \times I \cdot \vec{\omega}]$$

$$\tilde{F}^*_\zeta = -m(b_{21}\vec{i}_1 + b_{22}\vec{j}_1 + b_{23}\vec{k}_1) \cdot \vec{a}_{gc} - (a_{21}\vec{i}_1 + a_{22}\vec{j}_1 + a_{23}\vec{k}_1) \cdot [\vec{\varepsilon} \cdot I + \vec{\omega} \times I \cdot \vec{\omega}]$$

$$\tilde{F}^*_\phi = -m(b_{31}\vec{i}_1 + b_{32}\vec{j}_1 + b_{33}\vec{k}_1) \cdot \vec{a}_{gc} - (a_{31}\vec{i}_1 + a_{32}\vec{j}_1 + a_{33}\vec{k}_1) \cdot [\vec{\varepsilon} \cdot I + \vec{\omega} \times I \cdot \vec{\omega}]$$

$$\tilde{F}^*_{\omega x} = -m(c_{11}\vec{i}_1 + c_{12}\vec{j}_1 + c_{13}\vec{k}_1) \cdot \vec{a}_{gc} - \vec{i}_1 \cdot [\vec{\varepsilon} \cdot I + \vec{\omega} \times I \cdot \vec{\omega}]$$

$$\tilde{F}^*_{\omega y} = -m(c_{21}\vec{i}_1 + c_{22}\vec{j}_1 + c_{23}\vec{k}_1) \cdot \vec{a}_{gc} - \vec{j}_1 \cdot [\vec{\varepsilon} \cdot I + \vec{\omega} \times I \cdot \vec{\omega}]$$

$$\tilde{F}^*_{\omega z} = -m(c_{31}\vec{i}_1 + c_{32}\vec{j}_1 + c_{33}\vec{k}_1) \cdot \vec{a}_{gc} - \vec{k}_1 \cdot [\vec{\varepsilon} \cdot I + \vec{\omega} \times I \cdot \vec{\omega}]$$

As we see, they are exactly same as those obtained in equation (3.1.35) of chapter 5. Similarly, other generalised forces also can be obtained from this method. As pointed out by Kane et al [1987], the generalised forces caused by conservative loads, such as internal strain energy, can similarly be obtained from the derivatives of the potential function.

APPENDIX 6A

The expressions of U_{T0}, $[U_{Tv}]$, $[U_{Td}]$, U_{p0}, $[U_{pv}]$, $[U_{pd}]$, U_{Tp0}, $[U_{Tpv}]$ and $[U_{Tpd}]$ in Equations (2.38-2.40) of Chapter 6 are listed below.

$$U_{T0} = v_\lambda^2 t_2^2 + 2v_\lambda t_2 v_y + 2v_\lambda t_2 \omega_z r + v_y^2 + \omega_z^2 r^2 + 2v_y \omega_z r$$

$$\begin{aligned} U_{Tv} = [&-2\{v_\lambda t_2 + v_y + \omega_z(r+u) - \omega_x w\}v' + 2\{v_\lambda t_1 + v_x + \omega_y w - \omega_z v\}v'^2, \\ &v_\lambda t_2 + 2v_y + 2\omega_z(r+u) - 2\omega_x w - 2\{v_\lambda t_1 + v_x + \omega_y w - \omega_z v\}v', \\ &0\ ] \end{aligned}$$

$$\begin{aligned} U_{Td} = [&v_\lambda t_2 \omega_z + \omega_z^2(2r+u) + 2v_y\omega_z - 2\omega_x\omega_z w, \\ &-2\{v_\lambda^2 t_1 t_2 + v_\lambda t_1[v_y + \omega_z(r+u) - \omega_x w] + v_\lambda t_2[v_x + \omega_y w - \omega_z v] \\ &+ [v_x + \omega_y w - \omega_z v][v_y + \omega_z(r+u) - \omega_x w]\}D_r + \{v_\lambda^2 t_1^2 \\ &+ [v_x + \omega_y w - \omega_z v]^2 + 2v_\lambda t_1[v_x + \omega_y w - \omega_z v]\}\sqrt{D_r}, \\ &-v_\lambda t_2 \omega_x + \omega_x^2 w - 2v_y\omega_x - 2\omega_x\omega_z r] \end{aligned}$$

$$U_{p0} = v_\lambda^2 t_3^2 + 2v_\lambda t_3 v_z - 2v_\lambda t_3 \omega_y r + v_z^2 + \omega_y^2 r - 2v_z\omega_y r$$

$$\begin{aligned} U_{Pv} = [&-2\{v_\lambda t_3 + v_z + \omega_x v - \omega_y(r+u)\}w' + 2\{v_\lambda t_1 + v_x + \omega_y w - \omega_z v\}w'^2, \\ &0, \\ &2v_\lambda t_3 + 2\ v_z + 2\omega_x v - 2\omega_y(r+u) - 2\{v_\lambda t_1 + v_x + \omega_y w - \omega_z v\}w'] \end{aligned}$$

$$\begin{aligned} U_{Pd} = [&-2v_\lambda t_3 \omega_y + \omega_y^2(2r+u) - 2v_z\omega_y - 2\omega_x\omega_y v, \\ &2v_\lambda t_3 \omega_x + \omega_x^2 v + 2\omega_x v_z - 2\omega_x\omega_y r, \\ &2(-v_\lambda^2 t_1 t_3 - v_z v_\lambda t_1 + \omega_y r v_\lambda t_1 + v_\lambda t_3 \omega_z v + v_z\omega_z v - \omega_y r\omega_z v)D_r \end{aligned}$$

$$-2\{v_\lambda^2 t_1 t_3 + v_\lambda t_1[v_z + \omega_x v - \omega_y(r+u)] + v_\lambda t_3[v_x + \omega_y w - \omega_z v]$$
$$+[v_x + \omega_y w - \omega_z v][v_z + \omega_x v - \omega_y(r+u)]\}D_r$$
$$+\{v_\lambda^2 t_1^2 + [v_x + \omega_y w - \omega_z v]^2 + 2v_\lambda t_1[v_x + \omega_y w - \omega_z v]\}w'D_r]$$

$$U_{TP\,0} = v_\lambda^2 t_2 t_3 + v_\lambda t_2 v_z - v_\lambda t_2 \omega_y r + v_\lambda t_3 v_y + v_\lambda t_3 \omega_z r$$
$$+v_y v_z - v_y \omega_y r + v_z \omega_z r - \omega_y \omega_z r^2$$

$$U_{TPv} = [-\{v_\lambda t_2 + v_y - \omega_x w + \omega_z(r+u)\}w' - \{v_\lambda t_3 + v_z + \omega_x v - \omega_y(r+u)\}v'$$
$$+2\{v_\lambda t_1 + v_x + \omega_y w - \omega_z v\}v'w',$$
$$v_\lambda t_3 + v_z + \omega_x v - \omega_y(r+u) - \{v_\lambda t_1 + v_x + \omega_y w - \omega_z v\}w',$$
$$v_\lambda t_2 + v_y - \omega_x w + \omega_z(r+u) - \{v_\lambda t_1 + v_x + \omega_y w - \omega_z v\}v']$$

$$U_{TPd} = [-v_\lambda t_2 \omega_y + v_\lambda t_3 \omega_z - v_y \omega_y + v_z \omega_z + \omega_x \omega_z v + \omega_x \omega_y w - \omega_y \omega_z(2r+u),$$
$$v_\lambda t_2 \omega_x + v_y \omega_x + \omega_x \omega_z r - \omega_x^2 w - \{v_\lambda^2 t_1 t_3 + v_\lambda t_1[v_z + \omega_x v - \omega_y(r+u)]$$
$$+v_\lambda t_3[v_x + \omega_y w - \omega_z v] + [v_x + \omega_y w - \omega_z v][v_z + \omega_x v - \omega_y(r+u)]\}D_r$$
$$+\{v_\lambda^2 t_1^2 + [v_x + \omega_y w - \omega_z v]^2 + 2v_\lambda t_1[v_x + \omega_y w - \omega_z v]w'\}D_r,$$
$$-v_\lambda t_3 \omega_x - \omega_x v_z + \omega_x \omega_y r - \{v_\lambda^2 t_1 t_2 + v_\lambda t_1[v_y - \omega_x w + \omega_z(r+u)]$$
$$+v_\lambda t_2[v_x + \omega_y w - \omega_z v] + [v_x + \omega_y w - \omega_z v][v_y - \omega_x w + \omega_z(r+u)]D_r]$$

Where, $D_r = \frac{d}{dr}(\ )$

REFERENCES

Bathe, K. J. 1982 : "Finite Element Procedures in Engineering Analysis" Prentice-Hall, Inc.

Bathe, K. J. and Wilson, E. L. 1976 : "Numerical Methods in Finite Element Analysis" Prentice-Hall, Inc.

Bauchau, O. A. 1985 : "A Beam Theory for Anisotropic Materials" J. Applied Mechanics, vol. 52, pp. 416-422.

Bauchau, O. A. and Hong, C. H. 1987a : "Finite Element Approach to Rotor Blade Modelling" Journal of American Helicopter Society, Vol. 32, No. 1, Jan. pp.60-67.

Bauchau, O. A. and Hong, C. H. 1987b : "Large Displacement Analysis of Naturally Curved and Curved and Twisted Composite Beams" AIAA J., vol. 25, no. 11, Nov. pp. 1469-1475.

Beddoes, T. S. 1976 : "A Synthesis of Unsteady Aerodynamic Effects Including Stall Hysteresis" Vertica vol. 1 pp. 113-123.

Bielawa, R. L. 1976 : "Aeroelastic Analysis for Helicopter Rotor Blades with Time Variable, Nonlinear Structural Twist and Multiple Structural Redundancy--Mathematical Derivation and Program User's Manual" NASA CR-2638.

Bisplinghoff, R. L. Ashley, H. and Halfman, R. L. 1955 : "Aeroelasticity" Addison-Wesley Publishing Company.

Bland, S. R. and Bennett, R. M. 1963 : "Wind-Tunnel measurement of Propeller Whirl Flutter Speeds and Static Stability Derivative and Comparison with Theory" NASA TN D-1807, Aug.

Borri, M. and Merlini, T. 1986 : "A Large Displacement Formulation for Anisotropic Beam Analysis" Meccanica, vol. 21, pp. 30-37.

Carr, L. W. McAllister, K. W. and McCroskey, W. J. 1977 : "Analysis of the Development of Dynamic Stall Based on Oscillating Airfoil Experiments" NASA TN D-8283.

Celi, R. and Friedmann, P. P. 1987 : "Aeroelastic Modelling of Swept Tip Rotor Blades Using Finite Elements" Proceeding of 43rd Annual National Forum of the American Helicopter Society, St. Louis, Mo., pp.257-269.

Coleman, R. P. and Feingold, A. M. 1958 : "Theory of Self-Excited Mechanical Oscillation of Helicopter Rotors with Hinged Blades" NASA TR-1351.

Craig, R. R. 1981 : "Structural Dynamics -- An Introduction to Computer Methods" John Wiley & Sons.

Crespo, Da Silva, M. R. M. and Hodges, D. H. 1986a : "The role of Computerised Symbolic Manipulations in Rotorcraft Dynamic Analysis" Comput. Math. Applic. Vol. 12A, pp.161-172

Crespo, da Silva, M. R. M. and Hodges, D. H. 1986b : "Nonlinear Flexure and Torsion of Rotating Beams with Application to Helicopter Rotor Blades" I. Formulation. Vertical, vol. 10, no. 2.

Dat, R. 1984 : "Development of Basic Methods Needed to Predict Helicopter Aeroelastic Behaviour" Vertica, vol. 8, no. 3, pp. 209-228.

Desai, C. S. and Abel, J. F. 1972 : "Introduction to the Finite Element Method - An Numerical Method for Engineering Analysis" Van Nostrand Reinhold Company.

Dinyavari, M. A. H. and Friedmann, P. P. 1985 : "Application of the Finite State Arbitrary Motion Aerodynamics to Rotor Blade Aeroelastic Response & Stability in Hover & Forward Flight" AIAA Paper 85-0763, proceedings AIAA/ASME/ASCE/AHS 25th SDM Conference, Orlando, Fla., Apr.

Done, G. T. S. Juggins, P. T. W. and Patel, M. H. 1988 : "Further Experience with a New Approach to Helicopter Aeroelasticity" Vertica, vol. 12, no. 4, p. 357-369.

Dowell, E. H. Traybar, J. and Hodges, D. H. 1977: "An Experimental Theoretical Correlation Study of Non-Linear Bending and Torsion Deformations of a Cantilever Beam" J. Sound and Vibration, vol. 50. no. 4, Feb. pp.533-544.

Friedmann, P. P. 1975 : "Influence of Structural Damping, Preconing, Offsets, and Large Deflections on the Flap-Lag-Torsional Stability of a Cantilevered Rotor Blade" AIAA Paper 75-780, Denver, Colo.

Friedmann, P. P. 1977a : "Influence of Modeling and Blade Parameters on the Aeroelastic Stability of a Cantilevered Rotor" AIAA J., vol.15, no. 2, Feb. pp. 149-158.

Friedmann, P. P. 1977b : "Recent Development in Rotary-Wing Aeroelasticity" J. Aircraft, vol. 14, pp.1027-1041.

Friedmann, P. P. 1983 : "Formulation and Solution of Rotary-Wing Aeroelastic Stability and Response Problems" Vertica, vol. 7, pp. 101-141.

Friedmann, P. P. 1986 : "Arbitrary Motion Unsteady Aerodynamics and Its Application to Rotary-Wing Aeroelasticity" Proceeding of the 42nd Annual National Forum of American Helicopter Society, Washington,D.C., June. pp. 757-776.

Friedmann, P. P. 1987 : "Recent Trends in Rotary-Wing Aeroelasticity" Vertica, vol. 11, no. 1/2, pp. 139-170.

Friedmann, P. P. 1990 : "Helicopter Rotor Dynamics and Aeroelasticity: Some Key Ideas and Insights" Vertica, Vol.14, No.1, pp.101-121, 1990.

Friedmann, P. P. and Straub, F. K. 1980 : "Application of Finite Element Method to Rotary-Wing Aeroelasticity" J. Am. Helicopter Soc., vol. 25, no. 1, Jan. pp. 36-44.

Friedmann, P. P. and Yuan, C. 1977 : "Effects of Modified Aerodynamic Strip Theories on Rotor Blade Aeroelastic Stability" AIAA J., vol. 15, no. 7, July pp. 932-940.

Gangwani, S. T. 1981 : "Prediction of Dynamic Stall and Unsteady Airloads for Rotor Blades" Proceedings 37th Ann. Forum Am. Helicopter Soc., New,Orleasn, pp. 1-17.

Gaonkar, G. H. and Peters, D. A. 1986a : "Effectiveness of Current Dynamic-Inflow Models in Hover and in Forward Flight" J. Am. Helicopter Soc., vol. 31, Apr.. pp. 47-57.

Gaonkar, G. H. and Peters, D. A. 1986b : " Review of Dynamic Inflow Modeling for Rotorcraft Flight Dynamics" AIAA Paper 86-0845-CP, proceedings of the AIAA/ASME/ASCE/AHA 27th SDM Conference, San Antonio, Tex.

Gaonkar, G. H. Mitra, A. K. Reddy, T. S. S. and Peters, D. A. 1982 : "Sensitivity of helicopter Aeromechanical Stability to Dynamic Inflow" Vertica, vol. 6, no. 1, pp. 59-75.

Gibbons, M. P. and Done, G. T. S. 1984 : "Automatic Generation of Helicopter Rotor Equations of Motion" Vertica, Vol. 8, pp.229-241

Greenberg, J. M. 1947 : "Airfoil in Sinusoidal Motion in a Pulsating Stream" NACA TN-1326.

Hammond, C. E. 1974 : "An Application of Floquet Theory to the Prediction of Mechanical Instability" J. Am. Helicopter Soc., vol. 19, no. 4, Oct. pp. 14-23.

Hoa, S. V. 1979 : "Vibration of a Rotating Beam with Tip Mass" J. of Sound & Vibration, Vol.67, No.3, pp.369-381.

Hodges, D. H. 1979a : "A Theoretical Technique for Analyzing Aeroelastic Stability of Bearingless Rotors" AIAA J., vol. 17, no. 4, Apr. pp. 400-407.

Hodges, D. H. 1979b : "Vibration and Response of Nonuniform Rotating Beams with Discontinuities" J. Am. Helicopter Soc., vol. 24, no.5,, Oct. pp. 43-50.

Hodges, D. H. 1985 : "Nonlinear Equations for Dynamics of Pretwisted Beams Undergoing Small Strains and Large Rotations" NASA TP-2470.

Hodges, D. H. 1987a : "Finite Rotation and Nonlinear Beam Kinematics" Vertica, vol. 11, no. 1/2, pp. 297-308.

Hodges, D. H. 1987b : "Nonlinear Beam Kinematics for Small Strains and Finite Rotations" Vertica, vol. 11, no. 3, pp. 573-589.

Hodges, D. H. and Dowell, E. H. 1974 : "Nonlinear Equations of Motion for the Elastic Bending and Torsion of Twisted Nonuniform Rotor Blades" NASA TN D-7818.

Hodges, D. H. and Ormiston, R. A. 1976 : "Stability of Elastic Bending and Torsion of Uniform Cantilever Rotor Blades in Hover with Variable Structural Coupling" NASA TN D-8192

Hodges, D. H. and Rutkowski, M. J. 1981 : "Free-Vibration Analysis of Rotating Beams by a Variable-order Finite Element Method" AIAA J., vol. 19, no. 11, Nov. pp. 1459-1466.

Hodges, D. H. Hopkins, A. S. Kunz, D. L. and Hinnant, H. E. 1986 : "Introduction to GRASP--General Rotorcraft Aeromechanical Stability Program--A Modern Approach to Rotorcraft Modeling" Proceedings of the 42nd Annual National Forum of the American Helicopter Society, Washington, D.C. pp.739-756.

Hodges, D. H. Ormiston, R. A. and Peters, D. A. 1980 : "On the Nonlinear Deformation Geometry of Euler-Bernoulli Beams" NASA TP-1566.

Hohenemser, K. H. and Crews, S. T. 1973 : "Model Tests on Unsteady Rotor Wake Effects" J. of Aircraft, Vol.10, No.1, Jan. pp.58-60.

Hohenemser, K. H. and Perisho, C. H. 1958 : "Analysis of the Vertical Flight Dynamic Characteristics of the Lifting Rotor with Floating Hub and Offset Coning Hinges" J. Am. helicopter Soc., Vol.3 No.4, Oct.

Hohenemser, K. H. and Yin, S. K. 1972 : "Some Applications of the Method of Multi-blade Coordinates" J. Am. Helicopter Soc., vol. 17, no. 3, July. pp. 1-12.

Hohenemser, K. H. and Yin, S. K. 1977 : "Finite Element Stability Analysis for Coupled Rotor and Support System" NASA CR-152024.

Hong, C. H. and Chopra, I. 1985 : "Aeroelastic Stability Analysis of a Composite Rotor Blade" J. Am. Helicopter Soc., vol. 30, no. 2, pp. 57-67.

Hong, C. H. and Chopra, I. 1986 : "Aeroelastic Stability of a Composite Bearingless Rotor Blade" J. Am. Helicopter Soc., vol. 31, no. 4, pp. 29-35.

Houbolt, J. C. and Brooks, G. W. 1958 : "Differential Equations of Motion for Combined Flapwise Bending, Chordwise Bending, and Torsion of Twisted Nonuniform Rotor Blades" NACA Report 1346.

Johnson, W. 1974 : "Theory and Comparison with Tests of Two Full-Scale proprotors" NASA SP -352.

Johnson, W. 1977 : "Aeroelastic Analysis for Rotorcraft in Flight or in a Wind Tunnel" NASA TN D-8515.

Johnson, W. 1980a : "Application of Unsteady Airfoil Theory to Rotary Wings" J. Aircraft, vol. 17 no. 4, Apr. pp. 285-286.

Johnson, W. 1980b : "Helicopter Theory" Princeton University Press.

Johnson, W. 1981a : "Development of a Comprehensive Analysis for Rotorcraft. Pt I. Rotor Model and Wake Analysis" Vertica, vol. 5, no. 2, pp. 99-129.

Johnson, W. 1981b : "Development of a Comprehensive Analysis for Rotorcraft. Pt II. Aircraft Model, Solution Procedure, and Applications" Vertica, vol. 5, no. 3, pp. 185-216.

Johnson, W. 1982 : "Influence of Unsteady Aerodynamics on Hingeless Rotor Ground Resonance" J. Aircraft, vol. 29, no. 8, Aug. pp. 668-673.

Juggins, P. T. W. et al. 1989 : "Experimental Activities to Support the EUROFAR Tilt Rotor Project Preliminary Phase" Proceedings of the Royal Aeronautical Society for EUROFAR--The European Future Advanced Rotorcraft, 11th April, London.

Kamman, J. W. and Huston, R. L. 1984 : "Dynamics of Constrained Multibody Systems" J. Applied Mechanics, Vol. 51, Dec.

Kane, T. R. and Levinson, D. A. 1985 : "Dynamics : Theory and Applications" McGraw-Hill Book Company.

Kane, T. R. and Ryan, R. R. 1987 : "Dynamics of a Cantilever Beam Attached to a Moving Base" J. Guidance, Control and Dynamics, vol. 10, no. 2, March-April, pp. 139-151.

Kaza, K. R. V. and Kvaternik, R. G. 1981 : "Application of Unsteady Airfoil Theory to Rotary Wings" J. Aircraft, vol. 18, no. 7, July. pp. 604-605.

Kosmatka, J. B. and Friedmann, P. P. 1987 : "Structural Dynamic Modeling of Advanced Composite propellers by the Finite Element Method" Proceedings AIAA/ASME/ASCE/AHS 28th Structures, Structural Dynamics and Materials Conference, Monterey, CA, vol. II, pp. 111-124.

Kosmatka, J. B. and Friedmann, P. P. 1989 : "Vibration Analysis of Composite Turbopropellers Using a Nonlinear Beam-Type Finite Element Approach" AIAA Journal, vol. 27, no. 11, Nov. pp. 1606-1614.

Kulla, P. 1972 : "Dynamics of Spinning Bodies Containing Elastic Rods" Journal of Spacecraft and Rockets, vol. 9, Apr. pp. 246-253.

Kvaternik, R. G. 1973a : "Studies in Tilt-Rotor VTOL Aircraft Aeroelasticity" NASA TMX-69496.

Kvaternik, R. G. 1973b : "Studies in Tilt-Rotor VTOL Aircraft Aeroelasticity" NASA TMX-69497.

Kvaternik, R. G. and Kohn, J. S. 1977 : "An Experimental and Analytical Investigation of Proprotor Whirl Flutter" NASA TP-1047.

Lee, S. W. and Kim, Y. H. 1987 : "A New Approach to the Finite Element Modeling of Beams" Int'l. J. for Num. Methods in Engr., vol. 24, pp. 2327-2341.

Likins, P. W. 1974 : "Geometric Stiffness Characteristics of a Rotating Elastic Appendage" International Journal of Solids and Structures, vol. 10, pp. 161-167.

Loewy, R. G. 1957 : "A Two Dimensional Approach to the Unsteady Aerodynamics of Rotary Wings" J. Aeronaut. Sci., vol. 24, no. 2. Feb. pp. 82-98.

Loewy, R. G. 1969 : "Review of Rotary-Wing V/STOL Dynamic and Aeroelastic Problems" J. Am. Helicopter Soc., vol. 14, pp. 3-23.

Luh, J. Y. S. Walker, M. W. and Paul, R. P. C. 1980 : "On-Line Computational Scheme for Mechanical Manipulators" Journal of Dynamic Systems, Measurements, and Control, vol. 102, June. pp. 69-76.

McCroskey, W. J. McAllister, K. W. Carr, L. W. Pucci, S.`L. Lambert, O. and Indergrand, R. F. 1981 : "Dynamic Stall on Advanced Airfoil Sections" J. Am. Helicopter Soc., vol. 26, July, pp. 40-50.

Meirovitch, L. 1980 : "Computational Methods in Structural Dynamics" Sijthoff and Noordhoff International Publishers.

Meirovitch, L. 1986 : "Elements of Vibration Analysis" McGraw-Hill Book Co. Second Edition.

Miller, R. H. and Ellis, C. W. 1956 : "Blade Vibration and Flutter" J. Am. helicopter Soc., Vol.1, No.3, July.

Minguet, P. and Dugundji, J. 1989a : "Experiments and Analysis for Structurally Coupled Composite Blades Under Large Deflections : Part 2 - Dynamic Behaviour" AIAA Paper No. 89-1366-CP, Proceedings 30th AIAA/ASME/ASCE/AHS/ACS Structures, Structural Dynamics and Materials Conference, Mobile, AL, Apr. pp. 1817-1827.

Minguet, P. and Dugundji, J. 1989b : "Experiments and Analysis for Structurally Coupled Composite Blades Under Large Deflections: Part 1 -- Static Behaviour" AIAA Paper No. 89-1366-CP, Proceedings 30th AIAA/ASME/ASCE/AHS/ACS Structures, Structural Dynamics and Materials Conference, Mobile, AL, April, pp. 1807-1816

Modi, V. J. 1974 : "Attitude Dynamics of Satellites with Flexible Appendages--A Brief Review" Journal of Spacecraft and Rockets, vol. 11, Nov. pp.743-751.

NAG Library : "Handbook for the NAG Fortran Workstation Library"

NAG Library : "NAG Fortran Library Manual"

Nagaraj, V. T. and Shanthakumar, P. 1975 : "Rotor Blade Vibrations by the Galerkin Finite Element Method" J. of Sound & Vibration, Vol.43, No.3, pp.575-577.

Ormiston, R. A. 1976 : "Application of Simplified Inflow Models to Rotorcraft Dynamic Analysis" J.Am. Helicopter Soc., vol.21 no. 3, July. pp. 34-39.

Ormiston, R. A. 1985 : "Rotor-Fuselage Dynamic Coupling Characteristics of Helicopter Air and Ground Resonance" Proceedings of the Theoretical Basis of Helicopter Technology, Nanjing Aeronautical Institute, Nanjing, China, Nov. 6-8.

Ormiston, R. A. and Bousman, W. G. 1975 : "A Study of Stall Induced Flap-Lag Instability of Hingeless Rotors" J. Am. Helicopter Soc., vol.20, no. 1, Jan. pp. 20-30.

Ormiston, R. A. and Hodges, D. H. 1972 : "Linear Flap-Lag Dynamics of Hingeless Helicopter Rotor Blades in hover" J. Am. Helicopter Soc.,vol. 17, no. 2, Apr. pp. 2-14.

Ormiston, R. A. and Peters, D. A. 1972 : "Hingeless helicopter Rotor Response with Nonuniform Inflow and Elastic Blade Bending" J. Aircraft, vol. 9, no. 10, Oct. pp.730-736.

Ormiston, R. A. Warmbrodt, W. G. Hodges, D. H. and Peters, D. A. 1987 : "Rotorcraft Aeroelastic Stability" NASA CP 2495 pp. 353-529.

Panda, B. and Chopra, I. 1987 : "Dynamics of Composite Rotor Blades in Forward Flight" Vertica, vol. 11, no. 1/2, pp. 187-209.

Patel, M. H. and Done, G. T. S. 1985 : "Experience with a New Approach to Rotor Aeroelasticity" Vertica, Vol. 9, pp.285-294

Pei, C. C. 1958 : "Pitch-lag Instability of Helicopter Rotors" J. Am. helicopter Soc., Vol.3, No.3 July.

Peters, D. A. 1974 : "Hingeless Rotor Frequency Response with Unsteady Inflow. Proceeding of the AHS/NASA Ames Specialists' Meeting on Rotorcraft Dynamics " NASA SP-352.

Peters, D. A. 1985 : "Toward a Unified Model for Use in Rotor Blade Stability Analyses" J. Am. helicopter Soc., vol. 30, July. pp. 32-42.

Peters, D. A. and Ormiston, R. A. 1973 : "The Effects of Second Order Blade Bending on the Angle of Attack of Hingeless Rotor Blades" J. Am. Helicopter Soc., vol. 18, no. 4, Oct. pp. 45-48.

Pitt, D. M. and Peters, D. A. 1981 : "Theoretical Prediction of Dynamic Inflow Derivatives" Vertica, vol. 5, no. 1, Mar. pp. 21-34.

Press, W. H. Flannery, B. P. Teukolsky, S. A. and Vetterling, W. T. 1989 : "Numerical Recipes--Fortran Version" Cambridge University Press.

Rand, O. 1990 : "Theoretical Modelling of Composite Rotating Beams" Vertica Vo. 14, No. 3, pp. 329-343.

Reddy, T. S. R. and Warmbrodt, W. 1985 : "The Influence of Dynamic Inflow and Torsional Flexibility on Rotor Damping in Forward Flight from Symbolically Generated Equations" NASA CP 2400 pp.221-239

Reed III, W. H. 1965 : "Propeller-Rotor Whirl Flutter : A-State-of-the-Art Review" Presented at the Symposium on the Noise and Loading Actions on Helicopter V/STOL Aircraft and Ground Effect Machines, England, Sep.

Reed III, W. H. and Bland, S. R. 1961 : "An Analytical Treatment of Aircraft Propeller Precession Instability" NASA TN D-659, Jan.

Runyan, H. L. and Tai, H. 1986 : "Application of a Lifting Surface Theory for a Helicopter in Forward Flight" Vertica, vol. 10, no. 3/4, pp. 269-280.

Sivaneri, N. T. and Chopra, I. 1982 : "Dynamic Stability of a Rotor Blade Using Finite Element Analysis" AIAA J., vol. 20, no. 5, May, pp. 716-723.

Sivaneri, N. T. and Chopra, I. 1984 : "Finite Element Analysis for Bearingless Rotor Blade Aeroelasticity" J. Am. Helicopter Soc., vol. 29, no.2, Apr.

Stemple, A. D. and Lee, S. W. 1988 : "Finite Element Model for Composite Beams with Arbitrary Cross-Sectional Warping" AIAA J., vol.26, no. 12, Dec. pp. 1512-1520.

Theodorsen, T. 1934 : "General Theory of Aerodynamic Instability and the Mechanism of Flutter" NACA Report 496.

Tran, C. T. and Petot, D. 1981 : "Semi-empirical Model for the Dynamic Stall of Airfoils in View of the Application to the Calculation of the Response of a Helicopter Blade in Forward Flight" Vertica, vol. 5 pp. 35-53.

Turcic, D. A. and Midha, A. 1984 : "Dynamic Analysis of Elastic Mechanism Systems. Pt I: Applications" Journal of Dynamic Systems, Measurement, and Control, vol. 106, Dec. pp. 249-254.

Venkatesan, C. and Friedmann, P. P. 1984 : "Aeroelastic Effects in Multirotor Vehicles with Application to a Hybrid Heavy Lift System. Pt I. Formulation of Equations of Motion" NASA CR-3822.

Venkatesan, V. and Friedmann, P. P. 1987 : "Aeroelastic Effects in Multirotor Vehicles. Pt II. Methods of Solution and Results Illustrating Coupled Rotor/Body Aeromechanical Stability" NASA CR-4009.

Warmbrodt, W. and Friedmann, P. P. 1979 : "Formulation of Coupled Rotor/Fuselage Equations of Motion" Vertica, vol. 3, no. 3, pp. 254-271.

Wright, A. D. Smith, C. E. Thresher, R. W. and Wang, J. L. C. 1982 : "Vibration Modes of Centrifugally Stiffened Beams" J. Applied Mechanics, vol. 49, March, pp. 197-202.

Zienkiewicz, O. C. 1977 : "The Finite Element Method" The Third Edition.